Adrian Falconer BSc (Hons)

The activation and disarming of Protease-activated Receptor 2: Implications for Osteoarthritis

Thesis submitted for partial fulfilment of the requirements of the regulations for the degree of Doctor of Philosophy

Newcastle University

Faculty of Medical Sciences

2017

Abstract

Osteoarthritis (OA) is a common degenerative disease of articular joints characterised by the enzymatic degradation of cartilage, mediated predominately by the collagenolytic matrix metalloproteinases (MMP)-1 and -13. Various stimuli have been identified as inducers of MMP expression in chondrocytes, including pro-inflammatory cytokines, abnormal mechanical load, and the activation of protease-activated receptor 2 (PAR2) by matriptase. Both PAR2 and matriptase are strongly implicated in OA. PAR2 is activated by cleavage at a distinct site to reveal the canonical tethered ligand, SLIGKV, which can bind and activate the receptor. PAR2 is also able to undergo non-canonical activation and receptor disarming by cleavage at different sites, revealing different tethered ligands or removing the extracellular domain.

This project aimed to identify novel PAR2 cleavages by incubated recombinant proteases with a PAR2 peptide sequence. The classical collagenases, MMP-1, -8 and -13, as well as the cysteine proteases cathepsins V, K, L and B, were all identified as novel PAR2 cleaving enzymes. The collagenases cleaved PAR2 at a distinct site a single amino acid to the C-terminus of the canonical site, and the putative tethered ligand, LIGKVD, was identified as a potential biased agonist for PAR2. The cathepsins generally cleaved PAR2 further towards the cell membrane, and cathepsin V was found to disarm against canonical PAR2 activation. Enzyme kinetics were examined for all novel proteases and compared with matriptase, identifying MMP-13 as the most potent collagenase for PAR2 cleavage, with all cathepsins exhibiting broadly similar kinetic profiles to each other.

Canonical PAR2 activation was further explored by DNA microarray analysis which identified a pro-inflammatory expression profile. Multiple identified downstream targets had previously been identified as MMP regulators induced by pro-inflammatory cytokine stimulation of chondrocytes, such as activating transcription factor (ATF) 3, and early growth response (EGR) 2. Furthermore, work performed on the mechanical loading of chondrocytes in 3-dimensional hydrogel culture identified the same regulators to be induced by abnormal load, with subsequent MMP-1 expression. Taken together, disparate stimuli were identified as having common downstream elements suggesting overlapping pathways resulting in a common outcome: the induction of MMP expression, and an increased potential for cartilage catabolism.

Table of Contents

Acknowledgements

I would like to begin by thanking my supervisor, Professor Drew Rowan for his help and support throughout my PhD. I would also like to thank Dr David Wilkinson, Dr Chun Ming Chan and Dr Joe Gray for their help, advice and discussion towards the competition of this thesis, and to all the other members of my group especially David Hodgson, Mari Arques Mengual and Hua Lin and to the whole department for making the past few years enjoyable.

Thank you to my parents for their encouragement and support throughout my PhD, and thank you especially to my father, Giles, and to my God-father, Dr John Reeve, for the proof reading of my thesis.

I would finally like to thank the FARNE fund at the Community Foundation for their funding of this project.

List of Figures

List of Tables

Abbreviations

3D	3-Dimensional
ADAMTS	A disintentegrin and metalloprotease with thrombospondin motifs
AEBSF	4-(2-aminoethyl)benzenesulfonyl fluoride
AMC	7-amino-4-methylcoumarin
ANOVA	Analysis of variance
APC	Antigen presenting cells
APMA	4-aminophenylmercuric acetate
APS	Ammonium persulphate
ARIA	Autosomal recessive ichthyosis with hypotrichosis
ATF3	Activating transcription factor 3
BNC	Bovine nasal chondrocyte
Boc	t-butyloxycarbonyl
BSA	Bovine serum albumin
cAMP	Cyclic adenosine monophosphate
cDNA	Complimentary deoxyribonucleic acid
CIA	Collagen-induced arthritis
CS	Chondroitin sulphate
CSRNP1	Cysteine And Serine Rich Nuclear Protein 1
CTD	C-terminal domain
CUB	Cls/Clr, urchin embryonic growth factor and bone morphogenic protein-1 domain
Cys	Cysteine-rich domain
(k)Da	(kilo) Dalton
ddH_2O	Double distilled water (Nanopure)
DESC	Differentially expressed in squamous cell carcinoma
DFP	Di-isopropyl-fluorophosphate
dH_2O	Distilled water
DHT1	Ortho-dihydrotanshinone
DMEM	Dulbecco's modified Eagle’s medium
DMM	Destabilisation of the medial meniscus
DMSO	Dimethyl sulphoxide
DNase	Deoxyribonuclease

dNTP	Deoxyribonucleotide triphosphate
DPP	Dipetidyl peptidase
DTT	Dithiothreitol
ECL	Enhanced chemiluminescent substrate
ECL (*n*)	Extracellular loop (number)
ECM	Extracellular matrix
EDTA	Ethylenedinitrilotetraacetic acid
EGR2	Early Growth Response 2
ELISA	Enzyme-linked immunosorbent assay
ERK	Extracellular signal–regulated kinases
FAP	Fibroblast activation protein
FBS	Foetal bovine serum
FS-6	Fluorescent substrate-6
GAG	Glycosaminoglycan
GAPDH	Glyceraldehyde 3-phosphate dehydrogenase
(E)GFP	(enhanced) green fluorescent protein
GPCR	G-protein coupled receptor
GPI	Glycosylphosphotidylinositol
HA	Hyaluronic acid
HAC	Human articular chondrocyte
HAI-1	Hepatocyte growth factor activator inhibitor-1
HAT	Human airway trypsin-like protease
HBSS	Hank's balanced salt solution
HCl	Hydrochloric acid
HEPES	2-[4-(2-hydroxyethyl)piperazin-1-yl]ethanesulphonic acid
HHBS	HEPES-buffered Hank's balanced salt solution
HI	Heat inactivated
HIV	Human immunodeficiency virus
HMGB1	High mobility group box 1
HPLC	High performance liquid chromatography
Hpx	Haemopexin-like domain
HRP	Horseradish peroxidase
HTRA	High temperature requirement A
Hz	Hertz

IC_{50}	Half maximal inhibitory concentration
ICL (*n*)	Intracellular loop (number)
IGD	Interglobular domain
IL-1	Interleukin-1
IPA	Ingenuity pathway analysis
JNK	c-Jun N-terminal kinases
KS	Keratan sulphate
LB	Lysogeny broth
LCMS	Liquid chromatography/ mass spectrometry
LDLRA	Low-density lipoprotein like receptor class A
LRP-1	Low density lipoprotein receptor-related protein 1
MAC	Membrane-attack complex
MAPK	Mitogen-activated protein kinase
MHC	Major histocompatibility complex
MMLV	Moloney murine leukemia virus
MMP	Matrix metalloprotease
MMTL	Medial meniscotibial ligament disection
mRNA	Messenger ribonucleic acid
MS	Mass spectrometry
MT-MMP	Membrane-type MMPs
NF-κB	Nuclear factor-κB
NOF	Neck of femur fracture
NR4A2	Nuclear receptor subfamily 4, group A, member 2
OA	Osteoarthritis
OSM	Oncostatin-M
(k)Pa	(kilo) Pascal
PAGE	Polyacrylamide gel electrophoresis
PAR	Protease-activated receptor
(D)PBS	(Dulbecco's) phosphate buffered saline
PCM	Pericellular matrix
PCSK9	Proprotein convertase subtilisin/kexin type 9
PDGF	Platelet-derived growth factor
PES	Polyethersulfone
PKA	Protein kinase A

PVDF	Polyvinylidene difluoride
(q)PCR	(quantitative) Polymerase chain reaction
RA	Rheumatoid arthritis
(r) (m) RNA	(ribosomal) (messenger) ribonucleic acid
RT	Reverse transcription
SD	Standard deviation
SDS	Sodium dodecyl sulphate
SEA	Sea urchin sperm protein, enterokinase, agrin domain
SEM	Standard error of the mean
SFM	Serum-free medium
SOC	Super optimal broth with catabolite repression
SOX(*n*)	SRY-Box (number)
TEMED	N,N,N',N'-Tetramethylethylenediamine
TGF-β	Transforming growth factor-β
TIMP	Tissue inhibitor of metalloprotease
TM	Transmembrane
TMPRSS	Transmembrane protease/serine
TNFα	Tumour necrosis factor-α
Tris	2-amino-2-hydroxymethyl-propane-1,3-diol
Triton X-100	Polyethylene glycol p-(1,1,3,3-tetramethylbutyl)-phenyl ether
TTSP	Type II transmembrane serine protease
Tween-20	Polyoxyethylenesorbitan monolaurate
TXNIP	Thioredoxin-interacting protein
uPA	Urokinase-type plasminogen activator
uPAR	Urokinase-type plasminogen activator receptor
v/v	Volume by volume
w/v	Weight by Volume

The Amino Acids

Amino Acid	3 letter code	1 letter code
Alanine	Ala	A
Arginine	Arg	R
Asparagine	Asn	N
Aspartic acid	Asp	D
Cysteine	Cys	C
Glutamic acid	Glu	E
Glutamine	Glu	Q
Glycine	Gly	G
Histidine	His	H
Isoleucine	Ile	I
Leucine	Leu	L
Lysine	Lys	K
Methionine	Met	M
Phenylalanine	Phe	F
Proline	Pro	P
Serine	Ser	S
Threonine	Thr	T
Tryptophan	Trp	W
Tyrosine	Tyr	Y
Valine	Val	V

Chapter 1. Introduction

1.1 Articular Cartilage

1.1.1 Structure and Function

The human body contains numerous cartilaginous tissues, classified as being hyaline, elastic or fibrocartilage from a histological standpoint[2]. The most abundant of these is hyaline cartilage which is found on various surfaces such as in the nose, larynx, trachea and bronchi, as well as on articular joint surfaces where it is known as articular cartilage[3]. The major function of articular cartilage is joint protection[4], by which it provides a low-friction surface over the joints to protect them from the almost constant movement of the average human body. Furthermore, it provides a resistant surface for load-bearing joints such as those in the legs[4].

Articular cartilage is a unique tissue. It contains no vascular, lymphatic or nervous system, and harbours a relatively low number of resident cells known as chondrocytes[2]. These mesenchyme-originating cells produce and maintain a complex extracellular matrix (ECM) responsible for the unique properties of cartilage. The cartilage ECM contains three major components – collagen, aggrecan and hyaluronan – with a multitude of less abundant components. The major protein in all ECMs is fibrillar collagen, and in articular cartilage, this is of a specific type – type II collagen[5]. These collagen fibrils confer strength to the tissue, and are resistant to proteolysis. Following collagen, the most abundant proteins are the proteolgycans, in particular aggrecan[2].

Articular cartilage consists of four distinct zones which differ in cellular morphology and ECM structure (Figure 1.1). The top layer which faces the synovial cavity is known as the superficial zone and accounts for 10-20% of total cartilage thickness[6]. This zone is characterised by a low proteoglycan content, and densely packed collagen fibres parallel to the articular surface[7]. In the middle zone, the proteoglycan content begins to increase and in the deep zone the collagen forms thick fibres perpendicular to the subchondral bone, surrounded by high levels of proteoglycan. This zone is key for the structural role cartilage plays in the joints[7].

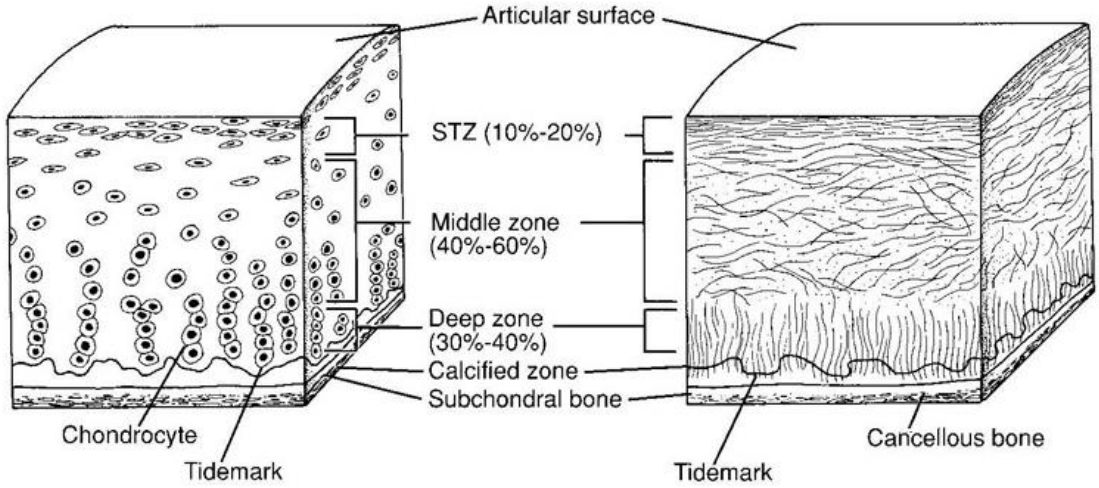

Figure 1.1: The zones of articular cartilage
Cartilage can be divided into 4 major zones: the superficial zone (STZ), the middle (or transitional zone), the deep zone and the calcified zone. Diagram taken from Buckwalter *et al.*, (1994).

1.1.2 Chondrocytes

The cartilage ECM is produced and maintained by the resident chondrocytes. It is thought that there is a slow turnover of cartilage, with the chondrocytes also producing enzymes which are able to break down the cartilage ECM, such as the collagenase Matrix Metalloproteinase (MMP)-13 and the aggrecanase, A Disintegrin And Metalloproteinase with Thrombospondin motifs (ADAMTS)-5[8].

As the cartilage is avascular, chondrocytes are unable to receive their nutrition and oxygen from blood, rather they are sustained by diffusion from the synovium and the majority of their energy requirements are obtained by anaerobic glycolysis[9]. Chondrocytes are immediately surrounded in an ECM which differs in structure to the general cartilage ECM, which is known as the pericellular matrix (PCM). The chondrocyte and its associated PCM are together known as a chondron[7]. The morphology of the chondrocytes and chondrons varies depending on their location in the cartilage (Figure 1.1). Furthest away from the subchondral bone in the superficial layer, the chondrocytes are smaller and flatter "disc-shaped" cells than those deeper within the cartilage. Within the transitional zone, the chondrocytes are rounder and more sparsely populated, before aligning themselves in clustered columns in the deep zone of cartilage[7]. In the calcified zone, the chondrocytes are small hypertrophic cells in uncalcified lacunae anchored within a calcified matrix which acts to attach the cartilage to the subchondral bone[7,10].

Despite having a very complex pathogenesis, one of the key concepts in osteoarthritis (OA) is an excessive level of ECM breakdown by chondrocyte-expressed proteinases, shifting the homeostatic balance away from ECM synthesis[11]. Type II collagen has an extremely long half-life, estimated to be around 117 years[12], meaning that its degradation is essentially an irreversible process, whereas aggrecan can more readily be remodelled[13].

1.1.3 The Extracellular Matrix

1.1.3.1 Collagen

Collagens are a large family of crucially important structural proteins, which compose a third of all protein in the human body. The collagens are defined by their structure, which is composed of three polypeptide chains, forming a right-handed triple helical structure. In order to form this tight helix, every third residue in the amino acid sequence is a glycine, the smallest amino acid. The overall primary structure of collagens is Gly-Xaa-Yaa, where Xaa is commonly a proline residue and Yaa is often a post-translationally modified hydroxyproline residue[14]. These collagen triple helices can then self-assemble together into microfibrils which can form huge macromolecular structures such as collagen fibres. Of particular interest to cartilage biology are the fibrallar collagens, especially the interstitial collagens (types I, II and III) which can form these fibres[15].

Collagen biosynthesis is a complicated process commencing with translation of collagen genes into proto-collagen strands. Type I collagen consists of two gene products, alpha 1 and alpha 2 chains (*COL1A1* or *A2*), whereas type II collagen consists of a single gene product, alpha 1 chain (*COL2A1*). Type I collagen forms helices with two alpha 1 chains and a single alpha 2 chain, whereas type II collagen forms trimers of alpha 1 chains[14].

1.1.3.2 Proteoglycans

Proteoglycans, as their name suggests, are heavily glycosylated proteins which usually consist of a core protein where the glycosylation occurs in the form of glycosaminoglycan (GAG) side chains[5]. The major proteoglycan in cartilage is aggrecan.

Aggrecan consists of three globular domains (G1, G2 and G3) separated by a long core region of around 230 kDa, glycosylated with the GAGs chondroitin sulphate (CS) and keratan sulphate (KS). The GAG side chains are separated in to KS- and CS-rich regions.

G1 and G2 are N-terminal to the long core region, and are separated from each other by a short region known as the interglobular domain (IGD) (Figure 1.2)[5].

The GAG side chains carry a negative charge which attracts positively charged water molecules, saturating the tissue and rendering it resistant to compressive forces[5]. Furthermore, aggrecan also undergoes various interactions with other matrix components, forming large aggregates. An important non-covalent interaction occurs between G1 of aggrecan and hyaluronic acid (HA), a large non-sulphated GAG, which can bind up to one hundred individual aggrecan molecules[2].

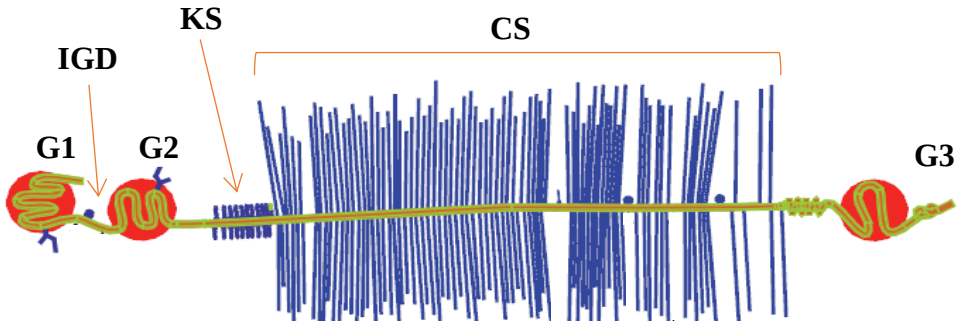

Figure 1.2: Structure of aggrecan
Aggrecan consists of three globular domains: G1, G2 at the N-terminus and G3 at the C-terminus, separated by a core region, heavily glycosylated by GAGs. KS Keratan sulphate-rich region, CS Chondroitin sulphate-rich region. IGD Interglobular domain. Diagram adapted from a figure in Heinegard (2009).

1.1.4 Mechanical Loading of Cartilage

In performing their physiological roles within joints, many articular surfaces are subjected to great loads on a near constant basis. The structure of cartilage allows for this loading, and it is known that experiencing "normal loading" is important in the maintenance of joint homeostasis. Indeed, physiological loads on cartilage and chondrocytes stimulate the cells to express anabolic mediators and effectors such as aggrecan and type II collagen[16,17].

Physiological loading as a result of moderate physical exercise has been suggested to be protective against OA development in humans[18], whereas moderate exercise may have positive effects on established OA[19].

Conversely, the non-physiological loading of cartilage (either excessive loading, or lack of physiological loading) has detrimental effects on cartilage health. Excess loading of cartilage in explant culture can lead to chondrocyte apoptosis[20] and the stimulation of multiple pro-inflammatory pathways leading to the expression of proteins such as MMPs which can lead to cartilage destruction[21,22] (Figure 1.3).

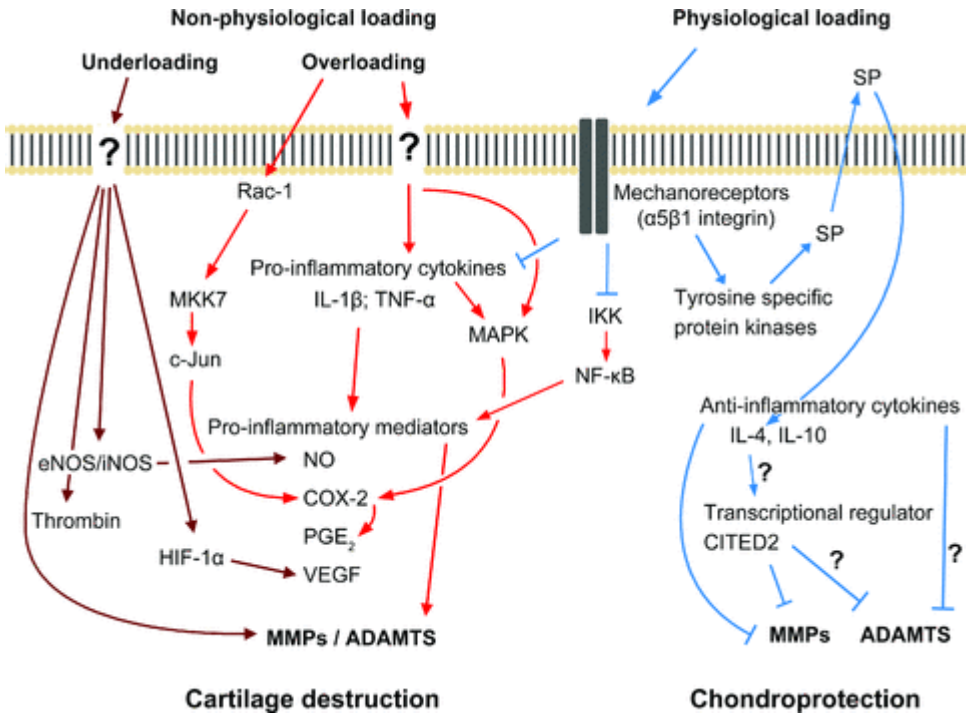

Figure 1.3: Signalling pathways mediated by mechanical loading of cartilage
Chondrocytes are responsive to both physiological and non-physiological loading, and multiple pathways have been identified as mechanosensitive. Diagram taken from Sun (2010).

1.2 Arthritis

"Arthritis" encompasses a huge range of diseases involving one or multiple joints with some level of inflammation. Indeed, the word arthritis comes from the greek "arthro-" meaning joint and "-itis" meaning inflammation. The most common forms of arthritis are osteoarthritis and rheumatoid arthritis (RA), however these also encompass many distinct sub-forms with differing aetiology and progression.

1.2.1 Rheumatoid Arthritis

Rheumatoid arthritis is an autoimmune disease of synovial joints characterised by a strong inflammatory response. The causes of RA are incompletely understood, with links to both genetic and environmental factors[23]. Despite the lack of an initial trigger being identified, it is likely that RA results from the recognition of an auto-antigen. During subsequent disease progression, a variety of immune cells such as T cells, B cells, macrophages, neutrophils and mast cells infiltrate the synovial space, and with the resulting release of a multitude of pro-inflammatory mediators, joint and bone is degraded, and the synovial membrane proliferates forming a pannus[23].

1.2.2 Osteoarthritis

Osteoarthritis is a common disease in the aged population, with some symptoms of the disease prevalent in the majority of people over 65 years of age[24]. OA is a disease best characterised by the degradation of articular cartilage, although the disease is considered a disease of the whole joint[25]. The joints most often affected by OA include joints of the hands, knees, hips and spine, with the major symptoms including pain, mild inflammation, stiffness and general loss of mobility[24].

There is some evidence that aggrecan cleavage is involved in the initiation of cartilage degradation in OA, as aggrecan is able to protect the type II collagen[26]. Pratta *et al*. (2003)[26], provide evidence that the selective inhibition of ADAMTS-4 and -5 (the aggrecanases) appears to offer protection against MMP-mediated collagen degradation in bovine explant cultures. In order to control for non-specific inhibition of MMPs by these aggrecanase inhibitors, the inhibitors were also added to the explant culture following aggrecan cleavage (but before collagen cleavage), and here they offered no protection, whereas MMP inhibition following aggrecan loss does offer collagen protection. The authors hypothesised that aggrecan offers the collagen physical protection from proteolytic attack via steric hindrance. Type II collagen is thought to bind to the KS-rich region of aggrecan[27] which would place the larger CS-rich region into close proximity of the collagen fibrils, thus protecting the collagen.

Conversely, there is opposing evidence which suggests that the cleavage of collagen is the initiating factor in cartilage degradation, with aggrecan loss being secondary to this. This idea was first suggested in the 1970s when it was noted that the breaking of the

collagen network results in localised swelling of the cartilage, as a result of the collagen no longer being able to partially "resist" the hydrophilic nature of the aggrecan[28]. Even though there is an eventual aggrecan loss in OA, and thus a loss of water, early disease phases are associated with an increase in hydration and swelling[29]. Furthermore, aggrecan loss has been shown to occur in areas where type II collagen fibrils are damaged[30,31]. Despite it not being definitively proven whether collagen or aggrecan cleavage are involved in the initiation of cartilage degradation, it is clear that a close interplay between these two key events is vital for disease initiation.

Aggrecan is able to undergo multiple cleavages (Figure 1.4), however the most important pathological cleavages are thought to occur within the IGD as these cleavages result in rapid loss of the whole GAG attachment region and thus is derogatory to the whole structure of the cartilage[32]. The IGD is able to be cleaved by various MMPs, including MMP-3[33], -2, -9[34], -1, -8[35], and -13[36] at asparagine-341 / phenylalanine-342. However, a key study in 1992 showed that these were unlikely to be the most pathologically relevant in OA. Sandy *et al*.[37] found that the synovial fluid collected from OA patients contained aggrecan fragments cleaved at the glutamic acid-373 / alanine-274. Subsequent studies confirmed that this cleavage was not undertaken by MMPs[38], and enzymes known as the aggrecanases (ADAMTS-4 and -5) were subsequently identified[39,40].

Mice studies using ADAMTS-4 and -5 null mice showed that the loss of ADAMTS-5 (but not ADAMTS-4) protected against OA, suggesting that ADAMTS-5 is the key aggrecanase in mice[41,42]. The situation in humans is more complex however, with evidence suggesting that ADAMTS-4 is also involved aggrecan degradation[43,44].

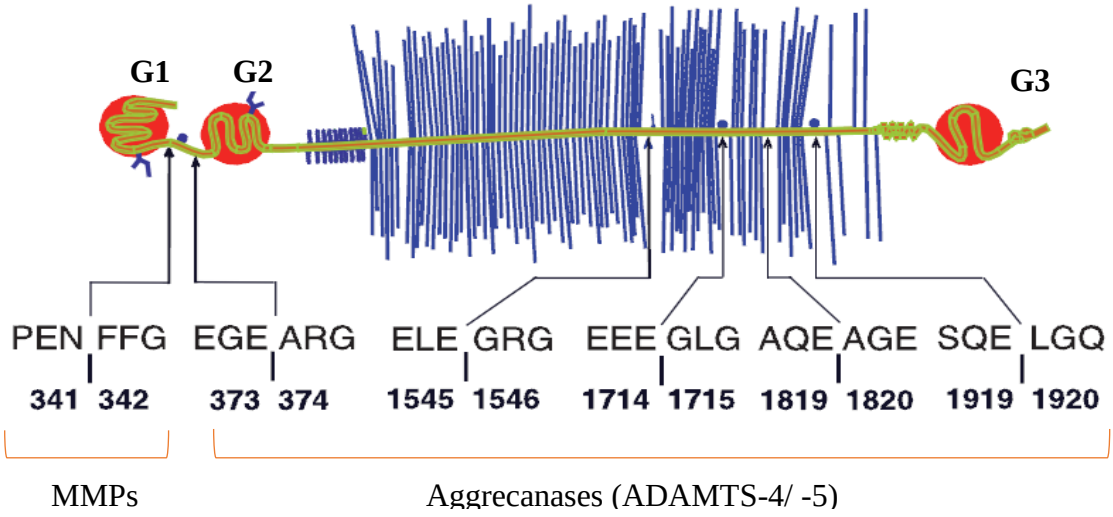

Figure 1.4: Aggrecan and its cleavage sites
Multiple cleavage sites have been identified on aggrecan mediated by both the MMPs and the aggrecanases (ADAMTS-4 and -5). Diagram adapted from a figure in Heinegard (2009).

1.3 Introduction to Proteases

Proteases are a class of enzymes which have the ability to catalyse the hydrolysis of a peptide bond. There are five classes of proteases, categorised based on their mechanism of catalytic action: serine proteases, metalloproteases, cysteine proteases, threonine proteases, and aspartic proteases. The total spectrum of proteases encoded by humans is known as the degradome.

There are currently 588 proteases identified within the human degradome: 192 metalloproteases, 184 serine proteases, 164 cysteine proteases, 27 threonine proteases and 21 aspartic proteases[45].

A nomenclature for naming substrate amino acid and protease enzymatic subsites was described in 1967 by Schechter and Berger[46], where the amino terminal side of the cleavage site (the scissile bond) is known as the non-prime side and the carboxy terminal side is known as the prime side. The amino acids of the substrate are subsequently numbered P4-P4', and the corresponding sites on the protease are numbered S4-S4' (Figure 1.5) which allows for description and comparison of enzyme specificities.

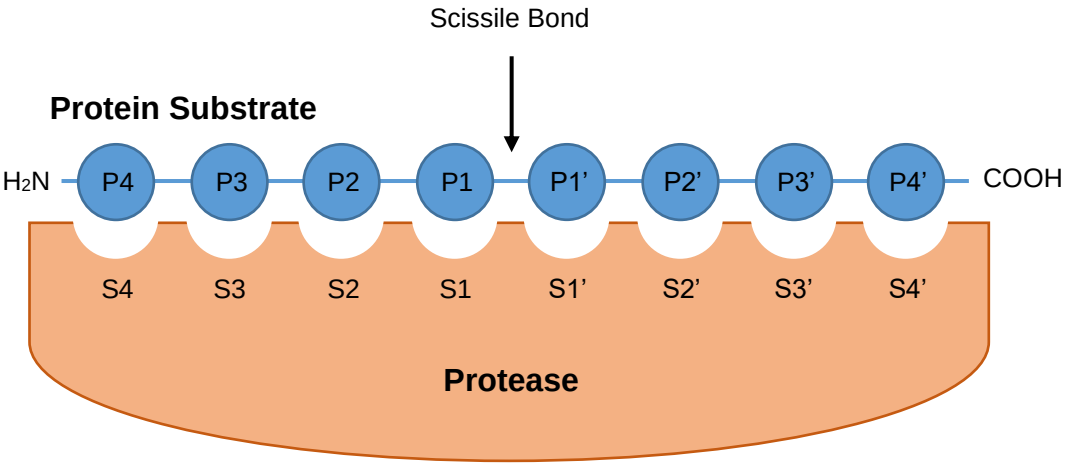

Figure 1.5: Schechter and Berger nomenclature for protease cleavage
The Schechter and Berger nomenclature describes the amino acids of the substrate as P4-P1 towards the amino terminus of the cleavage site, and P1' to P4' towards the carboxy terminus. These correspond to the subsites S4-S4' on the protease.

1.4 Metalloproteinases

1.4.1 Catalytic mechanism

Much understanding of the metalloproteinase catalytic mechanism is based on studies of thermolysin[47]. Metalloproteinases are thought to employ a single-step catalytic mechanism utilising a metal ion, often zinc (as is the case with all metzincins, such as the MMPs), co-ordinated by two or three histidine residues. Metalloproteinases further require a free water molecule to co-ordinate with the metal ion which is hydrogen bonded to a glutamate residue. The catalytic mechanism is thought to entail the binding of the substrate into the active site which displaces the hydrogens of the water molecule towards the glutamate residue whereas the oxygen remains associated with the zinc ions. The zinc ion also associates with the carbonyl oxygen of the substrate, forming the ES complex. The polarising activity of the zinc by the glutamate allows the oxygen of the active site water to perform nucleophilic attack on the carbonyl carbon of the scissile bond (Figure 1.6)[47,48].

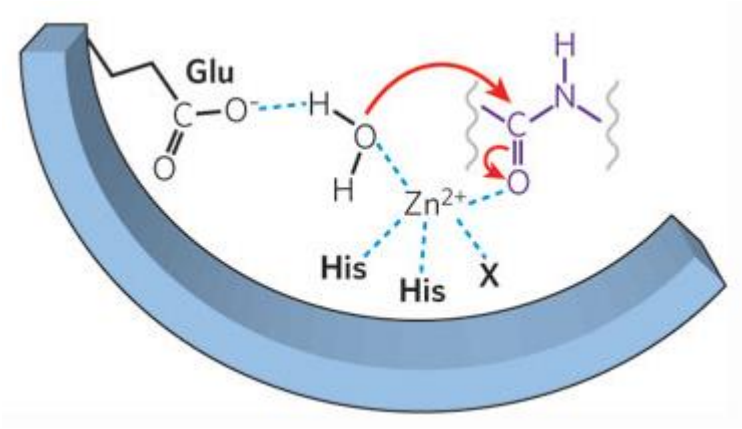

Figure 1.6: Metalloproteinase catalytic mechanism
Metalloproteinases require a co-ordinated metal ion (usually zinc) which is bound to two or three histidine residues as well as a water molecule. The water forms a hydrogen bond with a glutamate, which allows the water molecule to act as a nucleophile, able to attack the scissile bond of the substrate at the carbonyl carbon. Diagram taken from Erez *et al.*, (2009).

1.4.2 The Metzincins

The metzincins represent a superfamily of zinc-dependent metalloproteinases including the matrixins (MMPs), the astacins, the adamalysins and serralysin[49]. This superfamily shares certain features, most importantly the conserved zinc-binding motif (HEXXHXXGXXH, where the three conserved histidine residues bind the zinc ion) and a conserved methionine residue[49] located 6-53 amino acids after the zinc-binding motif, known as the "met-turn", a tight 1,4-β-turn which is thought to be key to the structural integrity of the metzincin active sites[50]. These two key features are indispensable to the metzincins; indeed, they lend their name to the superfamily[49]. Common to the metzincins is the presence of multiple non-catalytic domains[51]. Of the metzincins, the MMPs and the adamlysins play key roles in the remodelling of ECM components.

1.4.3 The Matrix Metalloproteinases

The first MMP was identified by Gross & Lapiere in 1962[52] as a collagenolytic activity in tadpole tails during metamorphosis. Subsequently, multiple family members have been identified and subdivided into one of six groups according to substrate preference or domain structure. These are the classical collagenases (MMP-1, -8 and -13); the gelatinases (MMP-2 and -9); the stromelysins (MMP-3, -10 and -11); the matrilysins (MMP-7 and -26); the membrane-type MMPs (MT-MMPs); and ungrouped MMPs (such as MMP-12 and -19)[53]. Despite these groupings of the MMPs, it is important to note that they all have multiple substrates. For example, MMP-1 cleaves not only collagen, but

other substrates such as protease activated receptor 1 (PAR1)[54]. Conversely, despite being classified as gelatinases, MMP-2[55] and MMP-9[56] further have the ability to cleave some collagens.

1.4.3.1 MMP Structure and activation

The MMPs share a domain structure consisting of an N-terminal pro-domain, a catalytic domain, a hinge region and (with the exception of MMP-7, -23 and -26) a C-terminal haemopexin-like (Hpx) domain (Figure 1.7), although some family members have variations on this structure, for example, the "membrane type" MT-MMPs. These either contain a transmembrane domain or glycosylphophatidylinositol (GPI)-anchor to the C-terminus of the Hpx domain[53].

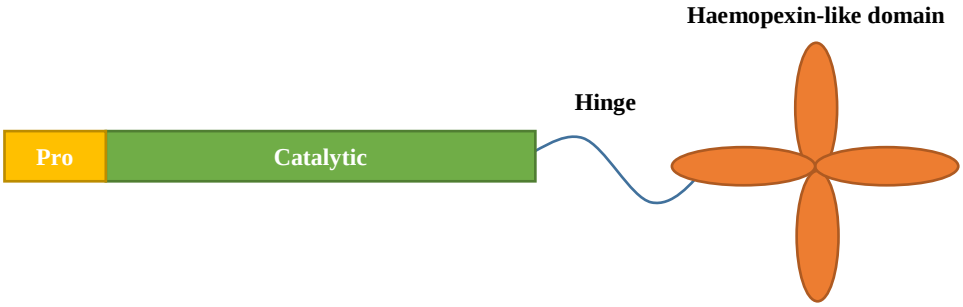

Figure 1.7: The basic structure of MMPs
The majority of MMPs share this basic domain structure, including the collagenases (MMP-1, -8 and -13), the gelatinases (MMP-2 and -9) and the stromelysins (MMP-3, 10 and 11) although other family members contain additional features. For example, several "membrane-type" MMPs (MMP-14, -15, 16, and -17) have an additional membrane binding domain, C-terminal to the Hpx domain, whereas the matrilysins MMP-7, -23 and -26 lack the haemopexin-like domain.

The role of the pro-domain is to keep the MMPs in their inactive, latent pro-forms. This is achieved via a mechanism called the "cysteine switch" whereby a conserved cysteine residue in the cysteine switch motif (PRCGXPD) ligates to the zinc in the MMP active site, preventing catalytic activity[57]. The majority of secreted MMPs are secreted in their pro-form and are activated by a mechanism known as "stepwise activation" where a proteinase-susceptible "bait" region in the pro-domain is cleaved by various proteinases[58]. At this stage, the pro-domain is only partially removed and the pro-MMP is only partially active. In order to fully activate the pro-MMP, the activity of other active MMPs is required, or the pro-MMP may undergo auto-catalysis[58].

Various MMPs contain a furin-like enzyme recognition sequence (RX-(K/R)-R), such as MMP-11 and the MT-MMPs[53]. These enzymes are able to be activated intracellularly by furin-like enzymes and secreted[59] or membrane bound[60] in an active form.

The activation of proMMPs is of great biological significance and is considered a key limiting step in MMP activity[61]. Indeed, the inhibition of proMMP activation could hold therapeutic relevance[62], which could be of particular importance as the therapeutic targeting of MMPs has to date been unsuccessful[63].

The Hpx domains of MMPs are thought to have a key role in ligand recognition of MMPs. For an excellent review on Hpx domains, the reader is directed to Piccard *et al*. (2007)[64].

1.4.3.2 The Collagenases

There are three "classical" collagenases: MMP-1, MMP-8 and MMP-13, with other MMPs also having identified collagenolytic activity such as MMP-14. The collagenases are defined by their ability to cleave fibrillar collagen and are all expressed in synovial joints[65].

The Hpx domains of the collagenases are indispensable for collagenolytic activity. MMP-1, -8 and -13 are all relatively unstable and are thought to undergo autoproteolytic events, separating the Hpx domain from the catalytic domain. MMP-1 and MMP-8 are hydrolysed in the hinge region, with MMP-1 being hydrolysed at the proline-250 / isoleucine-251 peptide bond[66] and MMP-8 is hydrolysed at the glycine-242 / leucine-243 or proline-247 / isoleucine-248 peptide bonds[67]. The auto-catalysis of MMP-13 does not occur in the hinge region, rather the cleavage site is at the C-terminus of the catalytic domain, at the serine-245 / leucine-246 peptide bond[68]. Following these auto-cleavage events, the ability of the MMPs to cleave collagen is lost, however their ability to cleave other non-collagen substrates remains. This led to the development of various studies using MMP-Hpx chimeras to explore the role of the Hpx domains in collagen recognition.

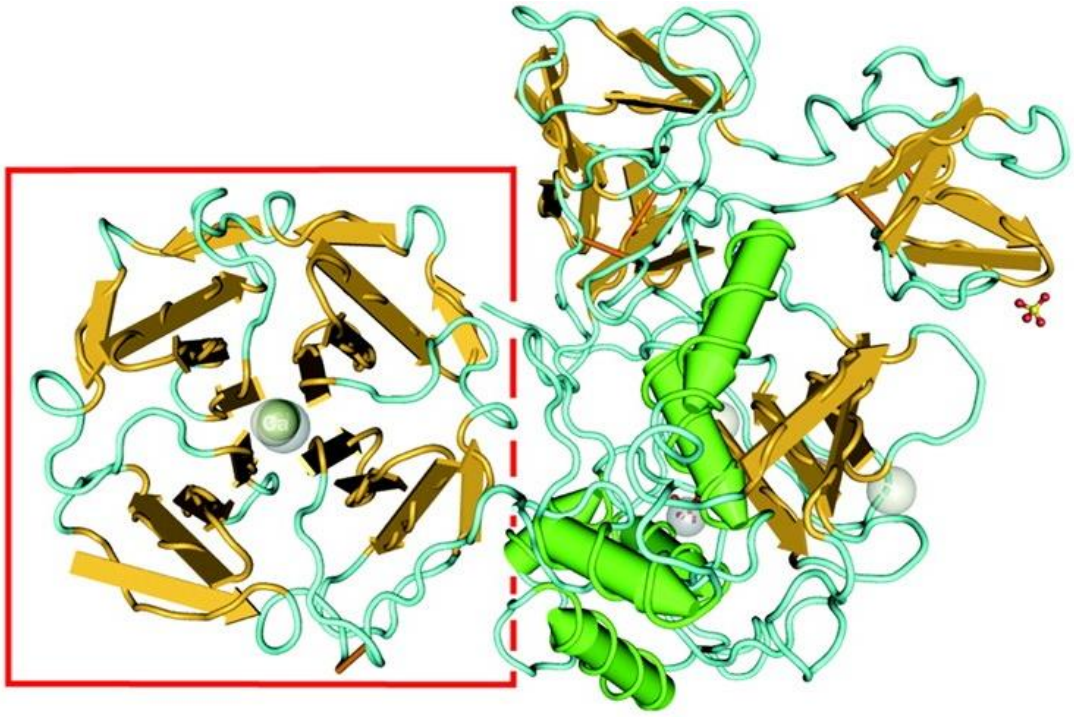

Figure 1.8: Structure of MMP-2
Crystal structure of MMP-2, with the Hpx domain boxed in red. The Hpx domain is formed by a four-bladed propeller structure with a co-ordinated calcium ion in the centre. Image adapted from a figure in Piccard *et al.* (2007).

MMP Hpx domains consist of around 210 amino acids, which form a four-blade propeller structure, with each blade consisting of four anti-parallel β-sheets[64] (Figure 1.8). The first and fourth blades are connected together via a disulphide bond[64]. When the catalytic domain from MMP-1 is ligated to the Hpx domain from MMP-3 (an MMP with no collagenolytic ability), its ability to cleave collagen is lost, confirming a vital role for the Hpx of MMP-1 in collagenolytic activity[69]. This study further created a chimera containing the catalytic domain of MMP-3 and the Hpx domain of MMP-1, and this was not sufficient to give MMP-3 collagenolytic activity, suggesting interplay of both the catalytic and Hpx domain of MMP-1 is required for binding to and cleaving collagen. Another study replaced blades two to four of the propeller in the MMP-8 Hpx domain for the corresponding blades in the MMP-3 Hpx domain, and this chimera showed 16.1% of the collagenolytic activity of MMP-8[70].

MMP-1 was the first MMP to be associated with pathological conditions when "collagenase" was detected in the synovium of patients with RA[71]. MMP-1 preferentially cleaves type III collagen, followed by type I and has its weakest activity on type II[72,73]. MMP-8 was originally purified from human neutrophils (and is thus often referred to as neutrophil collagenase), and has a similar cleavage profile to MMP-1, preferring to cleave

type I collagen over type II collagen, however unlike MMP-1, MMP-8 has a much lower activity on type III collagen. Indeed, the catalytic efficiencies for MMP-8 on all 3 fibrillar collagens are lower than those of MMP-1[73]. Furthermore, much lower levels of MMP-8 are expressed within articular cartilage[74], though higher expression levels are observed in OA[75]. Overall, MMP-8 is not considered to be a major contributor to cartilage degradation in arthritic conditions.

MMP-13 is thought to be the most important pathological collagenase in OA[76]. Even though cartilage is thought to express lower levels of MMP-13 compared to MMP-1[77], it has a much higher activity against type II collagen which is its preferred substrate, followed by type I and type III collagen[78]. The Hpx domain from MMP-13 has been shown to interact with a whole host of other cartilage ECM components, such as fibronectin, type VI collagen, decorin, syndecan 4 and serglycin[79], potentially highlighting a further role for this enzyme in the regulation of cartilage.

Despite neither MMP-1 nor MMP-13 being completely specific for either OA or RA[77], it is generally considered that MMP-1 is more important in RA whereas MMP-13 is more important in OA[61].

1.4.3.3 The Gelatinases

The gelatinase sub-family of MMPs consists of two members: MMP-2 and MMP-9 or gelatinase A and B, respectively. Despite being named for their ability to cleave gelatin, the mix of proteins and peptides generated from partial collagen hydrolysis, the gelatinases are able to cleave a much larger range of ECM components and have some roles identified in arthritic diseases[80].

Both MMP-2[55] and MMP-9[56] have been shown to also exhibit collagenolytic activity, with the ability to cleave type I collagen and both enzymes have had roles implicated in OA. The expression of both gelatinases is elevated in OA cartilage compared to normal adult human cartilage, with MMP-9 being expressed at a much lower level than MMP-2[81-83]. It is thought that in OA, gelatinase activity is higher in the subchondral bone, rather than in the cartilage[84], with a role in OA-associated bone changes speculated for them[80].

1.4.3.4 The Stromelysins

The stromelysin sub-family of MMPs consist of three members: MMP-3 (stromelysin-1), MMP-10 (stromelysin-2) and MMP-11 (stromelysin-3). None of the stromelysins are able to cleave fibrillar collagen, however are able to cleave several other cartilage components such as aggrecan[85].

MMP-3 and MMP-10 share 82% sequence homology with one another and have similar substrate specificities[86], however MMP-3 has much higher expression levels in cartilage[87]. Both of these enzymes are able to activate several proMMPs, including proMMP-1, -8 and -13[53,88,89], thus are able to initiate collagen degradation by activating the collagenases. Indeed MMP-3 is suspected to have an important role in cartilage turnover in both health and disease and elevated levels have been observed in synovial tissues of OA patients[90].

Despite being expressed at lower levels than MMP-3, MMP-10 expression can be induced by pro-inflammatory stimulation and subsequently induce collagen degradation by pro-collagenase activation[88].

1.4.3.5 The membrane-type MMPs

The cell anchored membrane-type MMPs (MT-MMP) sub-family of MMPs consists of six members of which four are transmembrane proteins: MT1-MMP, MT2-MMP, MT3-MMP and MT5-MMP, whilst two are glycosylphosphatidylinositol (GPI)-anchored: MT4-MMP and MT6-MMP[91]. These six MMPs may also be referred to as MMP-14, -15, -16, -24 -17 and -25, respectively. Whilst most soluble MMPs are secreted in an inactive pro-form, the MT-MMPs are activated intracellularly, and secreted to the cell surface in an active form. This activation is performed by furin-like proprotein convertases[91].

1.4.3.6 The Tissue Inhibitors of Metalloproteinases (TIMPs)

TIMPs are a family of endogenous metalloprotease inhibitors consisting of four members: TIMP-1, -2, -3 and -4, which are all 184-194 amino acids in length and consist of two key domains. The N-terminal domain is responsible for the inhibitory activity, and does so by folding into a “wedge-like” structure that is able to interact with the MMP active site[53]. TIMPs bind and inhibit MMPs in 1:1 stoichiometry[53], thus can be used experimentally to active-site titrate recombinant MMP. All four TIMPs can inhibit all MMPs, with the

exception of TIMP-1 which has negligible levels of inhibition against MT1-MMP (MMP-14)[92].

1.4.4 The Adamalysins

The adamalysin subfamily of the metzincins include the ADAM (A disintegrin and metalloproteinase) and the ADAMTS proteinases.

1.4.4.1 The ADAM family

The ADAMs are transmembrane and secreted proteinases with multiple roles including cellular adhesion and the proteolytic processing and shedding of various membrane-bound proteins, such as receptors and signalling molecules[93]. Despite not being key players in articular cartilage degradation, some ADAM members have been suggested to have roles in OA. For example, ADAM-8 has been identified in human OA cartilage as being able to cleave fibronectin, generating fragments that may then enhance collagenase and aggrecanase expression[94]. Furthermore, the serum levels of ADAM-12 appear increased in patients with knee OA[95] and *ADAM15* mRNA has been shown to be up-regulated in human OA cartilage compared to normal cartilage[96] whereas *ADAM15*$^{-/-}$ mice exhibit accelerated development of OA lesions[97].

Figure 1.9: The basic structure of ADAM proteinases
The ADAM proteinases are integral membrane proteins, containing a transmembrane domain (TM) at their C-terminus. Furthermore, the majority of ADAMs contain an epidermal growth factor-like (EGF) domain (ADAM-10 and -17 lack this). They also contain a cysteine rich domain (Cys) and a disintegrin-like domain (Dis).

The ADAM proteinases have a relatively complex domain structure, consisting of an N-terminal pro-domain, followed by its metalloproteinase catalytic domain, a disintegrin-like domain, a cysteine-rich domain and (apart from ADAM-10 and -17) and an epidermal growth factor (EGF)-like domain. They are transmembrane proteins, with a C-terminal transmembrane domain and a cytoplasmic tail which varies in length across the family members[98] (Figure 1.9). As with the MMPs, the pro-domain maintains the enzyme in a latent form via a cysteine switch mechanism[99], and activate intracellularly via the activity

of furin-like enzymes, similarly to some MMPs, ADAM pro-domains contain a RX-(K/R)-R motif[100].

To date, 21 human *ADAM* genes have been identified, of which only 13 have a catalytically active metalloproteinase catalytic domain, containing the classical HEXXHXXGXXH active site motif[93]. This suggests that the remaining 8 family members have evolved functions dependent on their non-catalytic domains.

1.4.4.2 The ADAMTS family

The ADAMTS family of proteinases are closely related to the ADAM proteinases, with two major differences. While the ADAMs are generally membrane-bound proteins, the ADAMTSs are secreted. Furthermore, the ADAMTSs have a thrombospondin type I repeat in between their disintegrin-like domain and cysteine-rich domain[101]. Following the cysteine-rich domain, ADAMTSs have a spacer region followed by a highly variable C-terminus (Figure 1.10).

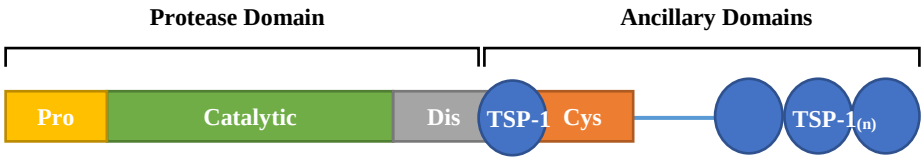

Figure 1.10: The basic structure of ADAMTS proteinases
The ADAMTS proteinases share an N-terminal protease domain consisting of a pro domain, a metalloproteinase catalytic domain and a disintegrin-like domain (Dis). The ADAMTS family also all contain a C-terminal ancillary domain, though these vary in content. They all commence with a single central thrombospondin type I motif (TSP-1) followed by a cysteine-rich domain (Cys) and a spacer region. Following this spacer, the family exhibits variation with either a few or several TSP-1 motifs and other domains such as CUB domains (ADAMTS13), mucin-like domains (ADAMTS7 and 12) and *gon-1*-like motifs (ADAMTS9 and 20)

Nineteen members of the ADAMTS family have been identified to date, with the ability to cleave a wide range of substrates[101]. As with the other metzincins, the ADAMTSs have a pro-domain with a vital role in enzyme latency, however it is thought that these pro-domains operate via a different mechanism as 13 members of the family lack a cysteine which would form the cysteine switch mechanism[101]. Like the ADAMs, the ADAMTSs are thought to be activated by furin-like enzymes[102].

ADAMTS-4 has the shortest ancillary domain out of the ADAMTS family, terminating following the spacer region, and containing no C-terminal thrombospondin type I

motifs[101]. However, ADAMTS-4 has been suggested to interact via its ancillary domain to the cell surface protein, syndecan 1, in a chondrocytic cell line[103] with the interaction requiring the central thrombospondin type I motif and the cysteine-rich domain. The ancillary domain is thought to undergo proteolytic processing which can alter aggrecanase specificity and activity, including a reduction in binding to GAGs and thus reduction in aggrecanolysis[104]. ADAMTS-5 has also been found to localise to the cell surface, and has been shown to interact with both GAGs[105] and hyaluronan[106], localising the enzyme to the chondrocytes with potential implications for OA.

1.5 Serine proteinases

1.5.1 Classification

The human genome encodes a predicted 184 serine proteinases, which have a wide variety of functions in human biology, and they are generally considered as extracellular proteases[45,107]. Whilst the majority of serine proteinases are soluble secreted proteins, some serine proteinases are found membrane-bound, either by a C-terminal GPI-anchor, a C-terminal transmembrane domain (type I transmembrane serine proteinases) or an N-terminal transmembrane domain (type II transmembrane serine proteinases, or TTSPs)[108].

Of particular interest to the current programme of research, matriptase is one of 17 identified human TTSPs, a family of enzymes characterised by a C-terminal catalytic domain separated from the membrane by a highly variable non-catalytic "stem region"[107]. TTSPs may be categorised into one of four subfamilies based on this variable stem region: the HAT/DESC (human airway trypsin-like protease/ differentially expressed in squamous cell carcinoma) subfamily, the hepsin/TMPRSS (transmembrane protease/serine) subfamily, the matriptase subfamily and the corin subfamily[107].

1.5.2 Catalytic mechanism

Common to the serine proteinases is the "catalytic triad", the presence of three amino acid residues: aspartic acid, histidine and serine, in the catalytic domain which are responsible for catalysis of substrate[109]. Chymotrypsin is considered the archetypal serine protease on which much of our understanding of catalysis is derived. Indeed, chymotrypsin numbering (histidine-57, aspartic acid-102, and serine-195) is used in all serine proteases,

despite these three amino acids not always being at these exact positions. Serine proteases employ a two-step mechanism of catalysis whereby the protease initially binds to the substrate in a covalent manner, forming an acyl-enzyme intermediate. This intermediate subsequently breaks down in the second step into two products and the protease is restored.

The substrate enters the active site and is initially held in position by non-covalent interactions. The hydroxyl group of serine-195 and the imidazole group of histidine-57 are hydrogen bonded together, which allows the serine hydroxyl group to perform nucleophilic attack on the carbonyl carbon in the substrate. This forms the acyl-enzyme intermediate where serine-195 is covalently bound to the carbonyl carbon of the former peptide bond, allowing C-terminal peptide fragment to dissociate away from the protease active site. A water molecule is then able to enter the active site and forms a hydrogen bond with histidine-57. This allows the water to perform nucleophilic attack on the carbonyl carbon within the acyl-enzyme intermediate. Serine-195 and histidine-57 re-form a hydrogen bond to restore the protease, and the second product is removed[110] (Figure 1.11).

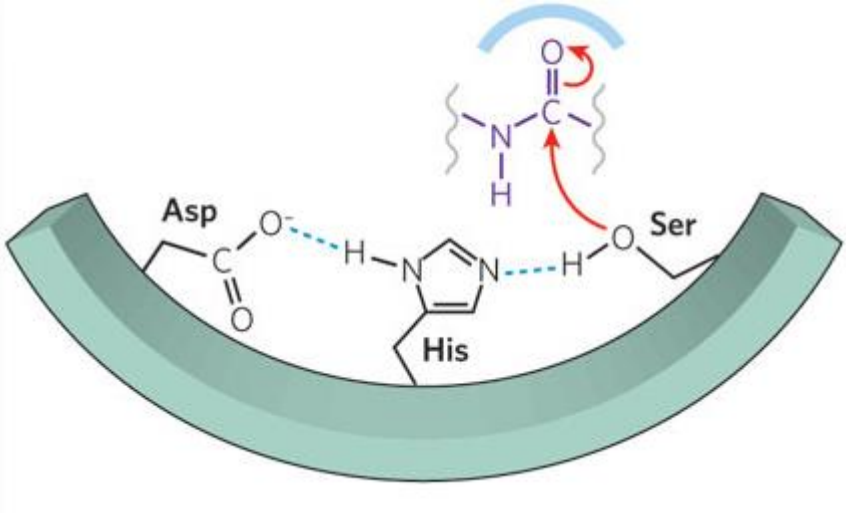

Figure 1.11: Serine protease catalytic mechanism
The catalytic triad of serine proteases consists of a histidine, a serine and an aspartic acid. The histidine is stabilised by the aspartic acid by forming a hydrogen bond with it, and deprotonates the serine, producing a strong nucleophile able to attack the substrate carbonyl carbon. Diagram taken from Erez *et al.*, (2009).

1.5.3 Matriptase

1.5.3.1 Structure and Function

Matriptase contains a single sea urchin sperm protein, enteropeptidase, agrin (SEA) domain, two Cls/Clr, urchin embryonic growth factor and bone morphogenic protein-1 (CUB) domains, and four low density lipoprotein receptor class A (LDLRA) domains (Figure 1.12).

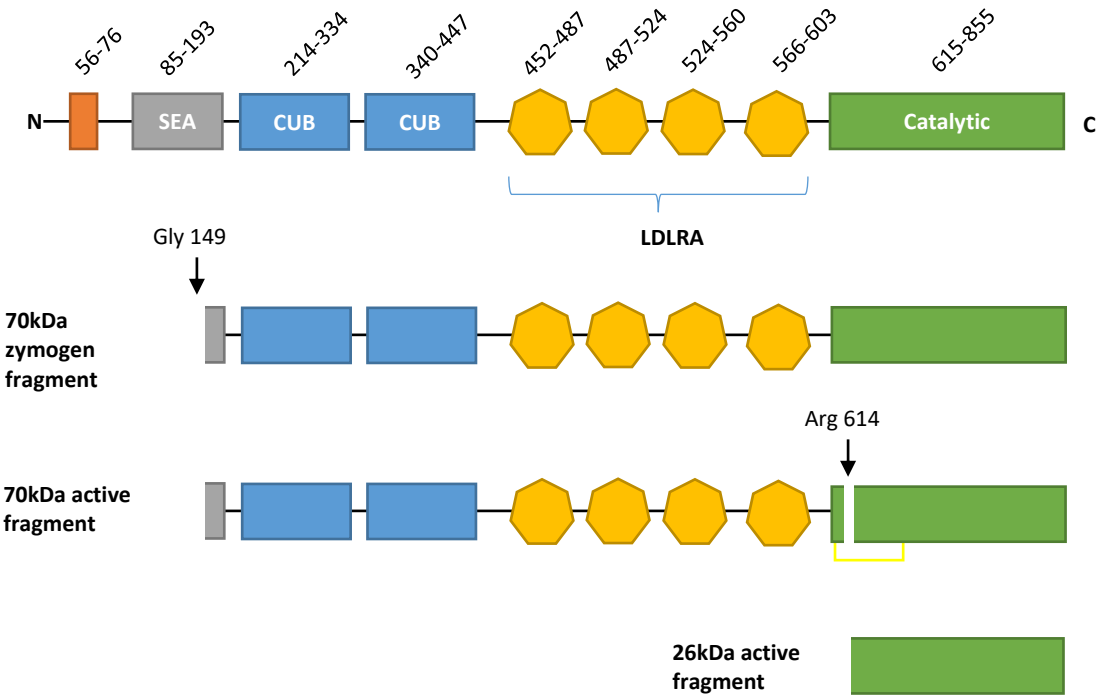

Figure 1.12: The domain structure of matriptase
Matriptase is a type II transmembrane serine proteinase consisting of an N-terminal transmembrane domain (orange), a C-terminal serine proteinase catalytic domain, as well as multiple non-catalytic domains in a stem region, including a SEA domain, two CUB domains and four LDLRA domains. Multiple processed forms of matriptase may be observed depending on progress through the maturation process. Full length matriptase is 95kDa, and undergoes early N-terminal processing to a 70kDa form, however it is thought these remain bound together. Matriptase undergoes activation from the zymogen by cleavage at Arg 614, resulting in a two chain disulphide linked form. When run by reducing SDS-PAGE, a 26kDa band is observed for the active catalytic domain.

Matriptase is best characterised as a proteinase expressed in epithelial tissues[108]. Matriptase null mice die shortly following birth as a result of dehydration from compromised skin integrity[111]. These mice exhibit an inability to process profilaggrin, a protein important in the arrangement of keratin filaments in the skin[112]. In humans, an important role in skin has been confirmed in patients with mutations in matriptase, such as G827R[113], which results in autosomal recessive ichthyosis with hypotrichosis (ARIA).

Matriptase has also been found to be overexpressed in a number of carcinomas (cancers derived from epithelial tissues), and correlations with negative prognostic outcomes have been identified[114].

A role for matriptase in OA was identified by Milner *et al*. (2010)[1] where it was found to be more highly expressed in OA patient samples compared to control NOF (neck of femur fracture) samples. The addition of matriptase to bovine explant cultures in the presence of pro-inflammatory stimulation resulted in enhanced levels of observed collagenolysis. Furthermore, the addition of matriptase to OA cartilage explant cultures resulted in an increase in the level of metalloproteinase-dependent collagenolysis, as well as an increase in the gene expression of MMP-1 and MMP-13, likely through the activation of the PAR2 receptor[1], a known substrate for matriptase[115], and will be further described in chapter 1.7.

1.5.3.2 Activation

The non-catalytic domains of matriptase are known to have several roles in the maturation and inhibition of matriptase, however it is likely they have further unidentified roles in matriptase activity. The successful maturation of matriptase is a complex and incompletely understood process, which is known to involve two sequential proteolytic cleavages as well as interactions with its cognate inhibitor, hepatocyte growth factor activator inhibitor (HAI)-1[108].

Matriptase is synthesised as a single chain 95kDa zymogen and enters the secretory pathway where it undergoes its first proteolytic cleavage, which occurs in the SEA domain after glycine 149 at a conserved GSVIA sequence, yielding a 70kDa zymogen form, although it is thought that the enzyme remains bound together[116]. It is unknown how this cleavage event occurs[117]. The second proteolytic cleavage event occurs after arginine 614, and is dependent on the first cleavage having occurred[118]. This is the cleavage which yields an active two-chain protease, and likely occurs as a result of a transactivation process on the cell surface as catalytic inactive mutants are unable to undergo this processing[118]. Furthermore, the zymogen form of rat matriptase has been shown to be able to cleave a synthetic peptide with sequence similarities to the arginine 614 cleavage site[119]. Rat matriptase shares a high degree of homology with the human enzyme[120].

1.5.4 Other serine proteases in Osteoarthritis

Aside from matriptase, multiple other serine proteases have been implicated in OA including the proteases involved in the complement and coagulation cascades (Figure 1.13)[121]. Abnormal complement activation is particularly associated with RA[122], however recent work has identified higher expression and activation of complement components in human osteoarthritic joints, such as activated fragments C3a and C5b-9[123]. Furthermore, mice deficient in either C5 or C6 protease are protected against OA, and CD59a (an endogenous complement inhibitor)-deficient mice experience more severe disease[123]. It is thought that this abnormal complement activation in OA could lead to cartilage damage by aberrant membrane-attack complex (MAC) deposition, the effector arm of the complement system, leading to production of inflammatory mediators or matrix-degrading proteases. Furthermore, the expression level of the competent proteases factor I, factor D and protease C2 have elevated expression levels in OA cartilage compared to normal[1].

Various proteases of the coagulation cascade have been linked to arthritic diseases, in particular RA[124]. One of the key proteases in coagulation, thrombin, has been implicated in arthritis. Thrombin is able to activate the PAR1 receptor (see chapter 1.7) which can instigate pro-inflammatory signalling. PAR1 deficiency in mice results in protection from antigen-induced arthritis, with a reduced expression of *MMP13*[125]. Furthermore, the inhibition of thrombin attenuates synovial hyperplasia in collagen-induced arthritis (CIA) in mice[126]. Coagulation factors X and VII have the ability to activate PAR2 (see chapter 1.7)[127], a pro-inflammatory receptor known to have an elevated expression in OA[128]. Furthermore, the expression of coagulation factor X is elevated in OA compared to normal cartilage[1].

The high-temperature requirement A (HTRA) family of serine proteases have been linked to arthritic diseases. Three out of the four family members (HTRA1, 3 and 4) have an elevated expression level in OA compared to normal cartilage[1,129]. These three members are all secreted proteases whereas HTRA2 functions within the mitochondria[130]. The expression of both HTRA1 and 3 is elevated in mouse models of arthritis[131,132]. HTRA1 has the ability to degrade cartilage components such as aggrecan and HTRA1-digested fragments of aggrecan have been identified in OA cartilage[133]. HTRA1 has also been

shown to digest soluble type II collagen[131], thus may act to further degrade partially digested collagen in cartilage.

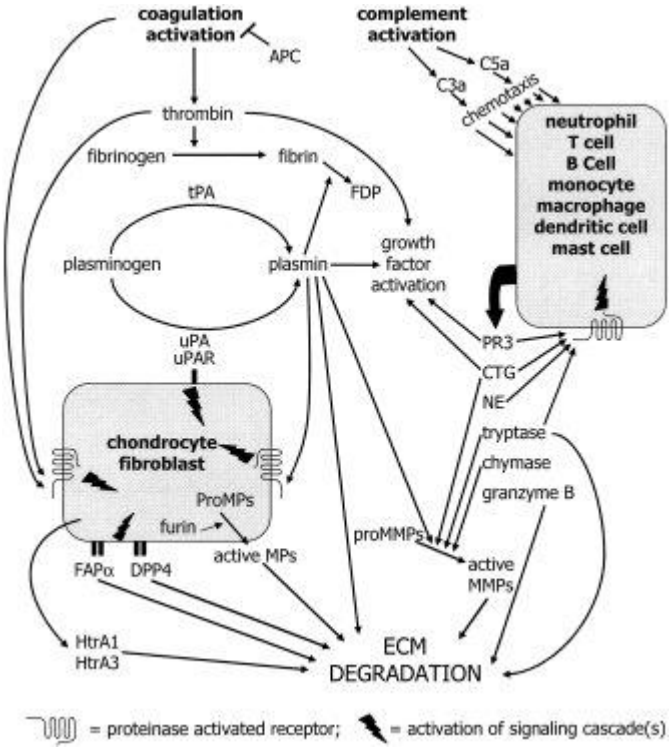

Figure 1.13: Roles of serine proteases in cartilage turnover in arthritic joints
Multiple serine proteases are expressed within the joint and are thought to play roles in arthritic diseases. Taken from Milner *et al.* (2008).

1.6 Cysteine proteinases

1.6.1 Classification and Structure

Cysteine proteases represent the third largest family of proteases, accounting for 164 proteases out of the 588 currently identified within the human degradome[45]. Members from this family are generally considered to be intracellular proteases which share a common catalytic mechanism[134]. They can be grouped into two major superfamilies: cytoplasmic caspase-1-like enzymes, and endosomal/lysosomal papain-like enzymes[135]. The research presented here utilises only papain-like superfamily enzymes, thus only these will be focused on in this section. Indeed, despite sharing an active site cysteine and catalytic mechanism, the two superfamilies share no other sequence homology and are thought to be evolutionary distinct families of enzymes[136]. The papain-like superfamily

also includes a subfamily of calpain-like proteases which are calcium-dependent cytoplasmic enzymes which share homology with the papain-like proteases[137].

The lysosomal papain-like cysteine proteases are referred to as the "cathepsins"[138], though this term is somewhat ambiguous as some enzymes such as cathepsin A, G (both serine proteases[139,140]), D and E (both aspartyl proteases[140,141]), share the name but have no relation to the lysosomal cathepsins. The research herein, the term "cathepsin" will refer to lysosomal cysteine proteases, unless otherwise stated. There are 11 lysosomal cathepsins in the human genome: B, C, F, H, K, L, O, S, V, X and W[142].

The cathepsins share a similar structure with the mature forms being composed of two domains of similar size with a total molecular weight of around 30 kDa. The two domains are referred to as the "left" and "right" domains with the left domain being formed by mainly the N-terminal half of the enzyme and vice versa, though the actual N-terminus is located in the right domain and the C-terminus is located in the left domain[143]. The left domain is composed of three helical regions, the longest of which contains the catalytic cysteine residue (position 25 in papain), whereas the right domain consists of a β-barrel structure made up of 5 or 6 strands. The structure is stabilised by two disulphide bonds in the left domain and a single disulphide bond in the right domain[143].

1.6.2 Catalytic mechanism

Cysteine proteases are thought to utilise a similar proteolytic mechanism to that of serine proteases, however it is not as well understood. Initial work undertaken on the prototypical cysteine protease, papain, identified a catalytic triad mechanism consisting of cysteine-25 in the left domain, with histidine-159 and asparagine-175 in the right domain[144]. Site-directed mutagenesis of the asparagine-175 to an alanine however suggested that this amino acid is not directly involved in catalysis as catalytic activity was partly retained, exhibiting an activity 150-fold lower than the wild type[145]. Mutating asparagine-175 to a glutamine however has little effect on catalysis, so it is thought that position 175 forms a hydrogen bond with histidine-159. This would fix the histidine residue in an orientation positioning its imidazole group in the proper position to act to deprotonate the sulphur on the cysteine, allowing it to act as a nucleophile able to attack the carbonyl carbon on the substrate[145,146] (Figure 1.14).

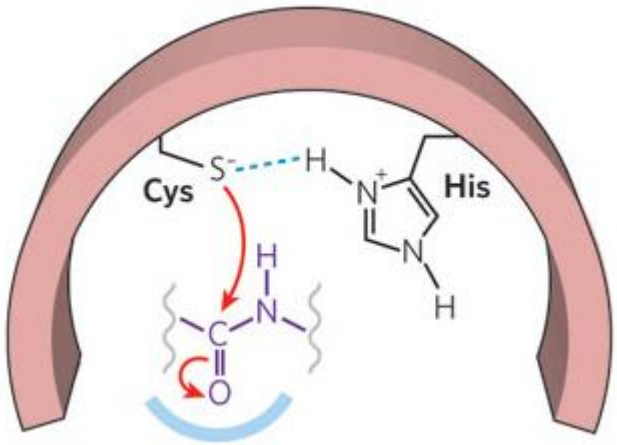

Figure 1.14: Cysteine protease catalytic mechanism
Cysteine proteases utilise a catalytic diad in which the imidazole group on a histidine is able to deprotonate the sulphur on a cysteine, allowing it to act as a nucleophile, able to attack the carbonyl group at the scissile bond on the substrate. Diagram taken from Erez *et al.*, (2009).

1.6.3 Regulation of activity

1.6.3.1 Activation

As cathepsins are synthesised as inactive pre-pro zymogens, they require activation to yield catalytic activity. The pre (signal) peptide is removed during intracellular trafficking while the enzymes are undergoing post-translational modifications and proper folding[147]. Insights to the pro-peptide inhibitory mechanism have been observed by the X-ray crystallography of several pro-cathepsins including human pro-cathepsin B[148], human pro-cathepsin L[149] and human pro-cathepsin K[150,151], which showed that the pro-domain physically blocks the properly-formed active site by simply running along the cleft (Figure 1.15).

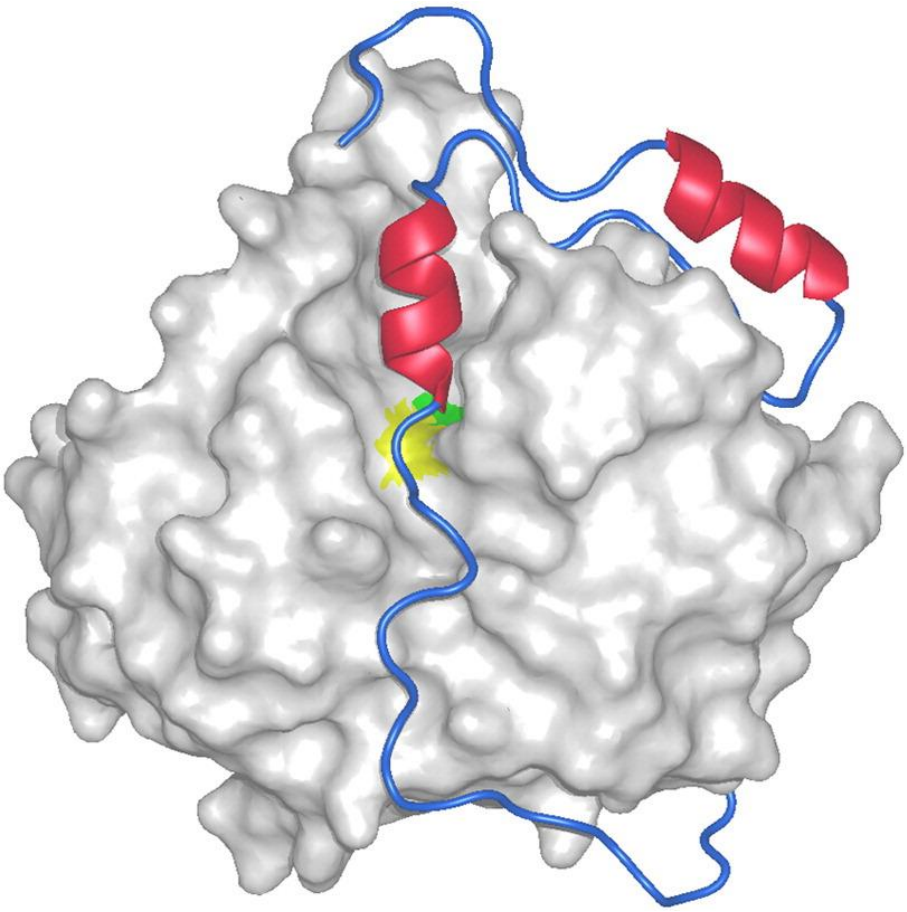

Figure 1.15: Crystal structure of pro-cathepsin B
Crystal structure highlighting the pro-domain (blue and red) over the mature domain of the enzyme (grey). The pro-domain sits in the active-site cleft blocking catalytic activity. The active site cysteine and histidine are coloured yellow and green, respectively. Taken from Turk *et al.* (2012).

Our understanding of the activation mechanisms of the cathepsins is incomplete, and variations between individual enzymes exist, but generally are thought to be a result of both proteolytic activities from other enzymes and autocatalytic activation. Insights into activation mechanisms have been obtained with work on pro-cathepsin B, which has been shown to have a low level of endogenous catalytic activity when exposed to low pH (as would be found in the lysosomes) presumably due to movement of the pro-domain from its normal inhibitory position. This partially active pro-cathepsin B is subsequently hypothesised to trans-activate other partially active pro-cathepsin B molecules by enzymatic cleavage of their pro-domains in a multi-step mechanism[152]. It is thought that this auto-activation mechanism is able to account in part for the activation of endopeptidase cathepsins (such as cathepsins B, H, K, L and S), however exopeptidase cathepsins (such as C and X) are unable to activate without the presence of an endopeptidase (such as L or S)[153,154].

1.6.3.2 Inhibition

Cathepsins are broad-spectrum proteases at very high concentrations within the lysosomes. As such, excessive activity of these enzymes can be potentially very damaging to cells. Cathepsin activity is curtailed by a variety of endogenous protein inhibitors such as cystatins, thyropins[138] and to a lesser extent, serpins[155].

1.6.4 Cathepsin B

Cathepsin B was one of the first identified cathepsins, and as such is one of the best described in this family[138]. Under normal physiological conditions, the activity of cathepsin B is tightly regulated, however there are multiple pathlogical conditions where this is no longer the case. The pathological condition most associated with cathepsin B is cancer, where overexpression is observed in malignancies such as brain, lung, prostate, breast and colorectal cancer. Indeed, the expression of cathepsin B correlates with invasive and metastatic cancers[156]. Cathepsin B is thought to exert both intra- and extra-cellular roles in cancer, such as promoting autophagy intracellularly[157], and activating important enzymes such as proMMPs via uPA[158] and degrading TIMP1 and TIMP2 extracellularly[159].

1.6.5 Cathepsin K

Cathepsin K is best known as an osteoclast-expressed collagenolytic enzyme with a key role in bone remodelling, however it is also expressed in cells such as macrophages, synovial fibroblasts, chondrocytes, and at sites of wound-healing and inflammation[160]. In osteoclasts, cathepsin K represents 4% of all mRNA, and constitutes around 98% of expressed cysteine proteases[161]. Despite the cathepsins being known as lysosomal proteases, cathepsin K can be secreted. In terms of bone remodelling, it carries out its function in resorption lacunae – a specialised compartment between the cell and the bone with conditions which are favourable for bone resorption – where it acts as a very potent collagenase breaking down the type I collagen of the bone[160].

The ability for cathepsin K to degrade triple helical collagen is unique among the cathepsins, and indeed unique amongst all known human proteases bar the collagenase MMPs and neutrophil elastase[162]. As with the collagenase MMPs, Cathepsin K is able to cleave both type I and type II collagens, however unlike the MMPs which cleave at a

specific site yielding characteristic ¼ and ¾ fragments, cathepsin K cleaves collagen at multiple sites[163]. In contrast with many cathepsins which are negatively charged overall, cathepsin K has several positively charged basic residues (lysine and arginine) which are on the opposite side of the enzyme to the active site (Figure 1.16). It is thought that these charges allow for interactions with the negatively charged GAGs of the ECM[164]. Indeed, cathepsin K exosite interactions with GAG are absolutely vital for collagenolytic activity[165] leading to the targeting of this region for the design of selective cathepsin K collagenase activity inhibitors such as ortho-dihydrotanshinone (DHT1) which do not inhibit cleavage of other cathepsin K substrates[166].

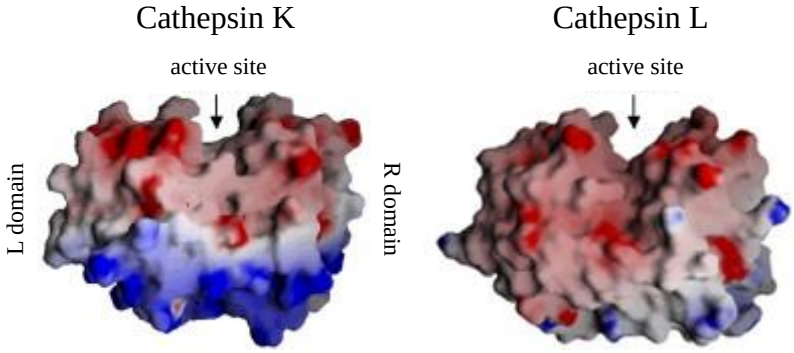

Figure 1.16: Surface charges of cathepsins K and L
Cathepsin L shares the most sequence homology to cathepsin K (60%) however cathepsin K has a region of net positive charge (blue) on the side furthest from its active site, whereas as with most cathepsins, cathepsin L has more net negative charge (red). Image taken from Lacaille *et al.*, (2008).

1.6.6 Cathepsin S

Cathepsin S is expressed mainly in cells of the immune system, namely antigen presenting cells (APCs) such as B cells, macrophages and dendritic cells where it has a vital role in antigen presentation[167]. During antigen presentation, the antigen presenting class II MHC molecules are expressed on the cell surface, containing a random peptide for presentation to other cells of the immune system. Class II MHC consists of αβ dimers, however in order to successfully form and then traffick to endosomes, they are associated with a chaperone known as the invariant chain which sits where eventually the presented peptide will sit. In order to successfully present antigen, lysosomal cathepsin S degrades the invariant chain from class II MHC which allows peptide antigen to bind it[167].

Uncommonly for lysosomal proteases, cathepsin S is highly active and stable at more neutral pHs[168], indeed it is the only cathepsin which is able to auto-activate at neutral pH as well as low pH[169], suggesting roles outside of lysosomal compartments. For example

cathepsin S is known to be a potent elastinolytic enzyme at neutral pH with implications for ECM degradation[170]. Cathepsin S has been implicated in the pathogenesis of a number of conditions such as RA[171], multiple sclerosis (MS)[172] and asthma[173].

1.6.7 Cathepsins L and V

Cathepsin L has had multiple intra- and extra-cellular physiological functions identified including lysosomal protein turnover, regulation of cell cycle and MHC class II processing, and has also been implicated in the pathogenesis of multiple malignancies[174].

Cathepsin V shares a high degree of homology with cathepsin L (78% homology, compared to <40% for the other cathepsins), indeed upon discovery it was named cathepsin L2[175]. A major difference between cathepsin V and cathepsin L is a much more restricted tissue distribution of cathepsin V, which is mainly expressed in the testes and thymus[176].

In terms of enzyme specificity, cathepsin V has a broader specificity in its S1 and S3 sites, compared to cathepsin L which has a preference for positively charged residues in these sites[177].

1.6.8 Cathepsins in Osteoarthritis

The cathepsins have been strongly implicated in arthritic diseases including RA and OA. Despite being best known as lysosomal proteases with optimal activity and stability at lower pH values, several of the family have also been shown to have activity at more neutral pH levels. Cathepsin S is well established to maintain its activity and stability at neutral pH with extracellular roles in degrading ECM components[168]. Cathepsin B, whilst most active at lower pH, is still thought to retain activity at neutral pH[178] and has also exhibited activity at cleaving ECM components[179]. As mentioned previously, cathepsin K is well established as being able to cleave triple helical collagen[160]. Cathepsin K has an optimal activity at pH 6, however is also fully active at neutral pH, but lacks stability and will rapidly lose activity[180]. Cathepsin L is thought to be one of the most unstable cathepsins at neutral pH[181], however it will exhibit short-term activity at more neutral pH levels[176,182]. Like cathepsin L, cathepsin V is most stable at more acidic pH levels, but will also exhibit activity at more neutral pH levels with a loss of stability[176].

As well as evidence of cathepsin activity at more neutral pH levels, there is also evidence of reduced pH levels in OA cartilage[183], which would theoretically allow for more stable active cathepsin enzymes. Indeed, cathepsin K degradation of type II collagen has been detected in human OA cartilage[184].

The first cathepsin to be implicated in OA was cathepsin B[185], where enzyme activity was found to correlate with disease activity[186]. In partial medial meniscectomy-induced arthritis in rabbits, cathepsin B expression is up-regulated in the synovium, but not in chondrocytes[187]. IL-1β stimulation of rabbit chondrocytes did however increase protein expression of cathepsin B[187]. The exact role for cathepsin B in OA is not fully understood. Cathepsin B has been shown to cleave aggrecan at the "MMP-specific" site between asparagine-341 and phenylalanine-342[188]. Cathepsin B has also been shown to cleave and reduce the activity of the protein deacetylase SirT1, an anti-inflammatory regulator in chondrocytes, following treatment by TNFα[189]. Interestingly, this role for cathepsin B is thought to occur within the nucleus[189].

Cathepsin S expression has also been shown to be induced by pro-inflammatory stimulation of chondrocytes by TNFα and IL-1β, with subsequent secretion of active enzyme, detectable in the conditioned medium[190]. Activity of both cathepsin S and cathepsin B has been detected in conditioned medium from OA cartilage in explant culture and in regions of degraded cartilage from patients[191].

Cathepsins V, L, K, B and S have all had multiple ECM substrates identified, including OA-relevant aggrecan and collagen. As mentioned previously, cathepsin B has aggrecanase activity, however cathepsins K, L and S have all also been shown to degrade aggrecan[192]. As discussed previously, cathepsin K is a well-established collagenase and the only cathepsin to cleave triple helical collagen. Cathepsins B, L and S have also been shown to have the ability to cleave collagen sequences, all being able to cleave the collagen non-helical telopeptide region[162,180]. Several other ECM substrates for these five cathepsins have also been identified, including elastin, fibronectin and type IV collagen, however these hold less relevance for OA. For an excellent review on cathepsin cleavage of ECM components, see Fonovic *et al*., (2014)[193].

Several animal models have implicated cathepsin K in the pathogenesis of OA, with most of the evidence suggesting a role in the progression of the disease. Mice constitutively

overexpressing cathepsin K spontaneously develop synovitis and exhibit degradation of articular cartilage[194], whereas cathepsin K protein and cathepsin K neo-epitopes were identified from post-mortems of horses which had naturally occurring OA, compared to healthy[195]. The inhibition of cathepsin K with the small molecule inhibitor SB-553484 following partial medial meniscectomy in a canine model of OA shows protective effects in terms of reduced cartilage degradation[196].

Studies undertaken in rabbits has described opposing effects. In one study, following anterior cruciate ligament transection-induced disease, cathepsin K expression was elevated in rabbits, however when the disease was induced following cathepsin K siRNA knockdown, disease progression was observed to be quicker, suggesting a protective effect by cathepsin K[197]. In a conflicting study, the inhibition of cathepsin K by a small molecule inhibitor, L-006235, protected against OA in the same anterior cruciate ligament transection model in rabbits[198]. In comparing these two studies, it is likely that the latter had a better methodology to ascertain the role of cathepsin K in OA. The use of siRNA in *in vivo* studies is known to have limitations, such as the ability to activate innate immunity[199], and is unlikely to be as efficient at inhibition as small molecule inhibitors. Furthermore, the latter study is more in line with the other literature regarding a role for cathepsin K in OA.

1.7 Protease-activated receptor 2 (PAR2)

1.7.1 The PAR family

The PAR family are unique amongst the G-protein coupled receptors (GPCRs) in that they are activated *in vivo* by an irreversible proteolytic cleavage event of their extracellular domain. Their peptide ligand is located within their extracellular domain, however upon cleavage, the neoepitope is able to bind to the active site of the receptor – this is known as a tethered ligand. The PARs are generally known as receptors for serine proteases. There are four members in the PAR family, PAR1, PAR3 and PAR4 which are known as thrombin receptors, and PAR2 which is a trypsin receptor. All four PAR members have, however, had additional agonist proteases identified[200].

The four PAR family members share a high degree of homology. PAR1 (*F2R*), PAR2 (*F2RL1*) and PAR3 (*F2RL2*) are located in a gene cluster of chromosome 5q13, whereas PAR4 (*F2RL3*) is located on chromosome 19p12[201]. As is conserved within the GPCR superfamily, the PARs are "7-TM" receptors containing 7 transmembrane helices. Furthermore, they have an N-terminal extracellular domain, three extracellular loops (ECL1-3), three intracellular loops (ICL1-3) and a C-terminal intracellular domain[200]. PAR1 and PAR3 further contain a hirudin-like motif within their extracellular domains to facilitate thrombin binding[202].

Following cleavage and removal of the N-terminal region, the tethered ligands of the PAR receptors are thought to interact primarily with ECL2, which results in a conformational change of the receptor and subsequent activation[200] (Figure 1.20). Following activation, the induced signalling cascades are typical for GPCRs in that they are mediated by association with heterotrimeric G-proteins. Heterotrimeric G-proteins consist of an α subunit (Gα) which associates with a βγ dimer (Gβγ). Multiple Gα proteins have been identified, which mediate different downstream signalling pathways[203]. The PARs have been shown to couple with multiple Gα subunits, including Gαq, Gαi, Gαs and $G\alpha_{12/13}$[204]. Furthermore, the PARs can also signal through Gβγ-dependent pathways[200] as well as G-protein-independent pathways such as β-arrestin signalling[204] (Figure 1.17). Our understanding of PAR2 signal transduction is incomplete, and further description is beyond the scope of this chapter. For an excellent review, the reader is directed to Soh *et al*. (2010)[204].

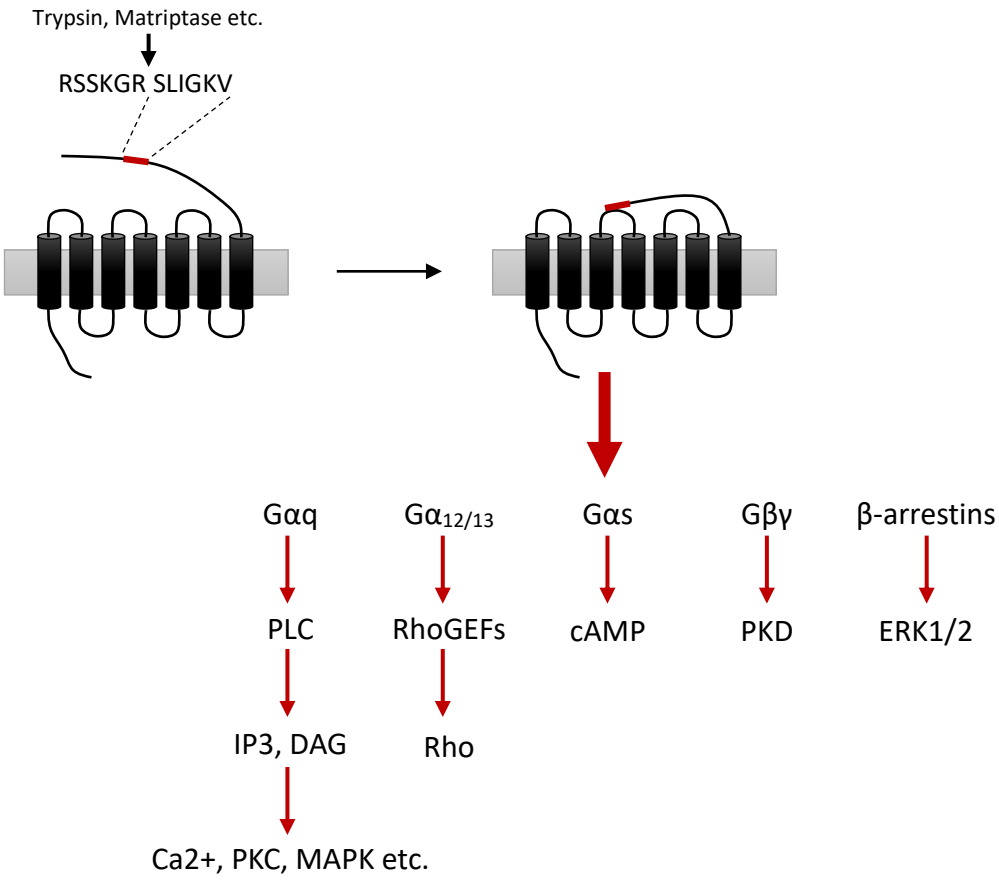

Figure 1.17: PAR2 activation mechanism and induced signalling pathways
The PAR family of GPCRs, including PAR2 as shown in the diagram, is activated by proteolytic cleavage in their extracellular domain which reveals a tethered ligand, for example SLIGKV in the case of PAR2. The tethered ligand then binds to and activates the receptor, and stimulates various signalling pathways. PAR2 signals through coupled G proteins, including various Gα proteins, as well as βγ dimers. PAR2 also signals independently of G proteins by β-arrestin signalling.

1.7.2 PAR2 agonists and antagonists

PAR2 is best known as a receptor for trypsin, which cleaves PAR2 after arginine-36 to reveal the tethered ligand SLIGKV and instigate full activation of PAR2 in what is known as canonical signalling[205]. Multiple other proteases have been identified to cleave PAR2 at this site, including coagulation factors X and VII[127], tryptase[206], trypsin IV[207], Granzyme A[208], kallikrein-2, -4[209], -5, -6 and -14[210], TMPRSS2[211], acrosin[212], human airway trypsin-like protease[213]. Of greatest interest to this study, matriptase has also been identified as a potent activator of PAR2[115]. In a challenge to the previous held dogma that thrombin was an agonist for PAR1, PAR3 and PAR4 but not PAR2, thrombin has in fact recently also been shown to have the ability to induce canonical PAR2 activation[214].

As well as the endogenous activators of PAR2, several exogenous activators have also been identified. The serine protease Pen c 13 is an allergen expressed by *Penicillium citrinum* (a mould) and has been found to induce canonical PAR2 activation, with associated pro-inflammatory outcomes[215]. The dust mite allergens and serine proteases Der P3 and Der P9 have also been shown to cleave and activate PAR2 at the canonical activation site[216]. Furthermore, the cysteine protease dust mite allergen Der P1 has also been shown to activate PAR2 and stimulate inflammatory responses[217,218]. A bacterial cysteine protease, arginine-specific gingipain from *Porphyromonas gingivalis* has been demonstrated to induce canonical PAR2 activation[219,220], as has a chitinase from the bacterium *Streptomyces griseus*[221].

A commonly used tool in PAR2 research is the use of synthetic peptides corresponding to the tethered ligand, either SLIGKV or SLIGRL, corresponding to the human or rat/mouse sequence, respectively. These peptides mimic the effect of canonical PAR2 activation, and by using mutant versions of them, much has been deduced about PAR2 agonist requirements. This is discussed in more detail in chapter 5.3. A modified synthetic peptide, 2-furoyl-LIGRLO-NH_2, where O corresponds to the non-proteinogenic amino acid, ornithine, is used as a synthetic PAR2 agonist with greater potency and bioavailability than SLIGKV/SLIGRL[222,223].

As well as the multitude of proteases identified as canonical activators of PAR2, several other proteases have also been identified as cleaving PAR2 at distinct sites. Some of these proteases can disarm the receptor by removing the extracellular domain and preventing the canonical cleavage producing the tethered ligand. Other proteases have, however, been identified as able to induce biased agonism, partially activating PAR2 by cleavage at a distinct site and either revealing a different tethered ligand or stimulating a conformational change of the receptor independently of a tethered ligand. Following cleavage by proteases able to induce biased signalling, a subset of PAR2 downstream signalling pathways are induced.

One of the first proteases identified as a disarmer for PAR2 was neutrophil elastase, which was found to disarm against trypsin-mediated Ca^{2+} mobilisation (a marker of Gαq activation)[224]. Subsequent work however identified elastase as able to induce biased signalling, in terms of ERK1/2 phosphorylation in a $G\alpha_{12/13}$-mediated Rho kinase activation mechanism[225]. It is thought that elastase acts as a biased agonist without the

need for a tethered ligand, rather directly activating the receptor by inducing a conformational change after cleavage. Elastase cleaves PAR2 after serine-68, resulting in an extracellular domain only 9 amino acids long, likely too short to act as a ligand. Furthermore, peptide agonists corresponding to the new N-terminus do not mimic the effect of the enzyme, as would be expected based on other activator peptides used in PAR2 research[225].

The serine proteases cathepsin G and proteinase 3 are both thought to be disarmers of PAR2 with no current evidence for biased agonism. Cathepsin G cleaves after phenylalanine-65 and proteinase 3 cleaves after valine-62, which as with elastase removes the majority of the extracellular domain, preventing canonical activation[225].

The cysteine protease cathepsin S has been identified as a biased agonist for PAR2[226]. Cathepsin S cleaves PAR2 after glutamic acid-56, revealing the tethered ligand TVFSVDEFSA. Cathepsin S is able to disarm against trypsin-mediated Ca^{2+} mobilisation, but induces cAMP formation, as a result of inducing coupling to Gαs, but not Gαq. The effects of cathepsin S are mimicked by TVFSVDEFSA which shows a tethered ligand mechanism is responsible for the activation.

1.7.3 PAR2 activation and termination

As previously mentioned, the PARs including PAR2 transduce signals via the coupling with various G alpha proteins. PAR2 is unique amongst the PAR family in that it also has the ability to bind to β-arrestins, which function to transduce G-protein independent signalling pathways (such as G-protein independent ERK1/2 signalling), as well as termination of PAR2 signalling[227]. PAR2 is also the only PAR that has been shown to interact with Jun activating binding protein 1 (Jab1), a protein involved in the activation of the AP-1 transcription factor[228].

Considering the unique activation mechanism of the PARs, it is clear that following activation, they cannot be "reactivated" due to the cleavage having already occurred. Following activation, PAR2 is therefore internalised and new PAR2 trafficked to the cell surface. PAR2 signalling is terminated by the phosphorylation of serine and threonine residues on the intracellular domain which aids the recruitment of β-arrestin 1 and β-arrestin 2[229], proteins which are essential for the termination of PAR2 signalling and

subsequent internalisation[227]. β-arrestin recruitment for internalisation is not unique to PAR2, rather is a common mechanism for GPCR inactivation and internalisation[230].

Following PAR2 internalisation, cell surface PAR2 is rapidly replenished by trafficking intracellular stores to the cell membrane. It is thought multiple stores of PAR2 are present within cells, at different stages of the secretion pathway. Following activation, PAR2 can quickly be trafficked from endosomal stores to the cell surface, and if activated again, further PAR2 can be trafficked from the Golgi. Additional activation would likely require *de novo* protein synthesis to replenish surface PAR2[231]. Recent work has shown that PAR2 Gβγ signalling leading to an activation of protein kinase D (PKD) is involved in the trafficking of PAR2 from the Golgi to the cell surface membrane[232].

There is currently no PAR2 crystal structure available, however structural models have been produced based on homology with other GPCRs (human PAR1, bovine rhodopsin and human ORL-1)[233].

1.7.4 Physiological and Pathological roles of PAR2

Roles for PAR2 in both normal physiology and pathological conditions have been identified in multiple tissues and systems, including the cardiovascular system, the respiratory system, the nervous system, gastrointestinal tissues, the renal system, and the musculoskeletal system[200]. A role for PAR2 is also implicated in various cancers and inflammatory conditions[200].

The physiological roles of PAR2 are complex and vary from cell type. Canonical PAR2 activation is pro-inflammatory in nature, resulting in the release of a host of inflammatory mediators such as various cytokines and chemokines. For a detailed description of the role of PAR2 in the aforementioned systems, the reader is directed to the review by Adams *et al*. (2011)[200].

1.7.5 PAR2 in Osteoarthritis

A role for PAR2 in OA was first speculated in the mid-2000s when the level of PAR2 gene expression was found to be elevated in OA chondrocytes compared to normal chondrocytes, and that pro-inflammatory (IL-1β or TNFα) stimulation of both normal or diseased chondrocytes increased PAR2 expression[128,234].

The canonical activation of PAR2 is known to induce the expression of the key catabolic mediators of articular cartilage, MMP1 and MMP13[128], and the PAR2 activator matriptase was found to also be significantly up-regulated in OA vs control cartilage[1]. Matriptase is thought to act in OA pathogenesis via PAR2 as it is unable to directly breakdown collagen, however its addition to OA cartilage in explant culture leads to enhanced collagenolysis which was found to be dependent on MMP activity[1]. Matriptase is able to induce MMP-1, -3 and -13 expression in OA cartilage, and subsequently it is able to activate proMMP-1 and proMMP-3 (with active MMP-3 further being able to activate proMMP-1 and proMMP-13)[1].

A role for PAR2 in OA pathogenesis is supported in mouse models where PAR2-deficient mice are protected in both the medial meniscotibial ligament disection (MMTL)[235] and destabilisation of the medial meniscus (DMM)[236] models of the disease. Further mouse studies have implicated PAR2 in some of the pathological changes observed in the joint, such as the formation of osteophytes and disease-related pain[237].

1.8 Scope of this thesis

Cartilage breakdown in OA is known to be a result of proteolytic cleavage mediated by proteases synthesised and secreted by the only resident cell within cartilage, the chondrocyte. The traditional view that metalloproteinases, specifically the collagenases and the aggrecanases, are the key enzymes in OA is looking increasingly simplistic, with increasing evidence that other families of enzymes such as the serine proteases and the cysteine proteases also having roles in OA. Whilst some of these enzymes, such as cathepsin K[184], may exert their role in OA by direct breakdown of cartilage, the role for other proteases are not so clear and likely exert their roles indirectly.

As described in this chapter, serine proteases partake in multiple complex networks of proteolysis, such as coagulation and complement activation, and many have roles in the regulation of protease activity, such as proMMP activation. Serine proteases are also able to regulate cell behaviour by direct receptor activation, such as uPA activation of uPAR and multiple serine proteases with the ability to activate protease-activated receptors, with PAR2 activation by matriptase of particular interest to this study.

Understanding how proteases can regulate chondrocyte behaviour is essential for understanding the molecular mechanisms underlying OA. Recent work has shown that the cysteine protease cathepsin S has the ability to activate certain PAR2 responses[226], challenging the dogma of this receptor being a receptor for trypsin-like serine proteases. Indeed, MMP-1 and MMP-13 can activate PAR1, highlighting the complexity of biology and the over simplification of considering PAR1 a "thrombin receptor" or PAR2 a "trypsin receptor". A multitude of proteases are expressed in cartilage in both normal physiological turnover and pathological OA[121], and how the majority of these interact with PAR2 is currently unknown. To date, no large scale screen of PAR2 cleavage by cartilage-expressed proteases has been performed, therefore this project aims to identify novel cleavages of PAR2. It is likely the *in vivo* situation is much more complicated than matriptase activation of PAR2 leading to an induction of *MMP1* and *MMP13*.

On the one hand it is of importance to understand how proteases can regulate chondrocyte behaviour, however since chondrocytes are the only cell type within the cartilage, it is also of importance to understand how protease expression is regulated in these cells. Pro-inflammatory stimulation is known to induce the expression of multiple proteases, and many studies have been undertaken to further understand this regulation. Mechanical loading of chondrocytes has also long been thought to be important in the regulation of chondrocyte function, including expression of various mechanosensitive genes, including MMP expression[22]. Matriptase is known to have an elevated expression level in OA[1], however it is unknown how its expression is regulated, therefore this project also aims to explore whether mechanical loading is involved in matriptase regulation.

1.9 Aims

- To explore the expression of matriptase and PAR2 in chondrocytes by mechanical loading.

- To perform a screen of cartilage and OA-expressed proteases for the ability to cleave PAR2.

- To explore the role of any novel cleavages of PAR2.

Chapter 2. Materials and Methods

2.1 Materials

2.1.1 Antibodies

Table 2.1: Antibodies used throughout this project

Antibody	Source	Manufacturer	Product Code
GAPDH	Mouse monoclonal	Abcam, Cambridge, UK	ab8245
Matriptase	Rabbit polyclonal	Merck Millipore, St Louis, USA	IM1014
Hepsin	Rabbit polyclonal	Cayman Chemical Company, Ann Arbor, USA	100022
Phospho-p38	Rabbit monoclonal	Cell Signalling Technology, Danvers, USA	4511
p38	Rabbit polyclonal	Santa Cruz Biotechnology, Dallas, USA	SC-535
Phospho-Erk1/2	Rabbit polyclonal	Cell Signalling Technology, Danvers, USA	#9101
Erk1/2	Rabbit polyclonal		#9102
PAR-2	Rabbit polyclonal	Santa Cruz Biotechnology, Dallas, USA	SC-5597
MMP-1	Mouse monoclonal	In-house	RRU-CL1

2.1.2 Recombinant Proteinases

Table 2.2: Recombinant proteases used throughout this project

Proteinase	Source	Manufacturer	Product Code
proMMP-1	High Five™ Insect Cells	Produced In-house	N/A
proMMP-8	Mouse myeloma cell line, NS0-derived	R&D Biosystems, Minneapolis, USA	908-MP-010
proMMP-13	High Five™ Insect Cells	Produced In-house	N/A
uPA	Purified from human urine	Merck Millipore, St Louis, USA	672112-10KU
HTRA1	Rosetta™(DE3)pLysS *E. coli*	Prof. Michael Ehrmann, University of Duisberg-Essen, Germany	N/A
HTRA3	Rosetta™(DE3)pLysS *E. coli*		N/A
Cathepsin G	Purified from human sputum leucocytes	Elastin Products Company, Owensville, USA	SG623
Neutrophil elastase	Purified from human sputum leucocytes		SE563
Hepsin	*Drosophila* S2 insect cells	Prof. Richard Leduc, University of Sherbrooke, Canada	N/A
Matriptase	*E. coli*	Prof. Alastair Hawkins, Newcastle University, UK	N/A
Factor I	Purified from human serum	CompTech, Tyler, USA	A138
Factor D	Purified from human serum		A136
ADAMTS-5	HEK 293-EBNA Cells	Prof. Hideaki Nagase, University of Oxford	N/A
Thrombin	Purified from bovine serum	Merck Millipore, St Louis, USA	605157-1KU
Cathepsin V	*Pichia pastoris*	Prof. Dieter Brömme, University of British Columbia, Canada	N/A
Cathepsin K	*Pichia pastoris*		N/A

Cathepsin S	*E. coli*	Merck Millipore, St Louis, USA	219323
Cathepsin B	Mouse myeloma cell line, NS0-derived	R&D Biosystems, Minneapolis, USA	953-CY-010
Cathepsin L	Mouse myeloma cell line, NS0-derived		952-CY-010
PCSK9	Mouse myeloma cell line, NS0-derived		3888-SE-010
FAP	*Spodoptera frugiperda*, Sf 21 (baculovirus)-derived		3715-SE-010

2.1.3 Synthetic peptides

Table 2.3: Synthetic peptides used throughout this project

Peptide	Sequence (N → C)	Source
PAR2 42mer	H-RSSKGRSLIGKVDGTSHVTGKGVTVETVFSVDEFSASVLTGK-OH	Dr. Hiroki Shimizu, AIST Hokkaido, Japan
PAR2 Trypsin AP	H-SLIGKV-NH2	Abcam, Cambridge, UK
PAR2 MMP AP	H-LIGKVD-NH2	
PAR2 MMP AP Reverse	H-DVKGIL-NH2	
Cathepsin S/V/L 10mer	H-TVFSVDEFSA-NH2	
Cathepsin S/V/L 6mer	H-TVFSVD-NH2	Peptide Synthetics, Fareham, UK
Cathepsin K 6mer	H-KVDGTS-NH2	
VETV	Abz-VETV-Y(3-NO2)	
FSVD	Abz-FSVD-Y(3-NO2)	
SY-9 peptide	Abz-SKGRSLIG-Y(3-NO2)	GL Biochem, Shanghai, China

2.1.4 Molecular Biology Reagents

For plasmid preparation, mini-prep kits were obtained from either GE Healthcare (Little Chalfont, UK) for illustra plasmidPrep Mini spin kit or Qiagen (Hilden, Germany) for QIAprep Spin Miniprep Kit. Maxi-prep kits were obtained from either Qiagen (Plasmid Maxi Kit) or Promega (Madison, USA) for PureYield™ Plasmid Maxiprep System.

For Polymerase Chain Reaction (PCR) amplification, Q5® High-Fidelity DNA Polymerase from New England Biolabs (Ipswich, USA) and *Pfx50*™ DNA Polymerase from Thermo Fisher (Waltham, USA) were used.

All custom primer oligos were synthesised by Sigma-Aldrich (St. Louis, USA). Plasmid sequencing was undertaken by Source Bioscience (Nottingham, UK).

For molecular cloning, all restriction endonucleases and their buffers were obtained from Thermo Fisher. Ligation was undertaken using an In-Fusion HD kit from Clontech (Mountain View, USA). For transient and stable transfection, the mammalian expression plasmid pcDNA3.1 (Thermo Fisher) was used and FuGene HD transfection reagent (Promega) was used for transfection.

2.1.5 Cell culture reagents

Interleukin (IL)-1α was provided by Dr Keith Ray at GlaxoSmithKline (Stevenage, UK) and is dissolved in Dulbecco's Modified Eagle's medium (DMEM), sterile filtered with a 0.22 µm polyethersulfone (PES) filter and stored at -20°C.

Oncostatin M (OSM) was produced in-house as previously described[238], and is dissolved in Dulbecco's Phosphate-buffered Saline (PBS) with 0.1% (w/v) Bovine serum albumin (BSA), sterile filtered with a 0.22 µm PES filter and stored at -80°C.

2.1.6 Chemicals

Unless otherwise stated, all chemicals were obtained from Sigma-Aldrich.

Unless otherwise stated, all cell culture medium was obtained from Thermo Fisher.

Dulbecco's PBS was obtained from both Sigma-Aldrich and Thermo Fisher.

2.1.7 Protease inhibitors

Table 2.4: Protease inhibitors used throughout this project

Protease	Inhibitor	Source
E64	Cysteine proteases	Sigma-Aldrich
AEBSF	Serine proteases	Sigma-Aldrich
DFP	Serine proteases	Sigma-Aldrich
TIMP-1	MMPs	Prof. Hideaki Nagase
MMP-8 inhibitor I	MMP-8	Merck Millipore
CL-82198	MMP-13	Sigma-Aldrich

2.1.8 Consumables

Unless otherwise stated, all consumables were obtained from Sigma-Aldrich.

Unless otherwise stated, all cell culture dishes, flasks and plates were manufactured by Corning (New York, USA) and purchased from Sigma-Aldrich or VWR International (Radnor, USA).

2.2 Bovine Nasal Chondrocyte Extraction

Primary chondrocytes were extracted from bovine nasal septa using a sequential digestion method. Bovine nasal septa were obtained from a local abbatoir.

Reagents:

- Antibiotic-supplemented PBS: Dulbecco's PBS, supplemented with 200 IU/mL penicillin, 200 ug/mL streptomycin and 40 IU/mL Nystatin.
- DMEM-F12, supplemented with 10% Foetal Bovine Serum (FBS), 200 IU/mL penicillin, 200 µg/mL streptomycin and 40 IU/mL Nystatin: "Complete DMEM-F12".
- Hyaluronidase (1 mg/mL in supplemented PBS, 4 mL/g cartilage).
- Trypsin (2.5 mg/mL in PBS, 4 mL/g cartilage).
- Collagenase (2 mg/ml in supplemented DMEM-F12, 3 mL/g cartilage).

Method: The nasal septum was isolated and removed from the nose and a scalpel was used to remove any non-cartilaginous material. The cartilage was then cut into small pieces and washed 3 x 5 minutes in antibiotic-supplemented PBS. The cartilage pieces were then weighed and no more than 5 g added to multiple 50 ml Falcon tubes. The cartilage was then incubated with hyaluronidase for 15 minutes at 37ºC with rotation. The hyaluronidase-containing supernatant was removed and the cartilage was washed 3 times with supplemented PBS. The cartilage was then incubated with trypsin for 30 minutes at 37ºC with rotation. The supernatant was removed and the cartilage washed 3 times with complete DMEM-F12, before incubating with collagenase for 15-20 hours at 35ºC with rotation. Following the collagenase digest, cells were allowed to settle and the chondrocyte-containing supernatant was passed through a 0.2 µm cell strainer to remove any undigested material. The cell solution was then centrifuged at 1100 x g and the pellet resuspended in growth medium and the cells counted.

2.3 Monolayer Cell Culture

2.3.1 SW1353 cell line

SW1353 cells are a chondrosarcoma immortal cell line purchased from American Type Culture Collection (ATCC) (Manassas, USA) and cryopreserved in SW1353 culture medium supplemented with 10% DMSO.

Reagents:

- SW1353 (complete) culture medium: DMEM-F12, supplemented with 10% FBS, 2 mM L-glutamine, 100 IU/mL penicillin and 100 µg/mL streptomycin.

SW1353 cells were resurrected from cryopreservation in liquid nitrogren, by rapidly thawing at 37°C, before adding drop-wise to 9 mL SW1353 complete culture medium and centrifuging at 1100 x g for 5 minutes before resuspending the pellet in 12 mL fresh SW1353 complete culture medium and seeding in a T75 flask. The SW1353 cell line was mainained in T75 flasks, passaging at a 1:6 ratio when reaching 90% confluency (roughly every 3-4 days) and plating cells for experiments as required. The cells were incubated at 37°C in 5% CO_2 in a humidified incubator.

In order to passage the cells, the cells were first washed with 10 mL Dulbecco's PBS, before incubating for 5 minutes at 37°C with 2 mL trypsin-EDTA solution (0.05% porcine trypsin and 0.02% (w/v) EDTA in HBSS) to dislodge the adhered cells. The trypsin was then inhibited by the addition of 8 mL SW1353 culture medium and the cells transferred to a 25 mL universal tube and centrifuged at 1100 x g for for 5 minutes. The cells were then resuspended and either counted for plating out experiments, and/or used to seed a new T75 to continue the cell line. SW1353 cells were typically utilised for 15-20 passages before resurrecting new cells.

In order to count cells, 10 µL of cell suspenstion was mixed with 10 µL of trypan blue solution (0.4% sterile-filtered) and well mixed. The 20 µL mixture was then added into the chamber of a Fuchs-Rosenthal haemocytometer and cells were counted under a microscope by averaging the counts obtained from three squares. Following counting, cells were plated according to experimental requirements.

2.3.2 Bovine nasal chondrocytes (BNC)

BNC are a primary chondrocyte cell type extracted from bovine nasal septa as outlined in chapter 2.2.

Reagents:

- BNC complete culture medium: DMEM-F12, supplemented with 10% FBS, 2 mM L-glutamine, 200 IU/mL penicillin, 200 µg/mL streptomycin and 40 IU/mL Nystatin

Following the counting step in chapter 2.2, cells were seeded into 96-well plates at a density of 1 x 10^5 cells per well in BNC complete culture medium. Cells were then incubated at 37°C in 5% CO_2 overnight before serum starving overnight in serum-free BNC culture medium and subsequently undertaking experiments.

2.4 3-Dimensional Cell Culture

Reagents:

- 2.5% SeaPlaque™ Agarose from Lonza (Basel, Switzerland). Made up in nanopure water and autoclaved.
- 1 M HEPES (Thermo Fisher)
- DMEM-F12 powder (Thermo Fisher)
- Insulin-Transferrin-Selenium (ITS -G) (Thermo Fisher)
- (+)-Sodium L-ascorbate
- 5x DMEM-F12 prepared using DMEM-F12 powder and supplemented with 10% FBS, 500 IU/ml penicillin, 500 ug/ml streptomycin and 50 mM HEPES.

Method: The 2.5% agarose was melted by heating in boiling water and then placed in a water bath set to 42ºC until the agarose reached 42ºC. Supplemented 5x DMEM-F12 is also heated to 42ºC and then mixed with the agarose in a 1:4 ratio to yield 2% Agarose and 1x culture medium. It is vital not to allow the temperature to drop in order to avoid premature gelling, the agarose/ medium solution is therefore kept at 42ºC until the cells are added. The cells are prepared by suspending the required cells and centrifuging to form a pellet. The pellet is then resuspended in the minimum possible amount of complete DMEM-F12, typically 500 µL. The concentrated cell solution is then added to the agarose/ medium solution and mixed taking care to avoid bubble formation. The solution is then placed in a 100 mm cell culture dish and quickly incubated at 4ºC for 2 minutes followed by 15 minutes at room temperature in order to allow the mixture to set.

Once set, the base of a sterile 5 ml micropipette tip is used to punch out discs of 13 mm diameter. Between 20 and 22 discs are obtained from a single 100 mm dish depending on the size of the meniscus around the edge and the presence of bubbles. It is important to avoid the meniscus and bubbles in order for the discs to have uniform thickness across the entire diameter. The discs which are destined to undergo loading are then carefully placed within the foam ring in the centre of each well of BioPress™ Compression Plates from Flexcell International Corporation (Burlington, USA). The corresponding unloaded controls are placed in regular 6-well cell culture dishes. “Day 0” (4 mL) culture medium (table 2.5) is then added to each well, and the plates incubated at 37ºC 5% CO_2. Culture medium is subsequently changed daily with the medium outlined in table 2.5, according to the method of Bougault *et al*., (2009)[239]. The benefits of this cell culture regimen are

twofold. Firstly, FBS is removed preventing adverse effects on downstream analysis, with the ITS being used to supplement for the lack of FBS. Secondly, the increasing levels of ascorbic acid help the cells to secrete a PCM/ECM[239].

In order to test for the secretion of PCM/ECM by the chondrocytes, the agarose-chondrocyte constructions either at day 0 or day 6 were fixed in 10% Formalin (Cellpath, Newtown, UK) for at least 24 hours before washing in 70% ethanol and embedding in paraffin wax (performed by the Newcastle University BioBank). Embedded constructs were then sliced and stained for ECM components using histological staining methods (performed by Sharon Watson).

Table 2.5: Progressive serum starvation and supplementation timetable for chondrocytes in 3D-agarose culture

Day	FBS (%)	HEPES (mM)	Ascorbic Acid (µg/ml)	ITS (%)
0	10	10	0	0
1	10	10	0	0
2	5	20	5	0
3	5	20	10	1
4	1	30	15	1
5	0	30	20	1
6	0	30	20	1

2.5 Cell loading studies using Flexcell® Compression System

Reagents:

- Laemmli buffer: 62.5 mM Tris-HCl pH 6.8, 5% (v/v) glycerol, 2.5% (w/v) Sodium dodecyl sulphate (SDS), 0.025% Bromophenol blue. Made fresh from a 4x stock and then β-mercaptoethanol added to 3% (v/v).

Method: Medium from each well of the BioPress plates was replaced with 3 ml of "day 6" medium. Stationary platens (Flexcell International Corporation) were sterilised in 70% ethanol and then prepared for compression by adjusting the centre screws so that the base

of the screw was at the same level as the base of the platen. A stationary platen was added to each well of the BioPress plates, and the centre screw adjusted so that it touched the top of the gel. The amount to adjust the screws can be calculated based on the known thickness of the gels using the following equation:

$$x = \frac{(3.11 - h)}{0.62}$$

Where *x* is the number of 180º clockwise turns required so that the bottom of the centre screw is in contact with the gel, and *h* is the known height of the chondrocyte-agarose construct in millimetres.

Following the preparation of the BioPress plates with the stationary platen, the plates were placed in the Flexcell® FX-5000™ Compression System (Flexcell International Corporation) by centering the plates over the gaskets in the baseplate and clamping the plates using the wing nuts on the clamping system until an airtight seal is formed between the BioPress plate and the baseplate of the Flexcell system. The Flexcell computer software is then used to create and run a regimen for cell loading. The system works by increasing air pressure in the baseplate below the BioPress plate, forcing the flexible bottom of the BioPress plate to rise and compressing the chondrocyte-agarose construct against the stationary platen.

A 30 minute loading regimen of 20-40 kPa with a square waveform with 1 second of 20 kPa for every 2 seconds of 40 kPa was utilised (Figure 2.1). Following the 30 minute loading regiment (referred hereafter as time point 0 minutes), the gels are processed for further analysis. For histological analysis, gels were fixed in 10% formalin, washed in 70% ethanol and embedded in paraffin wax as described in chapter 2.4. For protein analysis, gels are placed in a 15 ml Falcon tube and snap frozen in liquid nitrogen and stored at -80ºC before lyophilisation using a freeze-dryer. Following lyophilisation, the gels are resuspended in 200 µL Laemmli buffer and heated to 100ºC for 5 minutes. The gels were allowed to set at room tempterature and transferred to a minispin filter paper column with a 10 µm pore size and cut up with a spatula. The gels were then centrifuged at 12,000 x g for 1 hour at room temperature. This separates Laemmli buffer containing proteins in the filtrate from bits of agarose which cannot pass the 10 µm pores. 20 µL of filtrate is then used as loading samples for SDS-PAGE.

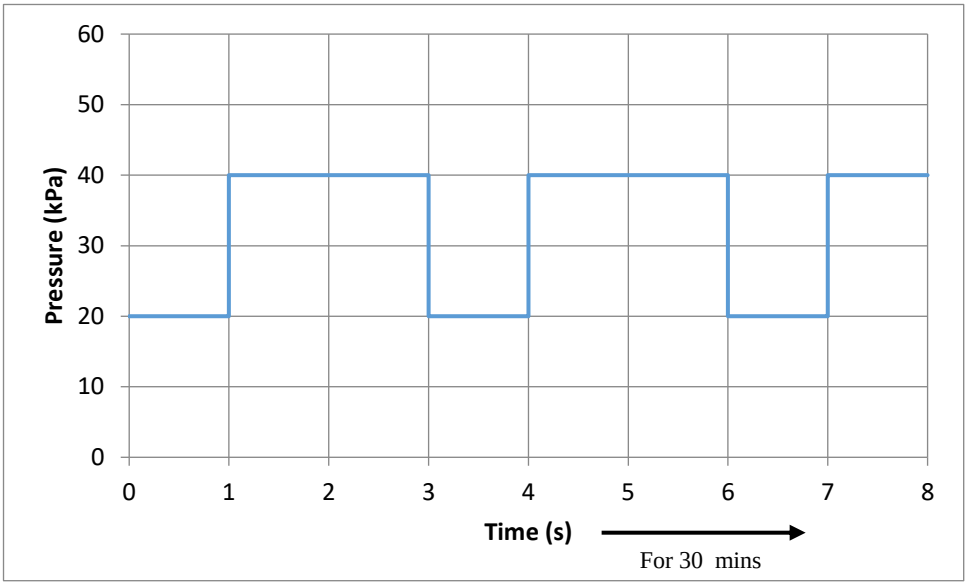

Figure 2.1: Loading regimen
Cells were loaded with a loading regimen of 20-40 kPa with a square waveform with 1 second of 20 kPa for every 2 seconds of 40 kPa.

2.6 SDS-Polyacrylamide gel electrophoresis (SDS-PAGE)

Background: SDS-PAGE is a commonly used laboratory technique in which samples containing proteins are separated in a size-dependent manner. Protein samples are denatured by heating to 98-105ºC in a buffer containing SDS. Under native conditions, proteins vary in net charge which would affect separation in electrophoretic techniques. The presence of SDS negates this variability in protein charges by binding the denatured polypeptide chains and giving all proteins a net negative charge and a uniform charge density thus allowing them to migrate in a manner relative to their size. The reducing agent β-mercaptoethanol may also be added to the sample, reducing disulphide bonds and further disrupting any tertiary structure.

The gel is placed in a tank containing a tris-glycine[240], or less commonly a tris-tricine[241], running buffer. An electric current is applied across the gel from negative at the top, to positive at the bottom, allowing anions to migrate down through the gel. There are three anions in SDS-PAGE: the negatively charged SDS/protein complexes, as well as chloride ions from the gel and glycine/tricine from the running buffer.

The polyacrylamide gel contains an upper “stacking gel” and a lower “resolving gel” which differ in pH, ionic content and acrylamide concentration. The different migratory

properties of the stacking gel allow the loaded sample to concentrate (or stack) into a single tight band before entering the resolving gel. This permits the proteins to commence separating according to their mass at the same starting point. The stacking gel has a larger pore size (typically resulting from a lower percentage acrylamide content) which allows larger proteins to move quicker and stack with smaller proteins. When a current is applied, the three anions enter the stacking gel, however they move at different speeds. The chloride ions move the quickest and the glycine/tricine moves slightly slower than the proteins. This traps the proteins between the chloride ions and the glycine/tricine, with the glycine/tricine "pushing" the proteins into the desired narrow bands. The lower pH (6.8) of the stacking gel is key, as this phenomenon is dependent on the pH. When the anions reach the higher pH of the resolving gel (pH 8), the glycine/tricine becomes more ionised and therefore, along with the chloride ions, migrates quicker than the protein. This allows the SDS-protein complexes to migrate based on size as a result of the pores in the acrylamide and not a result of their charge.

2.6.1 Tris-Glycine System

Method: Tris-glycine SDS-PAGE gels were cast with a either a 10 or12% resolving gel and (depending on the mass of protein of interest) a 4% stacking gel. Gels were loaded into gel running apparatus (Bio-Rad Mini-PROTEAN Tetra cell), and running buffer added.

SDS-PAGE samples are prepared by mixing 4 parts sample with 1 part 5x laemmli buffer. For denatured samples, a hotblock was used to heat at 100ºC for 3 minutes.

Prepared samples (10-25 µL) are then loaded into the SDS-PAGE gel at ran at 100 V for 10 minutes to allow the samples to stack, and then 160-190 V until the bromophenol blue dye front reached the bottom of the gel.

Protein was subsequently visualised by either Coomassie staining, silver staining or Western blot (chapter 2.6.3, 2.6.4 and 2.6.5, respectively).

<u>Lower Gel</u>
375 mM Tris pH 8, 0.1% (w/v) SDS, 10 or 12% (v/v) Acrylamide/Bis

Upper Gel

125 mM Tris pH 6.8, 0.1% (w/v) SDS, 4% (v/v) Acrylamide/Bis

Ammonium Persulphate (APS)

0.2% (w/v) APS

5x Laemmli (Sample) Buffer

625 mM Tris pH 6.8, 50% (v/v) Glycerol, 10% (w/v) SDS, 5% (v/v) β mercaptoethanol, 0.025% Bromophenol blue

Running buffer

25 mM Tris, 192 mM Glycine, 0.1% (w/v) SDS

2.6.2 Tris-Tricine System

Method: Tris-tricine SDS-PAGE gels were cast with a 20% resolving gel and a 4% stacking gel. Once cast, gels were either used or stored wrapped in damp blue roll at 4°C overnight. Gels were loaded into gel running apparatus (Bio-Rad Mini-PROTEAN Tetra cell), and running buffer added with the cathode buffer going between the the two gels and the anode buffer filling the rest of the tank. The tank was placed in a tray of ice prior to running to prevent overheating.

Samples were prepared by mixing in equal parts with 2x sample buffer, and heating to 60°C for 3 minutes. Samples were loaded into the gel, 10 µL per well. Gels were ran at 200 V until the dye front reached the bottom of the gel, typically 2 hours.

Tris-tricine gels were analysed by silver staining as described in chapter 2.6.4.

Lower Gel

1 M Tris pH 8.45, 333 mM HCl, 0.1% (w/v) SDS, 20% (v/v) Acrylamide/Bis

Upper Gel

1 M Tris pH 8.45, 333 mM HCl, 0.1% (w/v) SDS, 4% (v/v) Acrylamide/Bis

Ammonium Persulphate (APS)

0.1% (w/v) APS

2x Sample Buffer

150 mM Tris pH 7, 30% (v/v) Glycerol, 12% (w/v) SDS, 0.05% Coomassie G-250

Running buffer - Anode

100 mM Tris pH 8.9, 22.5 mM HCl

Running buffer - Cathode

100 mM Tris pH 8.25, 100 mM Tricine, 0.1% (w/v) SDS

2.6.3 Coomassie Staining

Background: Coomassie Brilliant Blue refers to two similar dyes, R-250 and G-250, which differ by the presence of two additional methyl groups on G-250. Despite both being blue dyes, G-250 has a more green tint whereas R-250 has a more red tint. Both dyes can be used to stain proteins, and this project utilised G-250. Coomassie dyes are able to bind to proteins through non-covalent interactions between sulphonic groups in the dye and amine groups within the protein.

Method: Following SDS-PAGE, the gels are briefly rinsed in ddH_2O and placed directly into Coomassie stain for 1 hour at room temperature on a rocker. There is no need for fixation as the stain contains the fixative, acetic acid.

Following staining, the gel is placed into destain solution for at least 1 hour with multiple changes of solution, until background staining is removed and the bands are clearly visible.

Coomassie Stain

50% (v/v) methanol, 10% (v/v) acetic acid, 0.25% (w/v) Brilliant Blue G-250

Destain Solution

40% (v/v) methanol, 5% (v/v) acetic acid

2.6.4 Silver Staining

Background: Silver staining is a sensitive method to stain for all proteins on a gel, typically 10-100 times more sensitive than Coomassie staining. The principle behind the stain is that silver ions from the silver nitrate solution are able to bind to various side groups in various amino acids, which are then reduced to elemental silver during development. The reaction can be stopped by introducing EDTA which can chelate any unreduced silver ions.

Method: Following SDS-PAGE, the gels are briefly rinsed in ddH_2O and placed in fixing solution for 1 hour. Following fixation, the gels are place in sensitising solution for an hour before rinsing 3 times for 5 minutes each. The gels are then placed in the silver nitrate solution for 30 minutes, before rinsing twice for 1 minute each and placing in developing solution. The gels are allowed to develop until clear bands are observed and then the reaction is stopped to prevent excessive background. All steps were undertaken at room temperature on a rocker.

Fixing solution

For Tris-Glycine gels: 40% (v/v) ethanol, 10% (v/v) acetic acid in ddH_2O

For Tris-Tricine gels: 12% (w/v) trichloroacetic acid (TCA), 30% (v/v) methanol in ddH_2O

Sensitising solution

30% (v/v) ethanol, 6.8% (w/v) sodium acetate, 0.2% (w/v) sodium carbonate, 0.125% (v/v) glutaraldehyde in ddH_2O

Silver nitrate solution

0.25% (v/v) silver nitrate, 0.0148% (v/v) formaldehyde in ddH_2O

Developing solution

2.5% (w/v) sodium carbonate, 0.029% (v/v) formaldehyde in ddH_2O

Reaction stopping solution

1.5% (w/v) EDTA in ddH_2O

2.6.5 Western blotting

Background: Western blotting is a protein visualation technique which utilises antibodies to specifically stain for target proteins of interest, unlike Coomassie or silver staining which simply stain for all present proteins. Following SDS-PAGE, the separated proteins are transferred from the gel to a membrane (either Polyvinylidene fluoride (PVDF) or nitrocellulose) which is then blocked with protein (usually BSA or milk proteins) before "probing" with a primary antibody specific to a protein of interest. After the primary antibody is allowed to bind to its target protein and excess is washed away, the antibody is detected. The most common detection method is to use a secondary antibody conjugated to horseradish peroxidase (HRP) enzyme which is specific to the species of primary antibody, for example "anti-mouse-HRP" or "anti-rabbit-HRP". After the secondary antibody is bound to the primary antibody and the excess washed away, the HRP is detected by a method known as enhanced chemiluminescence (ECL). HRP is able to convert the chemiluminescent substrate luminol into oxidised luminol in the presence of hydrogen peroxide, a chemical reaction that produces light which can be observed on X-ray film on in an imaging hood. The amount of light observed is relative to the amount of protein in the band, therefore Western blotting is a semi-quantitative method within a specific blot.

Method: A semi-dry transfer method was utilised in the project. Following SDS-PAGE, the gel was equilibrated in transfer buffer for two minutes before placement in a transfer stack. The transfer stack consists of two pieces of transfer buffer-soaked blotting paper, methanol-activated PVDF membrane, the polyacrylamide gel, and two more pieces of transfer buffer-soaked blotting paper. The stack was placed in an electroblotter from Bio-Rad (Hercules, USA) and the electroblotting was undertaken at 80 mA per gel for 1.5 hours.

Following transfer, the PVDF membrane was blocked for 1 hour at room temperature in either 5% BSA in Tris-buffered saline (TBS)-Tween (T) or 5% nonfat dry milk (Marvel brand) in TBS-T, depending on antibody preferences. Typically, 5% BSA was only used for antibodies which recognised phosphorylated proteins.

The membranes were subsequently incubated overnight at 4°C with the primary antibody at the manufacturer-recommended concentration, before washing in TBS-T and incubating with the appropriate HRP-conjugated secondary antibody (Dako, Agilent Technologies, Santa Clara, USA) for 1 hour at room temperature. Membranes were then washed in TBS-T prior to ECL detection using an ECL kit (GE Healthcare). The blots were then visualised using a Gbox EF Gel Documentation System with Genesnap software by Syngene (Cambridge, UK).

Tris Buffered Saline – Tween (TBS-T)

10 mM Tris pH 7.4, 150 mM NaCl, 0.1% (v/v) Tween 20

Transfer buffer

39 mM Glycine, 48 mM Tris, 0.0325% (w/v) SDS and 20% (v/v) methanol

2.6.5.1 Densitometric analysis (densitometry)

Densitometric analysis of Western blot allows for semi-quantification of band intensity and statisitical analysis to be undertaken. For analysis, high quality exported Tagged Image File Format (TIFF) were loaded into ImageJ software (National Institutes of Health, Bethesda, USA). Individual lanes were subsequently highlighted, background removed, and relative band intensity calculated. Intensities were normalised to appropriate loading control, typically GAPDH.

2.7 Agarose gel electrophoresis

Background: Agarose gel electrophoresis is used to visualise double-stranded DNA by first separating out different sized DNA in a sample by electrophoresis, and then visualising the gel by methods such as staining with a UV-sensitive dye (e.g. ethidium bromide) which can intercalate with double-stranded DNA.

Method: For a 1% gel, 1 g of agarose was measured out and dissolved in 100 mL TAE buffer and dissolved by microwaving until boiling. The liquid agarose solution was allowed to cool for 5-10 minutes and 1 µL ethidium bromide (at 10 mg/mL) was added and mixed. The solution was then placed into a gel tray and an appropriate comb added to form the wells. Once fully cooled, the gel set and was placed into a running tank and

filled with TAE buffer and the comb removed. Additional ethidium bromide (1 µL per 100 mL TAE) was added to the TAE buffer in the running tank and the samples loaded into the appropriate wells. The lid was then placed on the tank, and the gel ran at 80-110 V for 30-60 minutes, or until the dye front migrated an appropriate distance.

The gels were then visualised using a Gbox EF Gel Documentation System with Genesnap software (Syngene).

TAE buffer

40 mM Tris-base, 0.11% (v/v) Acetic acid, 1 mM EDTA in ddH_2O

2.8 Reverse-Transcription (RT) Real-time (q)PCR

2.8.1 mRNA extraction from monolayer cell culture

Background: In order to measure gene expression from cells in culture, the cells must first be lysed and the mRNA stabilised. Multiple methods exist to extract mRNA from cells, such as phenol-chloroform extraction or commercially available cell lysis and mRNA stabilisation buffers.

Reagents:

- Cells-to-cDNA II Cell Lysis Buffer (Thermo Fisher)

Method: For gene expression experiments, cells were typically cultured in 96-well plates. For mRNA extraction, all steps were performed on ice. Culture medium was aspirated from the cells, and each well washed with 200 µL of ice-cold PBS. After aspirating off the PBS, 30 µL of Cells-to-cDNA II Cell Lysis Buffer was added per well. Lysis was assisted by scratching with pipette tips on a multichannel pipette, before transferring the buffer/lysate mixture to a 96-well PCR plate. The lysates are then heated at 75°C for 10 minutes in a PCR thermocycler. Lysates were then stored at -80°C until required.

2.8.2 mRNA extraction from 3D cell culture

See chapter 3.2.2

2.8.3 Reverse Transcription

Background: In order to quantify gene expression, the extracted mRNA must first be converted into complementary (c)DNA, which is the DNA equivalent of the mRNA transcripts, thus differs from the genomic (g)DNA in that the introns have been spliced out.

Reagents:

- Moloney Murine Leukemia Virus Reverse Transcriptase (MMLV RT), 200 units/µL (Thermo Fisher)
- Random Hexamers (NNN NNN), 0.2 µg/µL (Integrated DNA Technologies, Coralville, USA)
- dNTPs, 2.5 mM each
- 100 mM Dithiothreitol (DTT) (Thermo Fisher)
- 5x First Strand buffer (250 mM Tris-HCl (pH 8.3), 375 mM KCl, 15 mM Magnesium Chloride) (Thermo Fisher)
- RNaseOUT™ Recombinant Ribonuclease Inhibitor, 40 units/µL (Thermo Fisher)

Method: Mix 1 (3 µL dNTPs, 1 µL random hexamers per well) and mix 2 (4 µL 5x first strand buffer, 2 µL DTT, 0.125 µL RNase OUT, 0.5 µL MMLV, 1.375 µL ddH_2O per well) made up for the required number of wells and placed on ice. 4 µL of mix 1 was added per well of a 96-well PCR plate, followed by 8 µL per well of cell lysates from chapter 2.8.1. The mixture was then incubated in a thermocycler at 70ºC for 5 minutes. The PCR plate was then instantly placed on ice and incubated for 2 minutes before adding 8 µL of mix 2 per well. The mixture plate was then centrifuged at 300 x g for 30 seconds to mix and the reverse transcription reaction undertaken in a thermocyler: 37°C for 50 minutes, followed by 70°C for 15 minutes. The resulting cDNA was then stored at -20°C (long-term) or 4°C (short-term). Prior to use in quantitative (q)PCR assays, the cDNA was diluted by adding 30 µL ddH_2O per well.

2.8.4 TaqMan® qPCR

Background: The TaqMan method of qPCR utilises a sequence-specific probe of the amplicon. The probe is a short oligonucleotide sequence with a fluorophore coupled to the 5’ end and a fluorescence quencher molecule at the 3’ end. The qPCR machine uses

a laser to excite the fluorophore, however when the probe is intact, the quencher quenches the emitted light and no fluorescence is observed. The probe binds to the template strand of cDNA and as the Taq polymerase extends the new strand, its 5' to 3' exonuclease activity cleaves the probe, thus separating the fluorophore from the quencher and a signal can be detected. The accumulated fluorescence is therefore directly proportional to the amount of generated product in the qPCR reaction.

Reagents:

- TaqMan® Gene Expression Master Mix (Applied Biosystems, Thermo Fisher)
- TaqMan™ Fast Advanced Master Mix (Applied Biosystems, Thermo Fisher)

Method: A mastermix for the required number of wells is made containing 4.5 µL of either Taqman gene expression mastermix (2x) (normal assay) or Fast Advanced Master Mix (2x) (fast assay), 0.2 µL of each forward and reverse primer (30 µM) and 0.1 µL probe (10 µM) per reaction. 5 µL of mastermix was added per well of an optical bottom 96-well qPCR plate (Applied Biosystems, Thermo Fisher). 5 µL of cDNA was then added per well and the plate given a 30 second spin at 300 x g to mix.

Cycling conditions (normal assay):

1. Initial denaturation stage of 95ºC 10 minutes
2. 40 cycles of 95ºC for 15 seconds, 60ºC for 60 seconds

Cycling conditions (fast assay):

1. Initial denaturation stage of 95ºC 30 seconds
2. 40 cycles of 95ºC for 1 second, 60ºC for 15 seconds

Table 2.6: Primers and probes for TaqMan assays, human genes

Gene	Sequence (5' - 3')
18S	Forward: CGAATGGCTCATTAAATCAGTTATGG Reverse: TATTAGCTCTAGAATTACCACAGTTATCC Probe: Fam-TCCTTTGGTCGCTCGCTCCTCTCCC-Tamra
GAPDH	Forward: GTGAACCATGAGAAGTATGACAAC Reverse: CATGAGTCCTTCCACGATACC Probe: Fam-CCTCAAGATCATCAGCAATGCCTCCTG-Tamra

MMP1	Forward: AAGATGAAAGGTGGACCAAAATT Reverse: CCAAGAGAATGGCCGAGTTC Probe: Fam-CAGAGAGTACAACTTACATCGTGTTGCGGCTC-Tamra
MMP13	Forward: AAATTATGGAGGAGATGCCCATT Reverse: TCCTTGGAGTGGTCAAGACCTAA Probe: Fam-CTACAACTTGTTTCTTGTTGCTGCGCATGA-Tamra
ATF3	Forward: TTTGCCATCCAGAACAAGC Reverse: CATCTTCTTCAGGGGCTACCT Probe: Probe #53 (Roche Probe Library, Roche, Basel, Switzerland)
CXCL8	Forward: AGACAGCAGAGCACACAAGC Reverse: AGGAAGGCTGCCAAGAGAG Probe: Probe #72 (Roche Probe Library)

For bovine *HPN* and *ST14*, TaqMan gene expression assay on demands were utilised.

2.8.5 SYBR green qPCR

Background: In contrast to the TaqMan method of qPCR where a sequence-specific probe is utilised to monitor the PCR amplification, SYBR green is a dye that simply binds to any double stranded DNA as is generated by the PCR reaction. As such, SYBR green PCR is not as specific as TaqMan, and more care must be taken to validate assays. This validation is in the form of a dissociation curve which occurs at the end of the amplification. The dissociation, or melt, curve gives an indication of the number of amplification products (there should only be one) and also indicates whether primer-dimers have occurred. The thermocycler begins the curve at a temperature below the T_m, and gradually increases to 95°C, the idea being that different products will melt at different temperatures thereby confirming the presence of a single amplicon.

SYBR green qPCR was utilised to measure expression levels of bovine genes in this project.

Reagents:

- Platinum® SYBR® Green qPCR SuperMix-UDG (Thermo Fisher)

Method: A mastermix for the required number of wells is made containing 10 µL Platinum® SYBR® Green qPCR SuperMix-UDG (2x), 0.4 µL of each forward and reverse primer (10 µM) and 5.2 µL H_2O per reaction. 16 µL of mastermix was added per well of an optical bottom 96-well qPCR plate. cDNA (4 µL) was then added per well and the plate given a 30 second spin at 300 x g to mix.

Cycling conditions:

1. UDG incubation stage of 50ºC 2 minutes
2. Initial denaturation stage of 95ºC 2 minutes
3. 40 cycles of 95ºC for 15 seconds, 60ºC for 60 seconds
4. Melt curve analysis

Table 2.7: Primers SYBR green assays, bovine genes

Gene	Sequence (5' - 3')
GAPDH	Forward: CCATCTTCCAGGAGCGAGAT
	Reverse: TCACGCCCATCACAAACATG
FOS	Forward: AAACCATGACAGGAGGCAGA
	Reverse: TCTAGTTGGTCTGTCTCCGC
JUN	Forward: TATGCTCAGGGAACAGGTGG
	Reverse: TCTGTTTCCCTCTCGCAACT
CSRNP1	Forward: TCACTCCCCTGTCCATTCTG
	Reverse: GCTTGCTCCTGGGTAAACTC
EGR2	Forward: AGGCCGTAGACAAAATCCCA
	Reverse: GTTGATCATGCCATCTCCGG
ATF3	Forward: CCTGCAGAAAGAGTCGGAGA
	Reverse: GGTTCCTCTCATCTTCCGGA
MMP1	Forward: TACACCCCAGACCTGTCAAG
	Reverse: TGTCACGATGATCTCCCCTG
MMP13	Forward: AGTCTCTCTATGGTCCAGGA
	Reverse: CATAGGCGGCATCAATACGG
F2RL1	Forward: CCGTCCCAGGAAACAAGTCT
	Reverse: CGGGGTGCTTCTTCTTTGTT

2.9 LIVE/DEAD® Viability/Cytotoxicity Assay

To test viability of cells following loading, a LIVE/DEAD® Viability/Cytotoxicity Kit for mammalian cells (Molecular Probes, Thermo Fisher) was utilised.

Background: The assay consists of two probes to simultaneously stain for both live and dead cells within a population. Live cells are measured by calcein-AM, a non-fluorescent precursor which can enter cells but is only cleaved to fluorescent calcein (λ_{ex} ~494 nm, λ_{em} ~517 nm) by intracellular esterase in cells which are alive. Dead cells are measured by ethidium homodimer (EthD-1), which can enter only cells with damaged membranes and fluoresces (λ_{ex} ~528 nm, λ_{em} ~617 nm) when bound to nucleic acid.

2.9.1 3D cell culture

Method: Prior to carrying out the assays on loaded cells, the concentrations of calcein-AM and EthD-1 required to stain BNCs in agarose to give optimal signal were determined experimentally, testing a range of concentrations of both probes (0.1 µM to 10 µM) on both live cells and cells killed using 70% methanol. Both probes were added to cells separately in PBS and incubated for 45 minutes at 37ºC.

Using this method, the optimal concentrations of probe to stain BNCs in agarose were 0.5 µM calcein-AM and 1 µM EthD-1 (data not shown). To expore the effect of loading on cell death, a small sample of the loaded construct was removed and washed in PBS, and subsequently incubating in PBS containing 0.5 µM calcein-AM and 1 µM EthD-1 for 45 minutes at 37ºC. Fluorescence was measured on a Zeiss Axiovert 200M inverted microscope (Carl Zeiss AG, Oberkochen, Germany).

2.9.2 Monolayer cell culture

Cells were plated in black-walled clear bottom 96-well plates. Cells were treated according to the conditions to be tested in terms of other assays of interest. To measure cell viability, only live cells were assayed using calcein-AM.

Cells to be assayed were PBS-washed, and 100 µL per well of 2.5 µM calcein-AM in PBS was added. The plate was placed into a FLUOstar Optima fluorometer (BMG labtech, Ortenberg, Germany) set to 37°C. The assay was carried out, monitoring

fluorescence progress at λ_{ex} 480 nm and λ_{em} 520 nm. The slope was taken for each condition and normalised to the negative control. As a positive control, cells were pre-treated for 30 minues with 70% methanol.

2.10 PAR2 overexpression in SW1353 cells

2.10.1 Stable transfection with expression plasmid

Background: The production of cell lines which express an expression plasmid in a stable manner is a commonly used laboratory technique with major advantages over the transient transfection of cells. The plasmid is transfected into the cells, where a selection marker, normally antibiotic restistance, is utilised to select only cells integrating the plasmid, killing off cells which have not integrated it. The major advantage over transient transfection is that low transfection efficiency is overcome by removing untransfected cells, resulting in a population of cells all of which overexpress the gene of interest. Futhermore, the cells subsequently behave like normal cells and can be passaged and plated out as such, without the need for repeated transient transfections, saving on time and expensive transfection reagents.

2.10.1.1 Cloning of FLAG-PAR2 into pcDNA3.1(+) vector

In order to clone the PAR2 gene (*F2RL1*) into the pcDNA3.1(+) vector, In-Fusion cloning was utilised (Clontech). Primers were designed in order to amplify the full-length *F2RL1* gene whilst simultaneously adding an N-terminal FLAG tag and overhangs with the plasmid cut sites. The pcDNA3.1 vector contains an ampicillin resistance gene for bacterial selection, and a neomycin resistance gene for mammalian cell selection.

The full-length *F2RL1* gene was obtained commercially (R&D Biosystems, Minneapolis, USA, catalogue #RDC0166) stored in a shuttle vector. A cloning strategy was developed by designing primers containing an overhang for the pcDNA3.1(+) vector, a kozak sequence in the forward primer, a FLAG tag in the forward primer and then an overhang for the *F2RL1* gene starting at the second amino acid position.

Primers:

Forward 5’ to 3’:

TACCGAGCTCGGATC-GCCACC-ATGGACTACAAGGATGACGATGACAAG-CGAAGTCCTAGTGCT

Reverse 5’ to 3’:

AAACGGGCCCTCTAG-TTAATAGGAGGTCTTAACAG

The sequences are coloured orange for pcDNA3.1(+) overhang, blue for kozak sequence, purple for FLAG tag, and green for *F2RL1* gene overhang.

Using the above primers, the *F2RL1* gene was amplified using Q5 polymerase (New England Biolabs) by performing a reaction containing 1 ng of template DNA (the *F2RL1* gene), 0.2 mM dNTPs, 0.5 µM of each forward and reverse primer and 0.5 units of Q5 polymerase, in Q5 polymerase buffer.

Cycling conditions:

1. Initial denaturation stage of 98ºC 30 seconds
2. 30 cycles of 98ºC for 10 seconds, 56ºC for 15 seconds and 72ºC for 15 seconds
3. Final elongation of 72ºC for 2 minutes

The pcDNA3.1(+) vector was double digested with the restriction enzymes XbaI and BamHI by incubating 1 µg of the vector with 20 units each restriction enzyme in 50 µL reactions with NEB buffer 3.1 at 37°C for 4 hours. Single digest control reactions were also carried out.

Following the restriction digests and PCR, samples were subjected to agarose gel electrophoresis to confirm successful digest and amplification (Figure 2.2), and the products were subsequently purified using a PCR clean up kit (Qiagen).

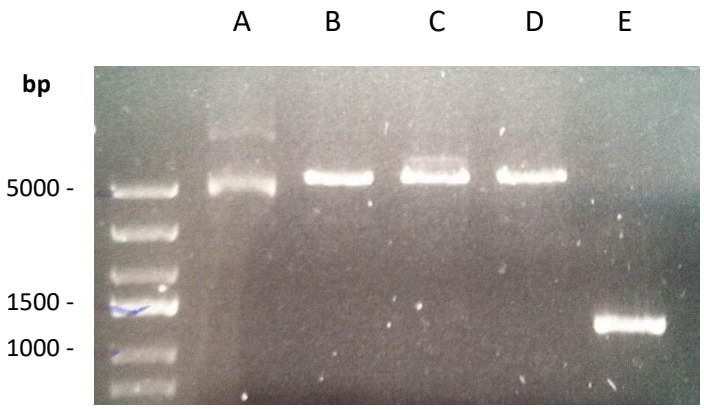

Figure 2.2: pcDNA3.1(+) digests and *F2RL1* insert
1% Agarose gel with pcDNA3.1(+) uncut (A), BamHI/XbaI double digest (B), BamHI single digest (C), XbaI single digest (D) and the PCR product encoding the kozak-FLAG-*F2RL1* insert (E).

The kozak-FLAG-*F2RL1* insert was ligated into the digested pcDNA3.1(+) vector using an In-Fusion cloning kit (Clontech) by incubating 50 ng of cut vector and 100 ng of insert with the kit components in a 10 µL reaction at 50°C for 15 minutes, according to the manufacturer's instructions.

The product was then transformed into "Stellar" *E. coli* (Clontech), by adding 2.5 µL of product into 50 µL of bacteria, and incubating for 30 minutes on ice. The transformation was then undertaken by heat shock (incubation at 42°C for 45 seconds), and then placed back on ice for 2 minutes. SOC medium (500 µL) (Clontech) prewarmed to 37°C was then added and the cells incubated at 37°C for 1 hour at 225 RPM in an orbital incubator. The bacteria were then incubated on LB agar plates supplemented with 100 µg/mL ampicillin overnight at 37°C. A control transformation was also undertaken.

Colony PCR reactions were performed to screen colonies for successful ligation reactions. Fourteen colonies were selected, and samples were obtained by touching the colony with a 20 µL pipette tip and then placing the tip in an Eppendorf tube containing 100 µL sterile water. The tubes were then heated for 3 minutes at 98°C to lyse the bacteria and release the DNA.

PCR reactions were set up by creating a mastermix and then adding 1 µL of the bacterial DNA-containing water to each reaction. The final reaction components per reaction were 0.3 mM dNTPs, 0.5 µM of each forward and reverse primers, 1.5 mM $MgCl_2$, 0.25 units recombinant Taq polymerase (Thermo Fisher) in the supplied buffer. The primers were

mismatched between the pcDNA3.1(+) vector (T7 promoter) and the *F2RL1* gene so that products would indicate successful ligation.

Primers:

Forward 5' to 3':

TAATACGACTCACTATAGGG

Reverse 5' to 3':

AGAGAGGAGGTCAGCCAAGG

Cycling conditions:

1. Initial denaturation stage of 94ºC 2 minutes
2. 35 cycles of 94ºC for 45 seconds, 42ºC for 30 seconds and 72ºC for 90 seconds
3. Final elongation of 72ºC for 10 minutes

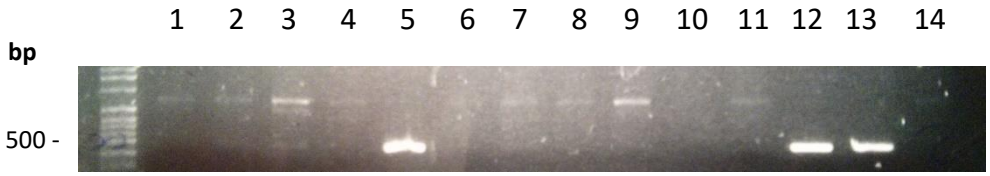

Figure 2.3: Colony PCR of pcDNA3.1(+)-FLAG-*F2RL1*
A 1% Agarose gel was run with the 14 colony PCR reaction products. The expected band size for successful ligation is 469bp, as observed in lanes 5, 12 and 13.

The colony PCR yielded three successful ligation bands (Figure 2.3), and colonies 5 and 12 were selected to further grow up and maxiprep. LB medium (250 mL) supplemented with 100 µg/mL amplicillin innoculated by each colony was grown overnight at 37°C at 225 RPM in an orbital incubator. Plasmid DNA was extracted using the PureYield™ Plasmid Maxiprep System (Promega) according to the manufacturer's instructions. A sample of each clone was sent for sequencing (Source Bioscience) which confirmed successful inframe cloning.

2.10.1.2 Optimisation of G418 concentration

In order to optimise the concentration of G418 to utilise on SW1353 cells, a kill curve was generated. SW1353 cells were cultured in black walled clear bottom 96-well plates and a titration of G418 100-1000 µg/mL was performed.

Reagents:

- DMEM-F12, supplemented with 10% FBS and 2 mM L-glutamine but no antibiotics.
- G418, stored dessicated then made up to 50 mg/mL in ddH_2O, filtered with 0.22 µm PES filter and stored at 4ºC for up to 3 months.

G418 was made up in DMEM-F12 at the desired concentration and 200 µL added per well. Cells were cultured at 37ºC in 5% CO_2 for either 3, 7, 10 or 14 days with medium replaced with freshly made medium at each time point.

In order to measure cell survival, a calcein-AM assay was undertaken as in chapter 2.9.2. Data were normalised to the negative control which was assumed to have 100% survival. A dose of 400 µg/mL was chosen based on the pcDNA3.1 vector manufacturer manual which stated that the minimum dose of G418 that kills the cells after 7 days should be used (Figure 2.4).

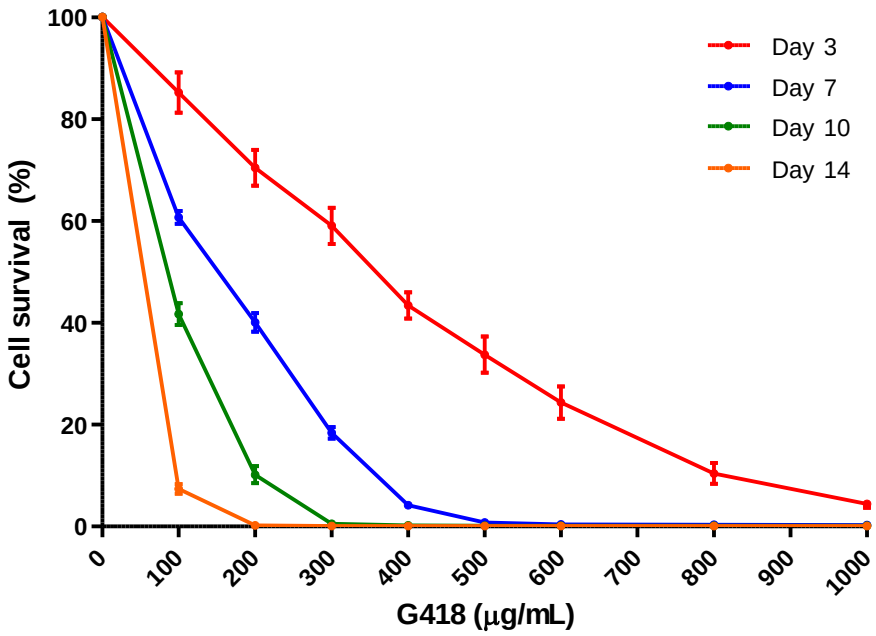

Figure 2.4: SW1353 sensitivity to G418
G418 was titrated onto SW1353 cells and cultured for up to 14 days. Cell survival was measured using a calcein-AM.

2.10.1.3 Stable transfection of pcDNA3.1_FLAG-PAR2

Reagents:

- DMEM-F12, supplemented with 10% FBS and 2 mM L-glutamine but no antibiotics.
- G418, stored desiccated then made up to 50 mg/mL in ddH_2O, filtered with 0.22 µm PES filter and stored at 4ºC for up to 3 months.

In order to create a stable cell line with pcDNA3.1, the plasmid was first linearised by digestion with BglII, as this restriction site is not located in an important region of the plasmid. A 100 µL reaction was set up containing 10 µg of pcDNA3.1_FLAG-PAR2 and 50 units of BglII in buffer 3 (New England Biolads, Ipswich, USA) which was incubated for 4 hours at 37°C. A 1% agarose gel was run to confirm successful digestion and the product was purified using a PCR clean up kit (Qiagen).

Two 60 mm dishes were plated with $2x10^5$ SW1353 cells each, and incubated overnight, before transfection was undertaken. Cells were transfected using FuGene HD transfection reagent according to the manufacturer's instructions. Plasmid DNA (2.75 µg) was used at a 1:3 ratio with 8.25 µL FuGene HD. A control transfection was also undertaken with water:Fugene HD.

Medium was replaced with fresh SW1353 cell culture medium 24 hours post-transfection, and with selective medium (400 µg/mL G418 in DMEM-F12, supplemented with 10% FBS and 2 mM L-glutamine but no antibiotics), 48 hours post-transfection. Selective medium was replaced every 2-3 days until the control transfection cells were all dead, and the pcDNA3.1_FLAG-PAR2 cells were 90% confluent. The dish was split 1:6 into 6 wells of a 6-well plate, and allowed to grow to 90% confluence. Each well was split into a T25 flask which was allowed to grow to 90% confluence, and then each flask was split into a T75 flask. A sample of each of the 6 clones was taken and lysed, and PAR2 Western blot analysis performed. The clone with the highest expression of PAR2 was selected for use in this project (data not shown).

2.10.2 Transient transduction with leniviral vector

Background: Lentiviral vectors use a highly modified version of the HIV-1 virus to introduce foreign DNA into the genome of cells. Numerous modifications have been

made on the native HIV-1 virus for use in gene delivery, removing multiple hazards including pathogenicity.

The majority of modern lentiviral expression systems are referred to as being either "second"- or "third"-generation. These are both highly safe and efficient lentiviral systems, however the third-generation introduces additional safety features, although they are more difficult to work with. As such, this project utilised a second-generation system.

A second-generation lentiviral expression system consists of three plasmids: an expression plasmid, in which the gene to be overexpressed is cloned into, a packaging plasmid (e.g. pCMV-dR8.91) and an envelope plasmid (e.g. pMD2.G) which produce virion proteins (the third-generation system splits the packaging components into three plasmids). The three plasmids are co-transfected into HEK293T cells, which then package live viral particles, which may then be collected and concentrated for subsequent use in lentiviral transduction experiments.

The PAR2-expressing and empty vector control lentiviruses were provided by Dr Chun Ming Chan, Newcastle University. The lentiviral expression plasmid utilised to construct the virus was pHR'-SINcPPT-SIEW (hereafter pSIEW). The vector drives gene of interest expression via a spleen focus-forming virus (SFFV) promoter, and also expresses enhanced green fluorescent protein (EGFP), produced as a separate protein from a single transcript as a result of an internal ribosome entry site (IRES) between the cloning site and the EGFP gene. The vector also contains other lentiviral elements, such as a central polypurine tract (cPPT), a Woodchuck hepatitis virus post-transcriptional Regulatory Element (WPRE), and the HIV Rev response element (RRE). Lentiviruses expressing either PAR2 (pSIEW_PAR2) or empty vector control (pSIEW_Empty) were produced by co-transfecting HEK293T cells with plasmids containing the remaining components required for producing active virion particles. Active virus was harvested, concentrated and stored at -80°C.

Reagents:

- Polybrene, 8 mg/mL, stored at -20°C
- Heat-inactivated (HI)-FBS, made by heating FBS at 56°C for 30 minutes
- Complete HI-DMEM-F12, supplemented with 10% HI-FBS, 100 IU/mL penicillin, 100 µg/mL streptomycin and 2 mM L-glutamine

- SFM, DMEM-F12, supplemented with 100 IU/mL penicillin, 100 µg/mL streptomycin and 2 mM L-glutamine

Method: SW1353 cells were seeded into appropriate cell culture plate at a seeding density of 30,000 cells/cm^3 and allowed to adhere overnight. On the day of transduction, cells were expected to be at 50% confluency. Transduction was undertaken by supplementing complete HI-DMEM-F12 with 4 µg/mL polybrene, then thawing out lentivirus and diluting in the supplemented medium at 1:200. The mixture was then added to the cells at an appropriate volume for the plate used (100 µL/well in 96-well plate and 1000 µL/well in 12-well plate). Cells were then cultured for 48 hours at 37°C, 5% CO_2 before checking EGFP expression using an inverted fluorescence microscope. Following confirmation of successful transduction by EGFP expression, cells were serum-starved overnight in SFM and subsequently used for experimentation.

2.11 Calcium mobilisation assay

Background: Activation of Gαq-coupled GPCRs results in Ca^{2+} flux which acts as a second messenger to transduce signal downstream within the cells. In order to assay for GPCR activation, Ca^{2+} flux can be measured utilising fluorescent Ca^{2+}-binding probes. Multiple probes exist, and this project utilised Rhod-4 AM, a fluorescent probe with excitation and emission wavelengths towards the red end of the spectrum. This probe was chosen as the lentiviral construct expresses GFP which would interfere with assays in the green part of the spectrum (such as Fluo-4 AM).

Reagents:

- Hank's Balanced Salt Solution (HBSS)
- 1 M HEPES, pH 7 in ddH_2O
- HEPES-buffered Hank's Balanced Salt Solution (HHBS), HBSS supplemented with 20 mM HEPES, pH 7
- 2 M $CaCl_2$ in ddH_2O
- HHBS (2 mM Ca^{2+}), HHBS supplemented with 2 mM $CaCl_2$
- 25 mM Probenecid (Santa Cruz Biotechnology, Dallas, USA), 72 mg dissolved in 300 µL 1 M NaOH, made up to 10 mL with HHBS (2 mM Ca^{2+})
- 20% Pluronic F-127 (Thermo Fisher), in DMSO

2.5 mM Rhod-4 AM (Santa Cruz Biotechnology), in DMSO, stored at -20ºC, protected from light
2 mM Ionomycin (Santa Cruz Biotechnology), in DMSO

Method: Cells transduced with PAR2-expressing lentivirus (chapter 2.10.2) in a black-walled clear bottom 96-well plate were washed with 200 µL HHBS (2 mM Ca^{2+}). Rhod-4 AM was made up to 5 µM in HHBS (2 mM Ca^{2+}) supplemented with 2.5 mM probenecid and 0.02% pluronic F-127. Pluronic F-127 helps to increase the solubility of the probe, whereas probenecid is an inhibitor of organic-anion transporters within the cell membrane and thus helps to prevent the export, and therefore loss, of the probe. Rhod-4 AM (50 µL) was added to each well and the plate incubated at room temperature in the dark for 45 minutes.

Following Rhod-4 AM loading, the cells were washed with 200 µL HHBS (2 mM Ca^{2+}), and then incubated in 100 µL HHBS (2 mM Ca^{2+}) for 20 minutes at room temperature to allow for complete de-esterfication of the probe. Meanwhile, the flourometer (FLUOstar OPTIMA, BMG labtech) was prepared for the assay. Both injection pumps were primed with 2 mL of HHBS (2 mM Ca^{2+}), before priming in 1 mL of test compounds. Test compound in pump A was always at 2x final concentration, whereas test compound in pump B was at 3x final concentration.

Following de-esterfication of the probe, each well was replaced with 30 µL HHBS (2mM Ca^{2+}), and placed in the fluorometer pre-heated to 37ºC. The flurometer was programmed to read in single-well mode with a reading taken every second at λ_{ex} 520 nm and λ_{em} 590 nm. Per well, a baseline was established for 10 seconds before 30 µL from pump A was injected, then at 90 seconds, 30 µL from pump B was injected. Readings were taken up to 120 seconds before moving onto the next well.

2.12 PAR-2 Activation and Disarming Assays

To test the effect of proteases and peptides on PAR2-expressing SW1353 cells, activation and disarming experiments were undertaken, measuring various downstream outcomes.

Cells were seeded according to the requirements of the experiment and the method of over expression. For gene expression studies by RT-qPCR and calcium mobilisation

assays, cells were plated in 96-well plates. For experiments requiring Western blotting, either 6 or 12-well plates were used. Prior to carrying out experiment, cells were serum-starved overnight.

Reagents:

- SFM, DMEM-F12, supplemented with 100 IU/mL penicillin, 100 µg/mL streptomycin and 2 mM L-glutamine
- HEPES-buffered Hank's Balanced Salt Solution (HHBS), HBSS supplemented with 20 mM HEPES, pH 7

2.12.1 Matriptase and SLIGKV activation assays

Matriptase and SLIGKV activation assays consisted of simulating PAR2-overexpressing cells which had been serum-starved overnight, with either matriptase or SLIGKV and analysing by various methods.

For all assays except those measuring calcium mobilisation, matriptase or SLIGKV was diluted into SFM at the appropriate concentration and pre-heated to 37°C. Medium was aspirated from the cell culture plates, and the matriptase or SLIGKV in SFM added to the cells. Typically, 50 µL was utilised for 96-well plates, and 500 µL for 12-well plates. The cells were incubated for varying durations depending on the assay, and then harvested by either extracting protein or mRNA as previously described.

For experiments measuring calcium mobilisation, SLIGKV or matriptase was diluted into HHBS at twice the final assay concentration, and then used to prime the fluorimeter pump. The cells were then aspirated, and HHBS added to each well. The amount of HHBS added depended on the final assay concentration for that well. For example, if 20 µM SLIGKV was primed into the pump, then by placing 30 µL of HHBS on the cells and injecting 30 µL in the assay would result in final stimulation of 10 µM.

2.12.2 Cathepsin V disarming assays

PAR2 disarming assays consisted of pre-incubating PAR2-expressing SW1353 cells with a cathepsin and then measuring a PAR2 activation readout following matriptase or SLIGKV stimulation. These assays were performed in 96-well plates, and consisted of

either measuring calcium mobilisation or gene expression by RT-qPCR of PAR2-responsive genes.

Experiments were performed following overnight serum starvation of the cells. For measuring calcium mobilisation as a read out, the cells were first loaded with calcium indicator as outlined in chapter 2.11.

The cathepsin enzymes were activated by diluting 1:10 in activation buffer, then further diluting to final concentration in assay buffer, and 50 µL was added to each appropriate well. Cells were incubated with cathepsin for 10 minutes at 37°C, before being washed in assay buffer (calcium mobilisation) or SFM (qPCR). For measuring calcium mobilisation, the plates were then directly placed in the fluorometer, and the assay undertaken by injecting PAR2 agonist using the fluorometer pumps. When using qPCR as a read out, the PAR2 activator was diluted into SFM and added to the cells before further incubating at 37°C for the required time.

Cathepsin V, K, S, L activation buffer
100 mM Sodium acetate pH 5.5, 2.5 mM DTT, 2.5 mM EDTA

Calcium assay buffer
HHBS (2 mM Ca^{2+})

2.13 Enzymatic digestion of PAR2 42mer

Background: In order to screen proteases for their ability to cleave PAR2, incubations were carried out with various proteases of interest and a 42 amino acid peptide (hereafter "PAR2 42mer") consisting of the extracellular region of PAR2 that all previously identified cleavages have occurred (see chapter 4.1.2.1) .

Reagents:

- PAR2 42mer, at 100 µM in 0.1% TFA in ddH_2O, stored at -80°C.
- Various recombinant and purified proteases, see chapter 2.1.2.

Method: Reactions were set up using the buffer conditions recommend for the specific protease. Typically, the experiments were set up by making dilutions of PAR2 42mer at

20 µM and protease at 2x final concentration (typically in the range of 0.1 nM to 200 nM) before mixing together in equal parts (typically 20-40 µL) yielding a final peptide concentration of 10 µM. Reactions were incubated at 37°C for varying amounts of time.

Following enzymatic digests, the reactions were either analysed by tris-tricine SDS-PAGE (chapter 2.6.2), HPLC (chapter 2.14.1) or nanoLCMS (chapter 2.14.3).

Cathepsin V, K, S, L buffer

100 mM Sodium acetate pH 5.5, 2.5 mM DTT, 2.5 mM EDTA, 0.05% (w/v) Brij 35

Cathepsin B buffer

25 mM MES pH 5, 5 mM DTT, 0.05% (w/v) Brij 35

MMP-1, -8, -13 and ADAMTS5 buffer

100 mM Tris-HCl pH 7.5, 100 mM NaCl, 10 mM $CaCl_2$, 0.05% (w/v) Brij 35, 0.01% (w/v) PEG 6000.

Matripase, Hepsin buffer

100 mM Tris pH 8.5, 150 mM NaCl, 0.01% Brij-35

Neutrophil elastase, Cathepsin G, FAP buffer

100 mM Tris pH 7.5, 150 mM NaCl, 0.01% Brij-35

Thrombin, uPA buffer

100 mM Tris-HCl pH 7.5, 150 mM NaCl, 0.01% Brij-35

HTRA1, HTRA3, Factor I, Factor D buffer

50 mM Tris pH 8, 150 nM NaCl, 0.01% Brij-35

PCSK9 buffer

50 mM Sodium Citrate pH 5, 75 mM NaCl, 2 mM $CaCl_2$, 0.01% Brij-35

2.14 Mass Spectrometry of PAR2 42mer digestion products

Background: In order to identify specific cleavage sites of enzymatic cleavages of PAR2, mass spectrometry (MS) was used. Samples were either separated by HPLC and ionised in direct-infusion MS, or the reaction mixture was directly subjected to nanoLCMS.

2.14.1 High Performance Liquid Chromatography

High performance liquid chromatograpgy (HPLC) was used to examine the enzymatic digestion products and to subsequently isolate specific products for MS.

An autosampler was used to inject either 10 µL or 30 µL of digestion reaction for analytical or preparative HPLC, respectively, onto an ACE 3 C18 column (Advanced Chromatography Technologies, Aberdeen, UK) fitted to an 1100 series HPLC system (Agilent Technologies). The 5% to 60% acetonitrile gradient was run as detailed below. Gradients were run at 35°C at a flow rate of 0.2 mL/min.

Run conditions:

1. 5% to 60% buffer B in 27 minutes
2. 60% to 100% buffer B in 1 minute
3. 100% to 5% buffer B in 2 minutes
4. Re-equilibration at 5% buffer B for 15 minutes

Buffer A

0.1% Formic acid in ddH2O

Buffer B

0.1% Formic acid in acetonitrile

2.14.2 Direct-infusion MS

Samples fractionated by HPLC were loaded onto a TriVersa NanoMate (Advion, Ithaca, USA) and electrosprayed into a Thermo Finnigan LTQ FT Ultra High Performance Mass Spectrophotometer (Thermo Fisher) using a 2.4 kV voltage.

2.14.3 NanoLCMS

For nanoLCMS, an Acquity UPLC system (Waters, Elstree, UK) was connected to the Thermo Finnigan LTQ FT.

Samples were diluted 1:10 in 0.1% Formic acid and loaded into the autosampler. Sample (1 µL) was injected onto the system and gradients were run on an in-house packed column (Dr. Joe Gray) of 20 cm length x 0.1 mm width, with 5 µm partical size at 5 µL/min.

Run conditions:

1. 5% to 55% buffer B in 35 minutes
2. 55% to 85% buffer B in 3 minute
3. 85% to 5% buffer B in 2 minutes

Products were trapped using an Agilent ion trap (Agilent Technologies) at 0.4 µL/min and sprayed using a PicoTip silica tip (New Objective, Woburn, USA).

Buffer A

0.1% Formic acid in ddH2O

Buffer B

0.1% Formic acid in Acetonitrile

2.14.3.1 Data analysis

NanoLCMS identifies all cleavages within a sample and thus the data required analysis to identify the cleavages and order the relative abundance of products.

Firstly, the NanoLCMS traces were loaded onto Xcalibur™ Software (Thermo Fisher), and all the data between 10 and 50 minutes on the gradient were compiled. These times were chosen as they avoid the injection peaks at the start and the acetonitrile peak at the end. After compiling the data from this timespan, a list of the 20 most abundant masses was acquired. Subsequently, a search was undertaken using Mascot software (Matrix Science, Boston, USA) where the peptide sequence was uploaded into the database, and the raw nanoLCMS data file uploaded and cross-checked with the peptide sequence. This resulted in a list of peptide fragments identified as belonging to the PAR2 42mer peptide,

which was then cross-referenced with the top 20 list obtained from the Xcalibur™ Software, to give the top cleavages generated by each enzyme.

2.15 Enzyme Activity Assays

Background: Enzymatic reactions can be explored using quenched-fluorescent substates. These substrates are composed of short peptide sequences, specific for various protease preferences, as well as a quencher group and a fluorophore. In its intact state, the quencher prevents the observation of the fluorophore emission following excitation, however when the protease cleaves the substrate, the quencher spatially moves from the fluorophore allowing fluorescence to be observed (Figure 2.5). Some fluorescent peptide substrates, such as Boc-QAR-AMC, do not require a quencher as the binding of the AMC flurophore to an amino acid results in quenching, and fluorescence is observed when the AMC is cleaved away from the peptide.

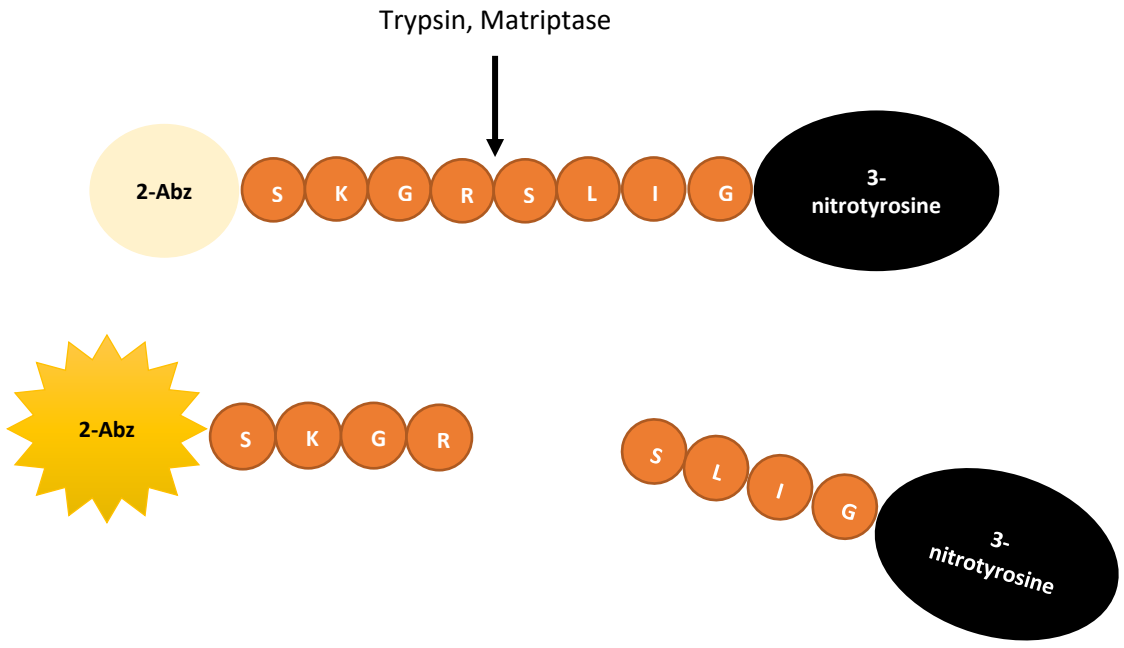

Figure 2.5: Example of a quenched-fluorescent substrate: SY-9 PAR2 activation peptide
Quenched-fluorescent peptides are composed of a specific peptide sequence, with a quencher group as well as a flurophore. For example, the PAR2 activation peptide, SY9, consists of 8 amino acids around the canonical activation site, as well as a 2-aminobenzyl flurophore and a trinitrotyrosine quencher.

2.15.1 FS-6 assay

Background: FS-6 is a quenched-fluorescent hexapeptide with the sequence AMC-Lys-Pro-Leu-Gly-Leu-Dpa-Ala-Arg-NH_2 where AMC is the fluorophore 7-amino-4-methylcoumarin, and Dpa is quencher N-3-(2,4-dinitrophenyl)l-α,β-diaminopropionyl. FS-6 is a general MMP substrate cleaved by several MMPs including all MMPs utilised in this project.

Reagents:

- FS-6 substrate at 5 mM in DMSO, stored at -20ºC protected from light
- AMC standard at 5 mM in methanol, stored at -20ºC protected from light

Method: 50 µL of MMP-containing sample made up to 1-5 nM (2x active concentration) in assay buffer was added to two wells of a white-walled white bottom 96-well plate (Perkin Elmer, Waltham, USA) per sample (two technical repeats). FS-6 substrate was diluted to 20 µM (2x final concentration) in assay buffer, and 120 µL added to a third well parallel to the assay samples. The plates were pre-incubated for at least 10 minutes at 37ºC to allow the reagents to reach assay temperature. Fluorescence was kept below 10% substrate hydrolysis using AMC standard at 1 µM. A multichannel pipette was then used to add 50 µL substrate to each sample well as quickly as possible to ensure that enzymatic reactions commenced essentially at the same time. Final substrate concentration was 10 µM, and fluorescence increase was monitored in the form of a progress curve on a FLUOstar Optima fluorometer (BMG labtech), at λ_{ex} 325 nm and λ_{em} 405 nm.

<u>FS-6 Assay buffer</u>

100 mM Tris-HCl pH 7.5, 100 mM NaCl, 10 mM $CaCl_2$, 0.05% (w/v) Brij 35, 0.01% (w/v) PEG 6000

2.15.2 Boc-QAR-AMC assay

Background: Boc-QAR-AMC is a fluorescent substrate for trypsin-like serine proteases with the sequence Boc-Gln-Ala-Arg-AMC, where Boc is N-*tert*-butoxycarbonyl, a blocking group.

Reagents:

- Boc-QAR-AMC substrate at 25 mM in methanol, stored at -20ºC protected from light
- AMC standard at 5 mM in methanol, stored at -20ºC protected from light

Method: Serine protease-containing sample made up to 1-5 nM (2x active concentration) in assay buffer, and 50 µL added to two wells of a white-walled white bottom 96-well plate (Perkin Elmer) per sample (two technical repeats). Boc-QAR-AMC substrate was diluted to 20 µM (2x final concentration) in assay buffer, and 120 µL added to a third well parallel to the assay samples. The plates were pre-incubated for at least 10 minutes at 37ºC to allow the reagents to reach assay temperature. Fluorescence was kept below 10% substrate hydrolysis using AMC standard at 1 µM. A multichannel pipette was then used to add 50 µL substrate to each sample well, as quickly as possible to ensure that enzymatic reactions commence as close to each other as possible. Final substrate concentration was 10 µM, and fluorescence increase was monitored in the form of a progress curve on a FLUOstar Optima fluorometer (BMG labtech), at λ_{ex} 360 nm and λ_{em} 460 nm.

Assay buffer

100 mM Tris pH 8.5, 150 mM NaCl, 0.01% Brij-35

2.15.3 Z-FR-AMC assay

Background: Z-FR-AMC is a fluoroescent substrate for papain-like cysteine proteases with the sequence Z-Phe-Arg-AMC, where Z is blocking group benzyloxycarbonyl. This substrate was used for all cathepsins in this project.

Reagents:

- Z-FR-AMC (Bachem, Bubendorf, Switzerland) at 20 mM in methanol, stored at -20ºC protected from light

Method: Cathepsin enzymes were stored in their pro-form and required activation by exposing to reducing conditions, as provided by DTT in their assay buffers. To activate, pro-cathepsins were typically diluted 1:10 in assay buffer and incubated at room temperature for 10 minutes. Cathepsin-containing samples were made up to 1-5 nM (2x

active concentration) in assay buffer, and 50 µL added to two wells of a white-walled white bottom 96-well plate (Perkin Elmer) per sample. Z-FR-AMC substrate was diluted to 20 µM (2x final concentration) in assay buffer, and 120 µL added to a third well parallel to the assay samples. The plates were pre-incubated for at least 10 minutes at 37ºC to allow the reagents to reach assay temperature. Fluorescence was kept below 10% substrate hydrolysis using AMC standard at 1 µM. A multichannel pipette was then used to add 50 µL substrate to each sample well, as quickly as possible to ensure that enzymatic reactions commence as close to each other as possible. Final substrate concentration was 10 µM, and fluorescence increase was monitored in the form of a progress curve on a FLUOstar Optima fluorometer (BMG labtech), at λ_{ex} 380 nm and λ_{em} 460 nm.

Cathepsin V, K, S, L assay buffer

100 mM Sodium acetate pH 5.5, 2.5 mM DTT, 2.5 mM EDTA, 0.05% (w/v) Brij 35

Cathepsin B assay buffer

25 mM MES pH 5, 5 mM DTT, 0.05% (w/v) Brij 35

2.15.4 Michaelis-Menten Kinetics

Background: Michaelis-Menten kinetics is a commonly used model of enzyme kinetics, able to relate the rate of reaction or velocity (V) with the concentration of substrate, [S]. Using Michaelis-Menten kinetics to explore how proteases can cleave their substrate, several important kinetic constants can be calculated which can give insight into their biochemistry.

The pioneering work by Leonor Michaelis and Maud Menten proposed a model for enzymatic reactions where enzyme (E) is able to bind to substrate (S) to form an enzyme-substrate complex (ES) which is a reversible reaction. The enzyme is then able to irreversibly catalyse the substrate to product (P) and release itself from the complex, able to catalyse another reaction (E):

$$E + S \rightleftharpoons ES \xrightarrow{k_{cat}} E + P$$

With certain assumptions, the Michaelis-Menten equation can be derived as:

$$V = \frac{V_{max}[S]}{K_m + [S]}$$

Where V_{max} is the maximal velocity, and K_m is the Michealis-Menten constant. The K_m is the substrate concentration at half V_{max} and is considered an inverse measure of the affinity of the enzyme for the substrate, thus a lower K_m is considered to be a higher affinity and thus the velocity will reach V_{max} more quickly. It is important to note that K_m is a kinetic constant and not an equilibrium constant (which would be the dissociation constant K_d for affinity). Using K_d to describe enzymatic affinity for substrate can be complicated since the enzyme also degrades the substrate rather than reaching a dissociation/association equilibrium. Under certain circumstances, K_m may be equal to K_d (when the rate of formation of the ES complex is much faster than the formation of E and P from ES)[242].

k_{cat} is known as the turnover number, and is a measure of the number of substrate molecules which are converted to product per active site per unit time. This can be calculated by knowing the active-site concentration of the enzyme at T=0 (E_0):

$$k_{cat} = \frac{V_{max}}{E_0}$$

As both k_{cat} and K_m give information about the relationship between enzyme and substrate, it is common to quote catalytic efficiency as:

$$\frac{k_{cat}}{K_m}$$

If an enzyme has a high turnover number as well as a high affinity for a substrate, then the catalytic efficiency will be very high, and a high value for k_{cat}/K_m would express this.

In order to generate kinetic constants experimentally, increasing concentrations of substrate are incubated with a constant concentration of enzyme, and the velocities are observed. The velocities will increase with substrate concentration until the system becomes saturated and V_{max} is reached. Velocity is plotted against substrate

concentration, and constants can be derived by methods such as Lineweaver-Burk plots, or by computer software.

2.15.4.1 PAR2 peptide kinetics

Background: In order to explore the enzyme kinetics for various proteases for PAR2, quenched-fluorescent substrates for three regions of PAR2 were utilised.

Reagents:

- SY-9 peptide at 1.748 mM in 20% (v/v) acetonitrile, stored at -20ºC protected from light.
- VETV peptide at 10 mM in DMSO, stored at -20ºC protected from light.
- FSVD peptide at 10 mM in DMSO, stored at -20ºC protected from light.

Method: Serial dilutions of the PAR2 peptides were undertaken in assay buffer, resulting in a series of enzyme concentrations at 2x final concentration. Each concentration was placed into duplicate wells of a white-walled, white-bottom 96-well plate (Perkin Elmer), 50 µL per well, and the plate pre-heated to 37ºC. Meanwhile, the enzyme was prepared in assay buffer at 2x final concentration and 120 µL added to a third well parallel to the assay wells. A multichannel pipette was then used to transfer 50 µL of 2x enzyme stock to each well of the substrate, and the reaction monitored in a FLUOstar OPTIMA fluorimeter at λ_{ex} 320 nm and λ_{em} 420 nm.

Velocities were taken in the linear phase at the start of the reaction, and plotted against substrate concentration. Velocity in arbitrary fluorescence units was converted to concentration of substrate per unit time by using a total hydrolysis standard curve (see Appendix 4). A plate was set up with concentration of substrate as used for kinetic determination, enzyme was added, but instead of measuring velocity, the plate was incubated for 2-4 hours at 37ºC before measuring fluorescence at total hydrolysis. The straightline equation was then used to relate arbitrary fluorescence to substrate hydrolysis. A different standard curve was used for each different buffer system.

To determine kinetic constants, non-linear regression analysis of velocities was performed using GraphPad Prism software. V_{max} and K_m. k_{cat} could then be determined based on the known active concentration of enzyme used.

Cathepsin V, K, S, L assay buffer

100 mM sodium acetate pH 5.5, 2.5 mM DTT, 2.5 mM EDTA, 0.05% (w/v) Brij 35

Cathepsin B assay buffer

25 mM MES pH 5, 5 mM DTT, 0.05% (w/v) Brij 35

Matriptase assay buffer

100 mM Tris pH 8.5, 150 mM NaCl, 0.01% Brij-35

MMP-1, -8, -13 assay buffer

100 mM Tris-HCl pH 7.5, 100 mM NaCl, 10 mM CaCl2, 0.05% (w/v) Brij 35, 0.01% (w/v) PEG 6000.

2.15.5 Active-site titration

Background: Throughout this project, quoted enzyme concentrations refer to the protein concentration of enzyme, however the enzyme might not be fully active. In order to calculate accurate kinetic constants to compare enzymes, an accurate active-site concentration must be obtained. In order to active-site titrate an enzyme, an inhibitor with 1:1 binding stoichiometry is required, and is titrated to a range of concentrations against a constant enzyme concentration. When plotted with velocity on the Y axis, and inhibitor concentration on the X axis, the X-intercept is the active concentration of enzyme.

2.15.5.1 Cathepsin active-site titration with E64

Background: *trans*-Epoxysuccinyl-L-leucylamido(4-guanidino)butane (E64) is an epoxide small molecule inhibitor of cysteine proteases, which exerts its effect by being able to bind to the active-site cysteine residue as a result of nucleophilic attack from its thiol group. It is commonly used to active-site titrate various cathepsins[243], including all cathepsins used in this project.

Reagents:

- Z-FR-AMC (Bachem) at 20 mM in methanol, stored at -20ºC protected from light.
- E64, at 1 mM in ddH_2O, stored at -20ºC

Method: Pro-cathepsins were activated by diluting 1:10 in their assay buffer and incubating at room temperature for 10 minutes. Subsequently, they were diluted to 3x final concentration (typically 1-5 nM) and 33 µL was added to 2 wells of a white-walled white bottom 96-well plate (Perkin Elmer) per sample. E64 was diluted in the same assay buffer, and a range of dilutions undertaken by either serial or parallel dilution. Typically, concentrations ranging from 10-fold lower to 10-fold higher than the enzyme concentration were used. 33 µL of each E64 concentration was added to the enzymes in the plate and incubated for 30 minutes at 37ºC to allow complete inhibition. Substrate Z-FR-AMC was diluted to 30 µM (3x final concentration) and 80 µL was added to a third well parallel to the assay wells. A multichannel pipette was then used to add 33 µL substrate to each sample well, as quickly as possible to ensure that enzymatic reactions commence as close to each other as possible. Final substrate concentration was 10 µM, and fluorescence increase was monitored in the form of a progress curve on a FLUOstar Optima fluorimeter (BMG labtech), at λ_{ex} 380 nm and λ_{em} 460 nm.

Cathepsin V, K, S, L assay buffer

100 mM sodium acetate pH 5.5, 2.5 mM DTT, 2.5 mM EDTA, 0.05% (w/v) Brij 35

Cathepsin B assay buffer

25 mM MES pH 5, 5 mM DTT, 0.05% (w/v) Brij 35

2.15.5.2 MMP active-site titration with TIMP1

Background: As described in chapter 1.4.1.6, MMPs are inhibited by their endogenous inhibitors which bind with 1:1 stoichiometry. This property can be exploited to active-site titrate MMPs, by titrating with a known concentration of TIMP. This project utilised TIMP1 as it is able to inhibit all the used MMPs. MMPs are produced recombinantly in their pro-form, thus require activating before carrying out the assay. They can be activated *in vitro* in the presence of 4-aminophenylmercuric acetate (APMA).

Reagents:

- TIMP1 at 5.6 µM, stored at -80°C.
- AMPA stock solution at 10 mM, made by dissolving 35.2 mg APMA in 200 µL DMSO, then made up to 10 mL in 100 mM Tris pH 8.5 stored at 4ºC protected from light for up to 3 months

Methods: Pro-MMPs were first activated by diluting 1:10 in their assay buffer with 1 mM APMA and incubating at 37ºC for 30 minutes (proMM13), 1 hour 30 minutes (proMMP8) or 3 hours (proMMP1). Subsequently, they were diluted to 3x final concentration (typically 1-5 nM) and 33 µL was added to 2 wells of a white-walled white bottom 96-well plate (Perkin Elmer) per sample. TIMP1 was diluted in the same assay buffer, and a range of dilutions undertaken by either serial or parallel dilution. Typically, concentrations ranging from 10-fold lower to 10-fold higher than the enzyme concentration were used. Each TIMP1 concentration was added (33 µL) to the enzymes in the plate and incubated for 30 minutes at 37ºC to allow complete inhibition. Substrate FS6 was diluted to 30 µM (3x final concentration) and 80 µL was added to a third well parallel to the assay wells. Subsequently, 33 µL of substrate was added to each sample well as quickly as possible. Final substrate concentration was 10 µM, and fluorescence increase was monitored in the form of a progress curve on a FLUOstar Optima fluorimeter (BMG labtech), at λ_{ex} 325 nm and λ_{em} 405 nm.

FS-6 Assay buffer

100 mM Tris-HCl pH 7.5, 100 mM NaCl, 10 mM CaCl2, 0.05% (w/v) Brij 35, 0.01% (w/v) PEG 6000.

2.16 Gene expression microarray

Background: A gene expression (or DNA) microarray is a powerful method for exploring the genome-wide gene expression status of a sample, utilising a chip containing thousands of oligomeric probes. High purity mRNA is extracted from a source such as a tissue or cells, which is then reverse-transcribed to cDNA, which is then hybridised to the chip and measured.

Method: SW1353 cells were seeded into a 6-well plate at a seeding density of 30,000 cells/cm^3 before transducing with pSIEW_PAR2 lentivirus as outlined in chapter 2.10.2 and cultured for 48 hours at 37°C 5% CO_2. The cells were serum-starved overnight, and stimulated with 10 nM matriptase, 100 µM SLIGKV (both dissolved in SFM) or unstimulated (SFM only). Stimulation was undertaken for either 90 minutes or 24 hours before extracting mRNA using an RNeasy kit (Qiagen). The mRNA was sent to the

Central Biotechnology Services at Cardiff University School of Medicine for gene expression analysis.

The microarray utilised a HumanHT-12 v4 Expression BeadChip Kit (Illumina Inc., San Diego, USA), able to measure 12 samples on a single chip, with 47,000 probes per sample. Samples were randomised over two chips.

The raw microarray data were analysed by the Musculoskeletal Research Group Bioinformatics Support Unit at Newcastle University. Pathway analysis was undertaken using Ingenuity Pathway Analysis software (Qiagen).

2.17 Statistical Analysis

Statistical differences between two parametric groups were compared using a student's two-tailed t-test. Where multiple comparisons were made within one experiment, a one-way analysis of variance (ANOVA) was performed. Graphpad Prism 5.0 software or Microsoft Excel were used to undertake statistical analysis. The significance levels used were: * = $p<0.05$, ** = $p<0.01$ and *** = $p<0.001$.

Chapter 3. Mechanical Loading of Chondrocytes

3.1 Introduction

As described in chapter 1, chondrocytes are cells which respond to mechanical load in a variety of manners, such as altered growth, metabolism and gene expression. Of particular interest to this project is the fact that various MMPs are known to be regulated by mechanical loading, such as MMP-1, -2, -3, -9 and -13[22] – which include the two key collagenases implicated in OA, MMP-1 and 13. Matriptase has been shown to be up-regulated in OA patients[1], however very little is currently understood about the mechanisms behind this up-regulation. This chapter aims to explore whether matriptase expression may be regulated by mechanical loading.

3.1.1 Chapter Aims

- To develop a system by which to encapsulate chondrocytes in a 3D hydrogel and to expose them to mechanical load, and to extract mRNA and protein for further analysis.
- To explore whether matriptase, and other serine proteases of interest such as hepsin, are regulated by abnormal loading.
- To further aim to understand genes regulated by mechanical loading in chondrocytes in the context of catabolism.

3.2 Results

3.2.1 Comparison of Bovine Nasal Chondrocytes with SW1353 cells

In order to test the mechanical loading of chondrocytes, a source of appropriate cells is required. Due to the relatively large numbers of cells required per experiment (5-10x10^6 cells), the utilisation of human articular chondrocytes (HAC) harvested from joint replacement patients would be inappropriate as these typically yield below 1x10^6 cells (unpublished observations). A comparison of a human chondrocytic cell line, SW1353, and primary bovine nasal chondrocytes (BNC) was therefore undertaken.

$10x10^6$ cells (either SW1353 or BNC) were utilised to make agarose/cell constructs and cultured for 6 days with progressive serum starvation and supplementation in order to allow the cells to secrete a PCM (chapter 2.2.8). Following day 6, histological staining was performed. These results clearly showed that BNCs, but not SW1353 cells, were able to synthesise and secrete proteoglycans in the pericellular space (Figure 3.1 C, D, G and H) as shown by Alcian Blue and Safranin O staining.

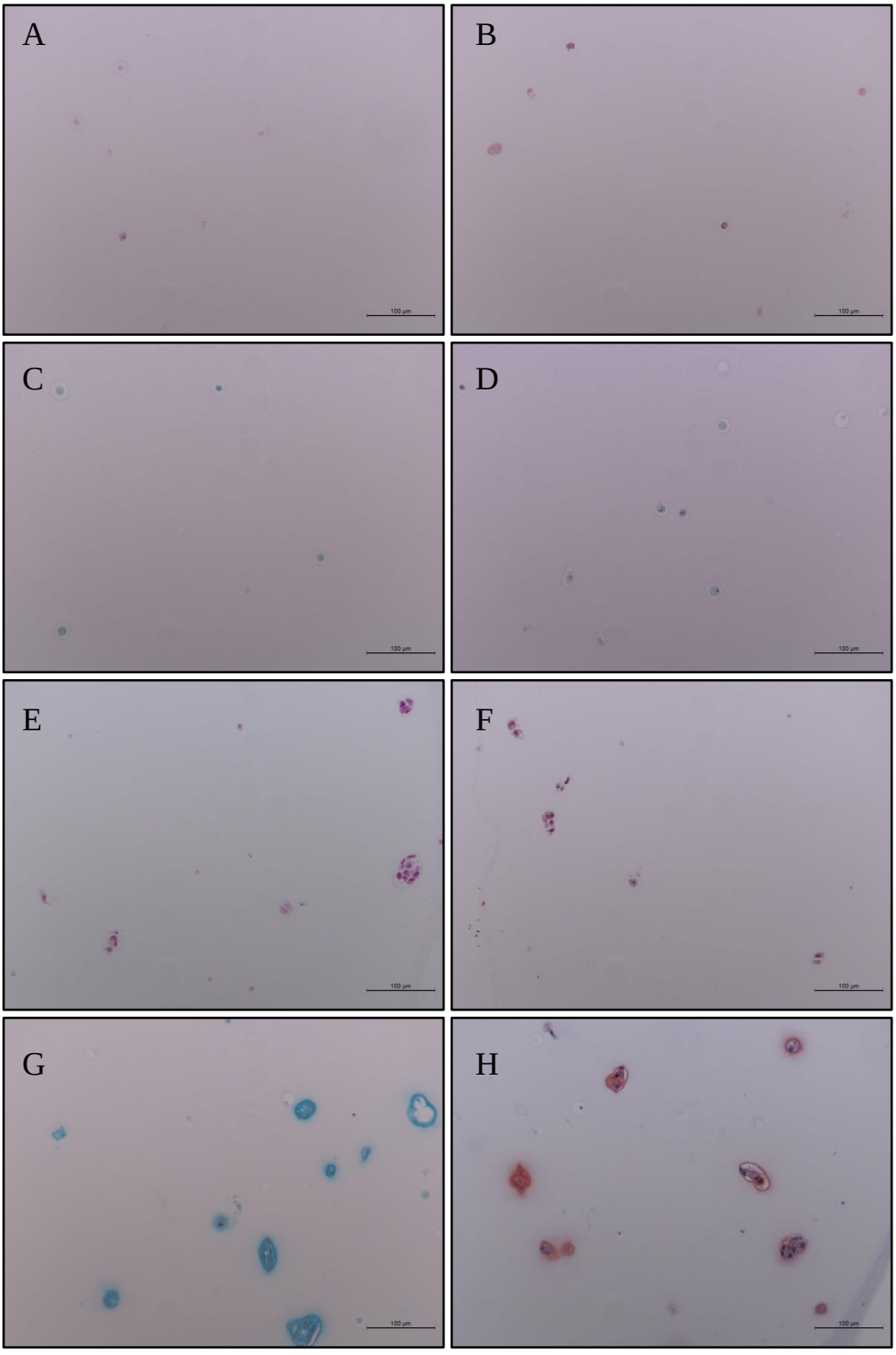

Figure 3.1: Histological staining of SW1353 cells and BNCs following 6 day culture
Chondrocyte/agarose constructs containing either SW1353 (A-D) or BNCs (E-H) were cultured for 6 days according to the method described in chapter 2.2.8, before fixing in formalin, embedding in paraffin wax and staining with H&E (A, E), Masson's Trichrome (B,F), Alcian Blue (C,G) or Safranin O (D, H). Scale bar = 100 μm.

Having ascertained whether the two cell types are able to secrete a PCM, their basic responses to loading were examined. It has been described in the literature that p38 is rapidly phosphorylated in response to loading[239,244-247]. Both SW1353 and BNC agarose constructs were therefore loaded with identical loading regimens and their responses examined by western blotting. Following a 30 minute loading regimen of 20-40 kPa at 0.33 Hz, the chondrocyte/agarose constructs were snap frozen in liquid nitrogen and processed for SDS-PAGE analysis, in a method designed to maintain the phosphorylated status of proteins in the cells[239]. Following mechanical loading, SW1353 cells did not appear to respond in terms of p38 phosphorylation (Figure 3.2). For BNCs however, there was a clear phosphorylation of p38 (Figure 3.3). When BNCs were loaded after two days in culture (before they had secreted a PCM), they did not respond to mechanical loading (Figure 3.4A). It appears that prior to secretion of PCM, there appears to be a space between the cell and the surrounding agarose matrix (Figure 3.4B-E).

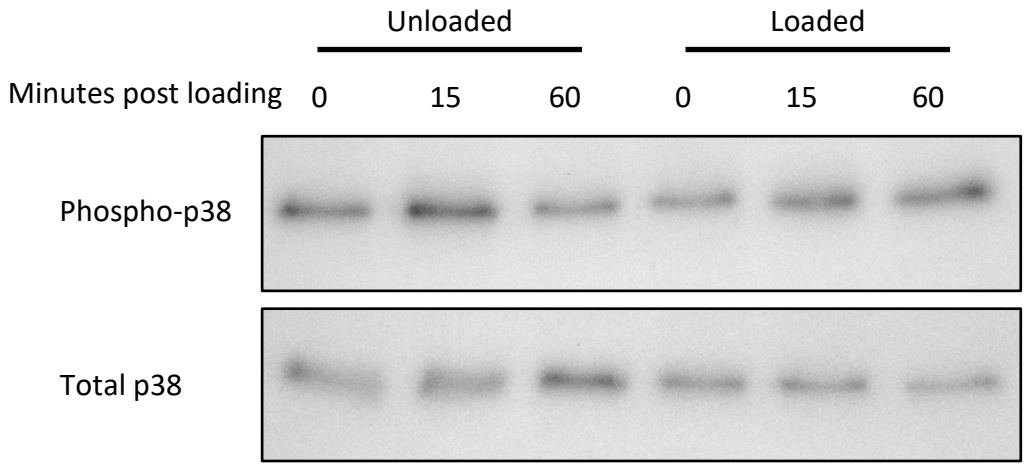

Figure 3.2: Western blot for SW1353 cells following dynamic loading
SW1353 cells encapsulated in agarose underwent 30 minutes of dynamic loading (20-40kPa at 0.33Hz), following which the gels were frozen in liquid nitrogen at 0, 15 or 60 minutes post-loading. Following processing, SDS-PAGE gels were run and Western blots for phospo-p38 and native p38 were undertaken.

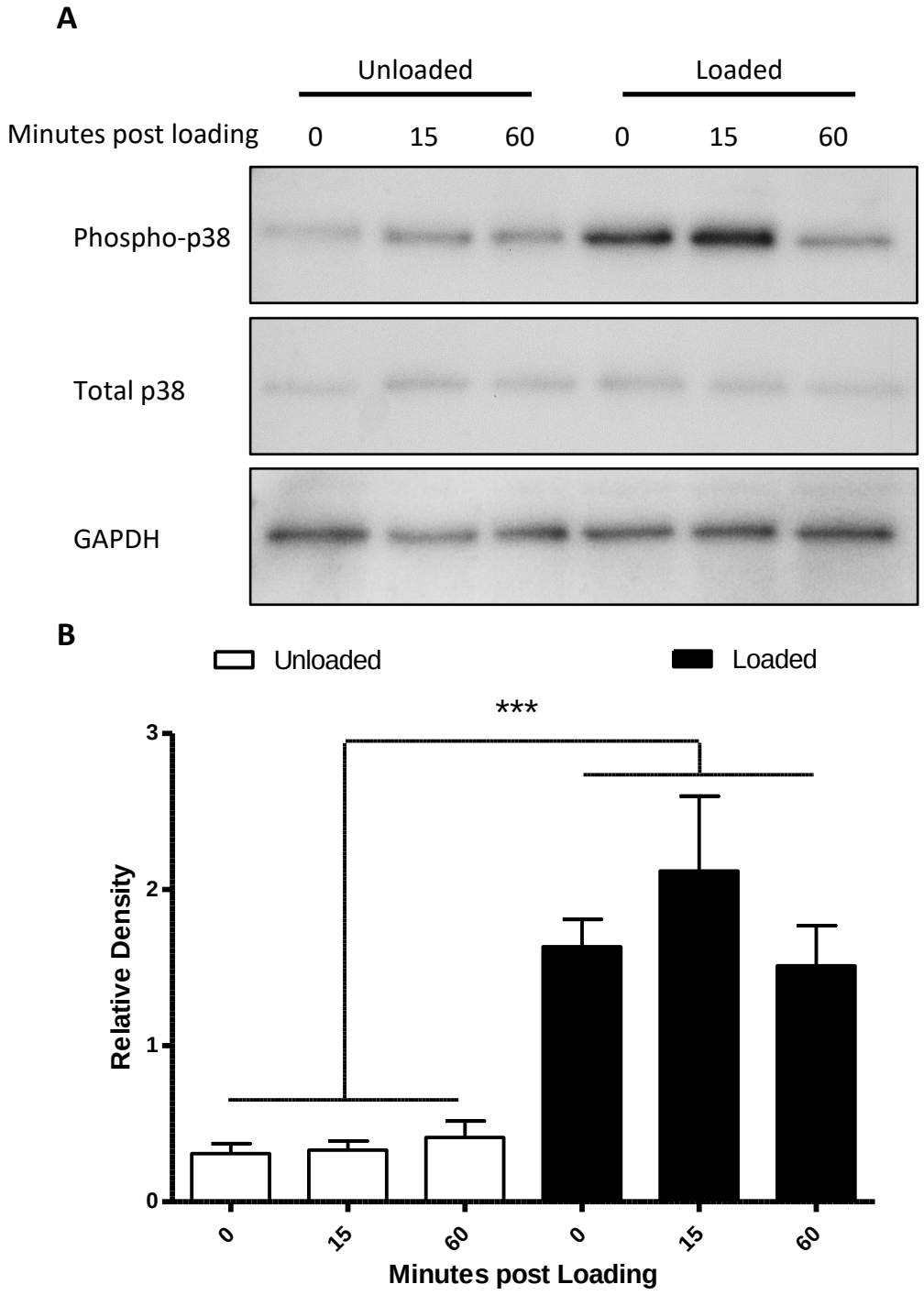

Figure 3.3: Western blot for BNC following dynamic loading

Following 7 days in culture, BNCs encapsulated in agarose underwent 30 minutes of dynamic loading (20-40kPa at 0.33Hz), following which the gels were frozen in liquid nitrogen at 0, 15 or 60 minutes post-loading. **A:** SDS-PAGE gels were run and western blots for phospo-p38 and total p38 were undertaken. Blot shown is representative of n=5 independent experiments with constructs generated from 5 bovine noses. **B:** Densitometric analysis of p38 phosphorylation was undertaken on the n=5 separate blots. Density is relative to appropriate total p38 time point (mean ± S.E.M; where *** $p < 0.001$ by two-way ANOVA comparing unloaded and loaded samples).

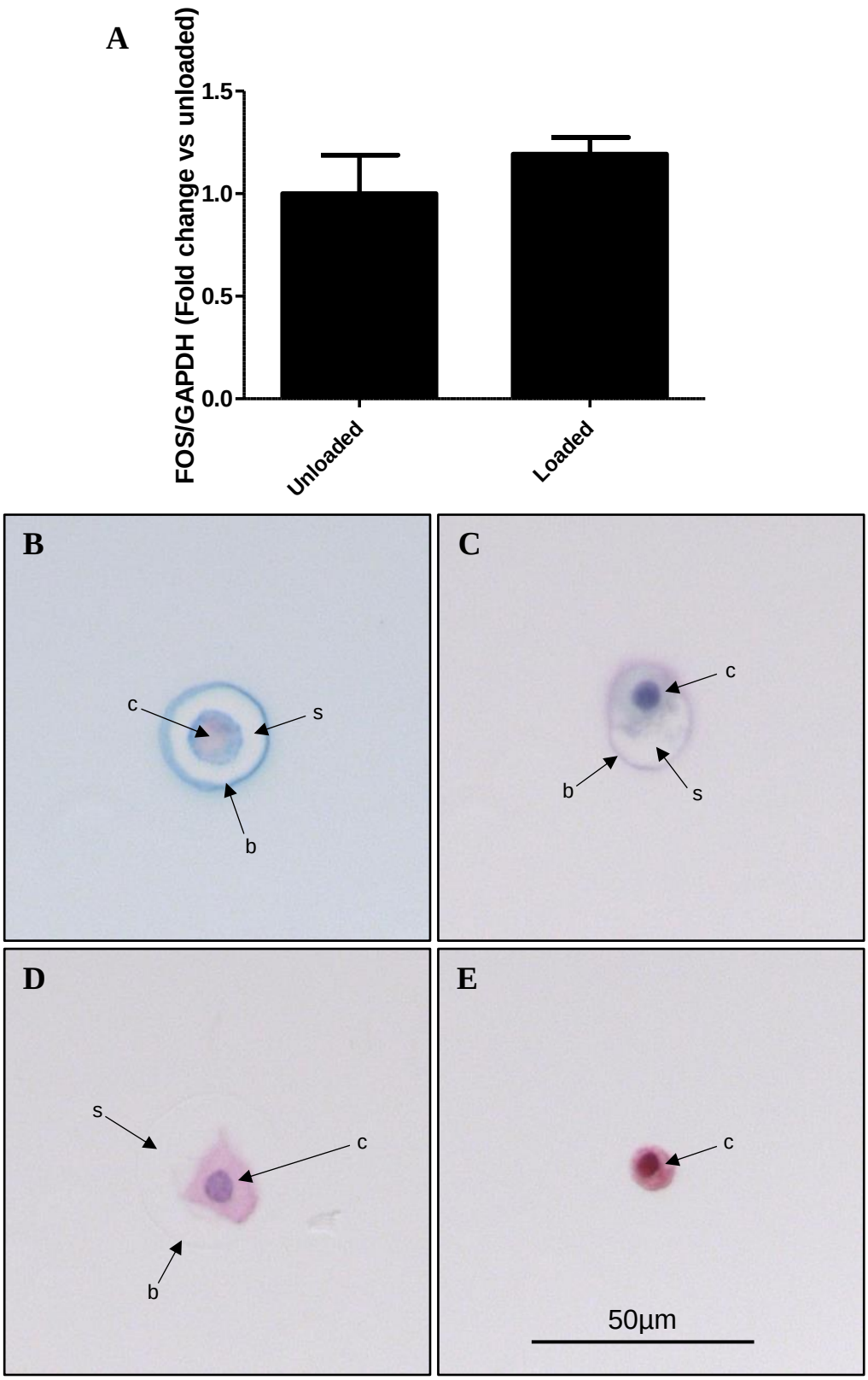

Figure 3.4: Histology and *FOS* expression post-loading after 2 days in culture
BNCs encapsulated in agarose were cultured for 2 days following seeding before either undergoing loading or processing for histological analysis. Loaded cells underwent dynamic loading (20-40kPa at 0.33Hz for 30 minutes) before extracting mRNA immediately post-loading, reverse transcribing to cDNA and running qPCR analyses for *FOS* (A). For histological analysis, BNC/agarose constructs were fixed in formalin, embedded in paraffin wax, sectioned and stained with Alcian Blue (B), Safranin O (C), H&E (D) or Masson;s Trichrome (E). c = cell, s = space between cell and agarose matrix, b = boundary between space and agarose matrix. qPCR data pooled from two separate chondrocyte populations. Cells selected for figure are representative of all cells on the slides.

3.2.2 Development of a method to extract RNA from chondrocytes embedded in agarose

In order to define the effects of mechanical loading on cells at the gene expression level, the ability to extract abundant and high quality RNA is of utmost importance. The extraction of RNA from cells embedded in agarose requires the dissolution of the agarose, the lysis of the cells and stabilisation of the RNA, whilst avoiding the interference of additional components of the gel, such as culture medium. As such, extraction of RNA from cells in agarose is known to be a relatively difficult process. Several methods, however, have been published with various levels of success. A selection of these methods were attempted to extract RNA, such as Bougault *et al.* (2009)[239], Wang & Stegemann (2010)[248] and Mio *et al*. (2006)[249], however none of these resulted in successful RNA extraction. A scouting experiment was undertaken based on the work of Mio *et al*. (2006)[249] where a range of extraction conditions were tested. Two key variables are considered to be vital in the extraction of RNA when utilising a Qiagen RNeasy kit, namely the amount of lysis buffer RLT used to dissolve the gel, and the final pH of the dissolved gel prior to loading onto the silica membrane of the Qiagen column. SW1353 cells were seeded into 13mm agarose gel discs at a density of 666 cells/µl. These constructs were dissolved in a range of buffer RLT volumes, 500-2000 µl. Following dissolution, the cells were homogenised by pipetting up and down, and then varying amounts of 2M Sodium Acetate (pH 5.5) were added, 5-50 µl. 0.71 volumes (of buffer RLT) of absolute ethanol was added, and the mixture loaded to a Qiagen RNeasy column. The subsequent method was as described by the manufacturer, including an on-column DNase digest. The RNA was eluted in 50 µl RNase-free H_2O, and concentrations measured.

It was evident that lower volumes of buffer RLT resulted in significantly higher yields of RNA, with a slight trend between RNA yield and pH within each buffer RLT group (Figure 3.5). These results disagree with Mio *et al*. (2006), who found that lower volumes of buffer RLT resulted in lower yields of RNA. Their optimum volume of buffer RLT was 1540 µl, which when taken into account with their agarose construct volume of 440 µl is 3.5 volumes of RLT to agarose/cell construct. The cell/agarose constructs utilised in this work have an estimated volume of 360 µl, of which the optimum volume of RLT 500 µl, or a 1:1.39 ratio.

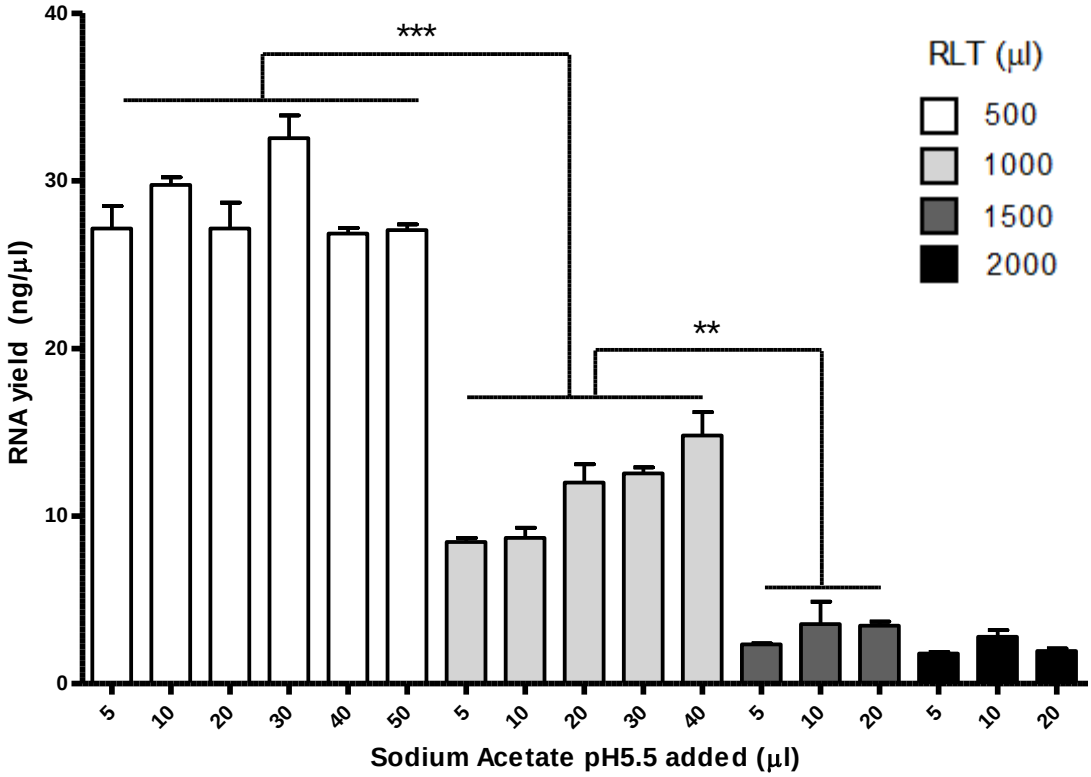

Figure 3.5: Optimisation of conditions to extract RNA from cells embedded in agarose
SW1353 cells were embedded in 2% agarose at a concentration of 666 cells/µl, prior to dissolution in 500-2000 µl Qiagen lysis buffer RLT, alteration of pH using 2M sodium acetate (pH 5.5) and addition of 0.71 volumes absolute ethanol before loading onto a Qiagen RNeasy column and subsequent clean-up, DNase step and elution (mean ± S.E.M; where ** $p < 0.01$; *** $p < 0.001$ by two-tailed unpaired T-test comparing the means of all the data for each buffer RLT value independent of sodium acetate amount). RNA extracted from n=2 gels from the same chondrocyte population per tested condition.

SW1353 cells were utilised in the optimisation of RNA extraction rather than BNCs due to the ease of obtaining the large quantities of cells required to test all possible conditions. After ascertaining the optimal conditions to extract RNA from SW1353 cells, it was important to carry out a similar experiment with BNCs due to potential differences in optimal conditions. As 500 and 1000 µl of buffer RLT were the only volumes to result in good yields of RNA from SW1353 cells, only these two volumes were tested in BNCs. As with SW1353 cells, using 500 µl of buffer RLT to dissolve the construct resulted in a significantly better yield of RNA compared to dissolving in a higher volume (1000 µl) (Figure 3.6). Furthermore, varying amounts of sodium acetate pH 5.5 were added to alter the pH of the solution prior to loading on the RNeasy column. Despite not being statistically significant, there was a trend of 30 µl sodium acetate pH 5.5 resulting in a better yield. These conditions were therefore chosen to be used in subsequent studies: dissolving the construct in 500 µl buffer RLT before adjusting the pH with 30 µl 2 M sodium acetate pH 5.5.

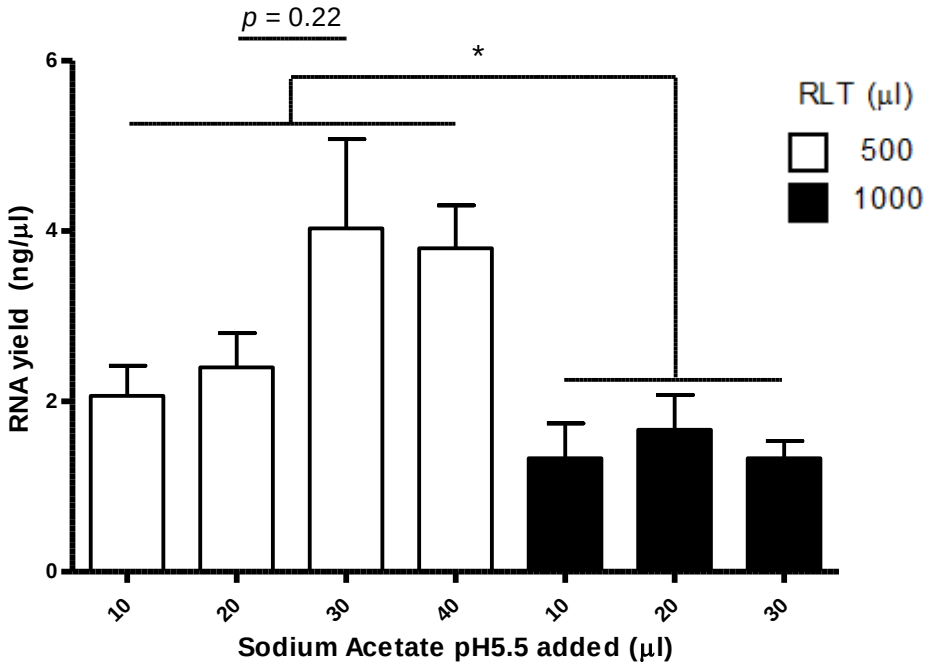

Figure 3.6: Optimisation of conditions to extract RNA from BNCs embedded in agarose
BNCs were embedded in 2% agarose at a concentration of 228 cells/µl, prior to dissolution in 500 or 1000 µl Qiagen lysis buffer RLT, alteration of pH using 2 M Sodium Acetate (pH 5.5) and addition of 0.71 volumes absolute ethanol before loading onto a Qiagen RNeasy column and subsequent clean-up, DNase step and elution (mean ± S.E.M; where * $p < 0.05$ by two-tailed unpaired T-test comparing the means of all the data for each buffer RLT value independent of sodium acetate amount). RNA extracted from n=3 gels from the same chondrocyte population per tested condition.

3.2.3 Exploration of the effect of mechanical loading on the regulation of matriptase and hepsin

Based on the results obtained in section 3.2.1, it was decided to focus solely on BNCs for the following work. After ascertaining that the mechanical loading of BNCs clearly results in the induction of certain early response genes, it was of interest to explore whether other known regulators of osteoarthritis were also differentially regulated following loading. Although matriptase was recently identified by this group as a key regulator in OA[1], little is known about the regulation of matriptase expression in cartilage. It was therefore of interest to explore whether the gene might be mechanically sensitive.

BNCs were loaded using the same regimen used to confirm the phosphorylation of p38, however different time points were chosen working under the assumption that new protein synthesis of a protease would require more than 60 minutes. The expression of matriptase following loading gave rise to mixed results with both striking up-regulation and no regulation or even down-regulation observed. When pooling together the data from densitometric analysis of the western blots from 5 independent experiments, there was no significant regulation of matriptase by loading observed (Figure 3.7 A). Hepsin is another serine protease of potential interest in OA, and its expression following load was also assessed. As with matriptase, no significant trends with loading were observed (Figure 3.7 B). To further validate the experimental set up, the expression of MMP-1, a protease previous described to be mechanically regulated, was examined. These results (Figure 3.7 C) suggest that MMP-1 is indeed regulated by loading, with significant increases in expression over time. Interestingly, the significant increases commenced immediately post-loading. Taken together, these data suggest that neither matriptase nor hepsin are mechanically regulated under tested conditions.

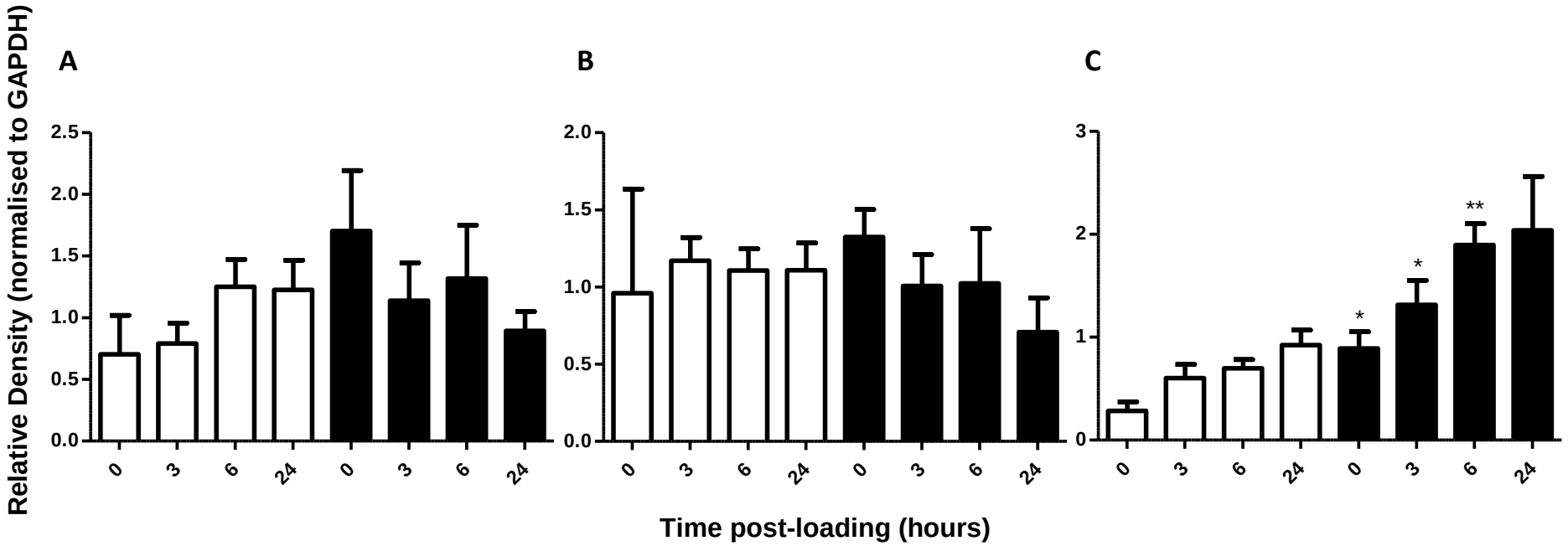

Figure 3.7: Exploration of MMP1, matriptase and hepsin expression following mechanical load

BNCs encapsulated in agarose underwent 30 minutes of dynamic loading (20-40kPa at 0.33Hz), following which the gels were frozen in liquid nitrogen at 0, 3, 6 or 24 hours post-loading. SDS-PAGE gels were run and western blots for matriptase (A), hepsin (B) and MMP1 (C) were undertaken. The blots were re-probed with GAPDH as a loading control and densitometric analysis was undertaken. Density is relative to appropriate GAPDH time point (mean ± SD; where * $p < 0.05$; ** $p < 0.01$, by unpaired two-tailed T Test compared to corresponding unloaded time point). Data generated from n=4 (MMP1) or n=5 (matriptase and hepsin) independent experiments from independent populations of chondrocytes.

With the western blotting data on matriptase regulation by loading being inconclusive, the effect on gene expression was explored. BNCs were loaded and mRNA was extracted 0, 6 and 24 hours post-loading and qPCRs were undertaken for *ST14* (matriptase), *F2RL1* (PAR2) and *HPN* (hepsin) (Figure 3.8). At 24 hours post-loading, there was a trend of up regulation of *ST14* though this was not statistically significant ($p=0.07$) and an up regulation of *F2RL1*. *HPN* however appeared to be down-regulated post-loading, but it is important to note that this gene had a very low expression level and thus very high cycle threshold (Ct) values making data analysis less robust.

It was observed that the Ct values for the housekeeping gene loading control *GAPDH* were higher at later time points post-loading (namely 24 hours) compared to earlier time points, implying a lower amount of starting cDNA. The average Ct value for *GAPDH* at 24 hours post-loading across four independent experiments was 22.3, whereas the average value for unloaded control, 0 and 6 hours post-load (pooled) for the same experiments was 19.2 – suggesting around 8.5 fold less *GAPDH* and thus starting mRNA. This raised concerns that the viability of the cells could be adversely affected by the loading regimen. Previously, cell viability in agarose culture had been ascertained indirectly by observing successful secretion of PCM and the observation of cell division by microscopy, however no assays had been undertaken to measure cell viability post-loading.

In order to explore cell viability post-loading, LIVE/DEAD® assays were undertaken on loaded constructs (see chapter 2.2.10) (Figure 3.9). Despite being unable to quantify cell death, it was clear that following loading there was cell death with the effects more pronounced at 24 hours post-loading. This increase in cell death correlates with the observed higher Ct values on qPCR undertaken at this point.

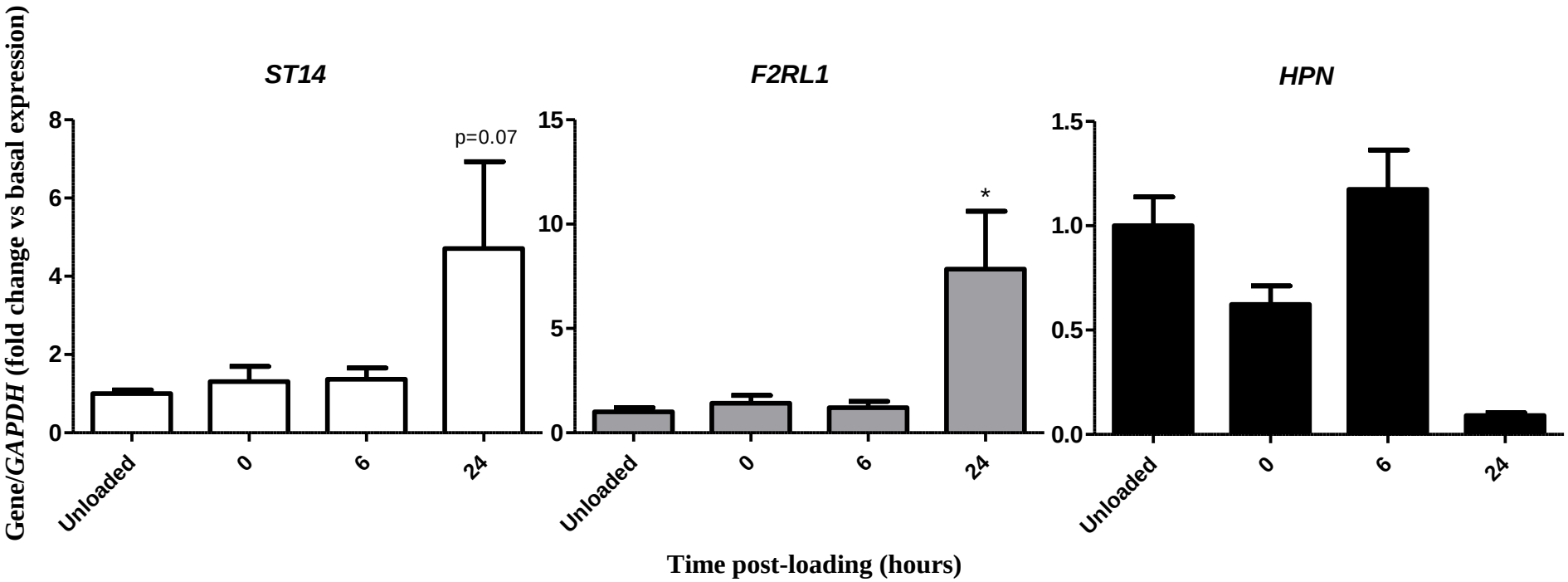

Figure 3.8: Exploration of *ST14*, *F2RL1* and *HPN* expression following mechanical loading

BNCs encapsulated in agarose underwent 30 minutes of dynamic loading (20-40kPa at 0.33Hz). Following loading, mRNA was extracted as described in chapter 3.2.2 and reverse transcribed to cDNA. qPCRs were undertaken for various indicated genes, normalised to *GAPDH* housekeeping gene (mean ± SD; where * $p < 0.05$, by unpaired two-tailed T Test compared to basal expression, unloaded control). Data pooled from four separate chondrocyte populations, and significant outliers were identified by a Grubb's test and removed from the analysis.

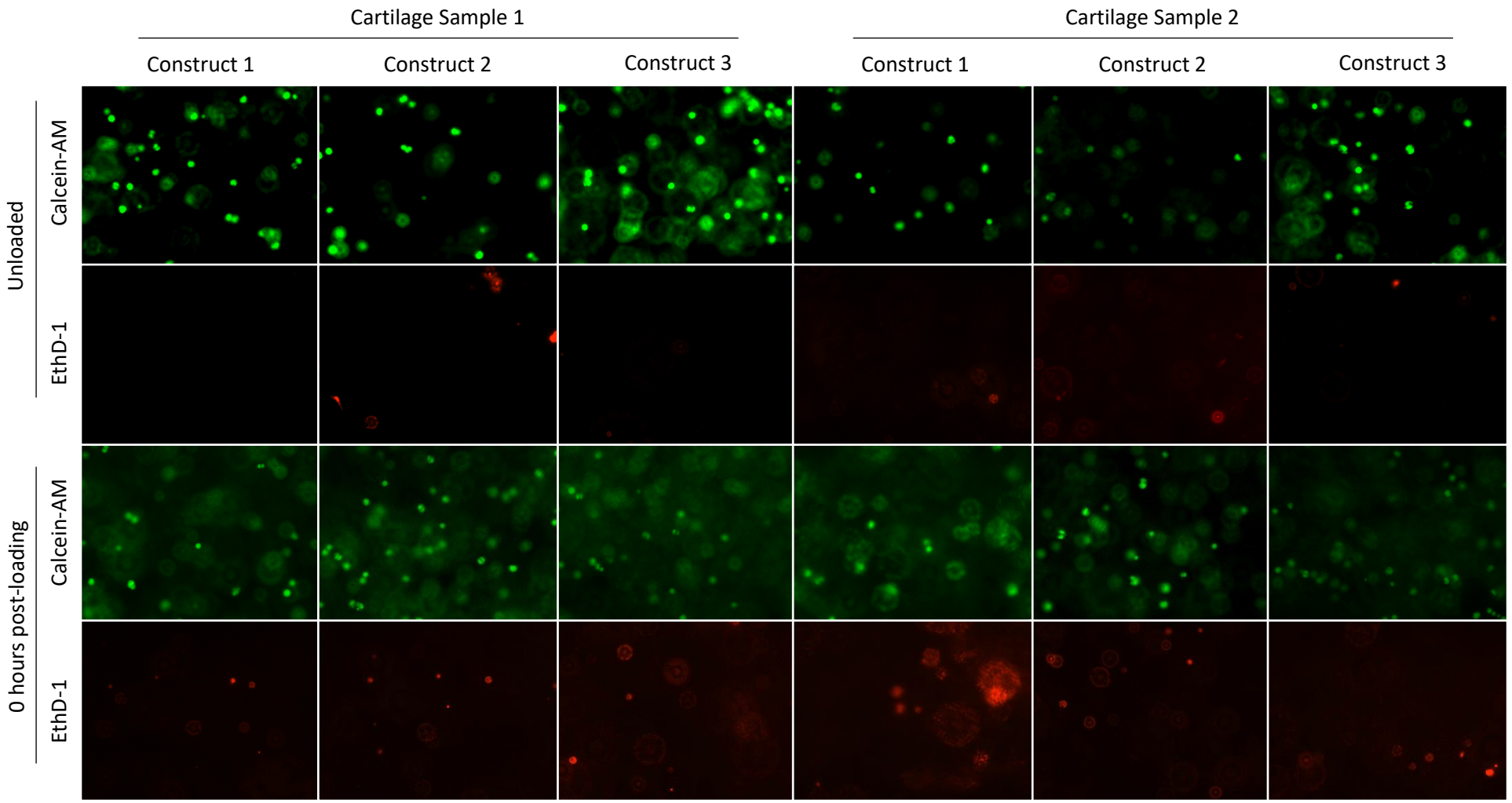
Cartilage Sample 1
Cartilage Sample 2
Construct 1
Construct 2
Construct 3
Construct 1
Construct 2
Construct 3
Unloaded
Calcein-AM
EthD-1
0 hours post-loading
Calcein-AM
EthD-1

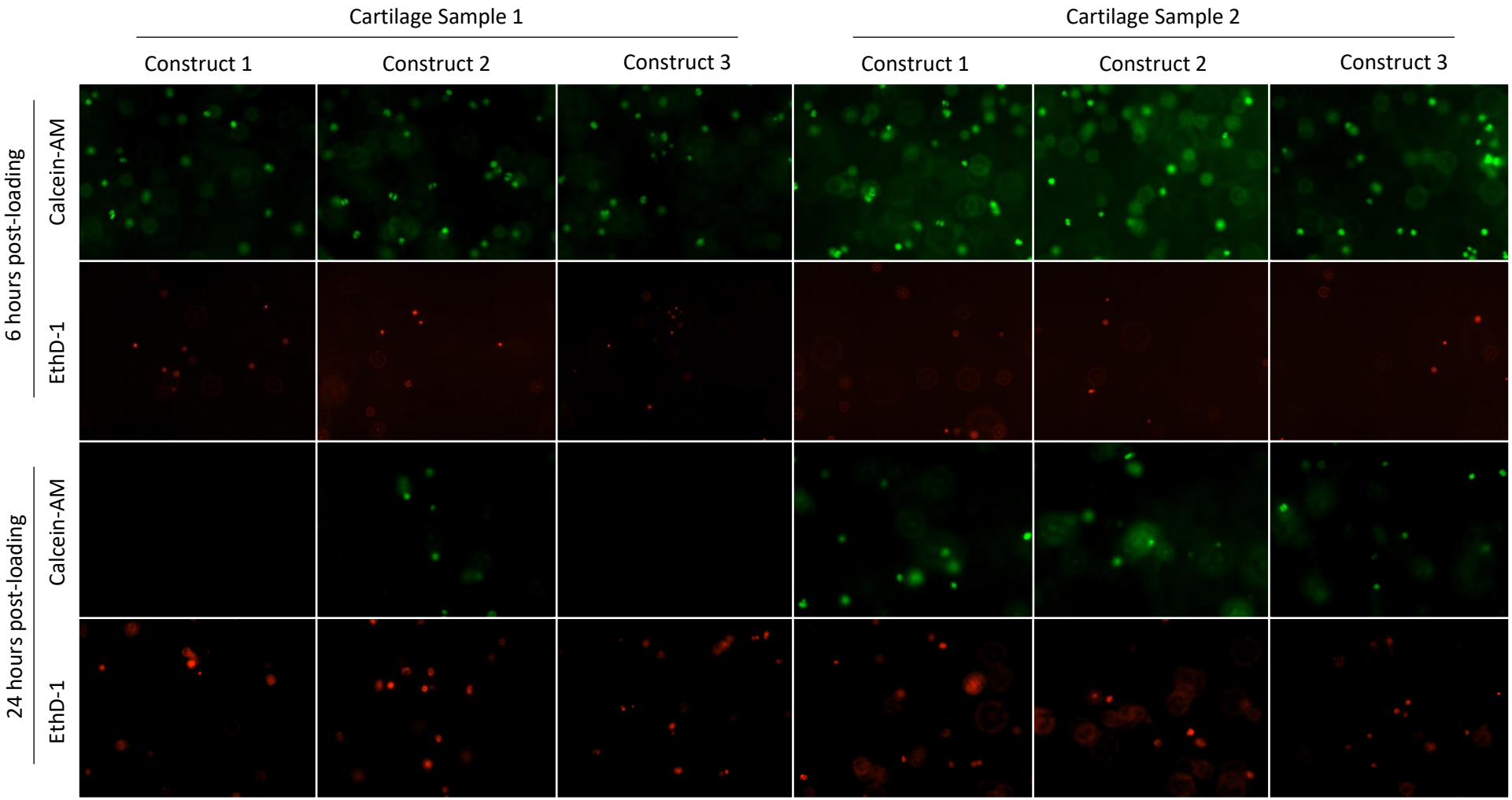

Figure 3.9: Exploration of cell death in BNCs following mechanical load

BNCs encapsulated in agarose underwent 30 minutes of dynamic loading (20-40kPa at 0.33Hz), following which a sample was taken to perform a LIVE/DEAD® assay as described in chapter 2.2.9. Calcein-AM stains only live cells, whereas EthD-1 stains only dead cells. Constructs were generated from BNCs obtained from two bovine noses, and each time point for each nose had three technical replicates (labelled construct 1, 2 or 3). Calcein-AM and EthD-1 images from corresponding sample are taken on the same field of view, simply taking images with different fluorescent filters.

Based on these results, it was difficult to draw firm conclusions on gene expression at later time points following loading, thus making this loading regimen inappropriate for exploring the effect of loading on the expression of genes such as *ST14* and *HPN*. Despite the utilised loading regimen having being previously described in the literature, regimens of lower pressures were tested to explore whether *FOS* could be up-regulated retaining greater cell viability. A loading regimen of 10-30 kPa at 0.33 Hz for 30 minutes was sufficient to upregulate *FOS* expression (Figure 3.8), however LIVE/DEAD staining revealed that cell death also increased following load (data not shown). Reducing the loading regimen to 0-20kPa at 0.33Hz for 30 minutes resulted in better cell viability immediately post-loading (data not shown), however the up regulation of *FOS* was at a much lower level, with a fold change of 1.46 compared fold changes of 7.42 and 5.73 for 20-40 kPa and 10-30 kPa regimens, respectively (Figure 3.10). This small fold-change was statistically significant, however due to its small magnitude it was decided not to pursue this regimen because of potential issues with sensitivity and resolution of other genes.

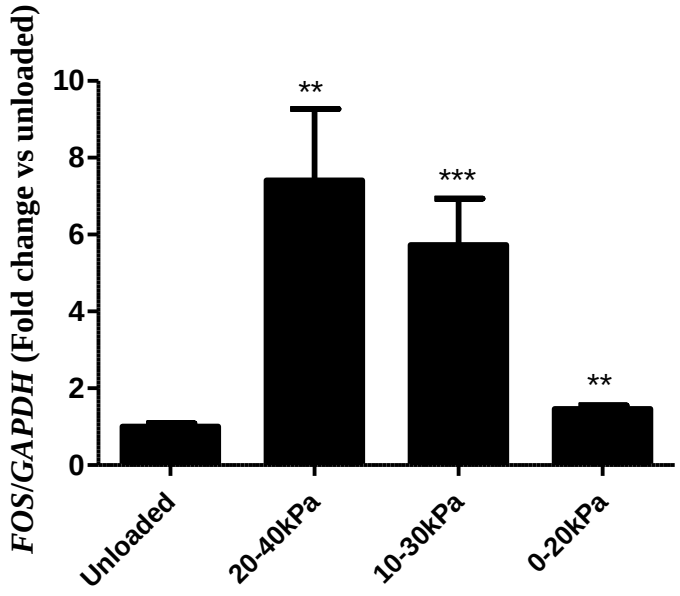

Figure 3.10: *FOS* expression following differing loading regimens
BNCs encapsulated in agarose underwent 30 minutes of dynamic loading of different loading regimens (20-40kPa, 10-30kPa or 0-20kPa, all at 0.33Hz). Immediately post-loading, mRNA was extracted as described in chapter 2.2.8 and reverse transcribed to cDNA. A qPCRs were undertaken for *FOS*, and normalised to *GAPDH* housekeeping gene (mean ± SD; where ** $p < 0.01$; *** $p < 0.001$, by unpaired two-tailed T Test compared to basal expression, unloaded control). Data pooled from either two (10-30kPa and 0-20kPa) or four (unloaded and 20-40kPa) separate chondrocyte populations.

Based on these issues with long-term viability of cells following loading, it was decided to examine gene expression changes at earlier time points post-loading when viability was not compromised.

3.2.4 Assessment of mechanical loading on known regulators of collagenase expression

Previous work in our group has identified key regulatory components of collagenase expression in chondrocytes following pro-inflammatory IL-1+OSM stimulation in HAC. It was hypothesised that abnormal loading on chondrocytes results in phenotypical changes similar to pro-inflammatory stimulation, therefore it was of interest to ascertain whether these regulatory components followed similar expression patterns following loading, to IL-1+OSM stimulation. Importantly, these regulators are thought to be slow immediate early genes (IEG), and thus are expressed in the first few hours of IL-1+OSM stimulation in HAC, and therefore are better candidates for study using the Flexcell BioPress system.

As prior work on these regulatory components was performed in HAC, it was of initial interest to explore the kinetics of gene expression following IL-1+OSM stimulation in BNC in monolayer culture before subsequently comparing the effect of loading (Figures 3.11 and 3.12). As expected, *FOS* expression is significantly elevated 1 hour following IL-1+OSM stimulation, before rapidly returning to lower levels. As in HAC, *ATF3*, *CSRNP1* and *EGR2* were all also rapidly up-regulated in BNC. Following the expression of these early response genes to pro-inflammatory stimulation, collagenase (*MMP1* and *MMP13*) expression gradually increases over the 24-hour time-course. Based on the data obtained from stimulating BNC in monolayer, it was clear that the first 3 hours of the time-course are of greatest interest for *ATF3*, *CSRNP1* and *EGR2* so a time-course of this length was undertaken following BNC loading. Furthermore, prior data (Figure 3.9) suggest that cell viability is higher in these early time points.

Interestingly, *FOS* expression hit a peak at 1-hour post-loading, reaching a fold increase of 38 compared to unloaded samples, whereas immediately post-loading, the fold increase was 10. Previously, *FOS* expression had been examined immediately post-loading for validating the compression system, as this was the time point utilised in the literature[239,244,245]. *ATF3* expression reached maximal expression immediately post-load, reducing but remaining significantly elevated for the remainder of the time-course, a similar profile to pro-inflammatory stimulation. *CSRNP1* and *EGR2* had highly similar expression profiles to each other, with maximum expression 2 hours post-load, which

differs from their expression following IL-1+OSM stimulation where their expression is more similar to *FOS*, reaching maximum expression early at 1 hour, before lowering 1.25 hours onwards. Based on the earlier concerns with cell viability, later time points were not examined, thus there is no examination of *MMP* expression at 6-24 hours, however protein expression data described in chapter 3.2.3 do suggest that MMP-1 protein expression is indeed elevated at 6 and 24 hours. Cell viability was also examined for the duration of this time-course, which appeared good for the duration with no observable cell death (data not shown).

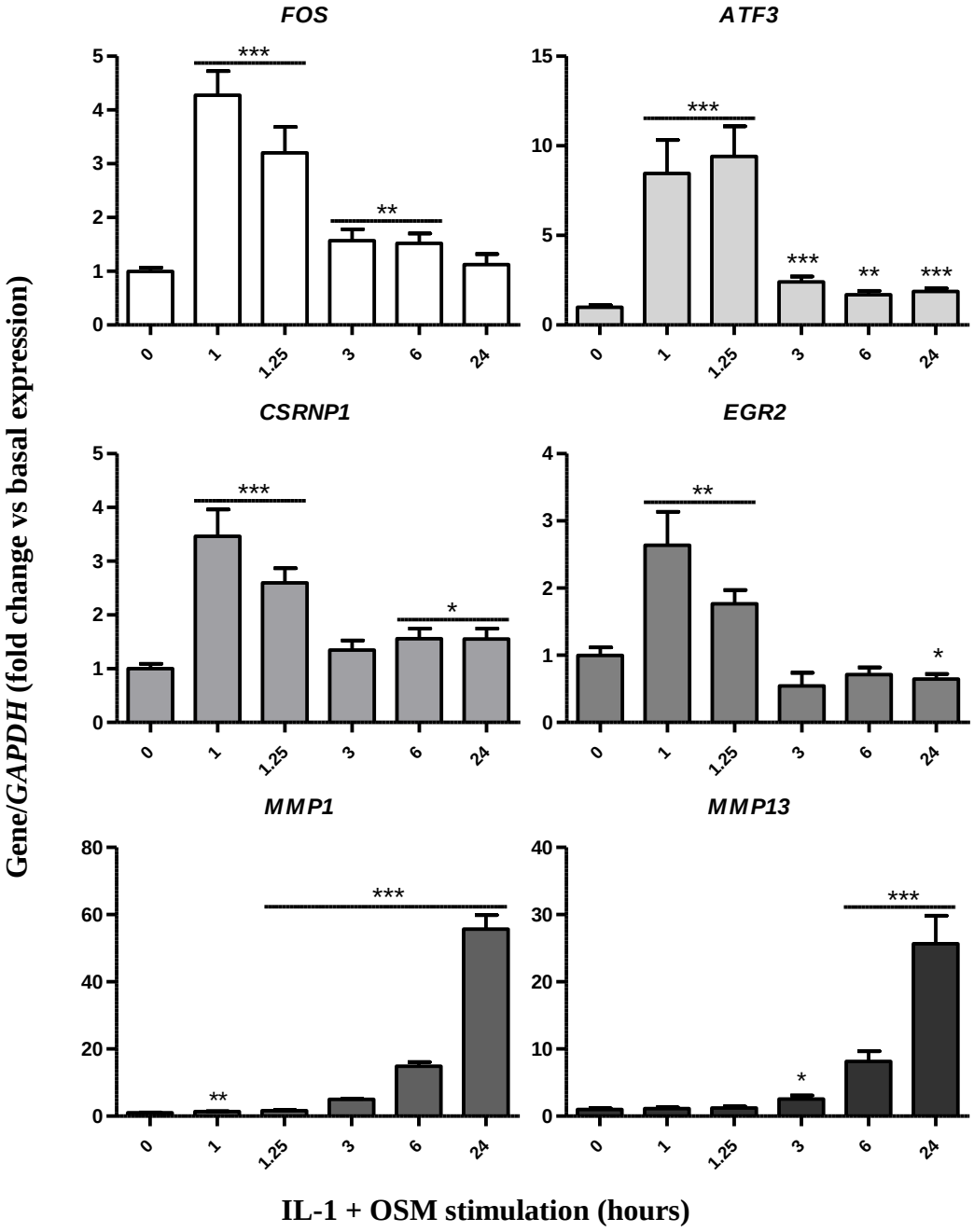

Figure 3.11: Exploration of gene expression changes following IL-1+OSM stimulation
BNCs seeded at a density of $10x10^4$ cells per well in a 96-well plate were cultured for 3 days before serum starving overnight and stimulating with IL-1 at 0.5ng/mL and OSM at 30ng/mL for varying lengths. Following stimulation, mRNA was extracted and reverse transcribed to cDNA and qPCRs were undertaken for various indicated genes, normalised to *GAPDH* housekeeping gene (mean ± SD; where * $p < 0.05$; ** $p < 0.01$; *** $p < 0.001$, by unpaired two-tailed T Test compared to basal expression, T=0). Data pooled from two separate chondrocyte populations.

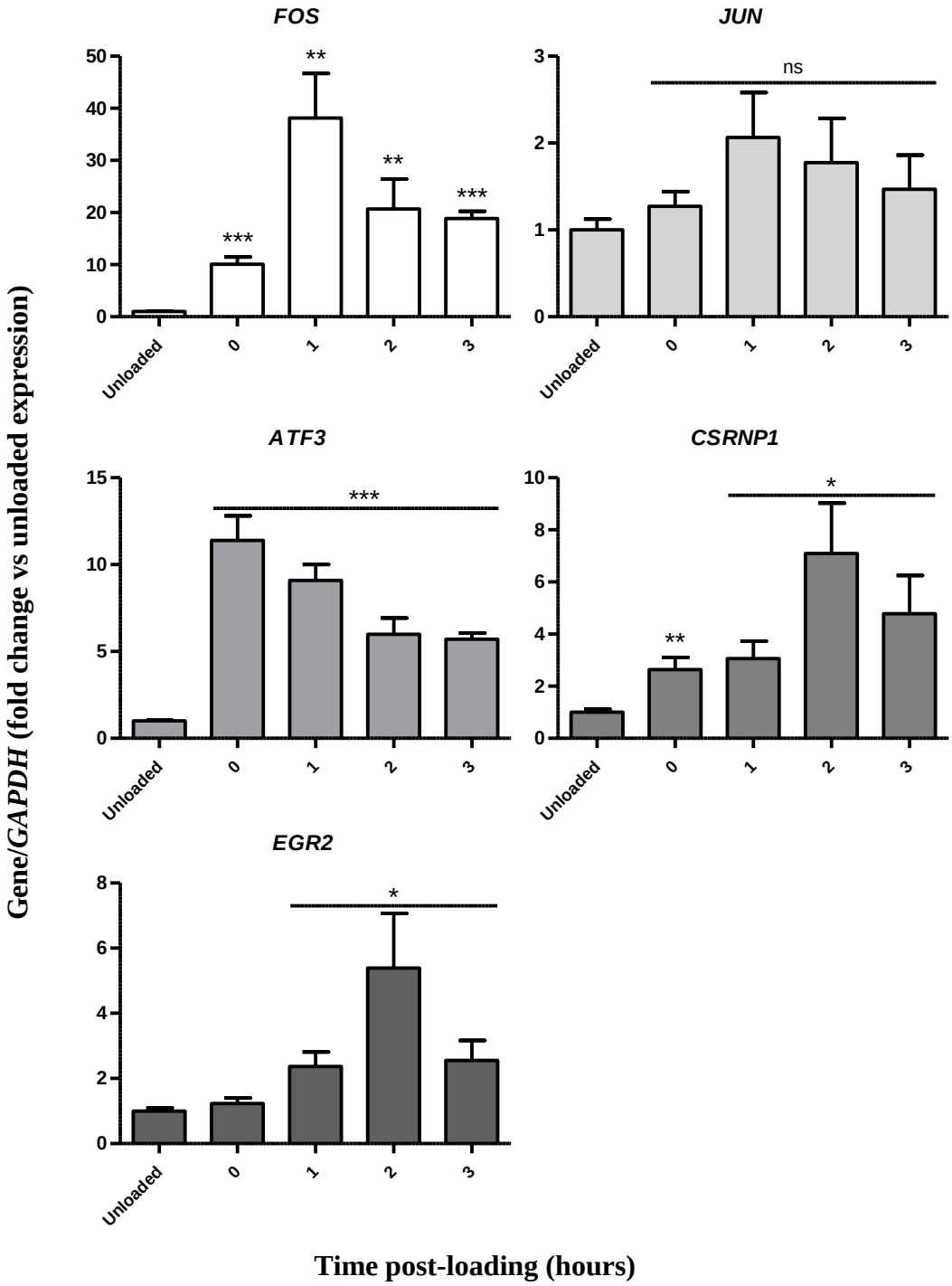

Figure 3.12: Exploration of gene expression changes following mechanical load
BNCs encapsulated in agarose underwent 30 minutes of dynamic loading (20-40 kPa at 0.33 Hz). Following loading, mRNA was extracted as described in chapter 3.2.2 and reverse transcribed to cDNA. qPCRs were undertaken for various indicated genes, normalised to *GAPDH* housekeeping gene (mean ± SD; where * $p < 0.05$; ** $p < 0.01$; *** $p < 0.001$, by unpaired two-tailed T Test compared to basal expression, unloaded control). Data pooled from two separate chondrocyte populations.

After showing that *ATF3* expression was increased post-loading, ATF3 expression was examined at the protein level also. Expression of ATF3 was clearly induced by mechanical loading in a time dependent manner (Figure 3.13), however as with the earlier protein expression experiments (chapter 3.2.3), there was variability between experiments, thus only densitometric analysis is presented here. CSRNP1 and EGR2 expression could not be examined due to lack of antibody cross reactivity with bovine proteins.

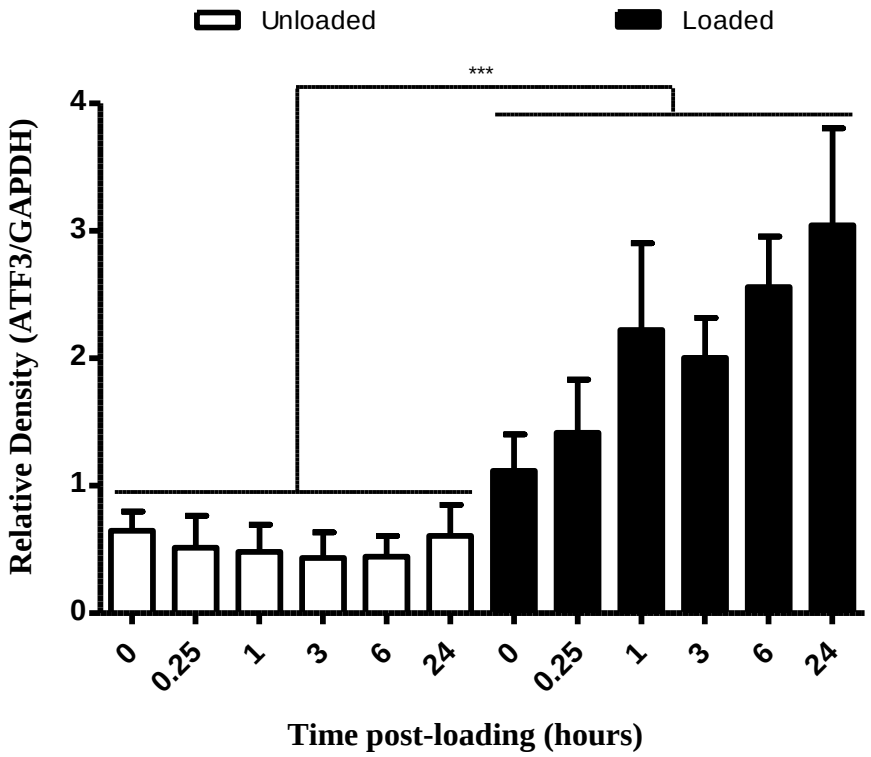

Figure 3.13: ATF3 expression following mechanical load
BNCs encapsulated in agarose underwent 30 minutes of dynamic loading (20-40 kPa at 0.33 Hz), following which the gels were frozen in liquid nitrogen at indicated time points post-loading. SDS-PAGE gels were run and western blots for ATF3 were undertaken. The blots were re-probed with GAPDH as a loading control and densitometric analysis was undertaken. Density is relative to appropriate GAPDH time point (mean ± S.E.M; where *** $p < 0.001$ by two-way ANOVA comparing all unloaded and loaded samples). Data generated from n=5 independent experiments from independent populations of chondrocytes.

3.3 Discussion

In this chapter, a method by which to explore the effect of mechanical loading of cells cultured in agarose was developed and optimised. Overall, data presented in this chapter suggest that the system has severe limitations in terms of cell viability over 24 hours, however this system was best suited over shorter term experiments.

A large amount of initial work using the Flexcell BioPress system was based on the methods described by Bougault et al (2009) in their detailed published protocols. Their methods for initial cell culture to produce PCM proved successful, and their loading regimen proved successful in BNCs, but not SW1353 cells. Their method to extract protein for SDS-PAGE also worked, however their method for RNA extraction was unsuccessful despite multiple attempts. Further published methods to extract RNA (for example, Wang & Stegemann (2010)[248] and Mio *et al*. (2006)[249]) were attempted, however no success was achieved with any of these methods. Subsequently, a condition scouting experiment was performed based on the method of Mio *et al*. (2006)[249] as their method appeared the most promising. Optimal conditions for the extraction of RNA from SW1353 cells which differed from that of Mio *et al*. (2006) was identified in dissolution of the construct in 500 µl Qiagen buffer RLT, as opposed to 1320 µl which their paper would suggest to be optimal for the construct size in the present study. Their paper also suggested a correlation between pH and RNA yield, where better yields were obtained when lowering pHs. Lower pH values act to neutralise electrostatic repulsion between the negatively charged silica membrane and negatively charged nucleic acid, thus resulting in higher RNA yields binding to the column[250].

A trend of increasing yields with lowering pH in the 1000 µl buffer RLT group was observed, however no such trend existed in the optimal 500 µl group. Extraction conditions for BNC/agarose constructs were further optimised as these were the cells to be utilised in subsequent gene expression experiments. As with SW1353 cells, the optimal volume of buffer RLT for dissolution was 500 µl and the optimal amount of sodium acetate pH 5.5 added appeared to be 30 µl, however this was not significantly higher than 20 µl ($p = 0.22$). The trend that 30 µl sodium acetate pH 5.5 resulted in a better yield in BNC whereas in SW1353 cells sodium acetate pH 5.5 appeared to make no difference could be explained by the fact that BNCs produce a PCM when cultured in agarose. This PCM stained positive for GAG, which is negatively charged and would therefore

contribute to the net negative charge of the lysis solution prior to column loading. It is possible that the higher volume of sodium acetate pH 5.5 required to optimise RNA yield from BNC reflects this GAG. These conditions were therefore used for subsequent RNA extractions.

It is difficult to explain the observed differences in optimal extraction conditions with Mio *et al.*[249], however differences in experimental setup are the likely reason. They observed agarose in the eluted RNA when using less than 840 µl buffer RLT, however samples in the present study were clear. A key difference in the experimental designs are that they used 1% agarose whereas 2% agarose was used in the present study, however this does not logically explain the observed differences. It would be reasonable to assume that the higher concentration of agarose would be more likely to result in carryover agarose in the eluted RNA, which did not prove to be the case.

A comparison of the human chondrosarcoma cell line SW1353 with BNCs was performed in order to decide which would be more suited to this research. SW1353 cells clearly did not secrete a PCM, nor were they responsive to loading in terms of p38 phosphorylation. It is known that the PCM plays an important role in the mechanical transmission of loading stimuli[251], therefore the fact that SW1353 cells did not respond to load could possibly be explained as such. SW1353 cells are a commonly used cell line for research on chondrocytes, however their use has several limitations. A comparison between SW1353 cells and HAC has revealed multiple differences in gene expression profiles between the two cell types[252]. Of greatest interest is the fact that SW1353 cells express very low levels of SOX9, a vital "master" transcription factor for all stages of chondrogenesis and chondrocyte function[253-256]. SOX9 is required for the formation of cartilage in terms of collagen type II expression[254], as well as aggrecan expression[257,258]. Staining for both collagen (Masson's Trichrome) and proteoglycans (Safranin O and Alcian Blue) show no matrix secretion, which could be a result of low SOX9 expression. SW1353 cells also express low levels of SOX5 and SOX6, which are two other SOX transcription factors important in cartilage, and have been shown to be important in the expression of aggrecan[258]. Reflecting this low expression of SOX genes, expression of key matrix genes such as collagen type II and aggrecan were hardly detectable in SW1353 cells[252]. Interestingly, when *SOX9* is overexpressed in SW1353 cells, their *ACAN* (aggrecan) expression also increases (David Young, personal communication).

After 6 days in agarose culture, BNCs did however secrete a PCM, which appeared to contain proteoglycans but not collagen, perhaps reflecting the additional time a collagen matrix requires to form[259,260]. This PCM was shown to be necessary for responding to loading in terms of *FOS* induction by testing the loading of BNCs after only 2 days in culture. The chondrocyte with its surrounding PCM is known as a chondron[261] and these are known to have a proteoglycan-rich matrix[7], a characteristic shared with the BNCs cultured in agarose in the present study. The PCM is thought to anchor the chondrocyte to the surrounding tissue by a network of type VI collagen[262] and is considered to act as a transducer of mechanical stimuli from the external environment of the tissue into the cell[263,264]. As such, it is perhaps unsurprising that when undertaking loading experiments on the BNCs before they secrete a PCM, there is no observed up-regulation of *FOS* expression. Indeed, on close examination, it appears that the cells are in limited contact with the agarose until they form a PCM (Figures 3.1 and 3.4). It is possible that the BNCs are suspended in an aqueous solution when first seeded in the agarose, which is gradually replaced by PCM over the 6 days. This aqueous space would not appear on the histological analysis, and appear as empty space under the microscope. When cells in this form are subjected to compressive load, they are likely protected from the compressive forces and do not have the forces applied to the agarose transmitted to the cell and thus there is no up-regulation of *FOS*.

After confirming that BNCs respond to mechanical loading by looking at previously described markers such as p38 phosphorylation and *FOS* induction[239,244,245], the key aims of this chapter were addressed – to explore the effect of mechanical loading on matriptase and hepsin expression. As proteinase expression is usually expected at later time points post-stimulus, a 24-hour time-course was decided upon. The effect of loading on matriptase and hepsin expression gave rise to mixed results. The experiment was repeated several times with chondrocytes extracted from multiple bovine nasal septa. Down and up-regulation of both proteinases was observed in these studies, and when densitometric analysis was undertaken and the data pooled, no significant effect of loading (up-regulation nor down-regulation) was observed. To validate the experiments, the expression of MMP-1 was assessed, and this was indeed significantly up-regulated in a time-dependent manner over the time-course. MMP-1 expression has been shown to be up-regulated in a variety of models including tensile strain of rabbit knee articular chondrocytes in monolayer culture[265]; unconfined compression of femoropatellar cartilage disks in explant culture[266]; and dynamic compression of calf femoropatellar

chondrocytes seeded in a poly(ethylene glycol) dimethacrylate hydrogel[267]. However, it is important to note that not all loading regimens result in MMP-1 up-regulation, as down-regulation has also been observed following cyclic tensile strain of rabbit knee and shoulder chondrocytes[268]. To our knowledge, this is the first study to describe MMP-1 up-regulation in chondrocytes cultured in agarose, but based on the literature, this result is likely to be expected. Taken together, these data suggest that the tested loading regimen successfully applies mechanical loading to the chondrocytes and results in elevated levels of MMP-1, however matriptase and hepsin expression are not regulated by this loading.

An interesting observation was that there was a significant increase in MMP-1 expression immediately post-loading, as well as some individual blots for matriptase and hepsin showing a similar effect. 30 minutes of loading would not allow for sufficient time for *de novo* protein synthesis of proteases such as MMP-1, matriptase or hepsin, so another explanation must be sought. A potential explanation could be that rather than being an up-regulation of the gene, there is in fact a reduction in protein turnover by loading, thus the observed increase in protease on the blot, though there is limited evidence in the literature to support this theory. There is however some evidence that protein turnover can be regulated by mechanical loading in muscle cells. For example actin[269], myosin[270] and collagen[271] have all been shown to have reduced protein turnover when undergoing mechanical strain. It is important to note that these three examples are all structural proteins, thus their mechano-regulation is not necessarily a surprise. Interestingly, proteases such as MMP-1 are key regulators of structural proteins, in that they cleave components such as collagen.

It is important to stress the fact that this is not a definite conclusion on the hypothesis of whether matriptase and hepsin are mechanosensitive, as there are a huge range of other loading regimens that could be tested if time and resources were not a limiting factor. What can be concluded is that under the tested conditions, where MMP-1 is clearly induced, matriptase and hepsin expression was more variable. Across the experiments, variation in responses was observed. In terms of causes, biological variability is a possibility, indeed it is known that the breed of cattle utilised, the Hereford, exhibits significant genetic variation within the breed[272] and the genetic diversity within the breed is considered to be as great as exists within human populations[273].

Another potential cause for variability is the Flexcell BioPress system itself. The preparation of the BioPress plates for loading requires the adjustment of the stationary platen to rest directly on top of the gel. As described in chapter 2.5, this can be calculated by knowing the accurate height of the gel. However, the "starting" position of the platen can only be set by eye and by touch, which is not a very scientific method as small discrepancies between platens can lead to differences in the loads given to each gel. If the platen is slightly too far away from the gel, but slightly too close to another gel – differences that the human eye cannot see – then both gels will receive different loads. As there are a limited number of gels obtained per bovine nasal septum, the protein expression experiments are undertaken with only a single technical replicate, which means that any variations within a time point will not be cancelled out.

Due to initial difficulties in extracting the RNA from the agarose constructs, the experiments exploring gene expression were undertaken after the experiments exploring protein expression. Based on the concerns with variability between experiments potentially being caused by the Flexcell system itself, the experiments exploring gene expression were designed to contain three technical replicates at each time point with the hope of generating more robust data. The expression of *ST14*, *HPN* and *F2RL1* were explored post-loading and there were hints that *ST14* and *F2RL1* might be up-regulated at 24 hours post-loading. In undertaking these experiments it was observed that the Ct values for *GAPDH* were higher at 24 hours post-loading compared to earlier time points and unloaded controls. This raised concerns that the cell viability over time might be affected by the application of load. To address this, cell viability assays were performed which suggested that the cells were indeed losing their viability over the time-course with the effect more pronounced at 24 hours post-loading.

It was not ascertained whether the cells are undergoing necrosis or apoptosis. As the cells appear to take time to die post-loading, apoptosis is the more likely culprit as if the cell loading machine was physically compressing the cells to death, then one would expect cell death to be observed earlier. Furthermore, following loading, the cells have a similar appearance compared to unloaded control cells, with no obvious signs of physical deformation. In terms of the causes of cell death, there is evidence in the literature that suggests c-Fos may act as a pro-apoptotic molecule in various cell types[274-277] and loading resulted in high expression levels of *FOS*, with a fold increase level of expression reaching 38 times that of basal (unloaded) levels 1-hour post-loading. This was a much

larger induction of *FOS* than was induced by IL-1+OSM stimulation which only reached an induction of 4.5 fold higher than basal (unstimulated). It is possible that this very high "dose" of *FOS* could be lead to apoptosis. Indeed, there are positive correlations between c-Fos expression levels and amount of apoptosis previously described[278,279].

Since it was possible cell death was linked to cell loading in a dose-dependent manner, other dynamic loading regimens with a lower pressure – 10-30 kPa and 0-20 kPa were tested, both for the same length and frequency as the previous experiments (30 minutes at 0.33 Hz). The 10-30 kPa also stimulated *FOS* at a slightly lower level than 20-40 kPa, however this did not result in better cell viability. The 0-20 kPa, however resulted in only a very small induction of *FOS* expression which would likely result in lower resolution of downstream genes of interest, so it was decided to be inappropriate to further test. These three tested regimens were all 30 minutes long, with the same dynamic waveforms (0.33 Hz, square waveform). There are a large range of other loading regimens possible to utilise by varying the conditions, using a different waveform, different frequency, different length etc. It is possible that there are loading regimens which would stimulate BNCs but not kill the cells. Unfortunately, due to the time-consuming nature of these experiments, it was not possible to explore further loading regimens.

The loading regimen used in this study has previously been described in the literature with no mention of adverse effect on cell viability[239,244,245], however these studies utilised a different type of chondrocyte – embryonic mouse chondrocytes. Bovine nasal septum cartilage does not undergo mechanical loading *in vivo*. A comparison of bovine nasal and articular chondrocytes with respect to loading as not been undertaken to date, however it is possible that BNCs are less able to tolerate mechanical loading. It has been shown that other non-loading cartilage, for example auricular cartilage, has different responses to articular cartilage differ in responses following dynamic loading in terms of collagen type I and II and aggrecan expression with articular cartilage showing greater increases in expression, although viability was not explored[280]. It is known that BNCs differ to bovine articular chondrocytes (BACs) (metacarpophalangeal) in that articular chondrocytes express more type II collagen and aggrecan, whereas BNCs express more type I collagen[281]. Furthermore, the response of BNCs and BACs to pro-inflammatory cytokines (IL-1α) differ in terms of subsequent *ADAMTS4* expression[282], and it is highly likely other responses differ between the two cell types. Interestingly, a study comparing the use of either human nasal or human articular chondrocytes in loading following tissue

engineering suggested that nasal chondrocytes were able to respond to and endure various loading regimens including a higher expression of matrix protein than articular chondrocytes, although cell viability was not explicitly tested nor discussed[283].

As cell viability and *GAPDH* Ct values appeared better at earlier time points post-loading, it was decided to look at other genes relevant to OA which would potentially be mechanosensitive. Our group has recently identified several transcription factors implicated in regulation of MMP-1 and MMP-13 following IL-1+OSM stimulation – *ATF3*, *CSRNP1* and *EGR2* (Chris MacDonald, unpublished). This prior work was performed in HAC, and was first successfully replicated in BNC before exploring in the loading model. Following loading the three genes did indeed get up-regulated, however the temporal regulation appeared to differ to pro-inflammatory stimulation. Following IL-1+OSM stimulation, *FOS*, *CSRNP1* and *EGR2* had very similar expression profiles of reaching peak expression at 1 hour, before beginning to reduce by 1.25 hours whereas *ATF3* also peaked early, at 1.25 hours. Following loading, however, *ATF3* peaked first, immediately post-loading, with *FOS* peaking at 1-hour post-loading whereas *EGR2* and *CSRNP1* peak 2 hours post-loading. It is likely that these slight differences in temporal regulation reflect the differing stimuli.

ATF3 has previously been shown to be mechanosensitive to stretch in human bronchial epithelial cells[284] and rat cardiomyocytes[285], whereas *EGR2* mechano-sensitivity to stretch has been demonstrated in both rat retinal glial cells[286] and in mouse osteoblastic cell line MC3T3-E1[287]. *EGR2* has also been shown to be mechanosensitive to loading *in vivo* in mouse tibiae[288]. In terms of mechanical loading in chondrocytes, *ATF3* and *EGR2* up-regulation were observed in a gene expression microarray following the loading of embryonic mouse chondrocytes with a very similar loading regimen (20-40 kPa for 30 minutes at 0.5 Hz, compared to 20-40 kPa for 30 minutes at 0.33 Hz in the present study) with fold increases of 1.47 and 2.60, respectively, immediately post-loading[245]. These data suggest that *EGR2* expression immediately post-loading has not yet significantly increased, with no significant effect observed until 1 hour, and then peaking at 2 hours. The present study also observed a much larger fold increase of ATF3 compared to theirs, potentially reflecting that adult bovine chondrocytes might be more responsive than embryonic mouse chondrocytes. Comparing these studies also highlights the importance of temporal kinetics of gene expression, and the limitations of only picking a single time point for analysis.

CSRNP1 (sometimes referred to as *AXUD1* in the literature), has been shown to be up-regulated following 6 hours of "compression" in human primary cementoblasts[289], however they used a centrifuge to apply the compression, which is less physiologically relevant than other systems. To our knowledge, the observation that *CSRNP1* is up-regulated in chondrocytes following mechanical loading is a novel observation.

3.4 Summary

- Chondrocytic cell line SW1353 does not secrete PCM whilst cultured in agarose and do not appear responsive to mechanical loading. BNCs however do secrete a PCM and do respond to mechanical loading in terms of p38 phosphorylation and *FOS* induction.

- Matriptase and hepsin do not appear to be regulated at the protein level post-loading, however MMP-1 is.

- Mechanical loading of BNCs appears to result in cell death, an effect pronounced with time post-loading. As the later time points are more of interest with regards to OA relevant genes, it is difficult to generate confident data with this system. The early time points appear more robust.

- The mechanical loading stimulation of BNCs appears to elicit a similar response to pro-inflammatory stimulation with IL-1+OSM

Chapter 4. Screening of novel proteases with the ability to cleave PAR2

4.1 Introduction

A role for canonical PAR2 activation in the pathogenesis of OA was described in chapter 1, where matriptase is able to cleave and activate PAR2, both of which have elevated expression levels in the disease. This can lead to the induction of many pro-inflammatory genes as well as the key collagenases in articular cartilage, MMP-1 and MMP-13[1].

Cartilage destruction in OA is much more complex than just the action of a single enzyme on a single receptor to induce the expression of a few important genes. Many other proteases have been identified as having roles in OA and other arthritic diseases. Whilst some may directly break down components of the cartilage, such as the aggrecanases ADAMTS-4 and ADAMTS-5[290], others exert their roles indirectly. For example, many enzymes have been identified as part of networks by activating other enzymes. The serine protease plasmin has long been known to possess the ability to activate various proMMPs[291], and subsequently several other proteases including thrombin, neutrophil elastase, and cathepsin G have also been found to possess this activation capacity[121].

The extracellular milieu of enzymes within cartilage (both normal and in disease) is complex, and therefore it is likely there are many unidentified roles for them. This chapter therefore aims to screen whether cartilage (and especially OA)-expressed proteases have the ability to cleave PAR2. The identification of novel cartilage-expressed proteases with the ability to cleave PAR2 could lead to the identification of novel mechanisms in the pathogenesis of OA.

4.1.1 Chapter Aims

- To develop a method to test protease ability to cleave a PAR2 42mer synthetic peptide.
- To screen for proteases from the serine, cysteine and metalloproteinase families for their ability to cleave this PAR2 42mer.

4.2 Results

4.2.1 Validation of a Tris-Tricine SDS-PAGE and silver staining method to visualise PAR2 42mer

4.2.1.1 Design of PAR2 42mer

A literature search was undertaken to compile a list of all previously identified cleavages of PAR2 (appendix 1). This demonstrated that all previously identified cleavages have occurred between positions 31 and position 76 of PAR2. The extracellular domain of PAR2 ends at amino acid 75, therefore it was decided to design a synthetic peptide ending at position 72 as any closer to position 75 would have limited physiological relevance due to enzyme not being able to bind to full-length transmembrane PAR2. The PAR2 sequence from arginine-31 until lysine-72 was therefore kindly synthesised by Dr. Hiroki Shimizu (National Institute of Advanced Industrial Science and Technology (AIST), Sapporo, Hokkaido, Japan) for use in the protease screen (Figure 4.1).

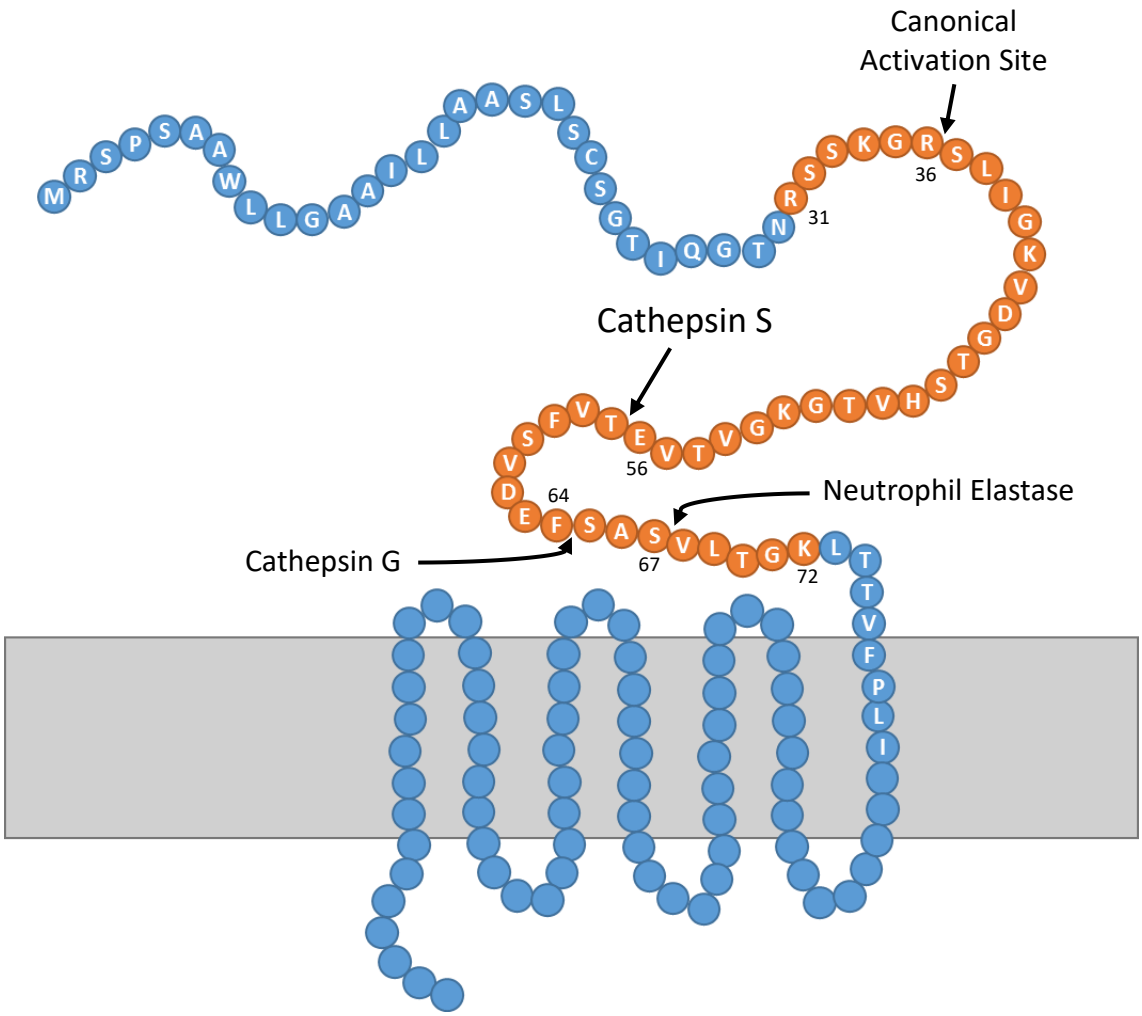

Figure 4.1: Location of PAR2 42mer peptide
A synthetic peptide corresponding from arginine-31 to lysine-72 (in orange) of PAR2 was designed and synthesised. The sites of several key cleavages are also highlighted.

4.2.1.2 Optimisation of Tris-Tricine system to separate peptides

In order to visualise cleavage events of the PAR2 42mer, it was decided to use SDS-PAGE followed by polypeptide staining. The PAR2 42mer is a peptide of 4324.86 Da and is therefore too small to be visualised by "conventional" SDS-PAGE which utilises a Tris-Glycine buffer system to separate the proteins. In order to visualise the PAR42mer and cleavage products, it was decided to utilise a Tris-Tricine system based on the method of Schägger (2006)[292].

Firstly, it was important to ascertain whether the Schägger method would be sufficient to stain for peptides as small as 4 kDa. SDS-PAGE gels with a 20% acrylamide resolving gel and 4% stacking gel were cast, electrophoresed and Coomassie-stained according to the Schägger method with a series of protein/peptide standards ranging from 1,060 Da to

26,600. Using this method, the 1,060 and 3,496 Da peptide/proteins did not successfully stain (Figure 4.2A). The Schägger method used a fixing solution containing 10% acetic acid, and it was hypothesised that this was not a strong enough fixative and the smaller peptide/proteins were able to diffuse out of the gel before being fixed. Glutaraldehyde was therefore utilised as a stronger fixative, and indeed lower MW peptide/proteins were visible following Coomassie staining (Figure 4.2 B).

Despite the tris-tricine system being sufficient to visualise peptide/proteins smaller than the PAR2 42mer, Coomassie staining is not sufficiently sensitive to visualise the PAR2 42mer on an appropriate scale for *in vitro* digests. Silver staining was therefore used. Initially, silver staining following glutaraldehyde fixation was utilised, however this resulted in a very high level of background on the gel (data not shown). Trichloroacetic acid (TCA) was therefore utilised as a stronger fixative than acetic acid, with a trade off against glutaraldehyde: despite poorer fixation, a lower background was observed (Figure 4.2 C).

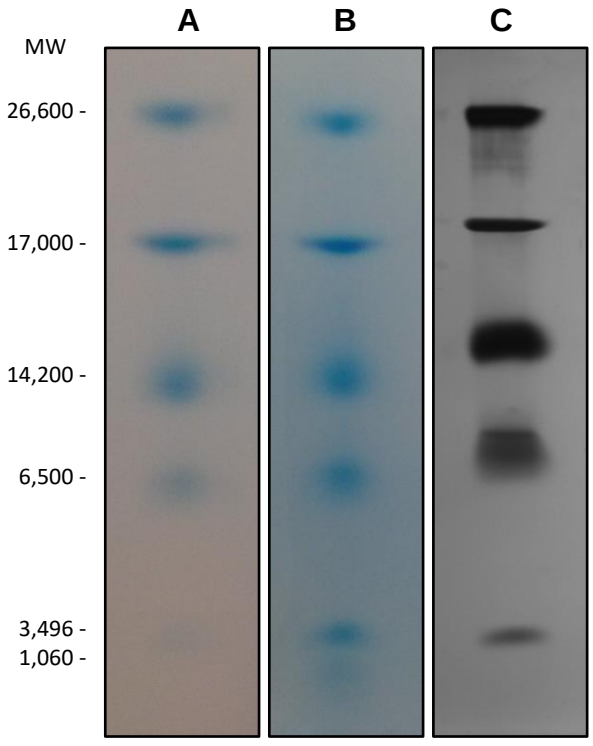

Figure 4.2: Optimisation of fixation and staining of Tris-Tricine SDS-PAGE gels
A series of protein/ peptide standards containing (from smallest to largest) bradykinin, bovine insulin chain B, bovine aprotinin, bovine alpha-lactalbumin, equine myoglobin, and rabbit triosephosphate isomerase were separated by SDS-PAGE. 16% acrylamide tris-tricine gels were cast, electrophoresed and fixed with either 10% acetic acid (A) or 5% glutaraldehyde (B) for 1 hour at room temperature before staining with Coomassie G-250. A 20% acrylamide tris-tricine gel was cast, electrophoresed and fixed with 12% TCA for 1 hour at room temperature before silver staining (C).

4.2.1.3 Screening a panel of proteases known to cleave PAR2

After optimising SDS-PAGE and silver staining for use with peptides the size of the PAR2 42mer, it was of interest to validate a system by which to identify cleavages of the peptide. Four proteases previously identified as being able to cleave PAR2 at various locations were selected for this: matriptase, hepsin, cathepsin G and neutrophil elastase. Matriptase and hepsin are both canonical PAR2 activators cleaving PAR2 at position 36 between arginine and serine[115,293]. Cathepsin G has been identified as a disarmer of PAR2, cleaving the protein at position 64 between phenylalanine and serine[225]. Neutrophil elastase is thought to be a biased agonist and disarmer of PAR2, cleaving at position 67 between serine and valine[225].

Incubation of hepsin and matriptase with PAR2 42mer resulted in a reduction of parent peptide and an accumulation of a single smaller product of >3.5kDa over time (Figure 4.3 A and D). The expected cleavage of matriptase and hepsin would result in fragments of ~3650 Da and ~670 Da, thus the observed product is likely to be the ~3650 Da fragment, whereas the smaller fragment would be too small to observe by this method. Neutrophil elastase and cathepsin G both also cleave the PAR2 42mer (Figure 4.3 B and C), however there was no accumulation of product observed, only a loss of the parent peptide, implying all fragments are too small to observe by SDS-PAGE.

It is important to note that the PAR2 42mer often runs as a doublet by SDS-PAGE. A doublet can be observed in Figure 4.3 D, however one of the gels run in the same experiment ran as a singlet (Figure 4.3 A). By running HPLC, it is clear that only a single product exists (see Figure 5.1 in chapter 5). It was never ascertained why this occurred, and thus it is important to compare the negative control lane to any cleavage lanes.

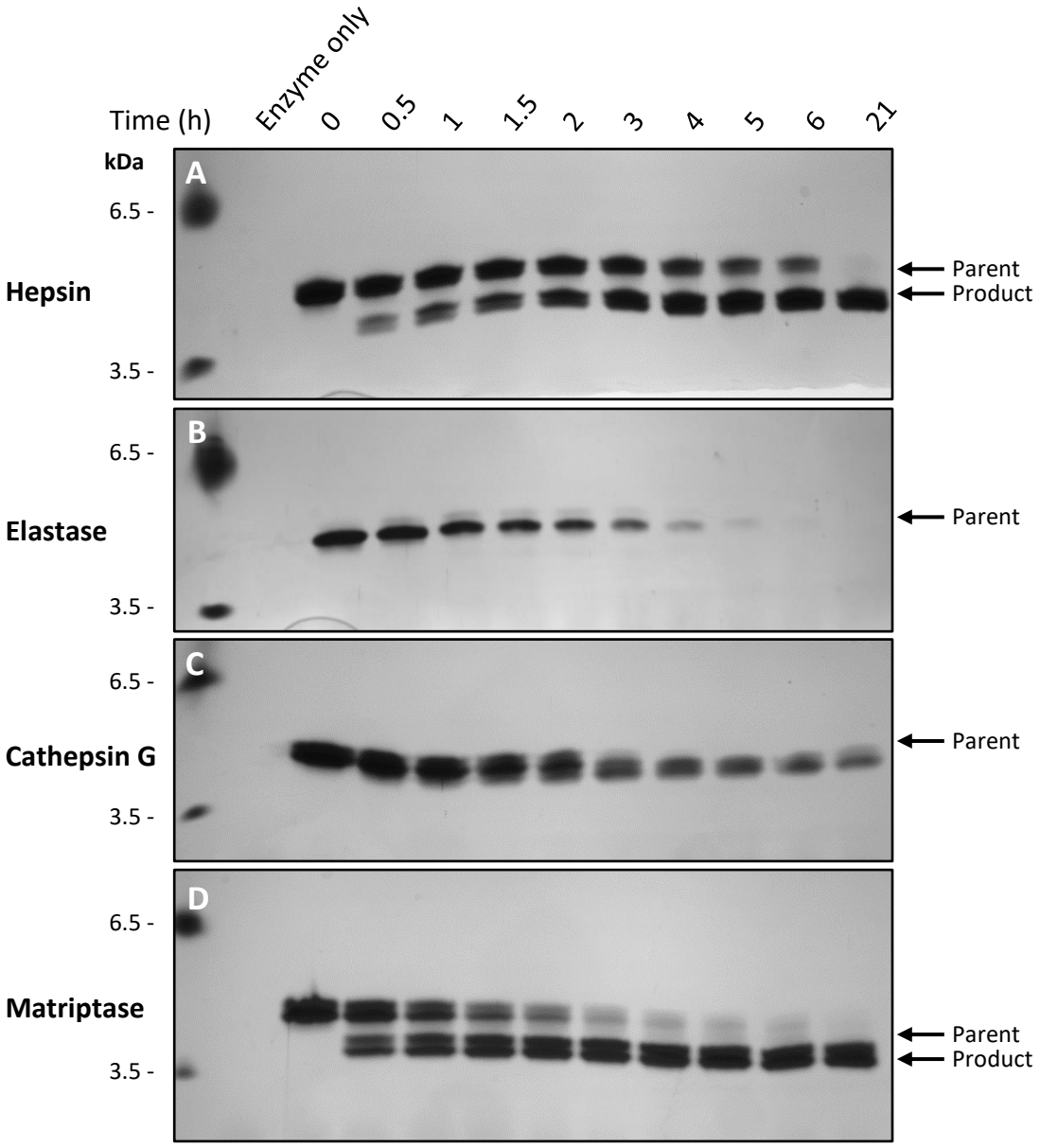

Figure 4.3: Validation of system with proteases known to cleave PAR2
10 µM PAR2 42mer was incubated with 10 nM of either hepsin (A) or elastase (B), 1 nM cathepsin G (C), or 0.1 nM matriptase (D) for varying durations before resolving the reaction products on 20% polyacrylamide gels and silver staining. All gels representative of 2 independent experiments.

4.2.2 Screen of proteases for ability to cleave PAR2 42mer

After validating the use of SDS-PAGE to identify the cleavage of the PAR2 42mer with enzymes known to cleave PAR2, the system was used to identify novel enzymes for their ability to cleave PAR2.

4.2.2.1 Serine protease screen

As PAR2 is considered primarily to be a receptor for serine proteases[294], and as a role for serine proteases in the pathogenesis of various arthritic diseases, including OA, is becoming well established[121], it was decided to screen novel serine proteases for their ability to cleave PAR2.

In order to keep the serine protease screen relevant to arthritis and in particular OA, a list of serine proteases that were found to be significantly dysregulated in OA versus control (neck of femur fracture samples) was drawn up (table 4.1), based on low-density array data generated during a previous study by our group[1]. Some of the dysregulated serine proteases in the screen are known PAR2 activators, such as matriptase[115], hepsin[293] and coagulation factor X[295].

Of the proteases identified in the serine protease screen, complement factor D, complement factor I, HTRA1, HTRA3, PCSK9 and FAP were sourced for screening of PAR2 cleavage ability. Furthermore, uPA and thrombin were sourced for screening. Despite not being identified in this screen, uPA has previously been implicated in arthritis pathogenesis[296] where its injection into mice joints resulted in rheumatoid arthritis-like morphological changes such as synovitis, pannus formation and some cartilage destruction.

Thrombin has also been implicated in arthritis. Aside from its role in thrombosis, thrombin also activates PAR1 to mediate various other roles including pro-inflammatory signalling. PAR1 deficiency in mice confers protection from antigen-induced arthritis, including reduced MMP-13 expression[125], whereas thrombin inhibition attenuates synovial hyperplasia in collagen-induced arthritis in mice[126].

Table 4.1: Differentially regulated serine proteases in OA, Low-density array analysis taken and modified Milner *et al.*, (2010)[1]

Gene	Protein	Fold change
BF	B-factor	0.3
C2	Complement component 2	7.24
DF	D component of complement	5.08
DPP4	Dipeptidylpeptidase 4	3.41
ELANE	Neutrophil Elastase	5.94
F10	Coagulation factor X	17.69
FAP	Fibroblast activation protein	2.36
GZMA	Granzyme A	18.97
GZMB	Granzyme B	3.7
GZMK	Granzyme K	10.81
HPN	Hepsin	0.09
HTRA1	HtrA serine peptidase 1	3.8
HTRA2	HtrA serine peptidase 2	0.67
HTRA3	HtrA serine peptidase 3	4.2
HTRA4	HtrA serine peptidase 4	20.23
IF	I factor	7.86
KLK13	Kallikrein 13	21.73
PCSK1	Proprotein convertase subtilisin/kexin type 1	0.11
PCSK6	Proprotein convertase subtilisin/kexin type 6	9.98
PCSK9	Proprotein convertase subtilisin/kexin type 9	14.48
PLAT	Plasminogen activator, tissue	0.22
PRSS15	Protease, serine, 15	0.57
PRSS23	Protease, serine, 23	5.89
PRSS3	Protease, serine, 3	0.24
ST14	Matriptase	5.92
TMPRSS4	Transmembrane protease, serine 4	0.02

Both uPA and thrombin displayed the ability to cleave the PAR2 42mer at higher concentrations after 24 hours (Figure 4.4). Signs of degradation by thrombin were observable as low as 10 nM of enzyme, and a dose-response was observed thereafter. It appears that thrombin digestion of PAR2 42mer results in a single product. uPA appeared less potent at degrading the peptide, however clear digestion was also observed.

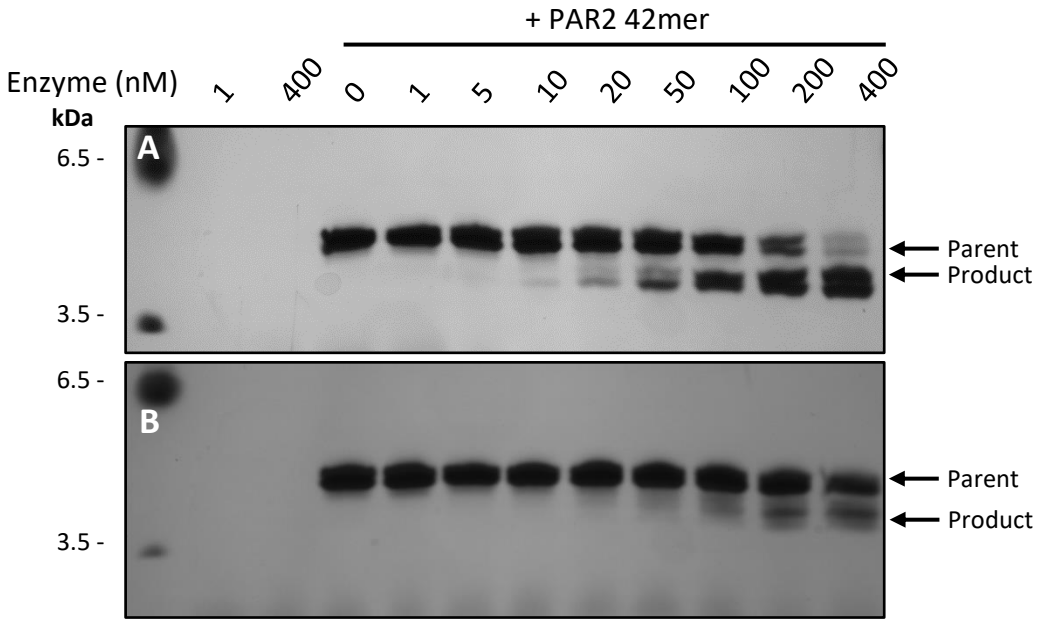

Figure 4.4: uPA and Thrombin cleavage of PAR2
PAR2 42mer (10 µM) was incubated with increasing concentrations (nM) of either thrombin (A) or uPA (B) for 24 hours at 37°C before resolving the reaction products on 20% polyacrylamide gels and silver staining. All gels representative of 2 independent experiments.

As recombinant HTRA1 and HTRA3 preparations were available at very high concentrations, PAR2 42mer digestion by a wide range of concentrations was tested. HTRA1 had the ability to degrade the PAR2 peptide, with evidence of cleavage as low as 20 nM with 500 nM resulting in a complete visual loss of peptide at 24 hours (Figure 4.5 A). Two bands are visible in the 20-200 nM digestions; thus it is likely multiple cleavages occur resulting in products too small to visualise by SDS-PAGE. The high concentrations of enzyme result in visual bands from the enzyme preparation visible in the gel, as shown in the 10000 nM enzyme only control. There was no evidence of HTRA3 being able to cleave PAR2 at all tested concentrations (Figure 4.5 B).

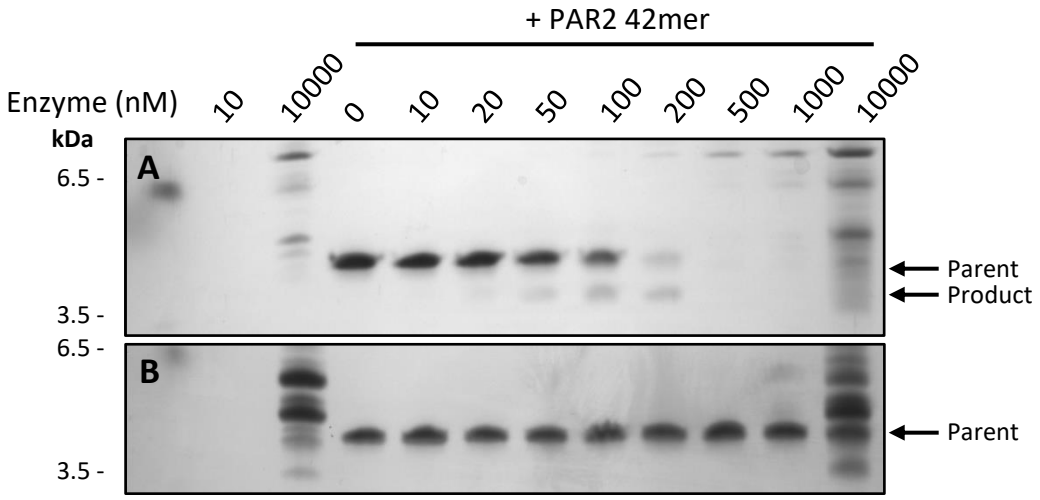

Figure 4.5: HTRA1, but not HTRA3, can cleave PAR2
PAR2 42mer (10 µM) was incubated with increasing concentrations (nM) of either HTRA1 (A) or HTRA3 (B) for 24 hours at 37°C before resolving the reaction products on 20% polyacrylamide gels and silver staining. All gels representative of 2 independent experiments.

The ability of complement factors D and I to cleave PAR2 was examined, and there was no evidence of either enzyme exhibiting such activity (Figure 4.6).

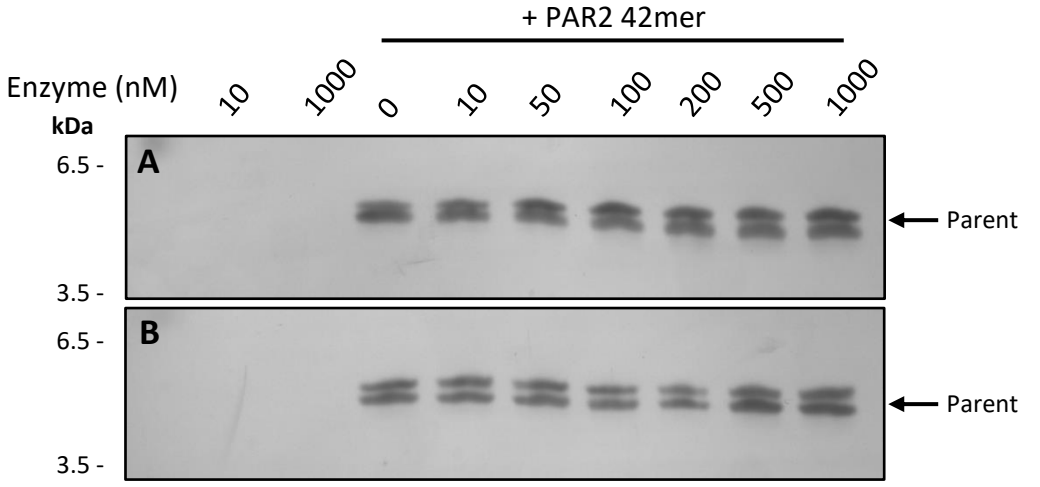

Figure 4.6: Factor D and Factor I do not cleave PAR2
PAR2 42mer (10 µM) was incubated with increasing concentrations (nM) of either Factor D (A) or Factor I (B) for 24 hours at 37°C before resolving the reaction products on 20% polyacrylamide gels and silver staining. All gels representative of 2 independent experiments.

Furthermore, neither PCSK9 or FAP displayed any evidence of being able to cleave the PAR2 42mer (Figure 4.7).

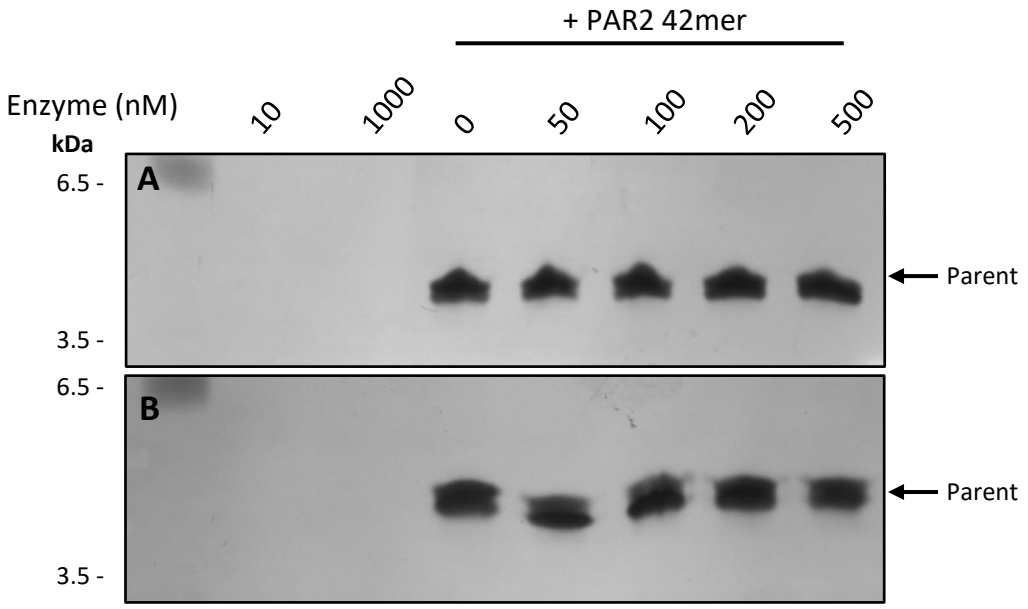

Figure 4.7: PCSK9 and FAP do not cleave PAR2
PAR2 42mer (10 µM) was incubated with increasing concentrations (nM) of either PCSK9 (A) or FAP (B) for 24 hours at 37°C before resolving the reaction products on 20% polyacrylamide gels and silver staining. All gels representative of 2 independent experiments.

4.2.2.2 Metalloprotease screen

The ability of MMPs to modify cell behaviour by cleaving receptors has previously been described in the literature with both MMP-1[297] and MMP-13[298] able to cleave and activate the thrombin receptor PAR1. Furthermore, it has been reported that MMP-1 may be able to act on PAR2 in an agonistic manner, which is further discussed in chapter 5.3. It was therefore of interest to ascertain whether the collagenolytic MMPs would have the ability to cleave PAR2, as both the MMPs and PAR2 are known to be involved in arthritis.

The incubation of proMMP-1, -8 and -13 in the presence of APMA with the PAR2 42mer for 24 hours resulted in observable cleavage (Figure 4.8). Both MMP-1 and MMP-3 appear to result in a single product with a dose-response observed, whereas MMP-8 at lower concentrations results in a single product, however both this product and the parent peptide were lost at higher concentrations.

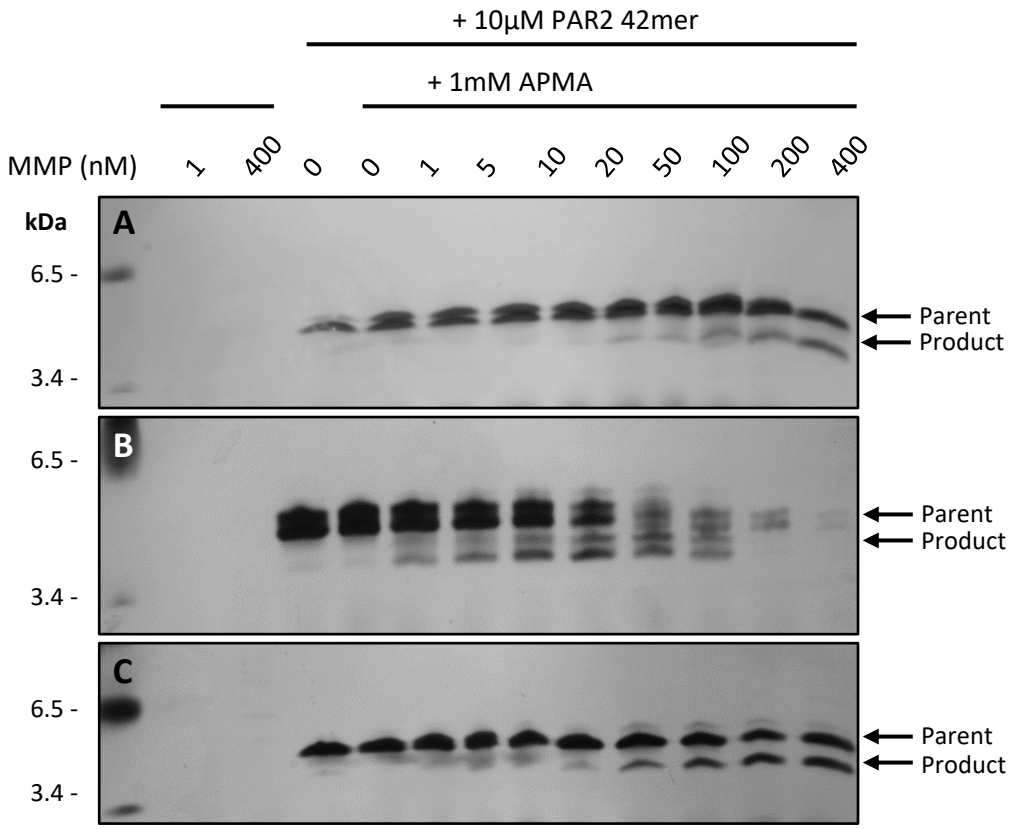

Figure 4.8: MMP-1, -8 and -13 cleavage of PAR2 42mer
PAR2 42mer was incubated for 24 hours with either proMMP-1 (A), proMMP-8 (B) or proMMP-13 (C) at various concentrations, activated by 1 mM APMA, before resolving the reaction products on 20% polyacrylamide gels and silver staining. All gels representative of 2 independent experiments.

In order to confirm that it was indeed metalloprotease activity responsible for cleavage of the peptide, experiments were undertaken in the presence of GM6001, which inhibited MMP-1, -8 and -13 cleavage of the PAR2 42mer (data not shown).

4.2.2.3 Cysteine protease screen

As described in chapter 1, several lysosomal papain-like cysteine proteases, often referred to as the "cathepsins", have been identified as having extracellular roles and implicated in arthritic disease. Furthermore, cathepsin S has been identified as a biased agonist for PAR2 activation[226]. Therefore, the ability of cathepsins V, K, B and L to cleave PAR2 was explored.

All tested cathepsins were able to digest the PAR2 42mer (Figure 4.9). Of these, cathepsin K appeared to result in an observable smaller band, whereas the other cathepsins resulted in a loss of PAR2 42mer but no additional bands, thus the product(s) were likely too small

to be visualised by this technique. The addition of E64 cysteine protease inhibitor resulted in the inhibition of PAR2 cleavage for each enzyme, showing that the cleavage of PAR2 was dependent on cysteine protease activity.

It is important to draw attention to a small band present in all lanes, including the controls. This band was not present in experiments undertaken earlier on in the project, thus it appears that the peptide was not stable in long-term storage.

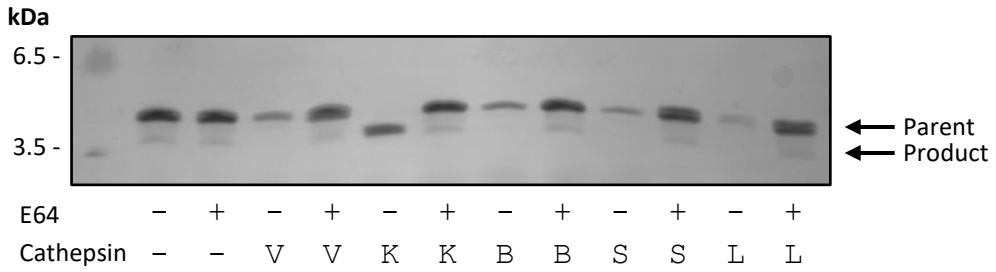

Figure 4.9: Cathepsin cleavage of PAR2 is dependent on cysteine protease activity
10 µM PAR2 42mer was incubated with either 1 nM cathepsin V, 5 nM cathepsin K, 10 nM cathepsin B, 20 nM cathepsin S or 0.5 nM cathepsin L 30 minutes at 37°C in the presence or absence of 10 µM E64, before resolving the reaction products on 20% polyacrylamide gels and silver staining. Gel representative of 2 independent experiments.

4.3 Discussion

In this chapter, a synthetic peptide was synthesised corresponding to the extracellular region of PAR2 where previously identified cleavages have been identified, and a method of visualising this peptide by SDS-PAGE was optimised. Subsequently, this system was validated by confirming a series of known PAR2 activators and disarmers could digest the peptide. Finally, a series of cartilage and arthritis-relevant proteases from the serine, cysteine and metalloprotease families were screened for their ability to cleave PAR2, which identified several novel activities of enzymes from these families.

In designing the sequence for the PAR2 42mer synthetic peptide, a list of all previously identified PAR2 cleavages was drawn up in order to design a peptide that could "cast the largest net" for identifying cleavages, and with consideration that solid-phase synthetic peptide synthesis becomes markedly more difficult with each increasing amino acid in length[299]. Indeed, in searching the literature, it appears that 42 amino acids is the longest PAR2 peptide sequence utilised for enzyme identification research to date, and previous

studies requiring large sequence coverage have utilised overlapping peptides[226], or otherwise have focused on smaller specific PAR2 regions[210,225,300]. Moreover, the PAR2 sequence utilised in this project (arginine-31 to lysine-72) is comparable to the sequence utilised in a study by Loew *et al*. (2000)[301] who made an arginine-31 to leucine-79 sequence, however this was not a synthetic peptide generated by solid-phase synthesis, but rather a recombinant protein expressed and purified from *E. coli*. Sequence analysis of PAR2 suggests that the extracellular domain ends at amino acid 75[302], thus the proteinase 3 and elastase cleavages identified at positions 74, 75 and 76 by Loew *et al.* (2000) are likely to be of low physiological relevance. Terminating the PAR2 42mer utilised in the project at lysine-72 was decided to encompass the whole physiologically-relevant range of residues.

Before screening novel enzymes for the ability to cleave PAR2, the system set up was validated by testing four enzymes previously identified as being able to cleave PAR2. Matriptase, hepsin, cathepsin G and neutrophil elastase were all tested for their ability to cleave PAR2. Matriptase and hepsin are both canonical activators expected to cleave after arginine-36[115,293], whereas cathepsin G is thought to be a disarmer and neutrophil elastase a disarmer of some responses and a biased agonist of others[224,225]. Multiple cleavage sites for cathepsin G and neutrophil elastase have been identified[301], however it this thought that the most important and physiologically-relevant cleavages are after phenylalanine-64 and after serine-67, respectively[225].

The cleavage of the PAR2 42mer by hepsin and matriptase was evident as early as 30 minutes, however even when digested for 21 hours, only a single product was observed, with no evidence of secondary cleavages or loss of peptide from the visible range of the SDS-PAGE system. This observation is in line with the literature where only a single cleavage site has been identified for the two enzymes – the canonical site. Electrospray MS was undertaken on the digestion product generated by matriptase and hepsin, and this confirmed the expected canonical cleavage (data not shown).

Neutrophil elastase and cathepsin G both also cleaved the peptide as expected, however this was observed by loss of parent peptide and no product was observed. This would imply that the products were too small to observe by SDS-PAGE, or there are multiple cleavages which result in multiple small fragments. The expected fragment size from the previously described major cleavage site for cathepsin G is 3581.00 Da and 3826.24 Da

for neutrophil elastase (based on the work of Ramachandran *et al*. 2011[225]), both would be expected to be visible by the SDS-PAGE method utilised. Indeed, the band generated by hepsin and matriptase was 3653.10 Da and was clearly detected by this method. Taken together, it is likely that multiple digestions have taken place by neutrophil elastase and cathepsin G resulting in a series of peptides too small to visualise. Multiple cleavage sites on PAR2 have previously been observed by both enzymes[225,301], so this observation is in line with the literature.

After optimising and validating a method to assess enzymes for their ability to cleave PAR2, a screen was undertaken and 9 novel enzymes were identified as being able to cleave PAR2 (table 4.2). Three metalloproteases, MMP-1, -8 and -13 were all able to cleave PAR2; two serine proteases, uPA and HTRA1 and four cysteine proteases, cathepsins V, K, B and L also had this ability.

Table 4.2: List of proteases tested for their ability to cleave PAR2

	Cleavages: Novel	**Cleavages: Not Novel**	**No Cleavage**
Metalloproteases	MMP-1*		ADAMTS-5
	MMP-8		
	MMP-13		
Serine Proteases	uPA	Thrombin	Factor I
	HTRA1	Cathepsin G	Factor D
		Neutrophil elastase	HTRA3
		Hepsin	FAP
		Matriptase	PCSK9
Cysteine Proteases	Cathepsin V	Cathepsin S	
	Cathepsin K		
	Cathepsin B		
	Cathepsin L		

*MMP-1 previously suggested to act on PAR2, however no identification of cleavage site nor direct evidence of PAR2 cleavage by active MMP-1 observed [303], see chapter 5.

It is important to draw attention to the relative concentrations of protease as well as length of incubation required to observe PAR2 42mer cleavage. Some proteases, for example matriptase, were very potent, able to cleave PAR2 with low concentrations (0.1nM matriptase for 30 minutes resulted in about 50% cleavage), whereas proteases such as the MMPs were much less potent. MMP-1 and MMP-13 required 400nM of protease for 24 hours to observe the same level of PAR2 42mer degradation. The cathepsins were generally very potent, whereas the other serine proteases exhibited a variable level of potency, for example thrombin, uPA and HTRA1 all required high protease concentration with a long incubation to observe cleavage.

The observation that HTRA1 was able to cleave PAR2 is an interesting one. This enzyme has been linked with multiple musculoskeletal disorders[304] including both RA and OA where elevated protein levels are observed in synovial fluids[305]. Furthermore, HTRA1 is expressed by chondrocytes, with elevated gene expression levels in OA[129] with high levels of the protein detected in cartilage extracts[306]. HTRA1 expression is also elevated in antibody-induced arthritis in mice[131]. The role of HTRA1 in arthritic diseases is incompletely understood. Recombinant HTRA1 is able to induce *MMP1* and *MMP3* expression in human synovial fibroblasts from both OA and RA patients in a mechanism that is thought to involve HTRA1 cleavage of fibronectin and subsequent fibronectin fragment induction of MMP expression[305]. HTRA1 has also been shown to degrade various cartilage components such as aggrecan with HTRA1-digested fragments identified in OA cartilage[133]. HTRA1 can also digest soluble type II collagen[131], and can potentially act to further degrade MMP-digested fibrillar collagen in disease.

Despite being a trypsin-like serine protease, HTRA1 does not have a preference for a charged amino acid in the P1 position[307], thus is unlikely to be a candidate for being a PAR2 canonical activator which would require cleavage after an arginine. HTRA1 prefers small- to medium-sized hydrophobic residues, as well as polar threonine and glutamine in the P1 position[307]. The bands observed on the gel suggest that multiple cleavages occur as first a single band appears, but at higher concentrations all bands disappear implying multiple peptide fragments too small to visualise by this method.

This project had initially included thrombin as part of the screen, which was identified as a novel enzyme with the ability to cleave PAR2, but a paper has since been published with identifies thrombin as a PAR2 activator[214]. Indeed, thrombin was identified as

cleaving the PAR2 canonical activation site, which is line with the cleavage observed in this project as thrombin digestion of the PAR2 42mer resulted in a band of the same size as matriptase and hepsin. The fact that the screening method in this project identified a cleavage which was subsequently published elsewhere further validates the system as a good system to screen PAR2 cleavages.

uPA is best known for its role in fibrinolysis, where it activates plasminogen to plasmin, but roles have also been identified in arthritic diseases[296] and it is able to activate various proMMPs including proMMP-3 and proMMP-13[291,308]. Interestingly, uPA is already known to be able to signal via a cell surface receptor, the uPA receptor (uPAR), which can induce multiple cell signalling pathways[309]. uPA has a preference for a basic arginine or lysine in the P1 position, as well as a small glycine or serine in the P2 position[310], and thus is a candidate for being a canonical PAR2 activator which would require cleavage after glycine and arginine. The motif glycine-lysine appears three times in the sequence also, so there is also potential for other uPA cleavages within the PAR2 sequence. The band observed on the gel appears to be of a similar size to that of hepsin, matriptase and thrombin.

Of the serine proteases screened, there was no evidence of factor I, factor D, HTRA3, PCSK9 or FAP being able to cleave PAR2. To date, only a single substrate has been identified for complement factor D which is complement factor B as part of the complement cascade[310]. Complement factor I, despite having slightly more identified substrates than factor D, still has a limited amount of substrates[310]. The complement system has however been linked to arthritic diseases, in particular RA[122] with factors I and D both being significantly up-regulated in OA compared to control cartilage[1]. Despite these links with arthritis, the known substrate specificities of these enzymes are in line with the findings presented here.

FAP is best known as a dipeptidyl peptidase (an exopeptidase which cleaves two amino acids from the N-terminus) with a preference for a P1 proline, however it has also been shown to exhibit endopeptidase activity[311]. Thus, it was relevant to include in this PAR2 cleavage screen. The PAR2 42mer peptide contains no proline residues, and despite being some evidence that FAP may also cleave substrates with alanine, arginine, glycine, lysine or serine in the P1 position[312], it is clear there is a strong preference for a proline in this

position[313]. The failure of FAP to cleave PAR2 means further research is required in order to identify potential substrates for this unusual protease.

The three major collagenases, MMP-1, -8 and -13 were all able to cleave PAR2. This was a fascinating observation, as it is known that canonical PAR2 activation is able to upregulate the expression of many MMPs, including *MMP1*, *MMP3* and *MMP13*[1]. Data presented in this chapter now suggests that active MMPs can act on PAR2, identifying a potential feedback system. Due to the vital importance of the collagenases in OA, as well as the importance of canonical PAR2 signalling in the disease, further work was undertaken on these cleavages, and is presented in chapter 5.

PAR2 has been mainly described as a receptor for trypsin-like serine proteases, however a recent paper described biased agonism via activation by the lysosomal cysteine protease cathepsin S[226]. As several other lysosomal cysteine proteases have had extracellular roles identified, and have been linked to arthritic diseases, a series of these were also screened. Cathepsins B, K, V and L were all identified as novel enzymes with the ability to cleave PAR2. These novel observations were very interesting, and opened up PAR2 as potentially much more than just a receptor for trypsin-like serine proteases. Therefore, more work was undertaken to further understand these cleavages, and is presented in chapter 6.

4.4 Summary

- A 42 amino acid peptide corresponding from arginine-31 to lysine-72 of PAR2, which contains the vast majority of previously identified PAR2 cleavage sites, was designed and synthesised.

- A method to visualise the PAR2 42mer was optimised, comprised of tris-tricine SDS-PAGE and silver staining.

- The system was validated by confirming that matriptase, hepsin, cathepsin G and neutrophil elastase could cleave the PAR2 42mer.

- A screen of novel enzymes from the metalloprotease, serine and cysteine protease families was undertaken, identifying 9 novel enzymes with the ability to cleave PAR2.

Chapter 5. Investigation of the role of the collagenolytic MMPs 1, 8 and 13 in PAR2 cleavage

5.1 Introduction

After identifying that MMP-1, -8 and -13 can enzymatically digest the PAR2 42mer peptide, work was performed to further explore these cleavages. To gain initial insights into potential roles of cleavages, it is important to know the specific cleavage sites, which were obtained by mass spectrometry. Subsequently, further insights into the relevance of the cleavages were obtained by generating kinetic parameters for the enzymes for their cleavage site. Biochemistry-based assays are useful to give insights into the cleavages, but to further to understand the biology, cell work also was performed.

5.1.1 Chapter Aims

- To identify the cleavage sites for MMP-1, -8 and -13 cleavage of PAR2.
- To explore kinetic parameters of MMP-1, -8 and -13 cleavage of PAR2.
- To explore a functional role for MMP-1, -8 and -13 cleavage of PAR2 in a chondrocytic cell culture model.

5.2 Results

5.2.1 Identification of PAR2 cleavage sites by MMP-1, -8 and -13

To identify the cleavage sites, mass spectrometry was used to identify the cleavage products generated by MMP cleavage. HPLC was used to remove detergents present in the digestion buffer and to visualise the contents of the enzymatic reaction. To be able to identify cleavage products, the undigested 42mer peptide was run as a control and the elution time noted for comparison with digestion products. The undigested PAR2 42mer yielded a single major peak which elutes at around 16.5-17 minutes on the gradient (Figure 5.1).

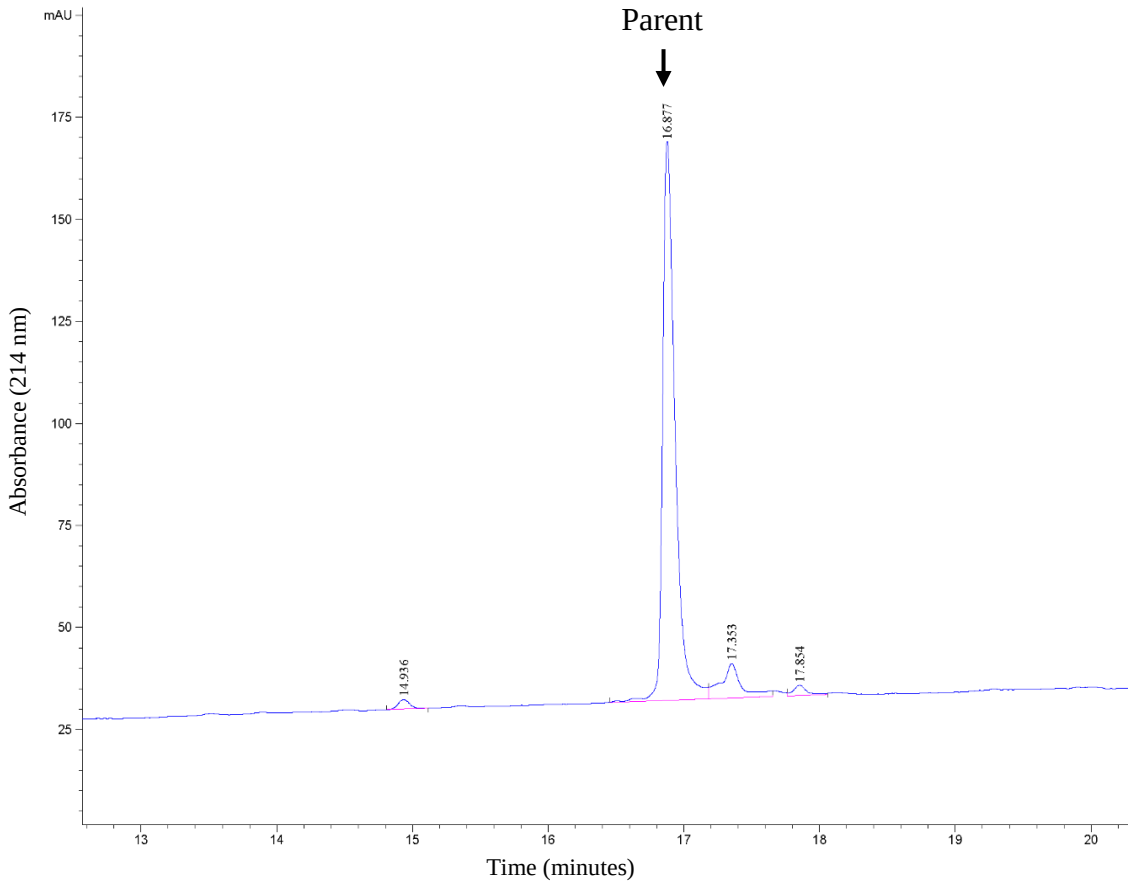

Figure 5.1: Reversed-phase HPLC trace for PAR2 42mer undigested
The PAR2 42mer peptide was diluted to 10 µM in 0.1% TFA and 30 µL was injected onto an ACE 3 C18 HPLC column. A gradient of 5-60% acetonitrile was run over 27 minutes at 35°C using a flow rate of 0.2 mL/min. The peptide elutes at around 16.9 minutes on the gradient. Chromatogram representative of three independent experiments.

To generate robust mass identification by electrospray MS, it is considered that a peak of greater than 50 mAU is required (Dr Joe Gray, personal communication). Thus, peaks greater than 50 mAU were selected for mass identification. The HPLC separation of a 24-hour digestion reaction containing 400 nM MMP-1 with 10 µM PAR2 42mer yielded two major peaks - a peak at 16.9 minutes which corresponds to the parent peptide, as well as a peak with a later elution time at 18.4 minutes (Figure 5.2). The peak was collected and the mass obtained by electrospray MS (an example MS trace is presented in appendix 2), yielding 3564.9 Da. FindPept software (ExPASy) was used to identify all possible cleavage sites on the PAR2 42mer, which identified a single site corresponding to the observed mass, which was a cleavage between serine-7 and leucine-8 of the peptide (and thus serine-37 and leucine-38 in full length PAR2). A small peak was also observed at 16.3 minutes, but it was below the sensitivity for electrospray MS.

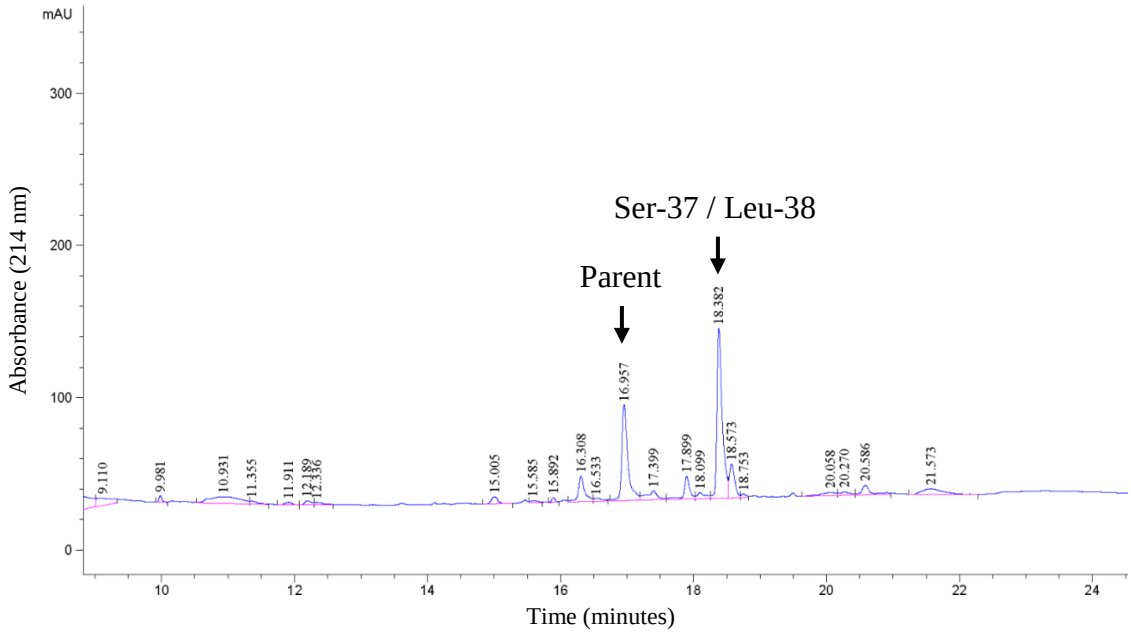

Figure 5.2: Reversed-phase HPLC trace for PAR2 42mer following MMP-1 digestion
PAR2 42mer (10 µM) was incubated with 400 nM MMP-1 for 24 hours at 37°C. 30 µL was injected to the HPLC system and ran through an ACE 3 C18 column on a 5-60% acetonitrile gradient over 27 minutes at 35°C using a flow rate of 0.2 mL/min. Peaks were collected manually for further analysis by electrospray MS.

A similar experiment using 20 nM MMP-8 resulted in the identification of three major peaks – at 16.3, 16.9 and 18.4 minutes (Figure 5.3). As previously described, the peak at 16.9 minutes corresponds to the parent peptide, and the peak observed at 18.4 minutes was likely to be the same product as observed by MMP-1 cleavage. A small peak at 16.3 minutes had been observed by MMP-1 cleavage of the PAR2 42mer (Figure 5.2), however it was too small to run by MS. The 16.3 and 18.4 minute peaks generated by MMP-8 cleavage were subjected to electrospray MS, and as expected, the peak at 18.4 minutes was the same product as generated by MMP-1. The peak at 16.3 minutes yielded a product of 3924.1 Da, which corresponded to a cleavage between valine-38 and leucine-39 of the peptide (valine-68 / leucine-69 in full length PAR2).

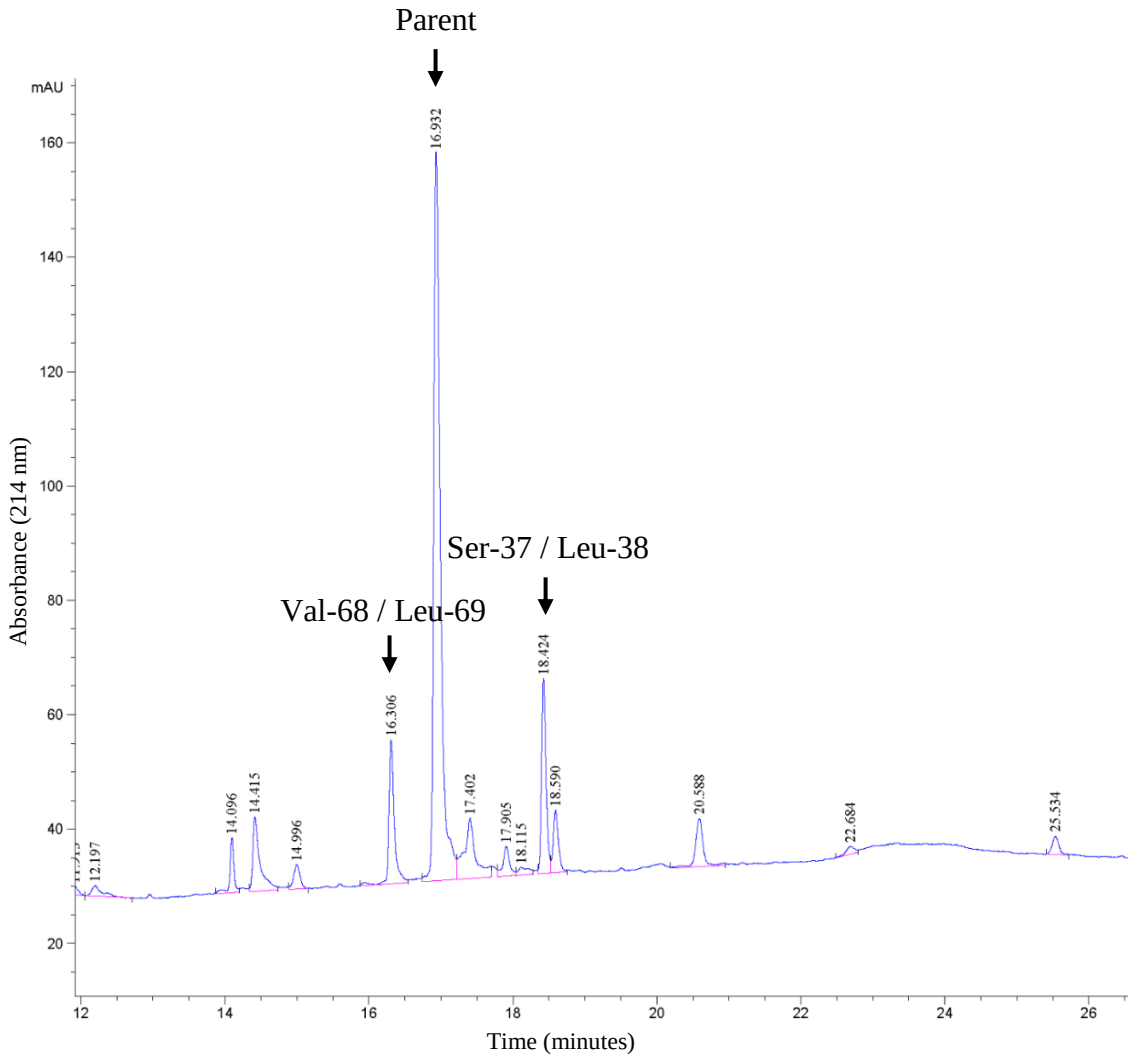

Figure 5.3: Reversed-phase HPLC trace for PAR2 42mer following MMP-8 digestion
PAR2 42mer (10 µM) was incubated with 20 nM MMP-8 for 24 hours at 37°C. 30 µL was injected to the HPLC system and ran through an ACE 3 C18 column on a 5-60% acetonitrile gradient over 27 minutes at 35°C using a flow rate of 0.2 mL/min. Peaks were collected manually for further analysis by electrospray MS.

The HPLC trace of the digestion of PAR2 42mer by 200 nM MMP-13 resulted in a chromatogram with many peaks (Figure 5.4). As insufficient peptide was used in the digestion for all the peaks to be product from the PAR2 42mer, it was hypothesised that MMP-13 had undergone autolysis as it is known to lack stability[68], thus resulting in observation of MMP-13 fragments. This was confirmed by running a HPLC trace of 200 nM MMP-13 following 24-hour incubation in the absence of PAR2 42mer (data not shown). The peaks at 17.9 and 18.4 minutes were selected for electrospray MS. There was no evidence of the parent peptide remaining in the chromatogram. As with MMP-1 and -8, the peak at 18.4 yielded the same product resulting from a cleavage between serine-7 and leucine-8 of the PAR2 42mer. The peak at 17.9 yielded a product with a mass of 3165.6 Da, which interestingly corresponded to a second cleavage event. This

product was a result of the previously observed cleavage at serine-7 and leucine-8, as well as a cleavage of its C-terminal fragment at valine-38 and leucine-39 – one of the cleavages observed by MMP-8 digestion of PAR2 42mer.

It was not possible at this stage to deduce which was the primary cleavage, however the fact that the 3564.9 Da peak was the larger peak, and the fact that the serine-7 and leucine-8 cleavage is present in both peaks, suggests that this is likely to be the case.

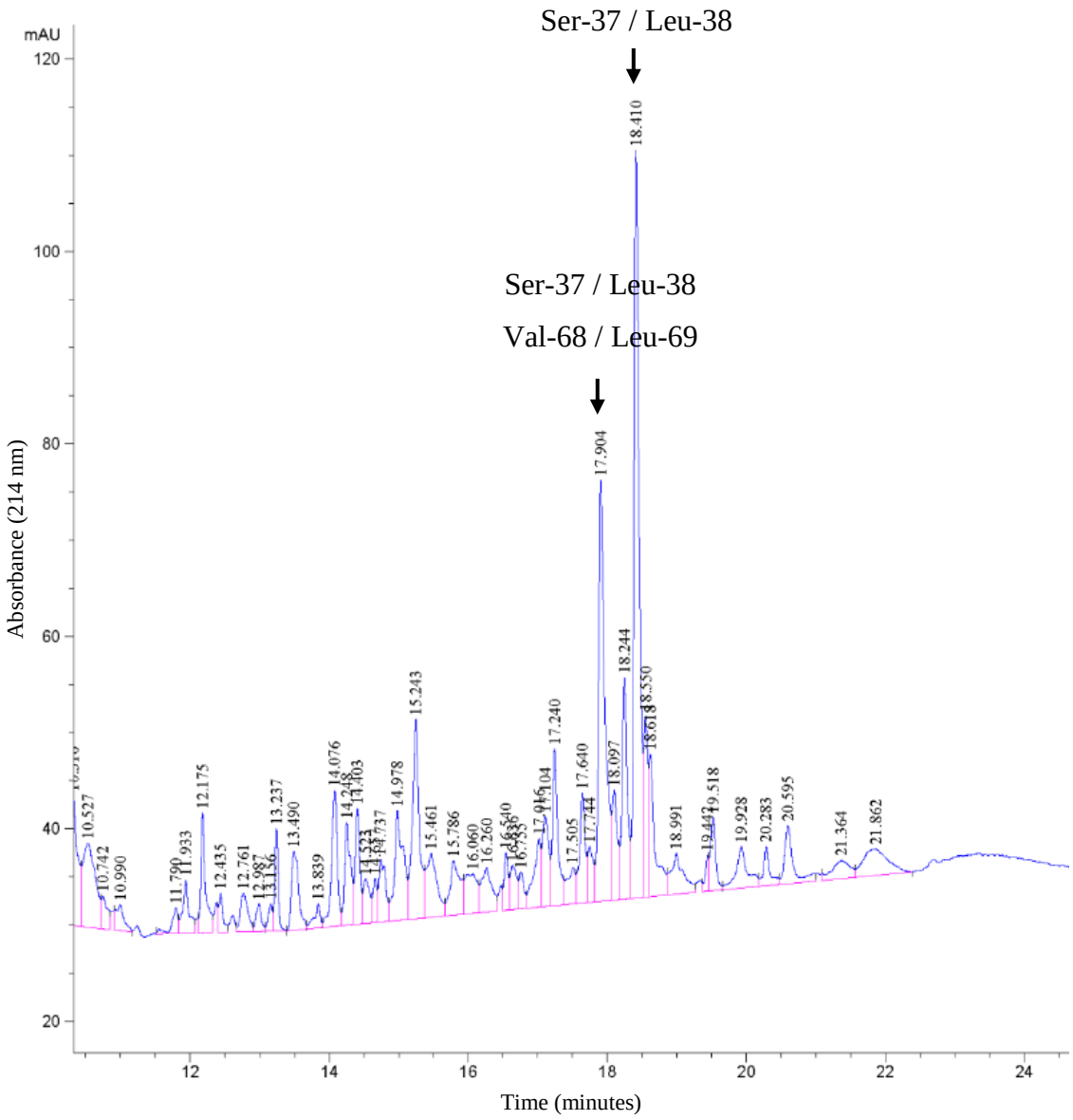

Figure 5.4: Reversed-phase HPLC trace for PAR2 42mer following MMP-13 digestion
PAR2 42mer (10 µM) was incubated with 200 nM MMP-13 for 24 hours at 37°C. 30 µL was injected to the HPLC system and ran through an ACE 3 C18 column on a 5-60% acetonitrile gradient over 27 minutes at 35°C using a flow rate of 0.2 mL/min. Peaks were collected manually for further analysis by electrospray MS.

Table 5.1: Identification of cleavage sites, highlighting the observed product in black

Protease	Mass (Observed) (Da)	Mass (Expected) (Da)	Sequence
MMP-1	3564.9	3564.9	(RSSKGRS)LIGKVDGTSHVTGKGVTVETVFSVDEFSASVLTGK
MMP-8	3924.1	3924.0	RSSKGRSLIGKVDGTSHVTGKGVTVETVFSVDEFSASV(LTGK)
MMP-8	3564.9	3564.9	(RSSKGRS)LIGKVDGTSHVTGKGVTVETVFSVDEFSASVLTGK
MMP-13	3165.6	3165.6	(RSSKGRS)LIGKVDGTSHVTGKGVTVETVFSVDEFSASV(LTGK)
MMP-13	3564.9	3564.9	(RSSKGRS)LIGKVDGTSHVTGKGVTVETVFSVDEFSASVLTGK

To ascertain which of the cleavages was the primary cleavage event, limited digests were undertaken at 3 and 6 hours for 200 nM MMP-13. At 3 hours, the parent peptide is still present, and approximately half had been converted to the 3564.9 Da peak, corresponding to the serine-7 and leucine-8 cleavage (Figure 5.5 A). By 6 hours, there is much less parent peptide remaining, having mostly been converted to the 3564.9 Da peak (Figure 5.5 B). Furthermore, at 6 hours the 3165.6 Da peak corresponding to the valine-38 and leucine-39 of the peptide begins to appear. Taken together, these data strongly suggest that for MMP-13, the primary cleavage is between serine-7 and leucine-8, and the secondary cleavage is between valine-38 and leucine-39.

MMP-1, -8 and -13 all cleave at an MMP-specific site which is one amino acid downstream of the canonical activation site of PAR2, which results from a cleavage with leucine in the P1’ position yielding a new product with an N-terminal leucine (Figure 5.6).

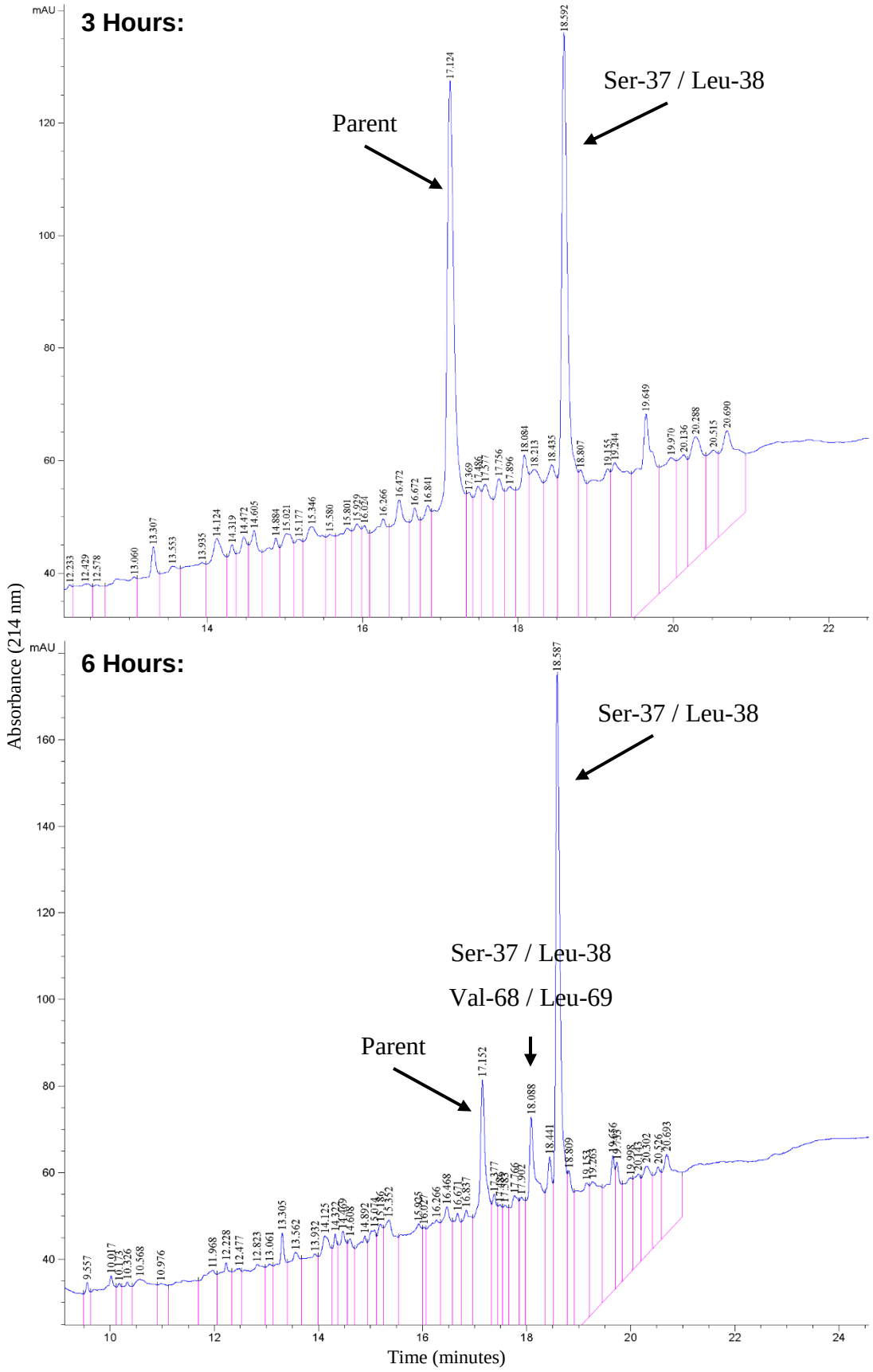

Figure 5.5: Reversed-phase HPLC trace for PAR2 42mer following MMP-13 digestion at 3 and 6 hours
PAR2 42mer (10 µM) was incubated with 200 nM MMP-13 for either 3 hours or 6 hours at 37°C. 30 µL was injected to the HPLC system and ran through an ACE 3 C18 column on a 5-60% acetonitrile gradient over 27 minutes at 35°C using a flow rate of 0.2 mL/min. Peaks were identified based on their elution time.

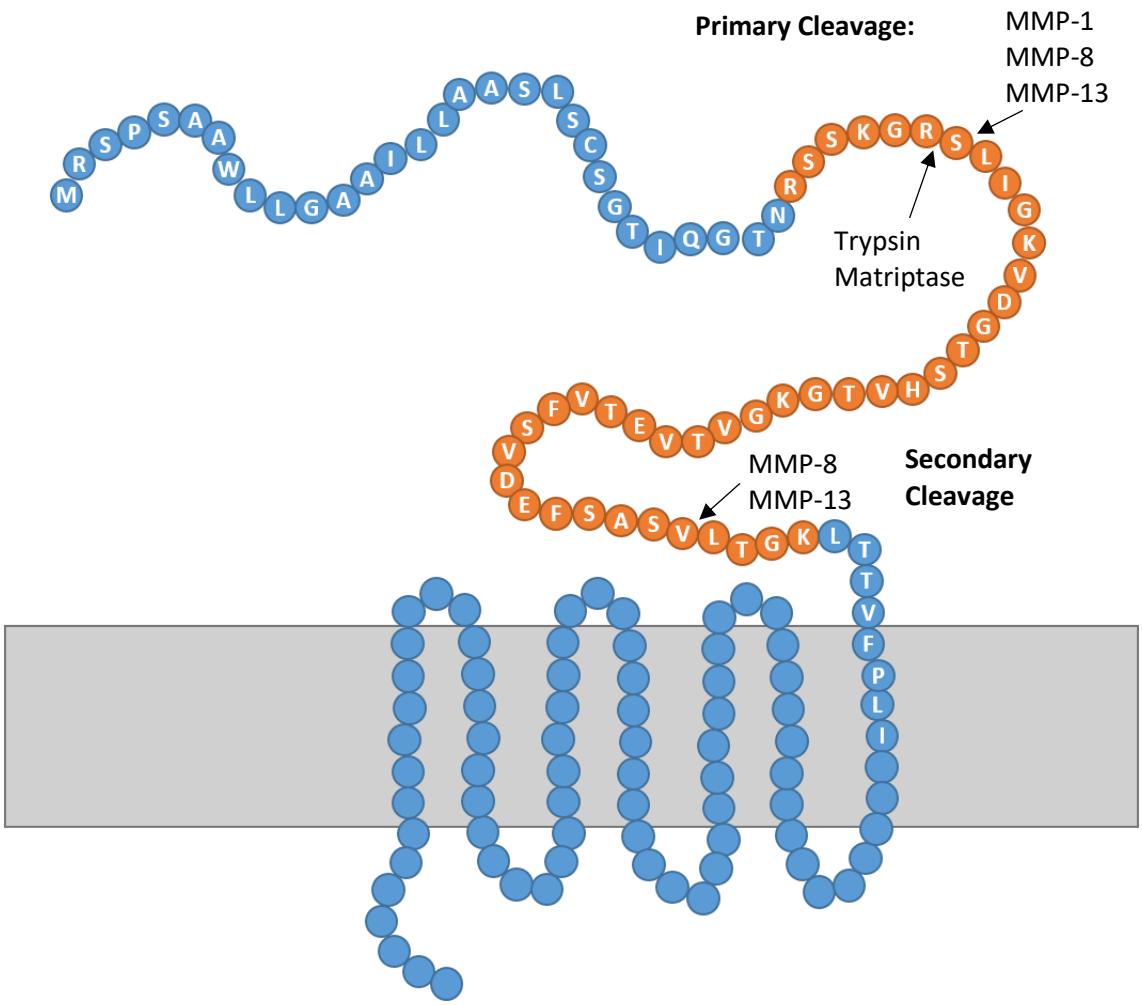

Figure 5.6: Summary of MMP cleavage sites on PAR2
Representation of the structure of the PAR2, highlighting the primary MMP cleavage site at serine-37 / leucine-38, and the secondary MMP cleavage site at valine-68 / leucine-69 as well as the canonical site for comparison.

5.2.2 Kinetic parameters of MMP-1, -8 and -13 for PAR2 substrate

Following the identification of an MMP cleavage site between serine-37 and leucine-38 of| PAR2, kinetic parameters were generated and compared to matriptase. For this work the SY-9 peptide was used, a quenched-fluorescent peptide containing 8 amino acids with the sequence SKGRSLIG, corresponding to P4 to P4' of the canonical cleavage site where matriptase and trypsin cleave. As the MMP cleavage site is only a single amino acid downstream from the canonical site, this peptide can also be used as a substrate for MMPs, and their kinetics directly compared to matriptase.

Michaelis-Menten kinetic experiments were undertaken for MMP-1, -8 and -13 (Figure 5.7), as well as for matriptase. By active-site titrating the enzymes (appendix 3), turnover numbers (k_{cat}) were able to be calculated for each one. Taken in combination with the K_m,

"enzymatic efficiency" was calculated for each enzyme in terms of k_{cat}/K_m. For further information regarding derivation of constants, see chapter 2.15.4.

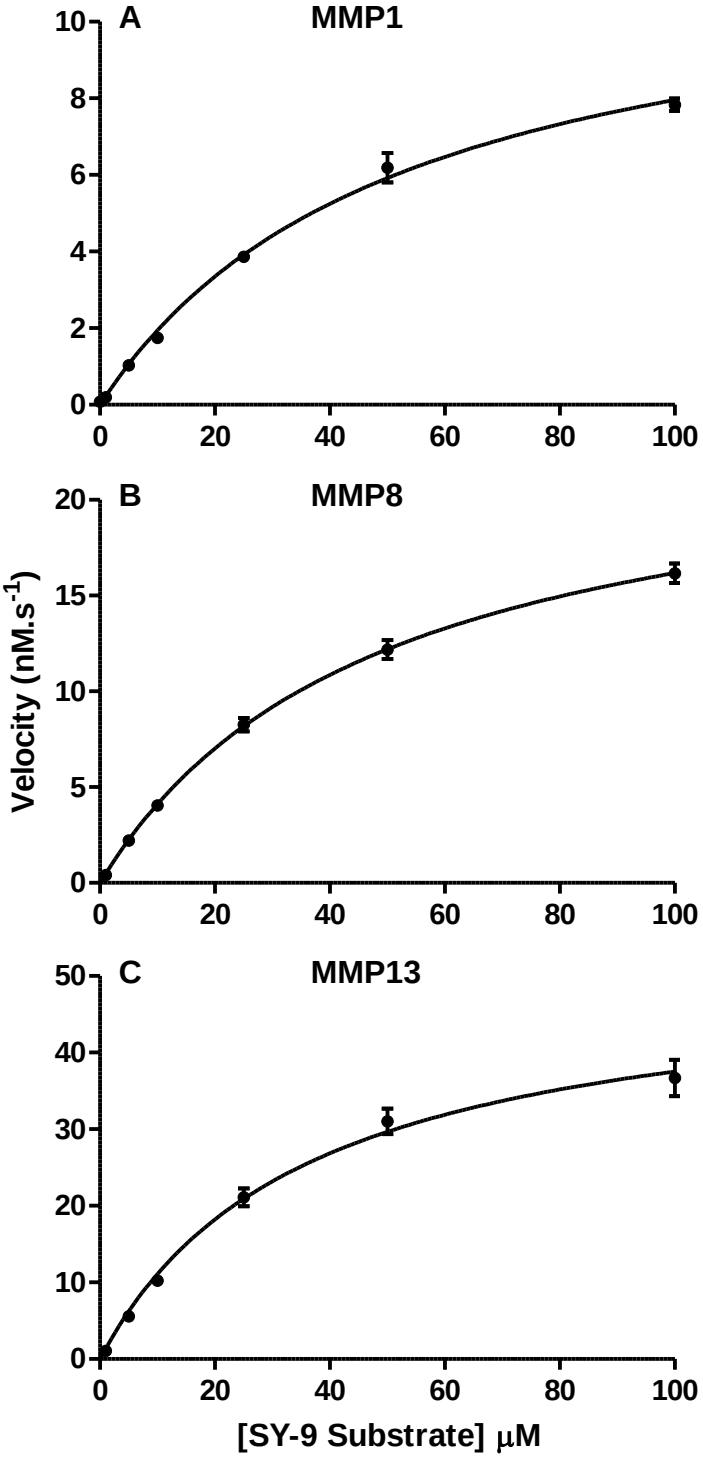

Figure 5.7: MMP-1, -8 and -13 Michaelis-Menten curves for SY-9 substrate
Michaelis-Menten curves for MMP-1, -8 and -13. Increasing concentrations of 2Abz-SKGRSLIG-3NY (SY-9) peptide were incubated with MMP. MMP-1 was at 400.4nM (A), MMP-8 was at 172.8nM (B) and MMP-13 was at 9.088nM (C). The fluorescence was measured at λ_{ex} 320 nm and λ_{em} 420 nm and the linear reaction velocities were obtained from linear gradients of the fluorescence progress curves at early timepoints. The hydrolysis of substrate was quantified ($nM.s^{-1}$) using a standard curve generated by total substrate hydrolysis. Graphpad Prism 5 software was used to plot velocity against substrate concentration and non-linear regression was used to generate constants K_m and V_{max}. k_{cat} was calculated from Vmax and enzyme active concentration. Curves shown are n=3 independent experiments, mean ± SD.

The kinetic constants for MMP-1, -8, -13 and matriptase are outlined in table 5.2. As expected, matriptase had a much higher k_{cat} than any of the MMPs with the ability to turnover 1720 molecules of substrate per minute per active site, compared to MMP-13 which can turnover 5.62. MMP-1 and -8 are however much less active on this substrate than MMP-13, with k_{cat} values of 0.03 and 0.14, respectively. In terms of Michaelis constant, an indicator of enzyme affinity for substrate, all four enzymes have comparable values, with MMP-13 having the lowest K_m. Taken together, these data suggest that the three MMPs have a similar affinity to matriptase for binding to the substrate SY-9, however are much less active at turning it over. In terms of k_{cat}/K_m, matriptase is two orders of magnitude more efficient than MMP-13 (6.13×10^5 $M^{-1}.s^{-1}$ and 2.6×10^3 $M^{-1}.s^{-1}$, respectively), which is in turn an order of magnitude more efficient than MMP-1 and -8 (0.09×10^2 $M^{-1}.s^{-1}$ and 0.47×10^2 $M^{-1}.s^{-1}$, respectively).

Table 5.2: Kinetic constants for MMP-1, -8, -13 and matriptase digestion of PAR2 peptide SY-9

Enzyme	k_{cat} (min^{-1})	K_m (μM)	k_{cat}/K_m ($M^{-1}.s^{-1}$)
MMP-1	0.03 ± 0.002	52.52 ± 5.73	0.09×10^2
MMP-8	0.14 ± 0.005	48.47 ± 4.10	0.47×10^2
MMP-13	5.62 ± 0.32	36.07 ± 4.89	2.6×10^3
Matriptase	1720 ± 113.90	46.73 ± 6.71	6.13×10^5

5.2.3 Exploration of the role of MMP-1, -8 and -13 in PAR2 cleavage

Identification of cleavage sites for MMP-1, -8 and -13 and subsequent deduction of kinetic constants for their cleavage site on PAR2 gives initial insights onto the role of these enzymes into PAR2 biology, however to further explore potential roles, cell culture work was undertaken.

5.2.3.1 Do MMP C-terminal domains (CTDs) act as competitive inhibitors of matriptase-induced PAR2 activation?

As MMP-1, -8 and -13 have relatively low turnover numbers for their PAR2 substrate, yet also have low Michaelis constants, it was hypothesised that the MMPs may be acting as competitive antagonists. If an MMP is bound to and cleaving PAR2 at position 37,

then it is unlikely the canonical site at position 36 can be also be cleaved to activate the receptor.

To test this hypothesis, a large quantity of MMP was required, however this represented a technical difficulty, therefore MMP C-terminal domains (CTDs) were used in lieu of full-length enzyme. These MMP CTDs are recombinant proteins consisting of the entire haemopexin-like domain of the MMP as well as a part of the linker domain. It is well established that the hameopexin-like domains play key roles in MMP binding to ligand[64], therefore it is possible that they could play a role in PAR2 binding and thus be able to block subsequent matriptase action.

Before testing the addition of matriptase on PAR2 in the presence of MMP CTD, it was important to make sure that matriptase does not directly act on CTD and thus give false results. Firstly, matriptase was incubated with either 10- or 100-fold excess MMP-1, -8 or -13 CTD and incubated for 3 hours. The reactions were separated out by SDS-PAGE and silver stained, which showed no evidence of matriptase digesting CTD (Figure 5.8 A). Secondly, the effect of CTD was tested on matriptase enzyme activity. Matriptase activity assays (Boc-QAR-AMC assays) were undertaken, in which a 1-1000-fold excess range of MMP-1, -8 and -13 CTDs were included in the assay. Once again, there was no evidence of MMP CTD interfering with the enzyme activity of matriptase (Figure 5.8 B). Taken together, these data suggest that matriptase had no interaction with MMP CTD in the absence of PAR2 and retains full activity; therefore, subsequent experiments could be undertaken.

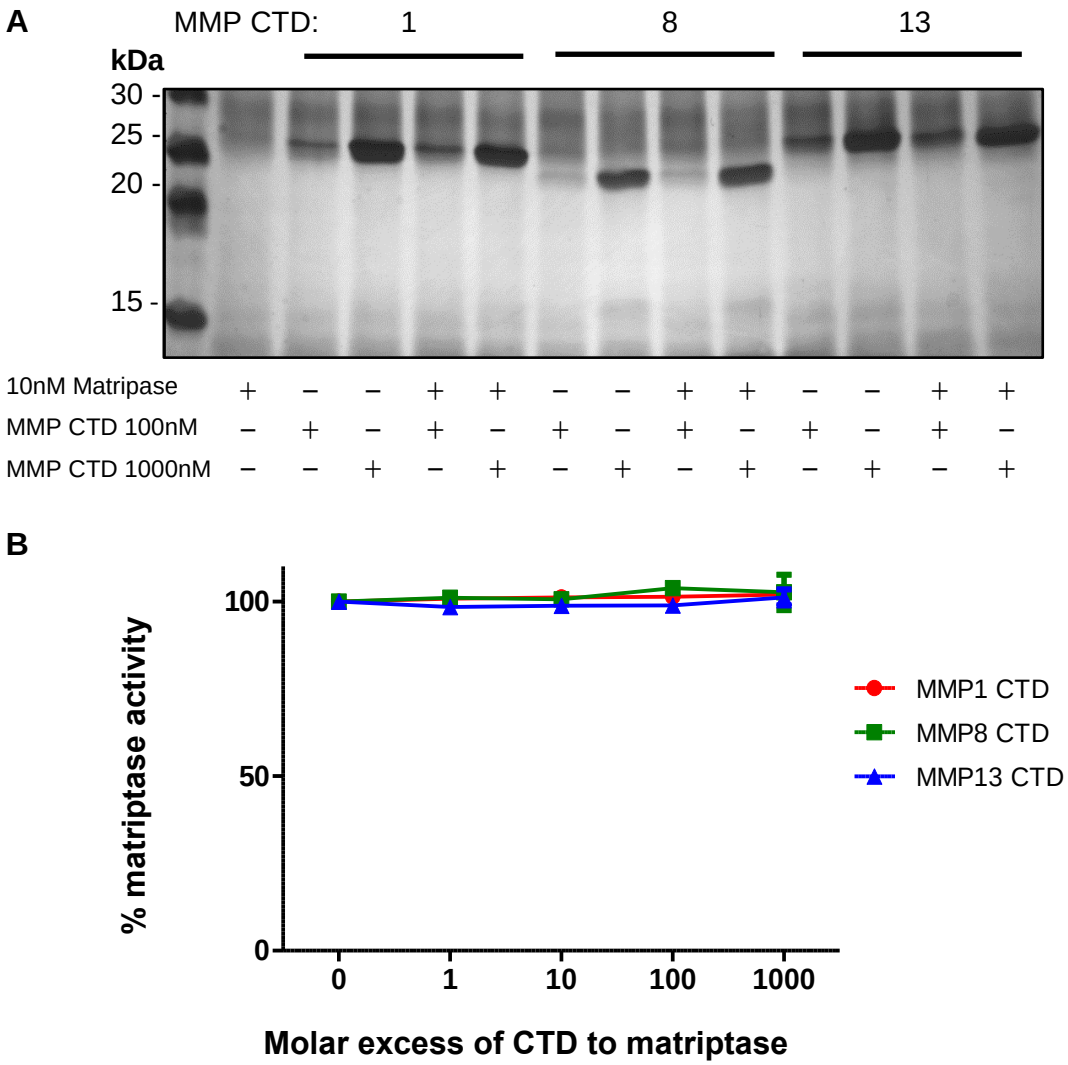

Figure 5.8: Incubation of MMP-1, -8 and -13 CTDs with matriptase
(A) MMP-1, -8 and -13 CTDs at either 100 or 1000 nM were incubated with Matriptase at 10 nM for 3 hours, after which samples were separated by SDS-PAGE and silver stained. Gel representative of n=2 independent experiments. (B) Boc-QAR-AMC assays were undertaken with 1 nM matriptase in the presence of CTDs at various molar excesses. Activity assay n=3 independent experiments.

To test the hypothesis that MMP CTD can act antagonistically to PAR2 activation by matriptase, an experiment was undertaken where PAR2-overexpressing SW1353 cells (see chapter 2.10) were pre-incubated with MMP-1, -8 or -13 CTD for 30 minutes. The cells were then stimulated with 10 nM matriptase in a calcium mobilisation assay. The presence of both MMP-1 and -13 CTD appeared to have a small antagonistic effect on calcium mobilisation following matriptase stimulation (Figure 5.9). When this effect was quantified, 1000 nM of MMP-1 CTD resulted in 91% of maximal calcium mobilisation, and 1000 nM MMP-13 CTD resulted in 82% of maximal calcium mobilisation (Figure 5.10). These two reductions were both statistically significant to $p < 0.05$, and were the only significant results from this experiment, despite a trend of reduction for 100 nM MMP-13 CTD.

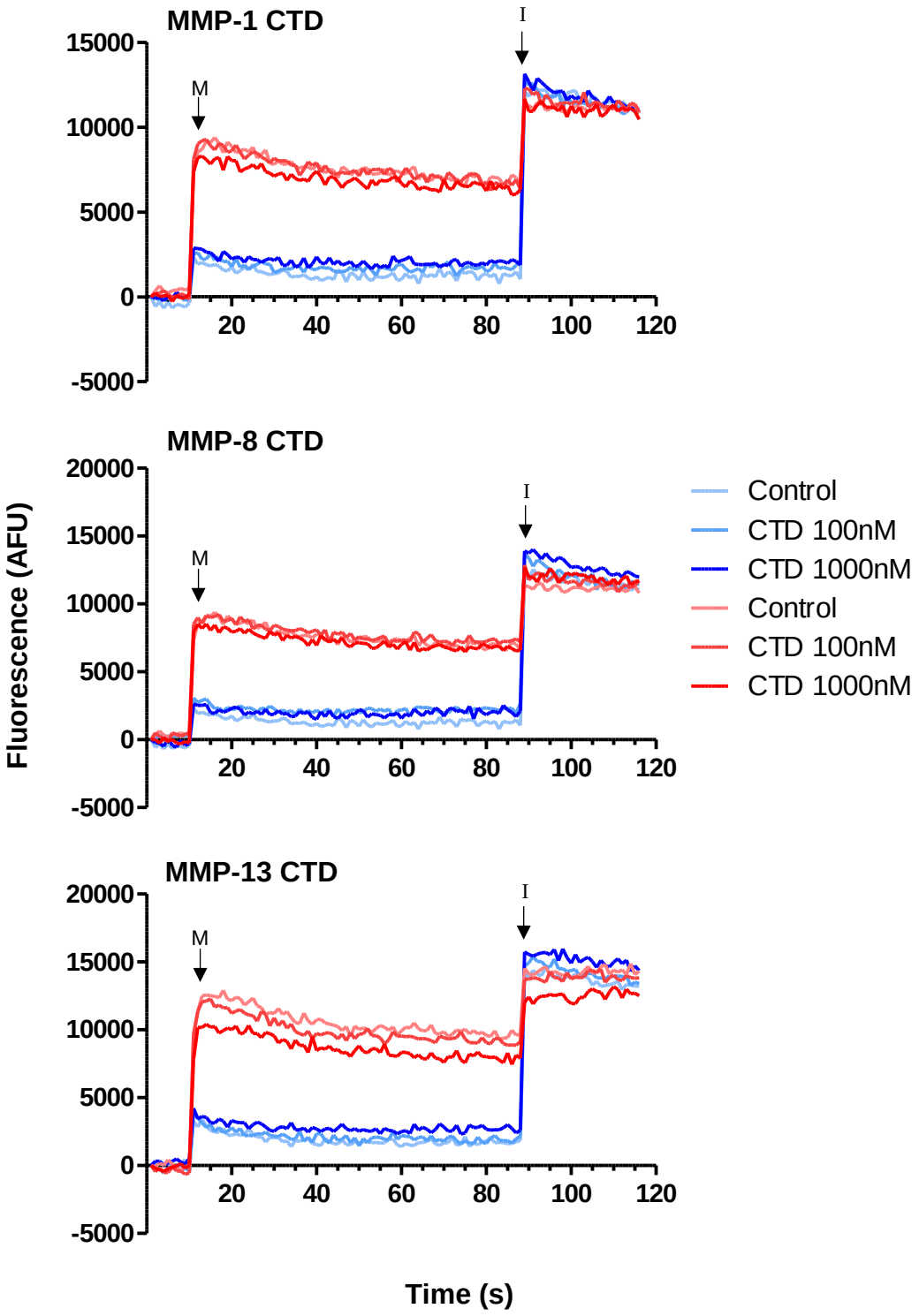

Figure 5.9: Calcium mobilisation following matriptase stimulation with MMP-1, -8 and -13 CTD pre-incubation

SW1353 cells were transduced with pSIEW_PAR2 (red lines) and pSIEW_Empty (blue lines) expressing lentivirus before culturing for 48 hours then serum starving overnight. Cells were loaded with Rhod-4-AM fluorescent calcium indicator and placed in a fluorimeter where the assays were undertaken. The cells were pre-incubated for 30 minutes with either MMP-1, -8 or -13 CTDs. Fluorescence was observed following 10 nM matriptase stimulation (M), and 5 µM ionomycin stimulation (I). Data shown are mean of n=2 independent experiments.

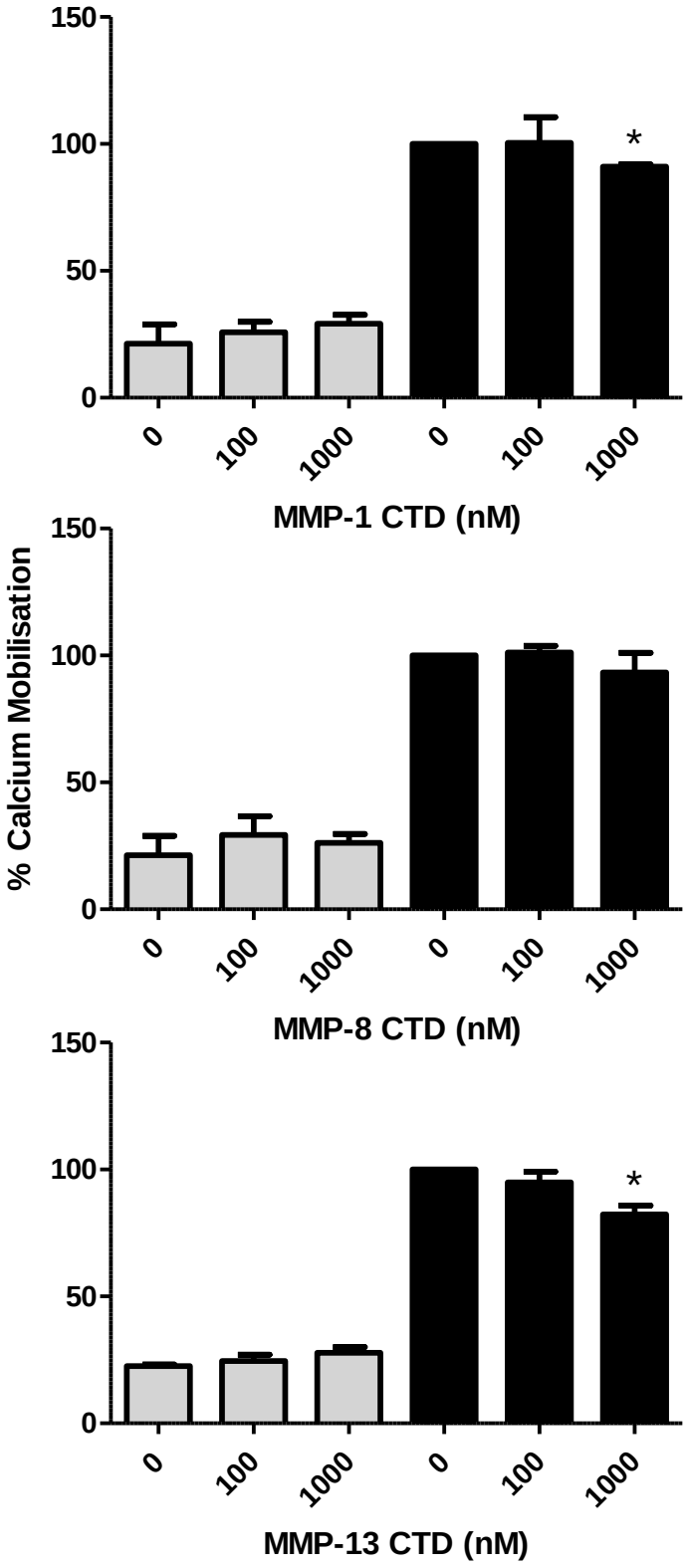

Figure 5.10: Calcium mobilisation following matriptase stimulation with MMP1, 8 and 13 CTD pre-incubation

Maximal calcium response (average calcium response in the 10 seconds immediately following stimulation) obtained from the data in figure 5.9 and normalised to the no CTD pre-treatment in PAR-2 expressing cells as 100% response. PAR2 expressing cells are black bars whereas empty vector control cells are grey bars. Mean ± S.E.M; where * $p < 0.05$ by unpaired T-test between 1000 nM pre-treatment group and no pre-treatment group in PAR2 expressing cells. Data shown is mean of n=2 independent experiments.

5.2.3.2 Testing putative MMP cleavage revealed tethered ligand, LIGKVD, for IL-8 expression

In order to study PAR2 biology, the synthetic peptide SKIGKV-NH_2 (hereafter SLIGKV) is commonly used as an agonistic "activator peptide" which mimics PAR2 canonical activation by trypsin[314]. Other activator peptides have been utilised in the literature, corresponding to other PAR2 cleavage sites, for example TVFSVDEFSA-NH_2 which is revealed by cathepsin S[226]. It was hypothesised that should MMP cleavage of PAR2 be agonistic for the receptor, then the revealed ligand would commence with leucine-37. The synthetic peptide LIGKVD-NH_2 (hereafter LIGKVD) was therefore synthesised and utilised as a putative MMP activator peptide. The reverse sequence peptide DVKGIL was used as a negative control.

Interleukin-8 (IL-8, gene *CXCL8*) is well established as a pro-inflammatory chemokine induced by canonical PAR2 signalling[315,316]. To explore whether LIGKVD might instigate pro-inflammatory PAR2 signalling, *CXCL8* expression was examined and compared with canonical SLIGKV stimulation. Both peptides were added to PAR2-overexpressing cells in increasing concentrations (10 to 300 µM) and stimulated for three hours, after which *CXCL8* expression was examined. As expected, there was a robust upregulation of IL-8 with all tested SLIGKV concentrations, however there was no effect by LIGKVD (Figure 5.11 A). Taking the concentration of SLIGKV as low as 1 µM still resulted in IL-8 upregulation significant to $p < 0.001$ (Figure 5.11 B).

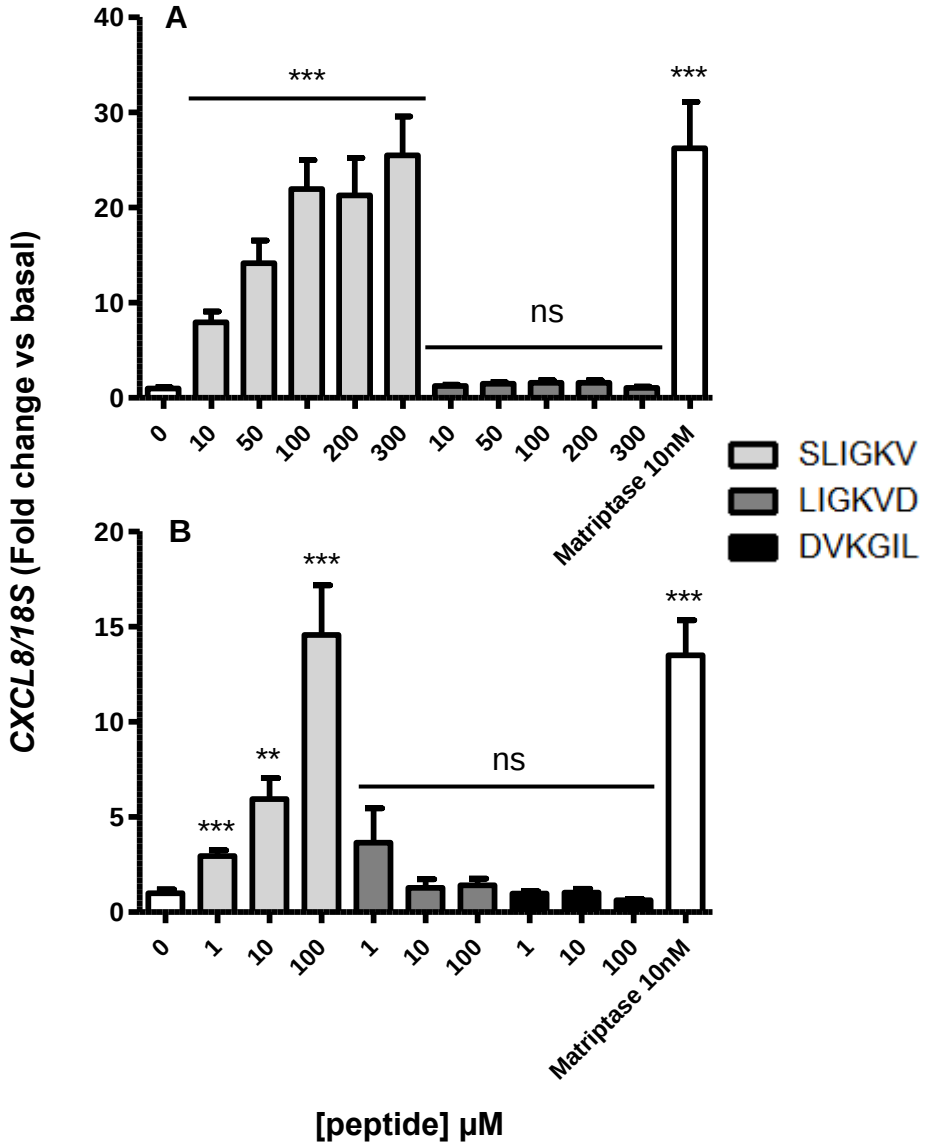

Figure 5.11: IL-8 expression following 3 hour SLIGKV, LIGKVD and DVKGIL stimulation in SW1353_FLAG-PAR2 cells

SW1353_FLAG-PAR2 cells were seeded in 96-well plates and stimulated for 3 hours with increasing concentrations of either 10-300 µM SLIGKV and LIGKVD (A) or 1-100 µM SLIGKV, LIGKVD and DVKGIL (B), as well as 10 nM matriptase as a positive control. Following stimulation, mRNA was extracted and reverse transcribed to cDNA. qPCR was were undertaken for IL-8 (*CXCL8*), normalised to *18S* ribosomal RNA (mean ± SEM; where ** $p < 0.01$ and *** $p < 0.001$, by unpaired two-tailed T Test compared to basal expression, unstimulated control). Data pooled from n=2 separate independent experiments.

5.2.3.3 Testing putative MMP cleavage revealed tethered ligand, LIGKVD, on calcium mobilisation

IL-8 is a useful readout for assessing canonical PAR2 activation, as instigated by matriptase or SLIGKV stimulation. The lack of response by LIGKVD suggests that it is not a canonical agonist, therefore other signalling pathways further upstream than IL-8 were investigated.

Firstly, calcium mobilisation assays were undertaken with increasing concentrations of SLIGKV on PAR2-overexpressing cells, and there were good responses at all tested concentrations from 0.2 to 20 µM (Figure 5.12). When undertaking similar experiments with LIGKVD concentrations up to 100 µM, there was no calcium response (Figure 5.13 A). The small "response" observed with the 100 µM sample is in fact a buffer injection artefact as a result of injecting a large volume on the cells and is often observed at the top concentration of such dose-response studies. This effect is also observed injecting 100 µM LIGKVD on the empty vector control cells. The reverse control peptide, DVKGIL, also had no effect on calcium mobilisation (Figure 5.13 B).

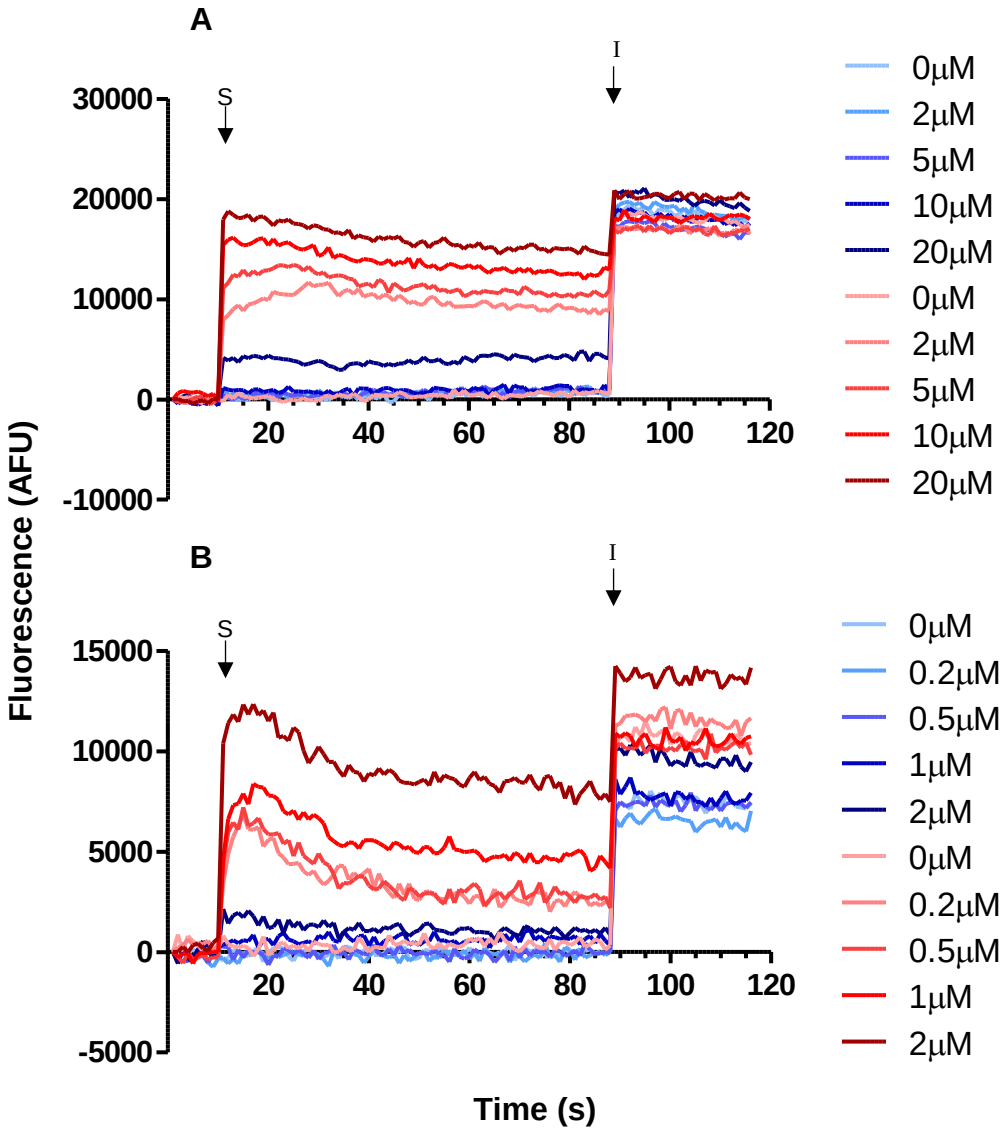

Figure 5.12: Calcium mobilisation following SLIGKV (canonical activating peptide) titrations
SW1353 cells were transduced with pSIEW_PAR2 (red lines) and pSIEW_Empty (blue lines) expressing lentivirus before culturing for 48 hours then serum starving overnight. Cells were loaded with Rhod-4-AM fluorescent calcium indicator and placed in a fluorimeter where the assays were undertaken. Titrations of SLIGKV peptide were undertaken using either 0-20 μM (A) or 0-2 μM (B) peptide. Fluorescence was observed following SLIGKV stimulation (S), and 5 μM ionomycin stimulation (I). Data shown is mean of two independent experiments.

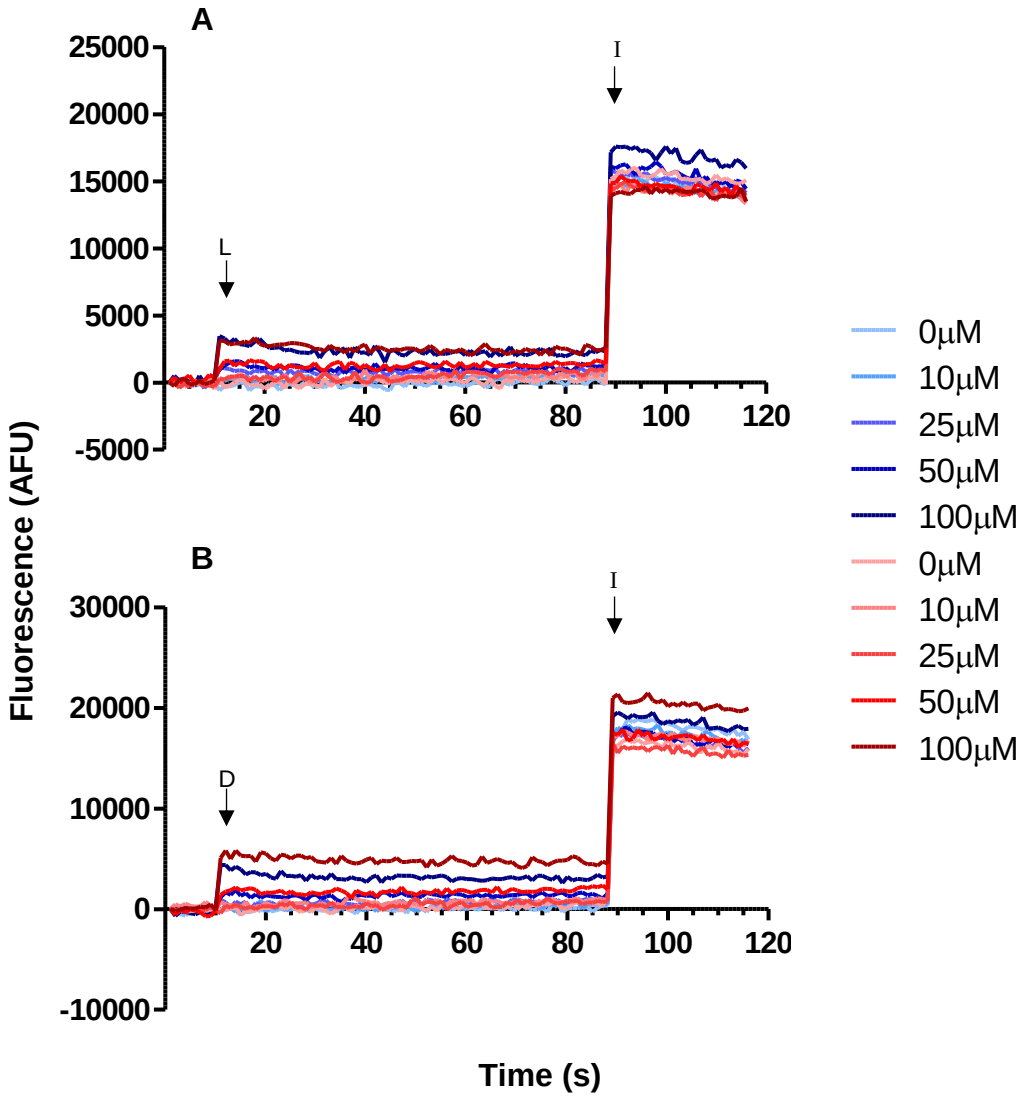

Figure 5.13: Calcium mobilisation following putative MMP activating peptide (LIGKVD) and reverse control peptide (DVKGIL) titrations

SW1353 cells were transduced with pSIEW_PAR2 (red lines) and pSIEW_Empty (blue lines) expressing lentivirus before culturing for 48 hours then serum starving overnight. Cells were loaded with Rhod-4-AM fluorescent calcium indicator and placed in a fluorimeter where the assays were undertaken. Titrations of 0-100 μM for either putative MMP activating peptide LIGKVD (A) or reverse control peptide DVKGIL (B) were undertaken. Fluorescence was observed following LIGKVD (L) or DVKGIL (D) stimulation, and 5 μM ionomycin stimulation (I). Data shown is mean of two independent experiments.

5.2.3.4 Testing putative MMP cleavage revealed tethered ligand, LIGKVD, on MAPK activation

Following the observation that LIGKVD does not stimulate calcium mobilisation, the activation of p38 and ERK1/2 MAPK signalling pathways was explored. It is known that both p38 and ERK1/2 are phosphorylated in response to PAR2 canonical activation, including activation by matriptase[317].

A time-course experiment was undertaken to explore the dynamics of both p38 and ERK1/2 phosphorylation in PAR2-overexpressing SW1353 cells following either 10 nM matriptase or 100 µM SLIGKV stimulation (Figure 5.14). As expected, both proteins are phosphorylated, with ERK1/2 reaching peak phosphorylation earlier than p38, after 5 minutes for matriptase, and 10 minutes for SLIGKV. p38 reached maximal phosphorylation at 40 minutes for both agonists (however the time-course was terminated thereafter, thus it is possible maximal p38 phosphorylation was later).

The same experiment was undertaken by stimulating the cells with either 100 µM LIGKVD or DVKGIL. Interestingly, the addition of LIGKVD resulted in a marked phosphorylation of ERK1/2 which mimics the phosphorylation observed following SLIGKV stimulation (Figure 5.15 A). These cells however had no evidence of p38 phosphorylation, indicating that biased signalling is occurring following LIGKVD stimulation. There was no evidence of MAPK phosphorylation following control peptide DVKGIL stimulation (Figure 5.15 B).

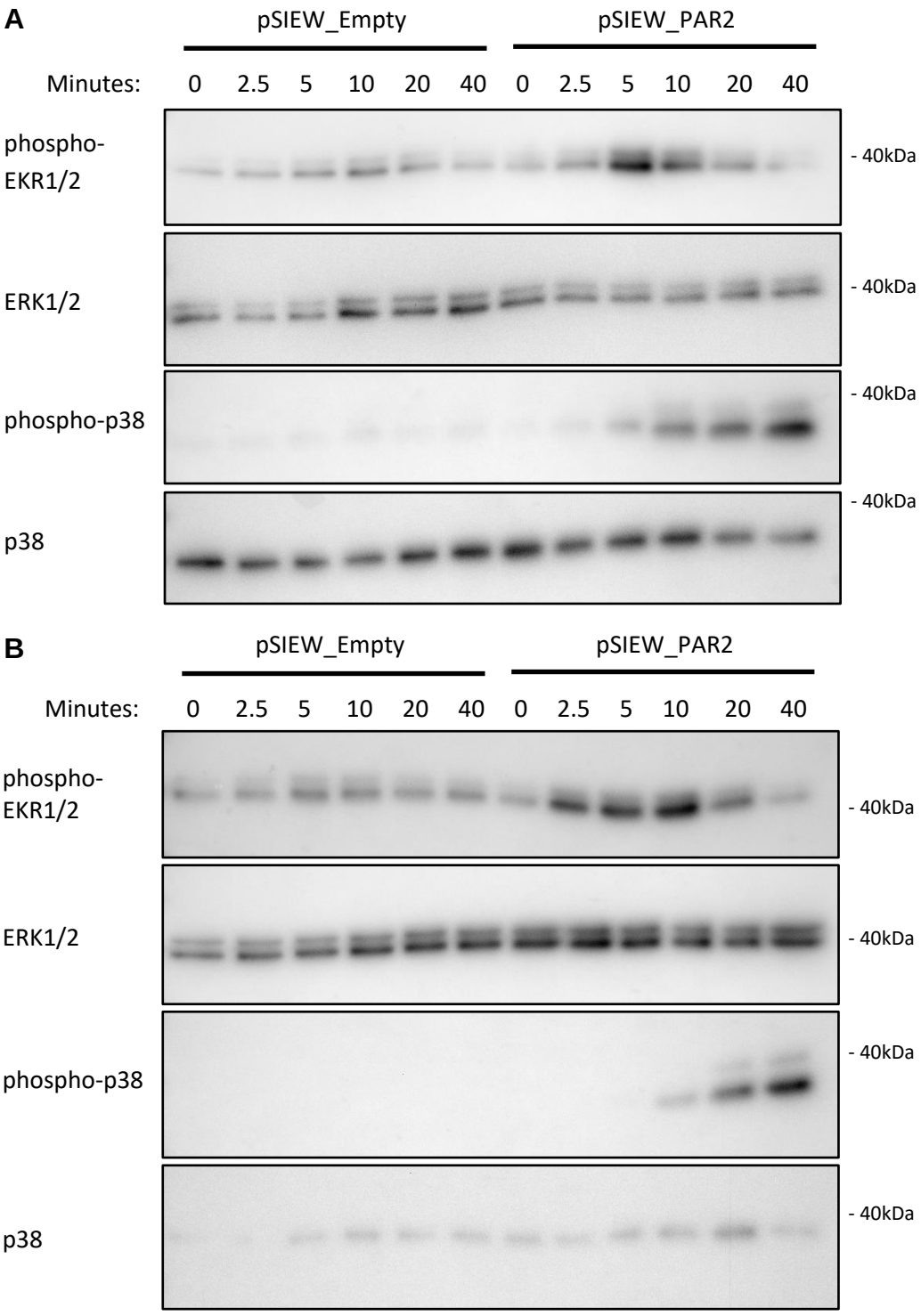

Figure 5.14: ERK1/2 and p38 phosphorylation following Matriptase and SLIGKV stimulation
SW1353 cells were transduced with pSIEW_PAR2 or pSIEW_Empty expressing lentivirus before culturing for 48 hours then serum starving overnight. A time course was undertaken by stimulating with either 10 nM matriptase (A) or 100 µM SLIGKV (B) and cells were lysed and proteins separated by SDS-PAGE before probing for either phospho-ERK1/2, native ERK1/2, phospho-p38 or native p38. Blots shown are representative of two independent experiments.

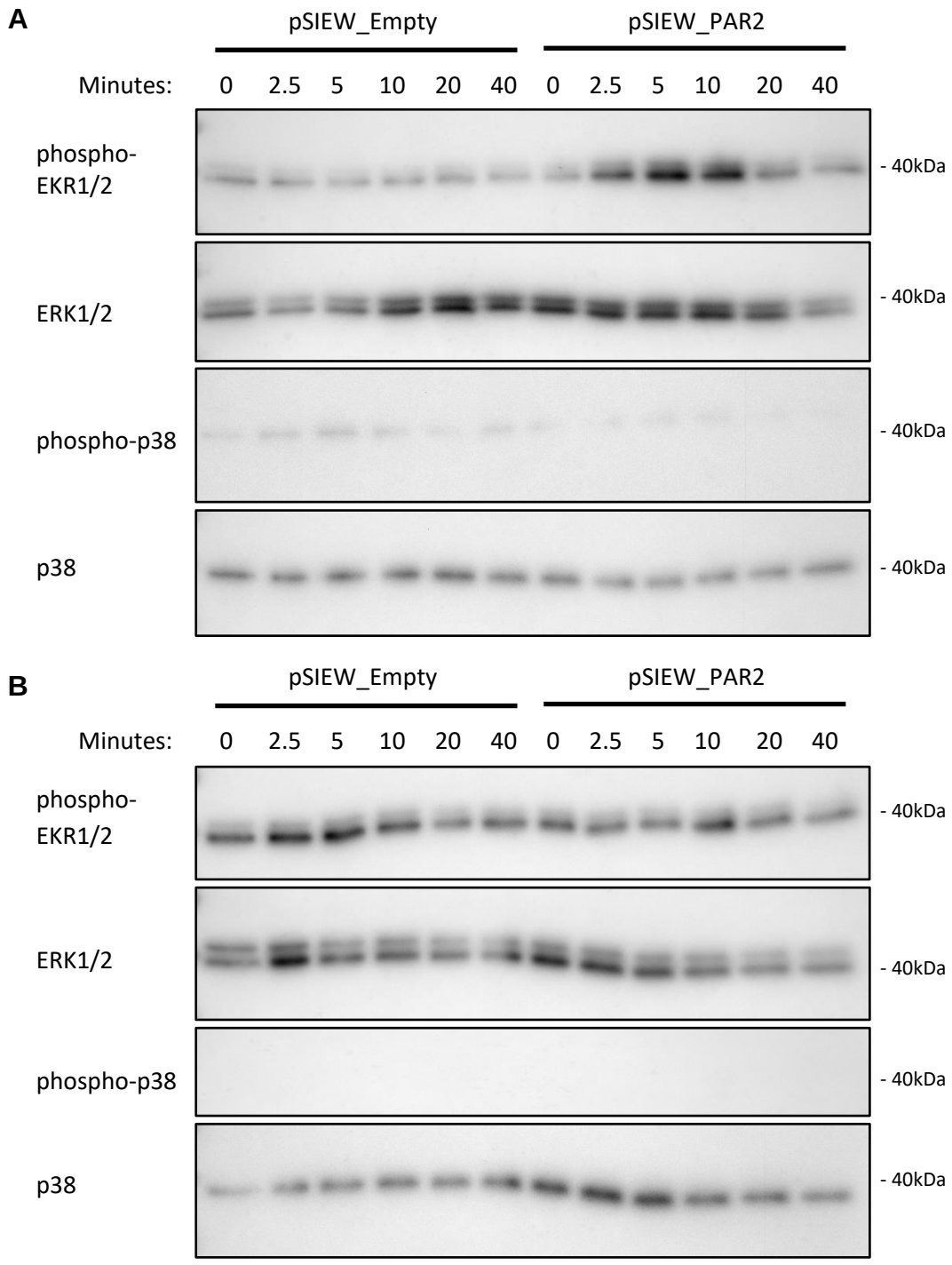

Figure 5.15: ERK1/2 and p38 phosphorylation following LIGKVD and DVKGIL stimulation
SW1353 cells were transduced with pSIEW_PAR2 or pSIEW_Empty expressing lentivirus before culturing for 48 hours then serum starving overnight. A time course was undertaken by stimulating with either 100 µM LIGKVD (A) or 100 µM DVKGIL (B) and cells were lysed and proteins separated by SDS-PAGE before probing for either phospho-ERK1/2, native ERK1/2, phospho-p38 or native p38. Blots shown are representative of two independent experiments.

ERK1/2 has previously been shown to be involved in the positive regulation of MMP-1 expression in various cell types[318,319], including chondrocytes[320]. Therefore, the regulation of *MMP1* by LIGKVD was explored.

As expected, SLIGKV resulted in significant upregulation of *MMP1* expression at all tested peptide concentrations, and control peptide DVKGIL had no effect. However, there was no evidence of LIGKVD regulating *MMP1* expression, even at the very high concentration of 500 μM (Figure 5.16).

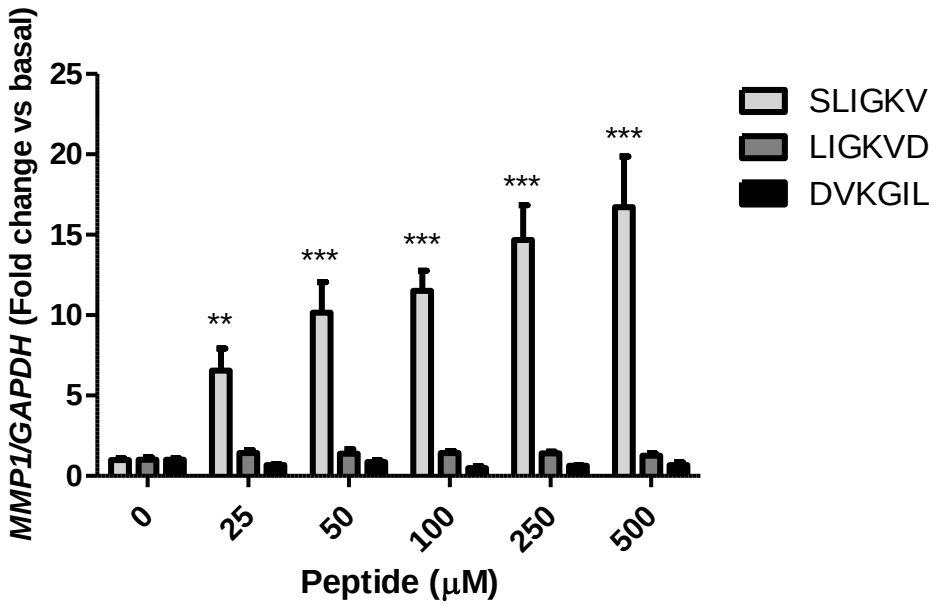

Figure 5.16: MMP1 expression following SLIGKV, LIGKVD or DVKGIL stimulation
PAR2-overexpressing cells were stimulated for 24 hours with 0-500 μM SLIGVD, LIGKVD or DVKGIL. Following stimulation, mRNA was extracted and reverse transcribed to cDNA. qPCR was were undertaken for *MMP1*, normalised to *GAPDH* (mean ± SEM; where ** $p < 0.01$ and *** $p < 0.001$, by unpaired two-tailed T Test compared to basal expression, unstimulated control). n=1 independent experiments.

5.2.3.5 MMP activity in IL-1+OSM-stimulated bovine nasal cartilage conditioned medium is able to cleave SY-9

The stimulation of bovine nasal cartilage with IL-1 in combination with OSM results in an MMP-dependent degradation of cartilage[321], a system used as a model for enzyme-mediated degradation of cartilage[1,322,323].

In order to test whether active MMP generated from this model would be able to cleave PAR2, conditioned medium was used in a SY-9 activity assay. It was clear that there was SY-9 degrading activity within the conditioned media, and this was clearly a result of MMP activity, as the effect was completely blocked by GM6001. The inhibition of serine proteases with DFP and cysteine proteases with E64 had no effect on the cleavage of SY-9 (Figure 5.17 A).

To ascertain specific MMPs involved in this activity, a selective MMP-8 inhibitor (MMP-8 inhibitor I) and a selective MMP-13 inhibitor (CL-82198) were utilised. This experiment suggests that the SY-9 cleaving activity is mainly as a result of MMP-13. CL-82198 inhibits MMP-13 with an IC_{50} of 3.2 µM[324], and 10 µM in this assay was able to almost inhibit all the SY-9 degrading activity of the bovine cartilage conditioned medium whereas 100 µM resulted in total inhibition (Figure 5.17 B). MMP-8 inhibitor I has an IC_{50} of 4 nM for MMP-8[325], and 10 nM had no effect on SY-9 degradation, whereas 100 nM only had a very small effect, however statistical analysis was not able to be undertaken (Figure 5.17 B).

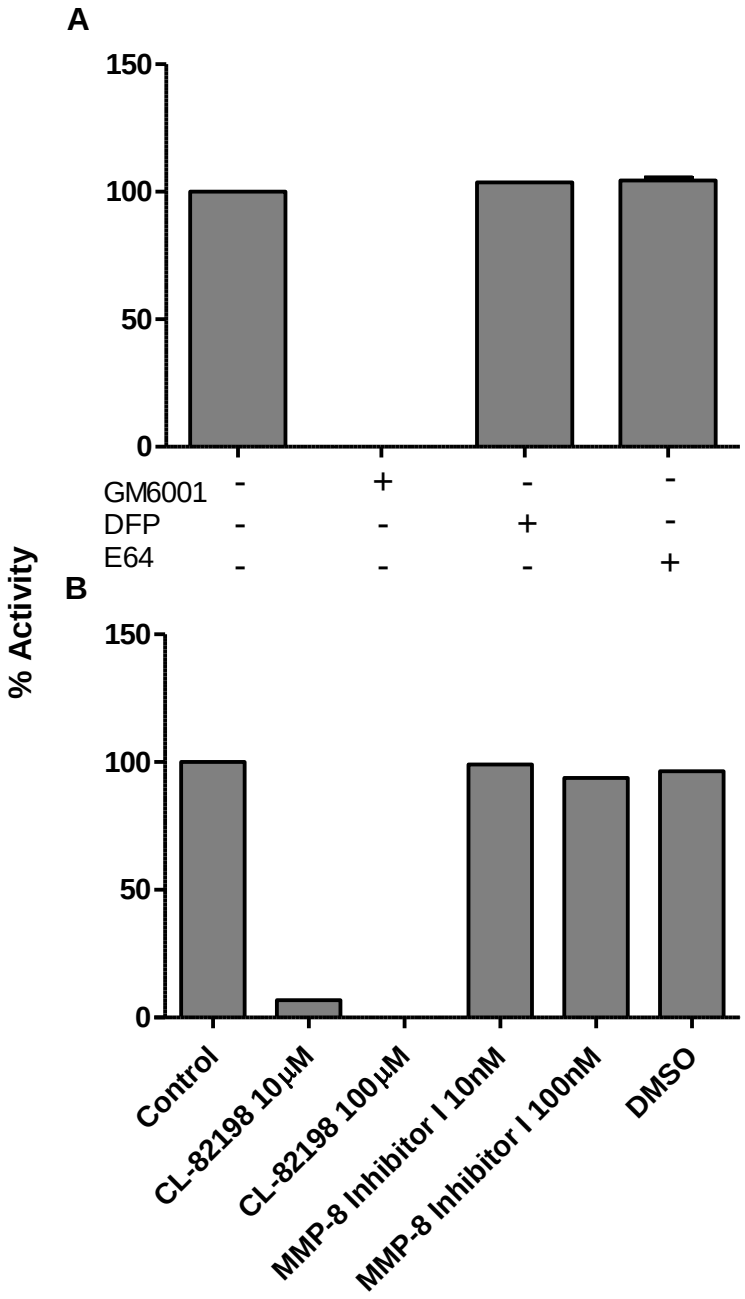

Figure 5.17: MMP activity in IL-1+OSM stimulated bovine nasal cartilage conditioned medium contains MMP activity able to digest SY-9 peptide

100 µL reactions containing 5 µL day 14 conditioned medium from an IL-1+OSM-stimulated bovine nasal cartilage explant experiment were incubated with 10 µM SY-9 peptide in the presence or absence of either 100 µM GM6001, 10 µM E64 or 2 mM DFP. Assays were undertaken in a fluorimeter to monitor SY-9 cleavage and velocities were obtained from the resulting progress curves. Data was normalised to the control wells, given as 100% activity (A). n=2 independent experiments with conditioned medium from different donors. Subsequently, a similar experiment was undertaken with MMP-13 inhibitor CL-82198 or MMP-8 inhibitor I (B). n=1 independent experiment.

5.3 Discussion

In this chapter, the specific cleavage sites generated by MMP-mediated PAR2 digestion outlined in chapter 4 were identified and subsequently the functional roles of these cleavages were explored. Overall, these results suggest that there might be a blocking effect of canonical signalling mediated by MMPs and that MMPs might be biased agonists of PAR2.

HPLC was undertaken on the products resulting from MMP-1, -8 and -13 digestion of the PAR2 42mer. Of these, MMP-1 yielded the "cleanest" digestion with a single major product, whereas MMP-8 and -13 yielded two major products. MS analysis of these products identified the cleavage sites as being serine-37 / leucine-38 for all three proteases, as well as valine-68 / leucine-69. Both these cleavage sites result from a leucine in the P1' position and a glycine in the P3' position, however the P2' position varies with an isoleucine at position 39 and a threonine at position 69. The collagenolytic MMPs have a preference for a hydrophobic amino acid at the P1' position, a basic or hydrophobic amino acid at the P2' position and a small amino acid (alanine, glycine or serine) at the P3' position[326,327]. Furthermore a search of these three proteases in the MEROPS database (which collates all previously identified MMP cleavage sites) indicates that the hydrophobic amino acid leucine is the preferred P1' amino acid for them[310]. The three proteases, in particular MMP-8 and -13, also have a preference for a glycine the P3' position of their substrate, which is also found in both sites identified on PAR2.

When comparing the two identified cleavage sites, the literature supports the observation that serine-37 / leucine-38 is the likely major cleavage event as the P1' – P2' – P3' positions are all chemical preferences for the collagenases, whereas the P2' for the valine-68 / leucine-69 cleavage site is a polar uncharged amino acid in threonine as opposed to the preferred basic or hydrophobic residue in that position. The observation that MMP-8 and -13 both cleaved in the additional site that MMP-1 did not, could possibly reflect the higher specificity for P3' glycine for MMP-8 and -13 compared to MMP-1[310]. It is likely that MMP-1 does indeed also cleave that site as a small peak was observed at the correct retention time by HPLC, but under tested conditions this was below the sensitivity range of electrospray MS.

In order to ascertain the relative importance of the two observed cleavages for MMP-8 and -13, a restricted digest experiment was undertaken using MMP-13. This clearly demonstrated that serine-37 / leucine-38 was the initial cleavage event, followed by valine-68 / leucine-69. It is well established that PAR2 activation is rapid following canonical activation, as demonstrated in this chapter by measuring calcium mobilisation following matriptase stimulation. It therefore follows that any activation by MMP-mediated cleavage at serine-37 / leucine-38 would likely be instigated before cleavage occurs at valine-68 / leucine-69. The second cleavage could also have a potential role as a limiting factor in any MMP-mediated activation. Indeed, mast cell tryptase has been identified as a canonical activator of PAR2, however its activation potential is limited by a secondary cleavage downstream of the canonical site[206].

In order to gain initial insights of the relevance of this MMP cleavage site on PAR2, enzyme kinetics were studied. As the SY-9 peptide substrate encompasses P4-P4' for matriptase and P5-P3' for the MMPs, it could be used to directly compare the kinetics for PAR2 cleavage by all the enzymes. Unsurprisingly, all three MMPs were far less efficient at cleaving the substrate compared to matriptase. Matriptase is known as a very potent PAR2 activator[293], and has previously had its cleavage of the SY-9 peptide explored. Béliveau *et al*. (2009)[328], found that matriptase cleaved PAR2 with a k_{cat}/K_m of 3.1 X 10^5 $M^{-1}.s^{-1}$, which is a Figure in the same order of magnitude as obtained in this study, 6.13 x 10^5 $M^{-1}.s^{-1}$. It is important to address the limitations of small peptide substrate experiments such as this, as they are unlikely to allow for exosite interactions, such as with MMP haemopexin domains, and thus the physiological enzymatic efficiencies are likely to be different. It is interesting to compare the kinetics for PAR2 cleavage by matriptase, and PAR1 activation by thrombin (the archetypal protease-mediated receptor activation). Thrombin cleaves PAR1 with a k_{cat}/K_m of 1.2 X 10^7 $M^{-1}.s^{-1}$, two orders of magnitude more efficiently than matriptase cleavage of PAR2[202].

When considering the enzyme kinetics for the collagenases, it is important to note that this projected utilised APMA-activated enzyme, however this is not considered to be fully active. When activated by either APMA or trypsin, the pro-collagenases are activated only to 10-25% of maximal activation. This results from cleavage within the bait region of the pro-domain, however for fully active enzyme, the whole pro-domain requires removal, which can be performed by enzymes such as MMP-3[329]. It is therefore possible that the kinetic data presented within this chapter underestimates the physiological

relevance of these cleavages, and the utilisation of MMP-3-activated collagenase would likely give higher k_{cat} values.

The relatively low k_{cat}/K_m values for MMPs on SY-9 are a result mainly of their low k_{cat} values, whereas their K_m values are comparable to matriptase. These low K_m values suggest a relatively high affinity for the substrate. Taking these data together, a hypothesis was developed where MMPs might act as competitive antagonists for PAR2 canonical activation. In a system where PAR2, matriptase and MMPs are all expressed, such as cartilage, it is possible that MMPs and matriptase compete for binding to PAR2. In such a system, irrespective of the subsequent functional role of the MMP cleavage and revealed ligand, canonical PAR2 activation by matriptase would be attenuated. The presence of MMP at its cleavage site would render it very unlikely to allow matriptase to bind there due to steric hindrance.

To test this hypothesis in a cell culture model, a blocking experiment utilising MMP CTDs was undertaken. MMP CTDs were utilised due to a lack of recombinant full-length MMPs and time constraints for producing sufficient quantities. The MMP CTDs consist of the entire haemopexin-like domain as well as part of the linker domains of MMP. It is well established that MMP haemopexin-like domains play key roles in substrate recognition and binding of MMP to substrate[64], therefore it is possible that this is true of MMP cleavage of PAR2. Whilst the haemopexin-like domain will not be binding to the cleavage site on PAR2, it is possible that it will be able to bind sufficiently close to also result in steric hindrance.

This experiment showed a modest blocking effect of MMP-1 and -13 CTDs on calcium mobilisation triggered by canonical matriptase activation of PAR2. A 100-fold excess of MMP-1 and -13 CTD over matriptase resulted in 91% and 82% of maximal calcium mobilisation, respectively. Background work suggested that this effect was not a result of interference by CTD on matriptase activity. Were this a result of CTD binding and blocking matriptase from fully activating the receptor, the modest effect does not reflect the K_m values for matriptase and MMP-1 and -13 could be a result of not using full-length MMP. Depending on where the CTD binds to PAR2, matriptase was not fully blocked from activating the receptor. It would be important in future work to utilise full-length MMP in similar experiments. Should the effect observed by CTD be a result of blocking the receptor, then utilising full-length MMP should result in a stronger blocking effect.

After exploring the effect of MMP CTD on canonical PAR2 signalling, an exploration of the potential role of the MMP cleavage and its revealed ligand was undertaken. The MMP cleavage site of PAR2 is downstream of the canonical activation site meaning it can either be a disarmer, a full agonist or a biased agonist. Unfortunately, sufficient quantity of active MMP was unable to be sourced for this work, so instead a synthetic peptide corresponding to the putative revealed tethered ligand, LIGKVD, was used.

This tethered ligand was compared to matriptase and SLIGKV canonical activation of PAR2, and it was found that LIGKVD was unable to activate the pathways resulting in IL-8 expression, as well as being unable to stimulate calcium mobilisation. When looking at MAPK signalling, LIGKVD was able to stimulate ERK1/2 phosphorylation, but not p38 phosphorylation, as opposed to the canonical activators which stimulated both.

Previous work has been undertaken on the canonical activator peptide, SLIGKV, exploring key residues for PAR2 activation. Al-Ani *et al.* (2004)[330] created a series of mutants substituting alanine into each position from 37 to 42 of full-length PAR2 for cell culture work, as well as synthetic peptides. As their work used rat cells, the canonical activator peptide was SLIGRL. Interestingly, when measuring calcium mobilisation, their ALIGRL mutant resulted in 95% activity in cell culture work following trypsin activation, whereas the synthetic ALIGRL peptide resulted in 9.5% residual activation in the same cells. In their study, substituting the P2' leucine for an alanine had a much larger reducing effect resulting in only 14% activation for trypsin activation, and no activity for the synthetic peptide SAIGRL. Taken together with their other mutants, it was concluded that the serine and leucine at the P1' and P2' position are key to activating PAR2, with leucine of particular importance. This leucine is present in the putative MMP activator peptide used in this study as the P1' position. This peptide however did not exhibit any stimulation of calcium mobilisation, despite being tested at a concentration of 500 times higher than for the observed calcium mobilisation by SLIGKV. The fact that LIGKVD in this study exhibited no calcium mobilisation whereas ALIGRL did in the Al-Ani *et al.* (2004)[330] study could reflect a species difference between rat and human, or the fact that despite leucine at P2' being more important than serine at P1', there is a requirement for the presence of an amino acid there, such as alanine. Indeed this is supported by the observation that synthetic PAR2 agonist 2-furoyl-LIGKV-OH (also known as ASKH95) is able to fully activate PAR2, including calcium mobilisation[331]. The 2-furoyl-LIGKV-

OH peptide was developed as a PAR2 agonist with a longer biological half-life than canonical activator peptide SLIGKV-NH_2, and has a higher affinity for PAR2 than the canonical activator[314]. Whilst the 2-furoyl group is not an amino acid, it is a similar size to an amino acid, and therefore could act to keep the leucine in the P2' position.

A subsequent study found that the peptide SLAAAA was able to stimulate ERK1/2 phosphorylation without stimulating calcium mobilisation, as observed with LIGKVD in this study but unfortunately they did not measure p38 MAPK[332]. It is thought that there is a requirement of a basic amino acid in position 5 of the tethered ligand/ activator peptide for triggering calcium mobilisation – lysine in the human sequence or arginine in the rat sequence[333]. The LIGKVD peptide used in this project has this basic lysine in position 4, and position 5 is subsequently occupied with a hydrophobic valine. It is unknown how the canonical peptide or LIGKVD docks into the active site of PAR2, however this loss of basic residue could contribute to the loss of calcium mobilisation observed.

An interesting study by Lin *et al*. (2008)[334], compared the rat activator peptide SLIGRL with a truncated version, LIGR and explored various signalling pathways. As with the peptide LIGKVD utilised in this study, LIGR was shown to instigate biased signalling. As with LIGKVD, LIGR was unable to stimulate calcium mobilisation, IL-8 induction or p38 MAPK phosphorylation, however unlike LIGKVD, there was no phosphorylation of ERK1/2 either. The biased signalling induced by LIGR involved activation of the Rho family of GTPases as measured by an increase in GTP-bound Rho.

Despite being able to induce the phosphorylation of ERK1/2, LIGKVD was unable to induce *MMP1* expression. Cell signalling is complex with much cross-talk between pathways. Whilst the inhibition of ERK1/2 will result in a suppression of *MMP1* expression following canonical PAR2 activation (Dr Chun Chan, unpublished), the suppression is not total, implying other pathways are also involved. Indeed, following IL-1β stimulation of chondrocytes, ERK1/2 inhibition will reduce *MMP1* expression, however so will p38 inhibition, albeit to a lesser extent[320]. In this study it is likely that despite inducing ERK1/2 phosphorylation, other pathways required for *MMP1* expression are not induced.

The observation that cell surface receptors may be activated by collagenolytic MMPs has previously been described. Both MMP-1 and MMP-13 have been shown to be able to

activate the PAR1 receptor. MMP-1 cleaves PAR1 two amino acids upstream of its canonical activation site, and results in an extended tethered ligand[297], whereas MMP-13 cleaves a single amino acid downstream of the canonical site[298]. Both MMP-1 and -13 are agonistic to PAR1, with some evidence of biased signalling generated by these cleavage sites[297,298].

Furthermore, Li and Tai (2013) published work that described MMP-1 acting on cells in a PAR2-dependent manner, by upregulating monocyte chemoattractant protein-1 (MCP-1) protein. Their work utilised A549 cells which are not as responsive to canonical PAR2 signalling as lentiviral overexpressed PAR2 nor PAR2 stable cell line (unpublished observations). The fact their paper observed a PAR2 activation effect with 5nM MMP-1 does not fit with data presented in this project. In this project, 5nM matriptase would be a low concentration to be used to activate PAR2 in highly expressing cells. Kinetic data presented here shows that matriptase is around 68000-fold more efficient at cleaving PAR2 than MMP-1 is based on respective k_{cat}/K_m values, therefore it is very unlikely that 5 nM MMP-1 would be sufficient to activate PAR2. Furthermore, to activate MMP-1 they used 10 µg/mL trypsin, which is approximately 416 nM, followed by subsequent inhibition with soybean trypsin inhibitor. Trypsin is difficult to completely inhibit (unpublished observations), and this paper failed to provide MMP inhibitor (e.g. GM6001) experiments, nor a trypsin/trypsin soybean inhibitor-only control to confirm that it was indeed MMP-mediated cleavage and not trypsin contamination responsible for the observed effect.

Both PAR2[234] and matriptase[1] are expressed significantly higher in OA chondrocytes than in normal chondrocytes, and it is known that canonical PAR2 activation results in *MMP1* and *MMP13* expression[128]. When recombinant matriptase is added to OA cartilage explant cultures, there is an enhanced level of collagen breakdown which is dependent on MMP activity and attenuated by PAR2 antagonists[1]. Matriptase is then subsequently able to directly activate proMMP-1, and indirectly activate proMMP-13 (by activating proMMP-3 which is able to activate proMMP-13) which is responsible for the observed collagenolysis in the explant experiments[1]. Data presented in this chapter further suggests that these active MMPs may be able to also act on PAR2 in a feedback loop (summarised in Figure 5.18). Further work will be required to elucidate the exact role of MMP cleavage of PAR2.

It remains to be deduced as to whether this feedback loop impacts negatively (i.e. prevents further PAR2 signalling) or positively (i.e. perpetuates PAR2 signalling) on ECM remodelling in OA. In either case, the findings of this chapter further highlight the inherent complexity regarding proteolysis and cell signalling in a disease setting.

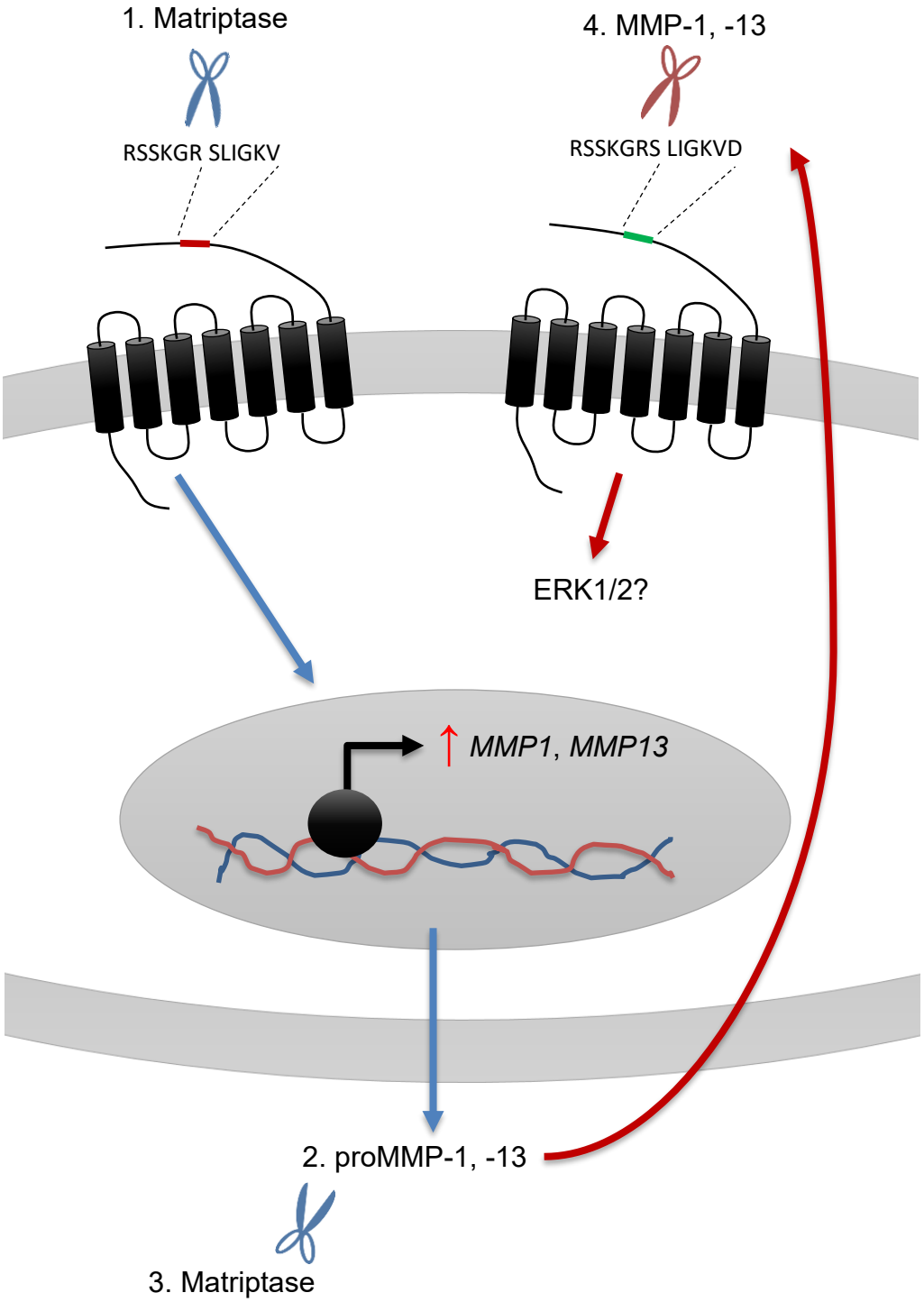

Figure 5.18: Chapter Summary

Both matriptase and PAR2 are more highly expressed in OA cartilage. It has previously been shown that PAR2 activation by matriptase results in the upregulation of *MMP1*, *MMP3* and *MMP13*, which are then secreted and can also be activated by matriptase directly (MMP-1 and MMP-3) or indirectly (MMP-13, via MMP-3[1]). Work presented in this chapter shows that MMP-1 and MMP-13 can both cleave PAR2 in *in vitro* assays and the putative revealed ligand, LIGKVD, is a biased agonist for MAPK signalling.

5.4 Summary

- MMP-1, -8 and -13 primarily cleaved at serine-36 / leucine-37 in PAR2, a single amino acid to the C-terminus of the canonical activation site.

- MMP-13 was the most catalytically efficient enzyme to cleave PAR2 followed by MMP-8 and then MMP-1, however all three were markedly less efficient than matriptase.

- The three collagenases had a similar affinity for PAR2 substrate, and using the C-terminal domains of MMP-1 and -13 resulted in small antagonistic effects on matriptase stimulation of PAR2.

- The putative MMP-revealed ligand, LIGKVD, was unable to stimulate IL-8 expression, calcium mobilisation, or p38 MAPK phosphorylation, however was able to stimulate ERK1/2 phosphorylation.

Chapter 6 - Investigation of the role of cathepsin-mediated PAR2 cleavage

6.1 Introduction

Data presented in chapter 4 identified a novel activity for four cathepsin enzymes in the ability to cleave PAR2. Furthermore, the previously described activity of PAR2 cleavage by cathepsin S was confirmed[226,300]. Data presented in this chapter aims to follow a similar work flow to the data presented in chapter 5 which explored MMP cleavage of PAR2. In order to understand cathepsin cleavage of PAR2, it is important to first identify the cleavage sites. Subsequently, generating kinetic parameters for the cleavages provides insights into functional relevance. Finally, to gain physiological relevance of the cleavages, cell culture-based work was performed to explore functional outcomes of this cleavage in PAR2.

6.1.1 Chapter Aims

- To identify the sites for cathepsin cleavage of PAR2.
- To explore kinetic parameters of cathepsin cleavage of PAR2.
- To explore a functional role for cathepsin cleavage of PAR2 in chondrocytic cells.

6.2 Results

6.2.1 Identification of cathepsin-mediated cleavage sites of PAR2

After identifying the ability of cathepsins V, L, B, S and K to cleave PAR2 in chapter 4, work was performed to identify the cleavage sites for these enzymes. For this work, nanoLCMS was utilised rather than direct infusion MS as was performed for MMP-cleavage of PAR2 in chapter 5. The reasons for this change of methodology were that as the stock concentrations of the recombinant cathepsins were higher than that of the MMPs, and that the cathepsins cleave PAR2 at a much lower concentration, a much larger dilution to assay concentration could be performed. The recombinant enzyme stocks all contained detergents which interfere with and damage nanoLCMS UPLC columns and thus were removed (by HPLC for the MMPs) or diluted out as per the cathepsins (Dr Joe

Gray, personal communication). The advantages of using nanoLCMS over direct infusion are a higher sensitivity and the ability to identify all cleavages within a sample.

NanoLCMS was performed on the 4 novel PAR2-cleaving cathepsins, as well as with cathepsin S (an example trace is presented in appendix 2). Multiple cleavages for each enzyme were identified and by using the analysis strategy described in chapter 2.14.3.1, these were ordered for each enzyme, and are shown in Figure 6.1 for cathepsins V, K, L and S.

The primary cleavage site for cathepsins V, S and L was between glutamic acid-56 and threonine-57, with secondary sites for cathepsins V and S between phenylalanine-59 and serine-60. A secondary site for cathepsin L was located towards the N-terminus between glycine-40 and lysine-41, which also corresponds to the primary site for cathepsin K. More minor sites were identified between serine-60 and valine-61 (cathepsins S and L), as well as between threonine-54 and valine-55 (cathepsin K).

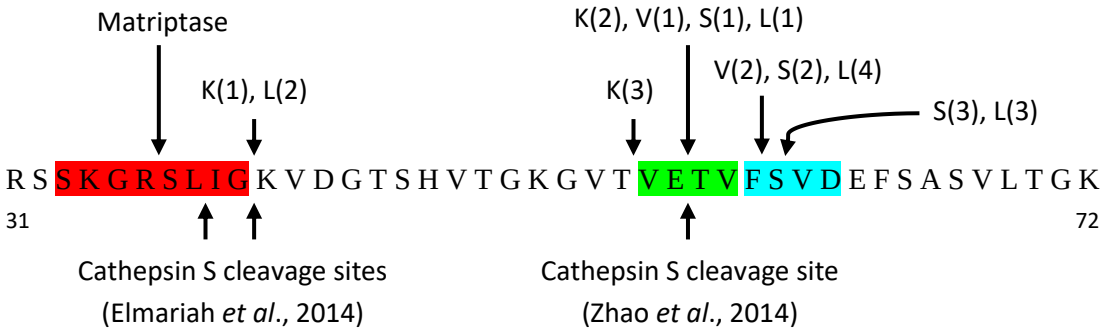

Figure 6.1: Cathepsin cleavage sites on PAR2
Schematic showing the amino acid sequence of the PAR2 42mer peptide, highlighting the identified cleavage sites by the cathepsin enzymes in this study, as well as the previously described cathepsin S cleavages of PAR2. Cleavage sites are numbered in brackets in order of importance according to nanoLCMS. Quenched-fluorescent peptides utilised for kinetic studies in this project are highlighted: red for SY-9 peptide, green for VETV substrate, and blue for FSVD substrate.

Cathepsin B resulted in more cleavages than the other enzymes, and it was more difficult to order them using the method utilised for the other cathepsins. Cleavages by cathepsin B were identified at all the same sites as for the other cathepsins, as well as several other sites (Figure 6.2).

Figure 6.2: Cathepsin B cleavage of PAR2
PAR2 42mer sequence showing the amino acid sequence of the PAR2 42mer peptide, highlighting the identified cleavage sites by cathepsin B.

As multiple cleavage sites were identified for each enzyme, it was of importance to validate the method for ordering the importance of the cleavages. Synthetic substrates were therefore designed to compare the potencies of the cathepsin enzymes for each cleavage site. It was difficult to design specific substrates for each enzyme, and it was decided to utilise two peptides of 4 amino acids each: VETV and FSVD (Figure 6.1). The VETV substrate contains the identified primary cleavage site of cathepsins V, S and L (glutamic acid-56 / threonine-57), whereas the FSVD peptide contains the site for the secondary cathepsin V, S and L cleavage at phenylalanine-59 / serine-60. The SY-9 peptide was used as the primary cleavage site for cathepsin K and the secondary site for cathepsin L (Figure 6.1).

6.2.2 Kinetic parameters of cathepsins V, L, S and K for PAR2 substrates

Kinetic parameters were generated for the cathepsin enzymes using the VETV, FSVD and SY-9 substrates, and compared with matriptase. Cathepsin B did not display Michaelis-Menten kinetics and therefore these data are not presented. The Michaelis-Menten curves for cathepsin V, L, S and K are shown in Figure 6.3, and the K_m, k_{cat} and k_{cat}/K_m values are all outlined in table 6.1.

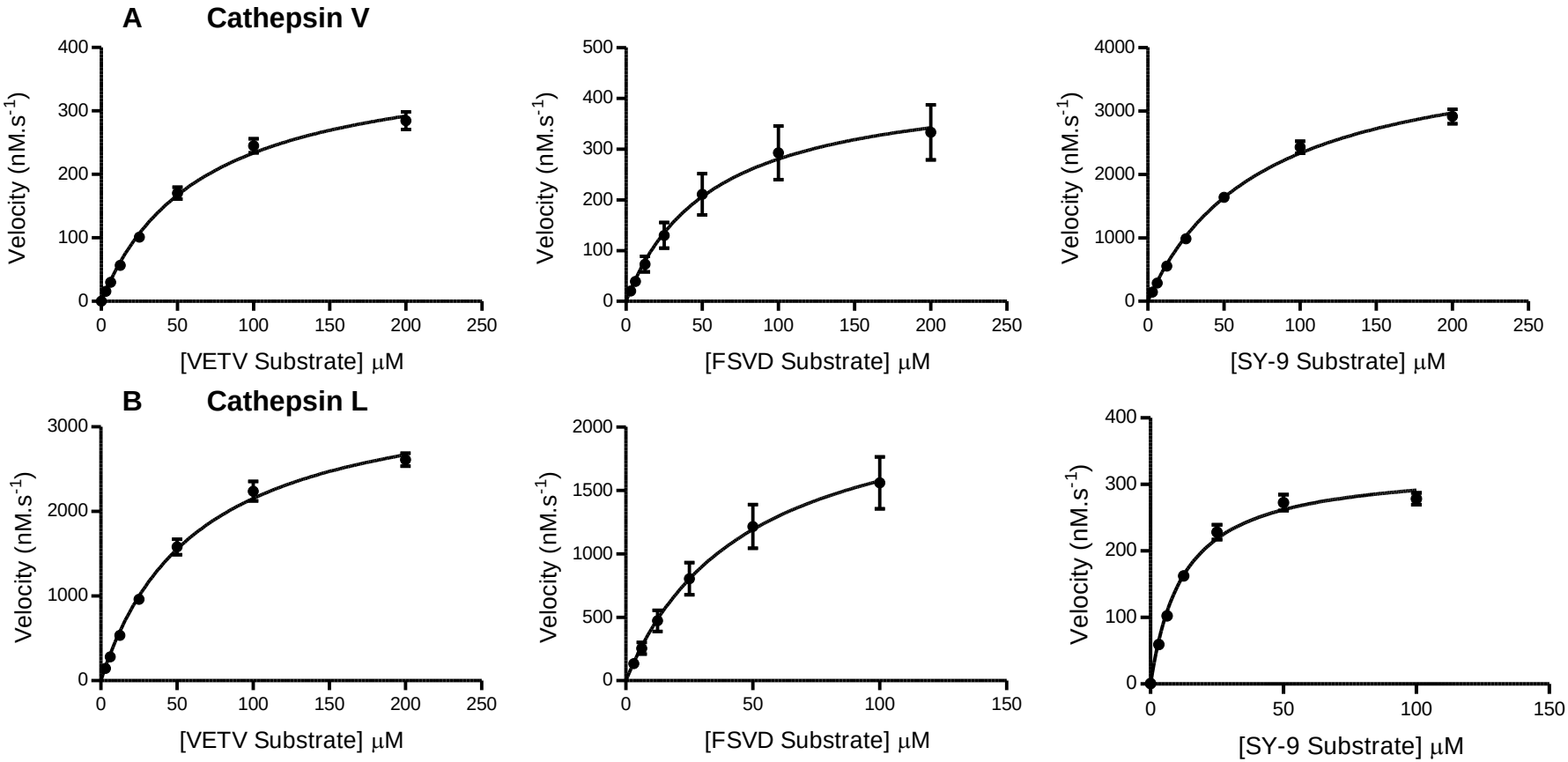
A
Cathepsin V
Velocity (nM.s-1)
[VETV Substrate] μM
[FSVD Substrate] μM
[SY-9 Substrate] μM
B
Cathepsin L
Velocity (nM.s-1)
[VETV Substrate] μM
[FSVD Substrate] μM
[SY-9 Substrate] μM

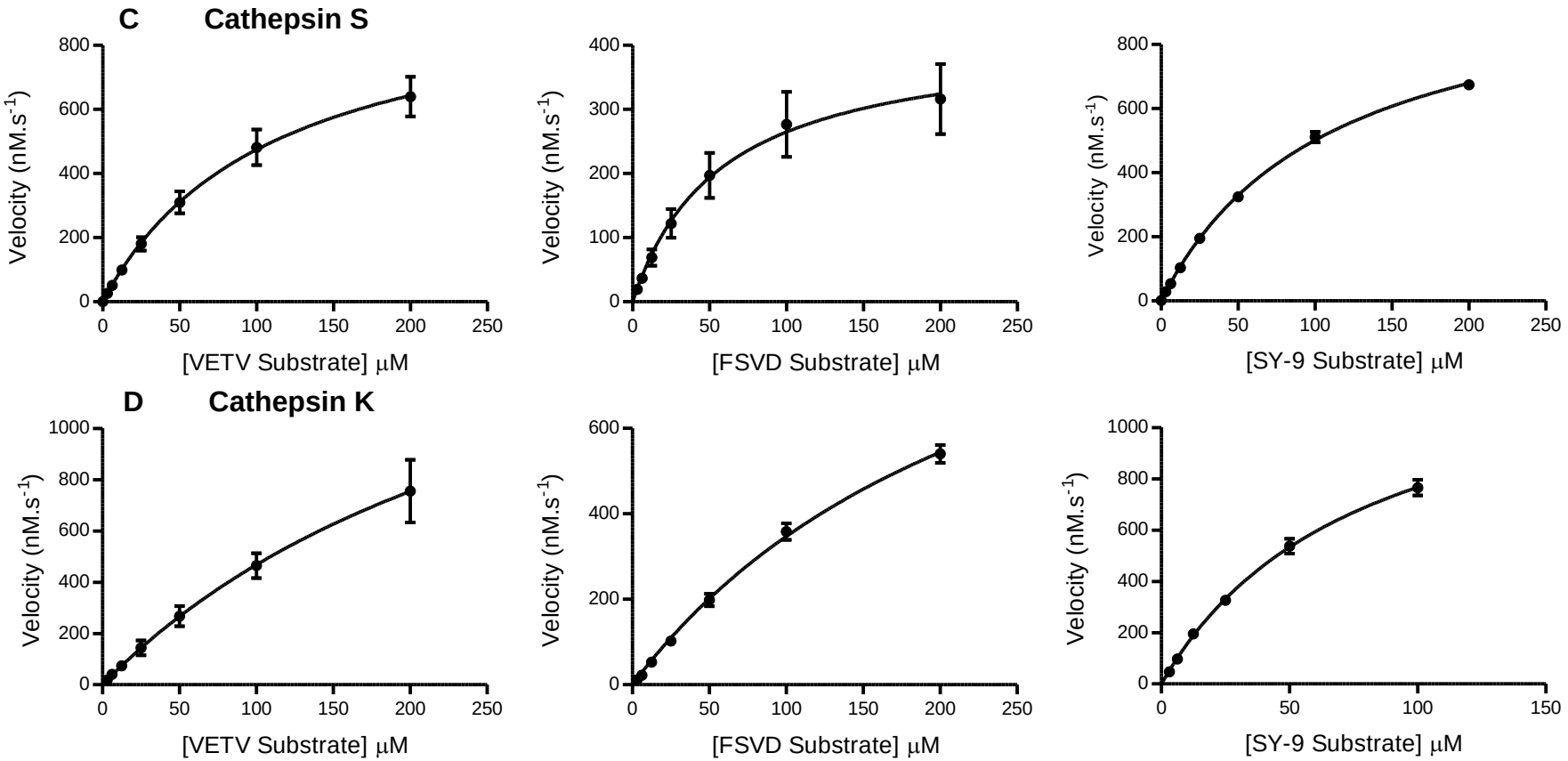

Figure 6.3: Cathepsin V, L, S and K Michaelis-Menten curves

Michaelis-Menten curves for cathepsins V, L, S and K. Increasing concentrations of VETV, FSVD or SKGRSLIG (SY-9) peptides were incubated with fixed concentrations of cathepsin enzyme. Cathepsin V was used at 5.32 nM for VETV, 10.65 nM for FSVD and 266.2 nM for SY-9 (A). Cathepsin L was used at 25 nM for all peptides (B). Cathepsin S was used at 10.77 nM for VETV and FSVD and at 21.54 nM for SY-9 (C). Cathepsin K was used at 10.69 nM for all peptides (D). The fluorescence was measured at λ_{ex} 320 nm and λ_{em} 420 nm and the linear reaction velocities were obtained from early gradients of the fluorescence progress curves. The hydrolysis of substrate was quantified ($nM.s^{-1}$) using a standard curve generated by total substrate hydrolysis. Graphpad Prism 5 software was used to plot velocity against substrate concentration and non-linear regression used to generate constants K_m and V_{max}. k_{cat} was calculated from Vmax and enzyme active concentration. See Chapter 2.15.4.1 for all experimental conditions. Curves shown are n=3 independent experiments, mean ± SD.

Table 6.1: Kinetic constants for cathepsin V, L, S and K, and matriptase digestion of PAR2 peptides VETV, FSVD and SKGRSLIG

Enzyme	Peptide	K_m (μM)	k_{cat} (min^{-1})	k_{cat}/K_m ($M^{-1}.s^{-1}$)
Cathepsin V	VETV	66.12 ± 4.60	72.95 ± 2.141	1.84×10^4
	FSVD	56.31 ± 10.61	41.14 ± 3.112	1.22×10^4
	SKGRSLIG	74.80 ± 6.274	15.32 ± 0.5641	3.41×10^3
Cathepsin L	VETV	63.14 ± 3.966	140.5 ± 3.673	3.71×10^4
	FSVD	47.46 ± 8.225	92.80 ± 7.611	3.26×10^4
	SKGRSLIG	12.53 ± 0.9363	13.11 ± 0.3062	1.74×10^4
Cathepsin S	VETV	110.6 ± 13.71	92.79 ± 5.728	1.40×10^4
	FSVD	57.77 ± 10.91	38.78 ± 2.965	1.12×10^4
	SKGRSLIG	109.6 ± 6.653	48.78 ± 6.653	7.4×10^3
Cathepsin K	VETV	316 ± 85.99	182.0 ± 33.96	9.60×10^3
	FSVD	262.8 ± 24.12	117.8 ± 7.046	7.47×10^3
	SKGRSLIG	78.15 ± 9.129	127.8 ± 8.312	2.73×10^4
Matripase	VETV	N/A	N/A	N/A
	FSVD	N/A	N/A	N/A
	SKGRSLIG	46.73 ± 6.711	1720 ± 113.9	6.13×10^5

N/A = No data as enzyme did not cleave substrate

Cathepsin V, S and L all had a primary cleavage site of glutamic acid-56 / threonine-57 according to the nanoLCMS data, and this was supported by the generated kinetic constants. These three enzymes had their highest turnover numbers (k_{cat}) and catalytic efficiencies (k_{cat}/K_m) for the VETV substrate which corresponds to this cleavage site. Cathepsin V, S and L had k_{cat}/K_m values of 1.84×10^4, 1.40×10^4 and 3.71×10^4 $M^{-1}.s^{-1}$, respectively. Therefore, these three enzymes can be ordered in terms of efficiency for the cleavage site as cathepsin L > cathepsin V > cathepsin S. Cathepsin S actually exhibited a higher k_{cat} value than cathepsin V (92.79 min^{-1} compared to 72.95 min^{-1}), but its lower affinity for the substrate resulted in a lower catalytic efficiency. Overall, these three proteases exhibited broadly similar kinetics for the VETV substrate.

Interestingly, all three enzymes had a higher affinity (lower K_m) for the FSVD substrate than the VETV substrate, suggesting they bind this substrate better, but do not cleave it as effectively. Both cathepsin V and cathepsin S had a much lower catalytic efficiency for the SY-9 substrate, an order of magnitude lower than for VETV and FSVD, though for cathepsin S, this was a result of a high K_m as its k_{cat} for SY-9 was in fact higher than for FSVD.

Cathepsin V and S had their secondary cleavage site based on nanoLCMS as phenylalanine-59 / serine-60, which is encompassed in the FSVD substrate. Once again, this is supported by the kinetic data which identify this substrate as their secondary substrate based on catalytic efficiency. Both these enzymes cleave the SY-9 substrate also, despite not being identified as doing so in Figure 6.1. When analysing the nanoLCMS data, a cleavage site at glycine-40 / lysine-41 can be observed, but it is not one of the top cleavages, thus was not included.

The secondary cleavage site for cathepsin L was glycine-40 / lysine-41, and this is further supported by kinetic data showing a higher catalytic efficiency for SY-9 than cathepsin V and S do. However, the cathepsin L catalytic efficiency for SY-9 is lower than for FSVD, which contains the cathepsin L preferred cleavage sites 3 and 4.

Unlike the other cathepsins, nanoLCMS identified the primary cathepsin K cleavage towards the N-terminus at glycine-40 / lysine-41, with secondary and tertiary cleavages located within the VETV substrate sequence. This observation is also fully supported by the kinetic data, which show that cathepsin K has the highest catalytic efficiency for the

SY-9 peptide compared to VETV and FSVD. Interestingly, cathepsin K has a similar k_{cat} value for the three substrates, with a highest value for VETV. The lower catalytic efficiency for VETV and FSVD is a result of very high K_m values, suggesting a low affinity for these substrates. It stands to reason in the cleavage of the PAR2 42mer substrate, the higher affinity for the glycine-40 / lysine-41 would result in preferential binding and thus cleavage at this location – as observed in the nanoLCMS experiments.

6.2.3 Cathepsin V and S do not stimulate PAR2 calcium mobilisation

Cathepsin S has previously been identified as a biased agonist for PAR2 able to stimulate cAMP production, but unable to stimulate calcium mobilisation, activate ERK1/2, recruit β-arrestins or endocytose PAR2[226]. As cathepsin V was identified to have a similar cleavage profile to cathepsin S, it was of interest to explore whether cathepsin V would behave in a similar manner in terms of cellular responses. Despite the majority of lysosomal cathepsin enzymes being active at lower pH levels, cathepsin S is known to retain activity at neutral pH[168]. Cathepsin V has been shown to lose stability rapidly at more neutral pH levels, being most stable at pH 5.5[176]. It was therefore important to test the stability of recombinant cathepsin V in a buffer system that is compatible with cell culture work.

A pH curve was performed testing pH 5.5-7.5 using 100 mM phosphate buffer, 150 mM NaCl, 0.01% Brij-35 (Figure 6.4). Under the tested conditions, cathepsin V was in fact most active at pH 7, but rapidly lost its activity at all tested pH values. After 15 and 30 minutes there was a higher residual activity at pH 6.5. Interestingly, under the tested conditions, at no time point was pH 5.5 the optimal pH.

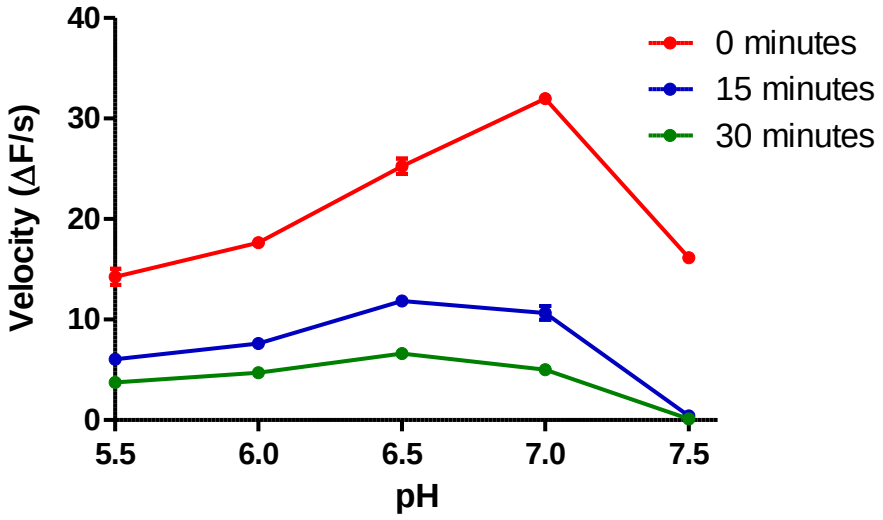

Figure 6.4: Cathepsin V pH curve
Cathepsin V was activated by diluting 1:10 in activation buffer (100 mM sodium acetate pH 5.5, 2.5 mM DTT, 2.5 mM EDTA) and incubating for 5 minutes at room temperature. Active cathepsin V was then diluted to 2x assay concentration in a pH range of 100 mM phosphate buffer, 150 mM NaCl, 0.01% Brij-35, and a Z-FR-AMC assay was performed as outlined in chapter 2. Velocities were calculated as change in fluorescence per second, taken from linear phase of the assay. n=3, error bars represent SD.

Even though cathepsin V rapidly lost its activity at neutral pH values, PAR2 responses are known to be rapid (see calcium mobilisation assays following matriptase stimulation in chapter 5), therefore cathepsin V assays could be performed as there is likely enough activity before the enzyme loses its stability.

The effect of cathepsin V on calcium mobilisation was explored, and compared to the effect of cathepsin S. Assays were performed with a stock of enzyme in assay buffer being prepared and loaded into the fluorimeter to inject onto the cells for the assay. The assay took 40 minutes to complete, therefore loss of activity was a concern. pH 6.5 was utilised for cathepsin V as there appeared to be the longest stability at this pH. Cathepsin S was utilised at pH 7. Neither cathepsin V nor cathepsin S could stimulate calcium mobilisation (Figure 6.5).

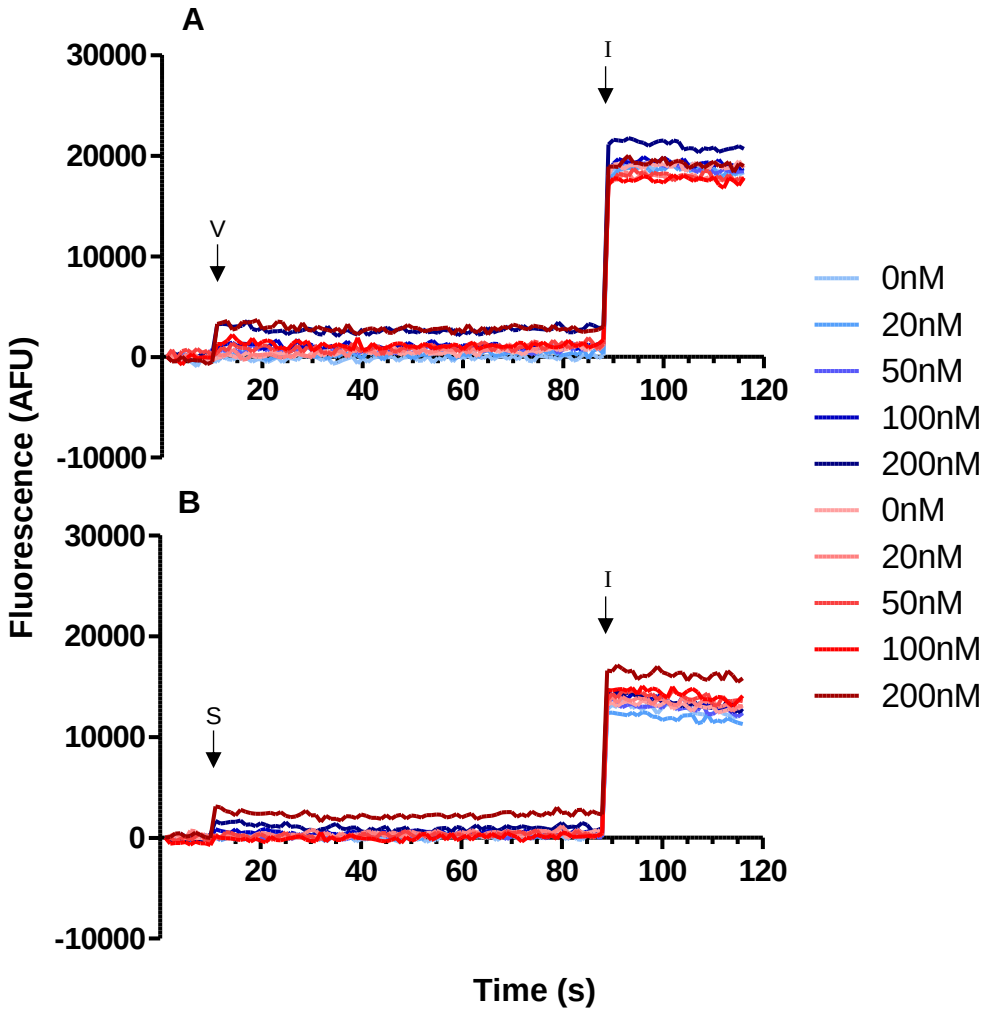

Figure 6.5: Calcium mobilisation following Cathepsin V and S titration
SW1353 cells were transduced with pSIEW_PAR2 (red lines) and pSIEW_Empty (blue lines) expressing lentivirus before culturing for 48 hours then serum starving overnight. Cells were loaded with Rhod-4-AM fluorescent calcium indicator and placed in a fluorimeter where the assays were performed. Titrations of activated cathepsin V (A) or cathepsin S (B) were performed using 0-200 nM enzyme. Fluorescence was observed following cathepsin injection stimulation (V or S, respectively), and 5 µM ionomycin stimulation (I). Data shown are mean of n=2 independent experiments.

After showing that recombinant cathepsin V and S were unable to stimulate calcium mobilisation, the experiment was repeated utilising cathepsin-revealed activator peptides. The revealed ligand for the primary cathepsin cleavage site of PAR2 between glutamic acid-56 and threonine-57 would be TVFSVDEFSA, which is the peptide utilised by Zhao *et al.*, (2014)[226] to mimic the effects of cathepsin S in their paper. As the canonical activator is shorter at 6 amino acids, a 6 amino acid version of the cathepsin activator peptide was also synthesised, TVFSVD. As expected, neither of these peptides had the ability to stimulate calcium mobilisation (Figure 6.6).

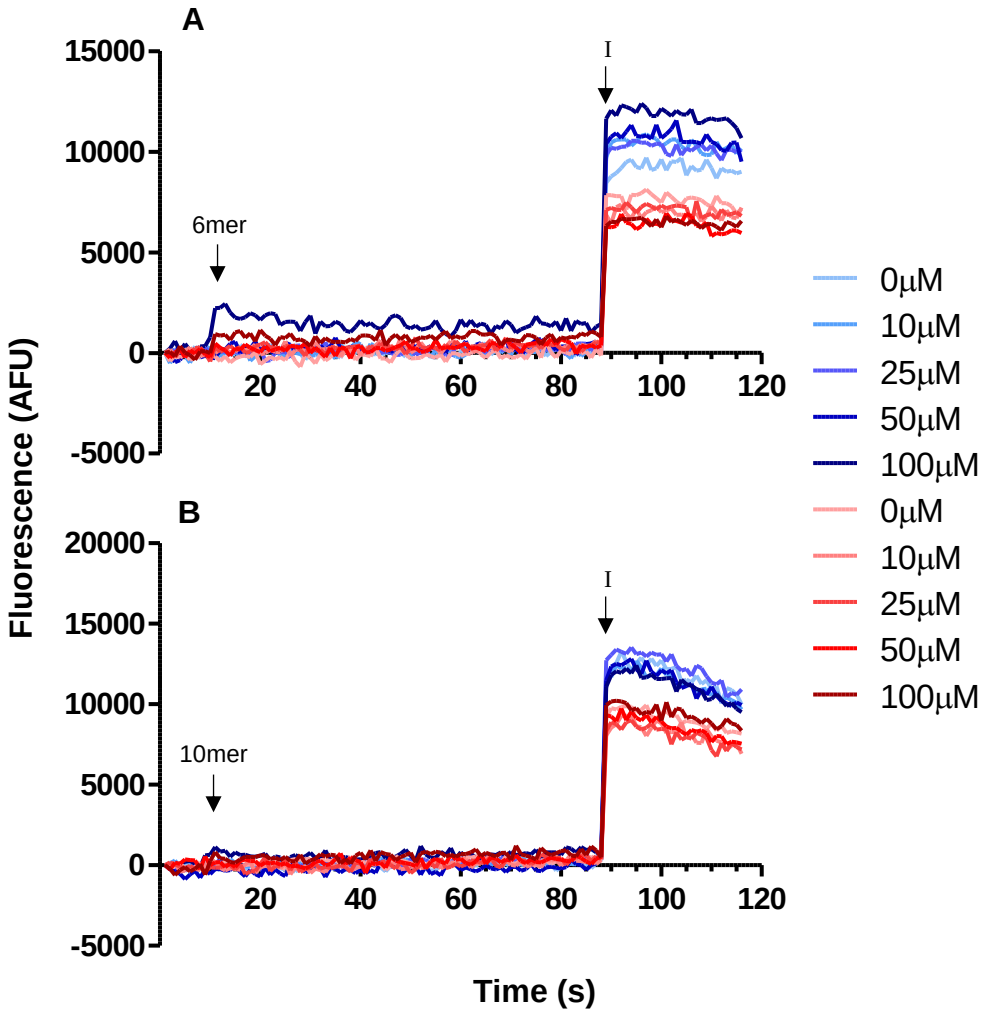

Figure 6.6: Calcium mobilisation following TVFSVD and TVFSVDEFSA titration
SW1353 cells were transduced with pSIEW_PAR2 (red lines) and pSIEW_Empty (blue lines) expressing lentivirus before culturing for 48 hours then serum starving overnight. Cells were loaded with Rhod-4-AM fluorescent calcium indicator and placed in a fluorimeter where the assays were performed. Titrations of cathepsin AP TVFSVD (A) or TVFSVDEFSA (B) dissolved in HHBS were performed using 0-100 μM peptide. Fluorescence was observed following peptide injection stimulation (6mer or 10mer, respectively), and 5μM ionomycin stimulation (I). Data shown are mean of n=2 independent experiments.

6.2.4 Cathepsin V is able to disarm matriptase-induced canonical PAR2 activation

As cathepsin V was unable to stimulate calcium mobilisation, but is able to cleave PAR2 downstream of the canonical activation site, it was of interest to explore whether cathepsin V could disarm against matriptase-induced canonical PAR2 activation.

Firstly, the disarming of PAR2 by the serine protease cathepsin G was explored to confirm that this system could be utilised to measure PAR2 disarming. Cathepsin G has previously been described as a PAR2 disarmer by Ramachandran *et al.*, (2011)[225], thus their methodology was replicated in the SW1353 cell overexpression system utilised in this

study. Cathepsin G was clearly able to disarm matriptase-induced canonical PAR2 activation of calcium mobilisation (Figure 6.7), thus the disarming by cathepsin V could subsequently be explored.

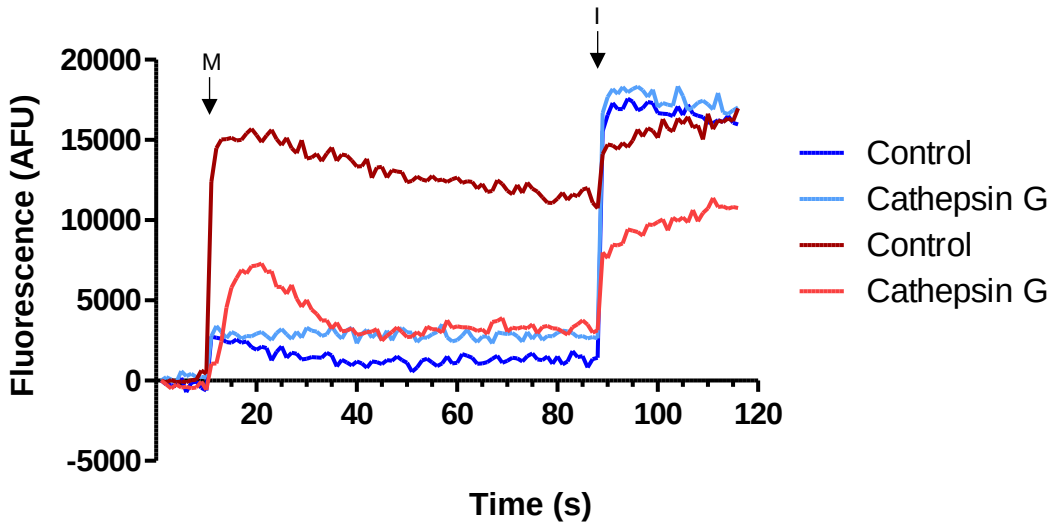

Figure 6.7: Cathepsin G disarming of canonical PAR2 activation
SW1353 cells were transduced with pSIEW_PAR2 (red lines) and pSIEW_Empty (blue lines) expressing lentivirus before culturing for 48 hours then serum starving overnight. Cells were loaded with Rhod-4-AM fluorescent calcium indicator and pre-treated. Cathepsin G was diluted to 0.3 units/mL in HHBS (2 mM Ca2+) and added to the cells for 15 minutes before removing, washing in HHBS (2 mM Ca2+) and undertaking the calcium mobilisation assay. Data shown is from n=1 experiment.

PAR2-expressing SW1353 cells were pre-stimulated for 15 minutes with various concentrations of cathepsin V, and subsequently challenged with matriptase. Cathepsin V could attenuate matriptase-induced calcium mobilisation in a dose-dependent manner, with the highest effect following 200 nM cathepsin V pre-treatment (Figure 6.8 A). The experiment was repeated, but instead of injecting ionomycin as a positive control, the PAR2 agonist peptide SLIGKV was injected. Cathepsin V-mediated disarming of PAR2 canonical activation would occur as a result of removal of the tethered ligand sequence of PAR2. The SLIGKV peptide activates PAR2 independently of the PAR2 extracellular domain by binding directly to the active site. Therefore, as expected, the SLIGKV peptide could restore the calcium response following cathepsin V disarming. This was confirmed as the control transduction cells did not respond to SLIGKV (Figure 6.8 B).

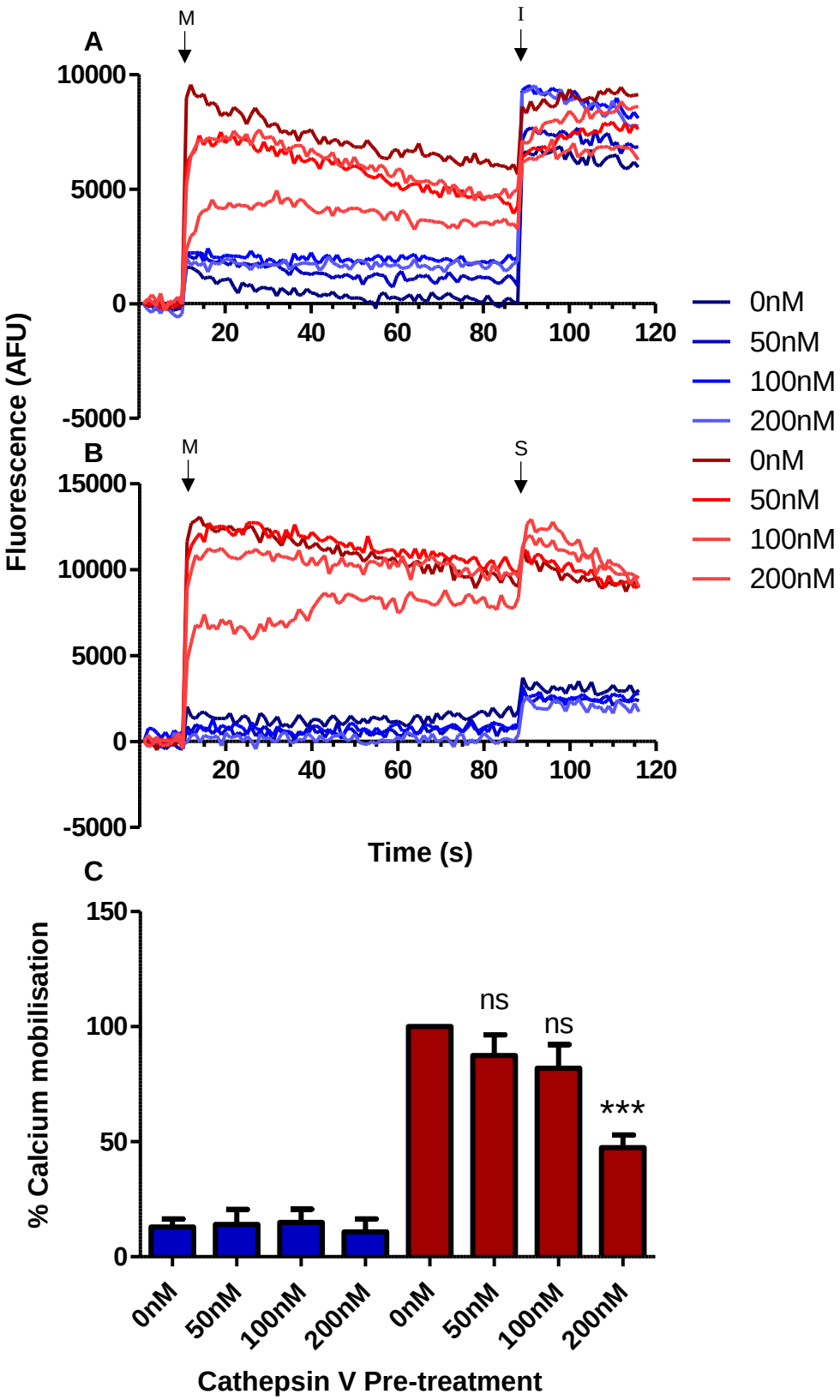

Figure 6.8: Pre-treatment PAR2 expressing cells with cathepsin V disarms canonical PAR2 activation
SW1353 cells were transduced with pSIEW_PAR2 (red lines) and pSIEW_Empty (blue lines) expressing lentivirus before culturing for 48 hours then serum starving overnight. Cells were loaded with Rhod-4-AM fluorescent calcium indicator and pre-treated (in order to disarm) with 0-200nM activated cathepsin V in 100 mM phosphate buffer pH 6, 150 mM NaCl for 15 minutes before placing in a fluorimeter and stimulating with 10nM matriptase (A and B), and subsequently stimulating with either 5 µM ionomycin (A) or 10 µM SLIGKV (B). Both n=2 independent experiments. To quantify disarming, maximal calcium response (average calcium response in the 10 seconds immediately following stimulation) was obtained from the experiments in A and B (therefore n=4 independent experiments) (C); where *** $p < 0.001$ by unpaired T-test between 200 nM pre-treatment group and no pre-treatment group in PAR2 expressing cells.

Calcium mobilisation was quantified, and statistical analysis performed, which confirmed the significant disarming by 200 nM cathepsin V (Figure 6.8 C).

Cathepsin V disarming of calcium mobilisation is an interesting observation, however to explore whether this could hold relevance for arthritic diseases, it was of interest to examine whether this effect is transmitted downstream to the expression of PAR2-regulated genes. PAR2-expressing SW1353 cells were disarmed as previously, but instead of undertaking calcium mobilisation assays, they were challenged with matriptase for 30 minutes, before incubating for 24 hours and gene expression examined for *MMP1* and *MMP13*.

Only the highest tested concentration of cathepsin V pre-incubation, 200 nM, showed any evidence of disarming *MMP* induction, where *MMP1* expression was significantly attenuated (Figure 6.9 A). In these assays, it appears that 10 nM matriptase was unable to stimulate *MMP13* upregulation. As with the calcium mobilisation experiments, the cathepsin V disarming of PAR2 followed by stimulation with the SLIGKV peptide did not result in any attenuation of *MMP1* expression (Figure 6.9 B).

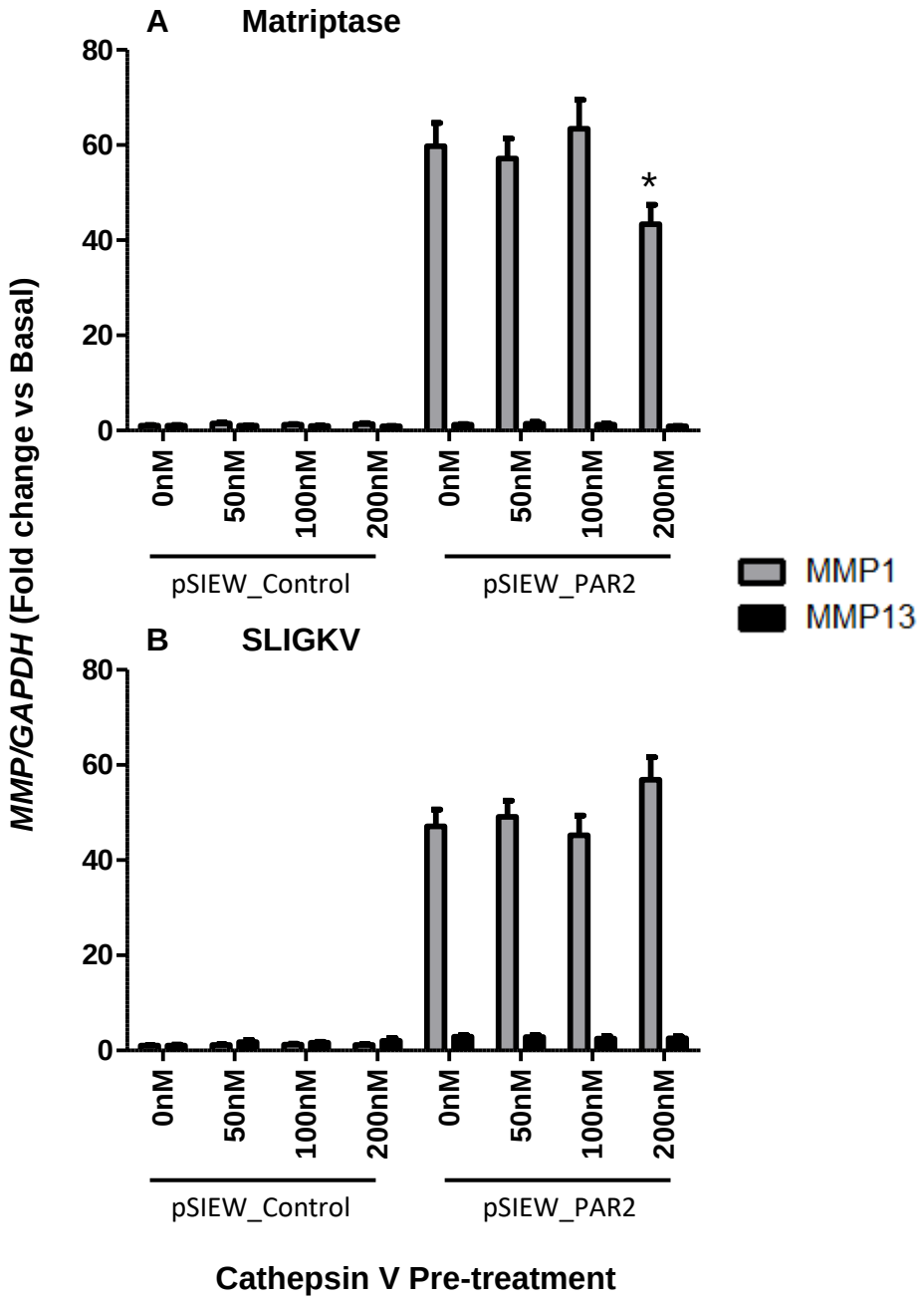

Figure 6.9: Cathepsin V can disarm against matriptase-induced *MMP* expression
SW1353 cells were transduced with pSIEW_PAR2 and pSIEW control-expressing lentivirus before culturing for 48 hours then serum starving overnight. Cells were then pre-treated with 0-200 nM activated cathepsin V in 100 mM phosphate buffer pH 6, 150 mM NaCl for 15 minutes before PBS-washing and stimulated with 10 nM matriptase (A) or SLIGKV (B) for 30 minutes, before PBS-washing and culturing in SFM for an additional 24 hours. Cells were then lysed and mRNA extracted and reverse transcribed to cDNA. *MMP1* and *MMP13* expression was measured by qPCR and normalised to *GAPDH*. where * $p < 0.05$ by unpaired T-test between 200 nM pre-treatment group and no pre-treatment group in PAR2 expressing cells. Data pooled from n=3 independent experiments for panel A, n=1 for panel B.

6.2.5 Putative cathepsin K activator peptide KVDGTS does not mobilise calcium

Cathepsin K has been shown to have optimal activity at pH 6, but is also nearly fully active at pH 7[180]. Cathepsin K is however much more stable at lower pH values, retaining 49% of its activity after 1 hour at pH 6.5, but none of its activity at pH 7.5. Cathepsin K is most stable at pH 5.5[180].

Cathepsin K activity was explored at a range of pH values. Cathepsin K appeared to have similar activity levels at pH 5.5 – pH 7 initially, but activity at higher pH levels decline by the 30-minute mark, with complete loss of activity at pH 7 but no loss of activity at pH 5.5 (Figure 6.10).

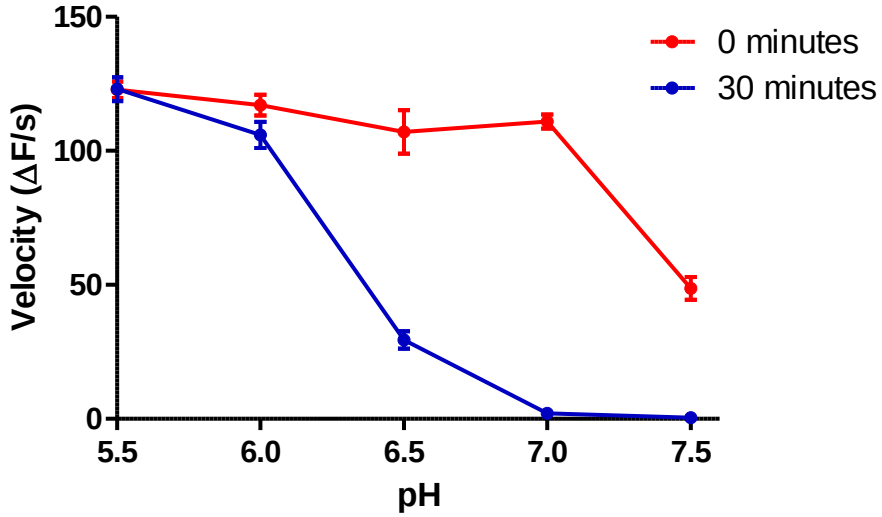

Figure 6.10: Cathepsin K pH activity curve
Cathepsin K was activated by diluting 1:10 in activation buffer (100 mM sodium acetate pH 5.5, 2.5 mM DTT, 2.5 mM EDTA) and incubating for 5 minutes at room temperature. Active cathepsin K was then diluted to 2x assay concentration in a pH range of 100 mM phosphate buffer, 150 mM NaCl, 0.01% Brij-35, and a Z-FR-AMC assay was undertaken as outlined in chapter 2. Velocities were calculated as change in fluorescence per second, taken from linear phase at beginning of assay. n=3, error bars represent SD.

The pH of cartilage has been shown to be reduced in OA[183], and the activity of cathepsin K has been observed in the disease[184], therefore cleavage of PAR2 by cathepsin K could hold physiological relevance and warrants further investigation. Unfortunately, limitations in the availability of sufficient quantities of recombinant cathepsin K meant that the required experiments could not be performed within the time frame of this project.

The primary cleavage site for cathepsin K was located between glycine-40 and lysine-41, thus should this be an activating cleavage, then the putative revealed ligand would be KVDGTS. This putative activator peptide was therefore synthesised and utilised in lieu of active cathepsin K. Testing the addition of KVDGTS on PAR2-expressing cells had no effect on calcium mobilisation at all tested concentrations (Figure 6.11).

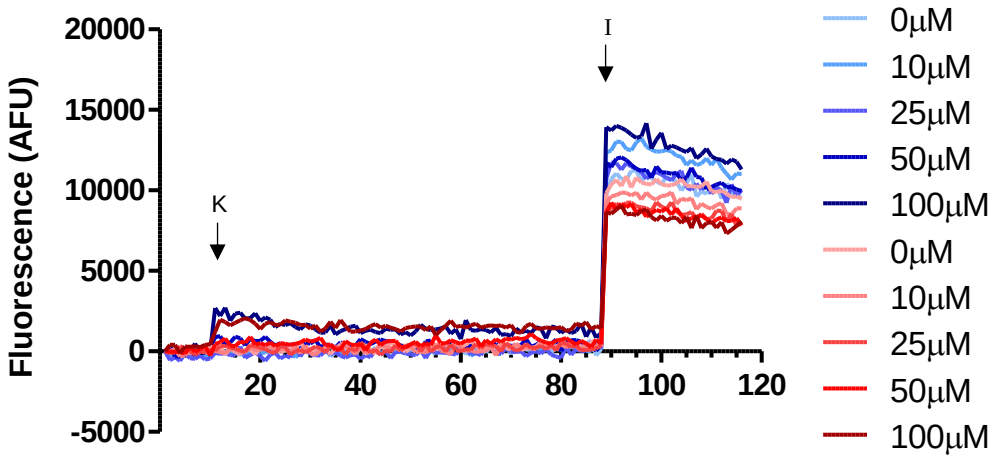

Figure 6.11: Calcium mobilisation following KVDGTS titration
SW1353 cells were transduced with pSIEW_PAR2 (red lines) and pSIEW_Empty (blue lines) expressing lentivirus before culturing for 48 hours then serum starving overnight. Cells were loaded with Rhod-4-AM fluorescent calcium indicator and placed in a fluorimeter where the assays were performed. Titrations of putative cathepsin K AP were performed using 0-100 µM peptide. Fluorescence was observed following peptide injection stimulation (K), and 5 µM ionomycin stimulation (I). Data shown are mean of n=2 independent experiments.

6.3 Discussion

All tested cathepsins were found to be able to cleave PAR2 potently, and at multiple sites. This is unsurprising due to the intracellular roles of this family of proteases, where they are best described as lysosomal proteases responsible for breaking down a wide range of proteins and peptides as part of normal protein turnover. Indeed, a search of these proteases in the MEROPS database shows little specificity in terms of amino acids able to interact within S4-S4' of the cathepsin active site clefts[310]. One might therefore ask the question of whether cathepsin-mediated cleavage of PAR2 is physiologically relevant or merely a product of incubating a protease with low specificity with a polypeptide and therefore cleaving the only heterologous protein substrate in the reaction. Indeed, cathepsins are likely to be involved in the recycling of PAR2 following canonical activation and subsequent internalisation[229]. This discussion will examine the potential

physiological relevance of cathepsin-mediated PAR2 cleavage by considering previously identified extracellular roles for the cathepsins.

To date, the only cysteine protease identified as being able to cleave PAR2 is cathepsin S[226,300]. Zhao *et al*., (2014)[1] identified a cathepsin S cleavage site between glutamic acid-56 and threonine-57, which reveals the tethered ligand TVFSVDEFSA. They showed cathepsin S to be a biased agonist, able to stimulate cAMP production, but unable to stimulate calcium mobilisation, activate ERK1/2, recruit β-arrestins or endocytose PAR2 in HEK293 cells overexpressing PAR2. Another study by Elmariah *et al*., (2014)[2] found cathepsin S to cleave at two locations further towards the N-terminus than the Zhao *et al*. (2014) study: between leucine-38 and isoleucine-39 and between glycine-40 and lysine-41. The Elmariah *et al*., (2014)[2] study described conflicting signalling outcomes following cathepsin S stimulation of PAR2 in that cathepsin S, as well as both putative activator peptides IGKVDG and KVDGTS, were all able to stimulate calcium mobilisation in HeLa cells overexpressing PAR2.

The reason for the identification of different cleavage sites in the two studies is likely to result from the fact that the Elmariah *et al*., (2014)[2] study utilised a shorter synthetic peptide to examine cleavage by cathepsin S which terminated at threonine-54, which would be too short to observe the Zhao *et al*., (2014)[1]-identified cleavage at glutamic acid-56. Indeed, data presented within this chapter using a peptide longer than the peptide used in both these studies, encompassing the whole region from arginine-31 to lysine-72, confirms the presence of the cleavage identified by Zhao *et al*., (2014)[1]. No cleavage was observed at the two cleavage sites identified by Elmariah *et al*., (2014)[2], however cathepsin S could cleave the PAR2 SY-9 peptide substrate, which encompasses the region serine-33 to glycine-40. Taken together, it is likely that cathepsin S can indeed cleave all the sites identified in both studies, however when presented with the full-length PAR2 sequence, there is a much stronger preference for the glutamic acid-56 / threonine-57 site, but it will cleave between leucine-38 and isoleucine-39 or between glycine-40 and lysine-41 in the absence of the preferred site as observed by Elmariah *et al*., (2014)[2], and within the SY-9 kinetics in the present study. Taken together, the data from these two previous studies and the present study, it is likely that the glutamic acid-56 / threonine-57 is the predominant cathepsin S cleavage of PAR2 and the most likely to hold physiological relevance.

As well as confirming the ability for cathepsin S to cleave at glutamic acid-56 / threonine-57, cathepsins V, L, K and B were all shown to cleave at this location, with this being the preferred site in PAR2 for cathepsins V and L, and a secondary site for cathepsin K. Zhao *et al*., (2014)[1] did not explore enzyme kinetics for this cleavage, however data presented in this chapter show that cathepsin V and L are more potent than cathepsin S at cleaving this site on PAR2. When considering the kinetic parameters for the three substrates, specificity for the glutamic acid-56 / threonine-57 can be ordered as cathepsin V > cathepsin S > cathepsin L. Cathepsin L has cleavage sites at all three sequences identified by nanoLCMS and had a similar potency for each site in terms of catalytic efficiency.

In agreement with the Zhao *et al*., (2014)[1] study, cathepsin S was unable to stimulate calcium mobilisation in PAR2 overexpressing SW1353 cells. Cathepsin V was also unable to do this, which is in line with the similar cleavage profiles observed by both enzymes on PAR2. Furthermore, the same activator peptide used in the Zhao *et al*., (2014)[1] study, TVSFVDEFSA, was unable to stimulate calcium mobilisation which is in agreement with that study. Futher work needs to be performed to explore whether cathepsin V, L and S are able to induce the same signalling outcomes in chondrocytes as were observed with cathepsin S in HEK293 cells[226].

The lack of calcium mobilisation by cathepsin S stimulation of PAR2 is in disagreement with Elmariah *et al*., (2014)[2] who observed calcium mobilisation following cathepsin S stimulation. It is unclear why calcium mobilisation was observed in their study, and not in the present study or the Zhao *et al*., (2014)[1] study, but all three studies utilised different cell lines, thus could be a result of different signalling mediators available following PAR2 cleavage. Futhermore, a contaminant can not be excluded on the recombinant cathepsin S stock utilised by Elmariah *et al*., (2014)[2] as no controls utilising a cathepsin S inhibitor were performed confirming the observed calcium mobilisation is indeed a result of cathepsin S activity.

Interestingly, the present study did identify a cathepsin cleavage site at glycine-40 / lysine-41, which was the primary cleavage site for cathepsin K, and the secondary site for cathepsin L. To test the role of this cleavage, the putative activator peptide, KVDGTS, was synthesised. This peptide is the same as the peptide utilised by Elmariah *et al*., (2014)[2] who incorrectly used it as the cathepsin S activator peptide. In that study, this peptide was able to stimulate calcium mobilisation in PAR2-overexpressing HeLa cells.

It was therefore hypothesised that cathepsin K and KVDGTS would induce calcium moblisation. Limitations in recombinant cathepsin K meant that this hypothesis could not be fully tested, however the addition of KVDGTS on PAR2-overexpressing SW1353 cells had no effect on calcium mobilisation, which is in disagreement with Elmariah *et al*., (2014)[2]. The reasons for this are unclear, but it could possibly be as a result of different cell types, and different availability of required signalling mediators. SW1353 cells however clearly have the capacity for inducing calcium mobilisation in a PAR2-dependent manner as shown with matriptase activation in this study. Despite the possibility for non-canonical calcium mobilisation explaining the observed differences, the Elmariah *et al*., (2014)[2] study suggests canonical calcium mobilisation occuring as measured by inositol monophosphate accumulation, a metabolite of inositol triphosphate – the agonist for the calcium channel responsible for canonical GPCR activation[335].

Cathepsin V was found to be able to disarm canonical PAR2 activation in terms of calcium mobilisation and *MMP1* induction. In this study, a pH curve was performed using a buffer system amenable to cell culture work, and interestingly, cathepsin V was found to be most active at pH 7 initially, and most active at pH 6.5 at the 15 and 30 minute marks. Cathepsin V was unstable at all pH values however, quickly reducing in activity. This observation conflicts with previous work which shows cathepsin V to be most active at pH 5.7, and completely stable for at least 2 hours at pH 5.5 but rapidly losing activity at pH 6.5 or 7[176]. It is extremely likely that these conflicting observations reflect the different buffer systems utilised within the two studies, with 100 mM phosphate buffer, 150 mM NaCl, 0.01% Brij-35 utilised in the present study clearly not an optimal buffer system for this enzyme. A trade off was however required to allow for cathepsin V activity in cell culture work, and there was clearly a disarming effect observed in the cell culture work, suggesting that activity did indeed occur in the cell culture model.

By considering the kinetic data presented in this chapter as well as the previous literature regarding cathepsin S cleavage of PAR2, it is reasonable to hypothesise that cathepsins V, S and L could hold relevance in PAR2 and OA biology.

Cathepsin V is one of the more recent and less well understood cathepsins, and currently there is not a lot of evidence for its expression in cartilage, involvement in OA or extracellular functions. Macrophage-expressed Cathepsin V has been shown to have the ability to potently digest the ECM-component elastin[336], although that study failed to

detect secreted cathepsin V, and suggested intracellular digestion of elastin. Other work has however shown cathepsin V to be secreted from cells[337]. Work presented in this chapter showed that cathepsin V was able to disarm against matriptase-induced canonical PAR2 signalling, including a reduction of *MMP1* expression which could hint at a protective effect for cathepsin V in OA. More work however needs to be undertaken on the role of cathepsin V in cartilage biology.

On the other hand, cathepsin L is a better candidate for having a role in cartilage biology, and in arthritis with respect to PAR2 cleavage. Cathepsin L has been detected in synovial fluid of patients with RA[338] and secretion has been observed in chondrocytes extracted from OA cartilage[191]. The enzyme is expressed in the synovium of both RA and OA patients[339]. Furthermore, cathepsin L has been shown to be able to cleave aggrecan[192]. Future work would need to be undertaken with cathepsin L in cell culture work to ascertain putative roles in chondrocyte and PAR2 biology. However, one would hypothesise that cathepsin V and L would exert similar effects *in vivo*.

As previously discussed, cathepsin S has been identified as a biased agonist for PAR2. A potential role for cathepsin S cleavage of PAR2 in OA is possible as cathepsin S activity has been previously detected in OA cartilage explant culture[191], therefore there is evidence for the presence of cathepsin S in a tissue and disease where PAR2 is expressed. Furthermore, the expression and secretion of cathepsin S from chondrocytes following TNFα or IL-1β stimulation has been described[190].

As described in chapter 1, a role for cathepsin K in OA is well established. Cathepsin K degradation of type II collagen has been detected in human OA cartilage[184], therefore the presence of cathepsin K in a tissue where PAR2 is expressed suggests potential physiological relevance for cathepsin K cleavage of PAR2. Further work will be required to ascertain the role for cathepsin K in PAR2 biology.

A role for cathepsin B in OA is also well established as outlined in chapter 1. In terms of cathepsin B cleavage of PAR2, there were too many cleavages observed to deduce the most physiologically relevent cleavages. Further work would be required untertaking more restricted digests to ascertain which cleavages occur first – it remains possible that there could be a physiological role for cathepsin B in PAR2 biology.

Taken together, there is potential for the cathepsins to have a role in PAR2 activation or disarming in OA. In particular, cathepsins S, L and K are strong candidates for this based on previously described roles of these enzymes in OA and general extracellular functions.

6.4 Summary

- Cathepsins V, K, L, B and S were all able to cleave PAR2 at multiple sites, with a primary cleavage site for cathepsins V, S and L between glutamic acid-56 and threonine-57, and a primary cleavage site for cathepsin K between glycine-40 and lysine-41. Cathepsin B cleaved at multiple sites along the sequence and cleavages were difficult to rank.

- The kinetic parameters for cathepsins V, K, L and S generally correlated with the ranking of cleavages as observed by nanoLCMS.

- Cathepsin V, as well as its putative activator peptide, were unable to stimulate calcium mobilisation.

- Pre-incubation of SW1353 cells with cathepsin V was able to disarm against matriptase-induced canonical activation of PAR2.

- The putative cathepsin K activator peptide was unable to stimulate calcium mobilisation.

Chapter 7 – Canonical PAR2 Activation: Gene Expression Microarray

7.1 Introduction

Data presented in chapters 4, 5 and 6 have identified and begun to describe the regulation of PAR2 activity by extracellular proteolysis mediated by enzymes involved in OA. Data presented in chapter 6 have also demonstrated the ability for cathepsin V to "disarm" canonical PAR2 activation by matriptase. Taken together, it is likely that a complex extracellular environment regulates chondrocyte behaviour in response to PAR2 in both the context of disease and normal physiology. It is not possible to understand the full relevance of extracellular events in PAR2 biology when intracellular events in terms of PAR2 signalling are incompletely understood. A gene expression microarray to assess global gene expression changes following canonical PAR2 activation was therefore performed.

There has been little work previously performed in chondrocytes with respect to PAR2 biology, and data presented and discussed in chapter 6 with respect to previously published data has suggested possible signalling differences between commonly used cell lines in response to PAR2 activation. Only a single study has previously explored global gene expression changes following PAR2 canonical activation, and this work was undertaken in HEK293 cells[340], a cell line with conflicting PAR2 responses as outlined in chapter 6. Furthermore, that study utilised both trypsin and the synthetic PAR2 agonist 2-furoyl-LIGRLO-NH_2 to stimulate canonical PAR2 activation. There is evidence that such synthetic PAR2 agonists can act on cells in PAR2-independent mechanisms[341], and that trypsin cleavage of other cell surface proteins may modify cell behaviour[342]. It was therefore of interest to explore global gene expression changes following matriptase and SLIGKV stimulation of PAR2 in chondrocytic cells.

Understanding the signalling outcomes of PAR2 activation in chondrocytes, stimulated by a physiologically relevant activator in matriptase, is of central importance to this study. Furthermore, as PAR2 canonical activation is generally considered to be pro-inflammatory in nature, it is of interest to compare some of the downstream targets of PAR2 activation with the downstream targets identified in chapter 3 of this study, where

mechanical loading of cells was found to induce the expression of various pro-inflammatory regulators such as *ATF3*, *CSRNP1* and *EGR2*.

7.1.1 Chapter Aims

- To optimise time points to explore SW1353 cell gene expression by microarray after canonical PAR2 activation.
- To perform a gene expression microarray following canonical PAR2 activation by either SLIGKV or matriptase.
- To carry out pathway analysis to explore the outcomes of canonical PAR2 activation.

7.2 Results

7.2.1 Optimisation of time points for microarray

As described in chapter 3.2.4, previous work undertaken in our group explored the expression of collagenases following IL-1+OSM stimulation in HAC and identified regulators such as *ATF3*, *CSRNP1* and *EGR2*. Studies undertaken using bovine nasal chondrocytes identified some of the same regulators that were mechanosensitive. In order to explore global gene expression changes in SW1353 cells, it was of importance to pick the most relevant time points for examination, and it was decided that the time required for maximal expression of genes such as *ATF3* would be of greatest interest.

Firstly, the kinetics of *ATF3* and *MMP* expression were explored following IL-1+OSM stimulation is SW1353 cells. *ATF3* expression peaked at 1.5 hours post-stimulation, reaching statistically significant upregulation at 0.5 hours and remained significantly up-regulated for the remainder of the time-course, until 24 hours (Figure 7.1 A). As expected, *MMP1* and *MMP13* expression were induced later in the time-course, reaching maximum level at the 24-hour mark (Figure 7.1 B).

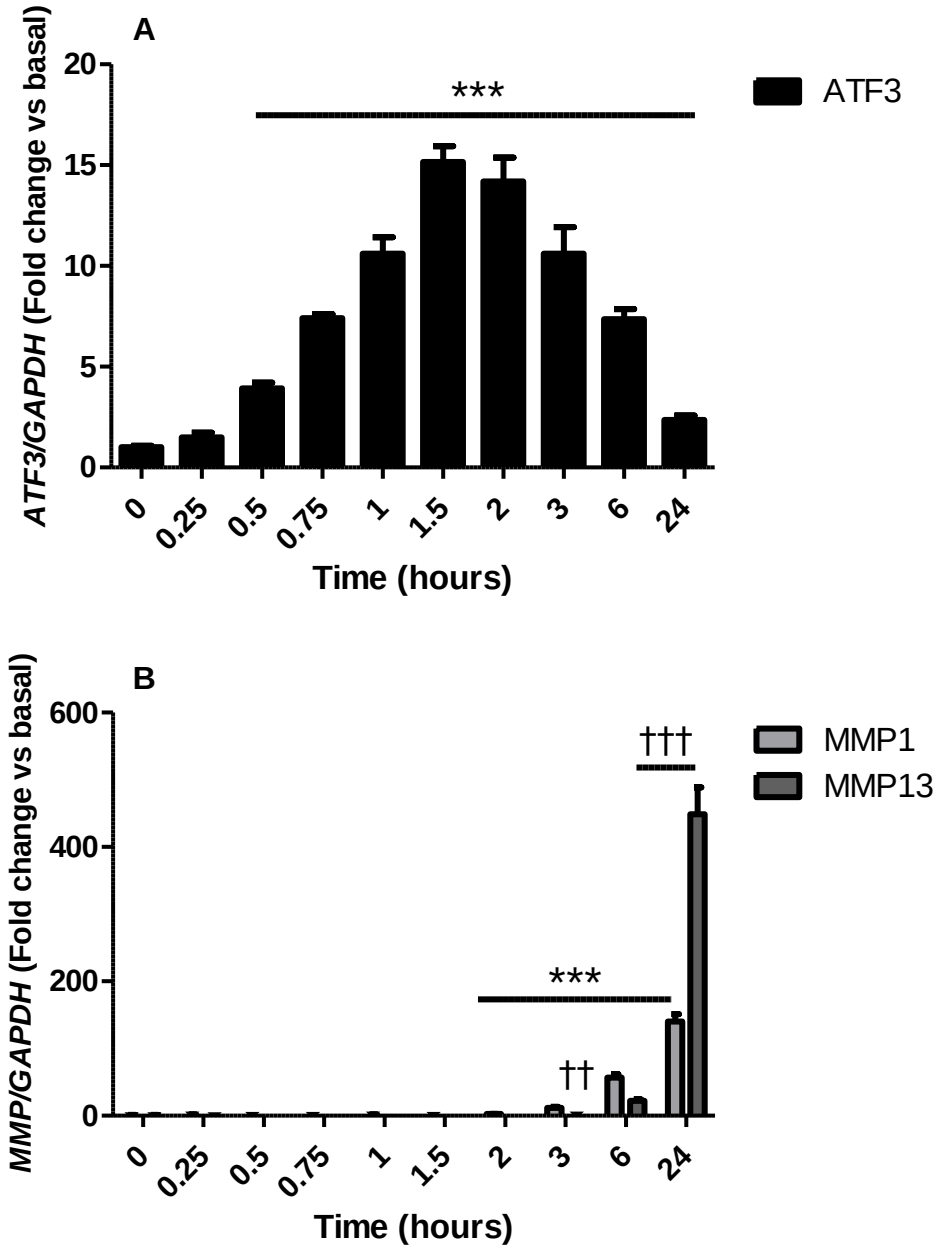

Figure 7.1: *ATF3, MMP1* and *MMP13* expression following IL1+OSM stimulation
SW1353 cells were stimulated with IL-1 at 0.5 ng/mL and OSM at 30 ng/mL for varying lengths of time before lysing the cells, extracting the mRNA, reverse transcription and qPCR examining *ATF3* (A) or *MMP1* and *MMP13* (B) expression. Mean ± S.E.M; where *** $p < 0.001$ by unpaired T-test between *ATF3* or *MMP1* basal expression (T=0) and time point; †† $p < 0.01$, ††† $p < 0.001$ by unpaired T-test between *MMP13* basal expression (T=0) and time point. Data pooled from n=2 independent experiments.

After exploring the kinetics of *ATF3* expression in SW1353 cells following IL-1+OSM stimulation, it was of interest to see whether PAR2 activation would also induce *ATF3* expression. Despite it being known that *MMP* expression is induced in chondrocytes following PAR2 canonical activation, the signalling pathways involved are not well established, and *ATF3* has not previously been explored as a PAR2 target.

ATF3 expression was indeed robustly induced by canonical PAR2 activation by both matriptase and SLIGKV, with maximal induction 1.5-hours post-stimulation (Figure 7.2).

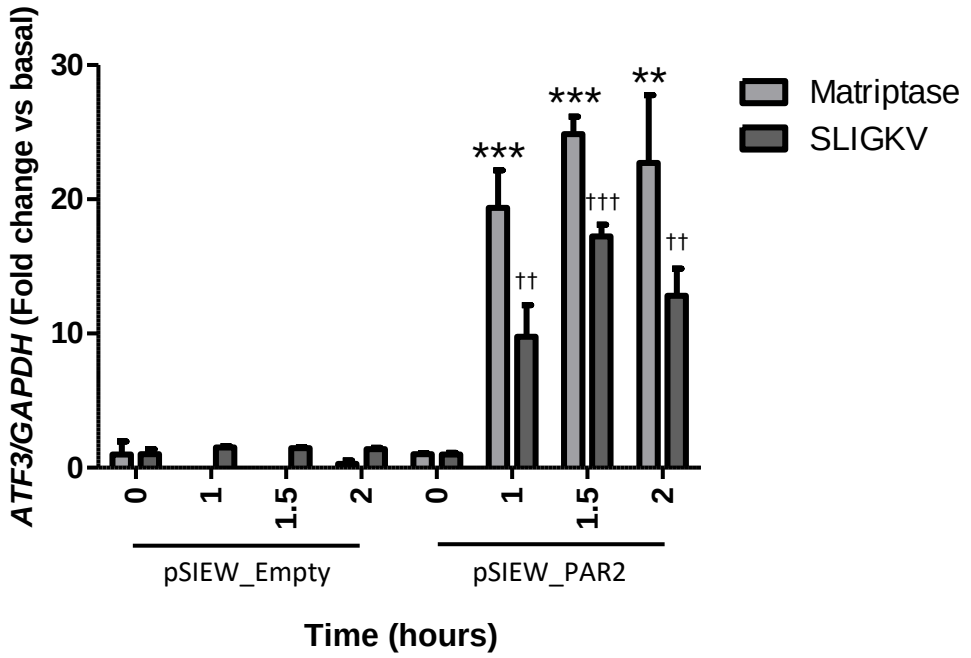

Figure 7.2: *ATF3* expression following matriptase and SLIGKV stimulation
SW1353 cells transduced with pSIEW_Empty or pSIEW_PAR2 were stimulated stimulating with either 100 µM SLIGKV or 10 nM matriptase for varying lengths of time before lysing the cells, extracting the mRNA, reverse transcription and qPCR examining *ATF3* expression. Mean ± S.E.M; where ** $p < 0.01$*** $p < 0.001$ by unpaired T-test between *ATF3* basal expression (T=0) and time point following matriptase stimulation; and †† $p < 0.01$, ††† $p < 0.001$ by unpaired T-test between *ATF3* basal expression (T=0) and time point following SLIGKV stimulation. Data pooled from n=1 experiment.

When comparing the IL-1+OSM and PAR2 activation data, it was decided that the use of 1.5 and 24 hours would be most appropriate for the microarray experiment, as this would give coverage for examining earlier expressed genes such as ATF3, as well as later genes such as the MMPs.

7.2.2 Microarray experiment validation

To generate the mRNA for use in the microarray analysis, three independent experiments were undertaken, overexpressing PAR2 in SW1353 cells and then stimulating with either 100 µM SLIGKV peptide, 10 nM matriptase, or control (serum-free medium), for either 90 minutes or 24 hours. mRNA was extracted and a small sample was taken to perform a reverse transcription to validate the experiments by qPCR. The expression levels for *ATF3* (90 minutes) or *MMP1* (24 hours) were examined at each time point. All three

experimental repeats exhibited successful induction of *ATF3* and *MMP1* at the expected time points (Figure 7.3) and the samples were therefore sent for microarray analysis.

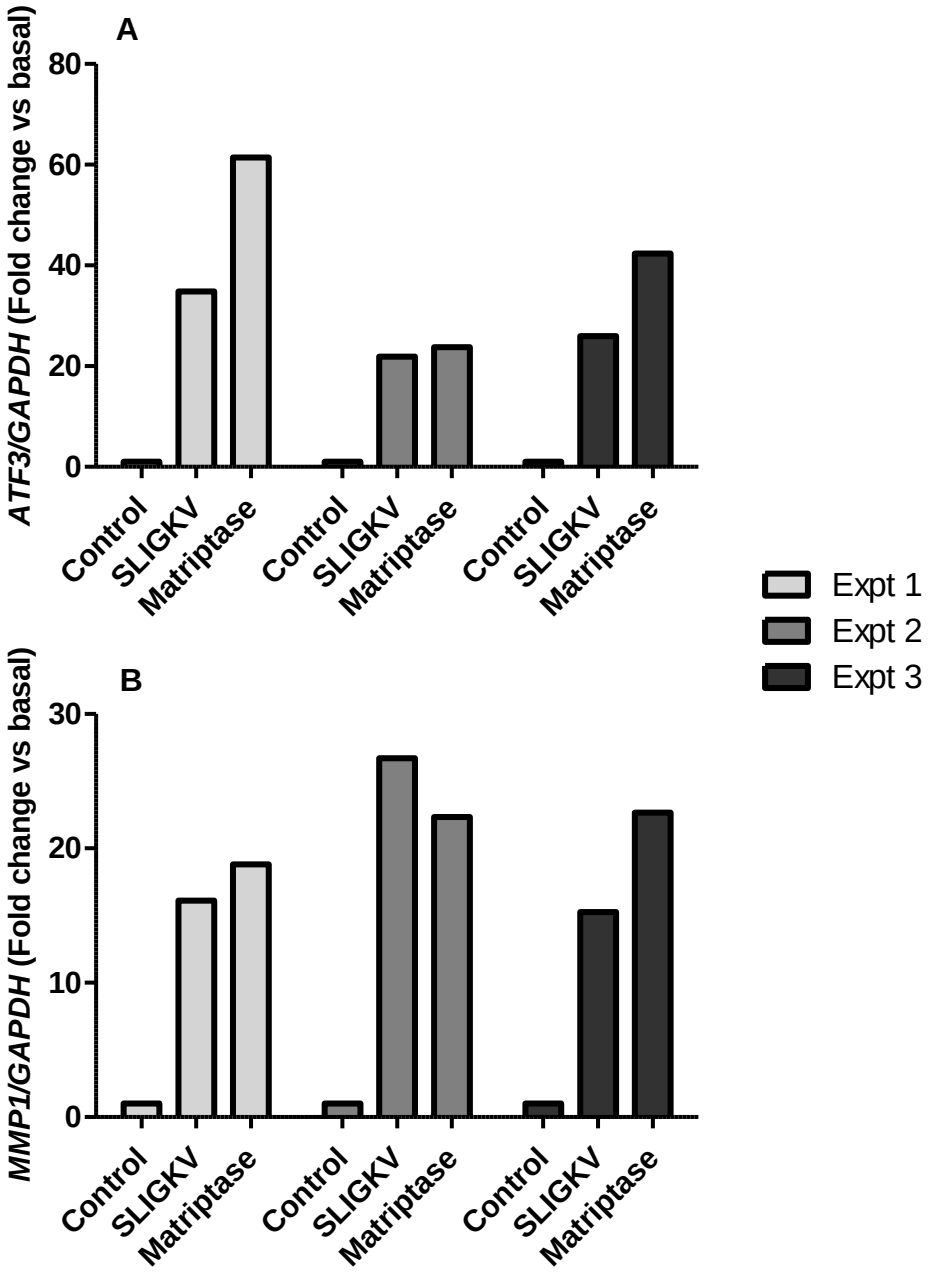

Figure 7.3: *ATF3* and *MMP1* expression of samples sent for microarray analysis
pSIEW_PAR2 transduced SW1353 cells were stimulated with either 100 µM SLIGKV or 10 nM matriptase for either 90 minutes (A) or 24 hours (B) before mRNA was extracted by an RNeasy kit. A sample of the mRNA from each replicate was reverse transcribed and qPCR was performed for either *ATF3* (A) or *MMP1* (B). Each bar represents a single sample, thus there is no standard deviation for error bars to be added. Each experiment was performed independently of each other.

7.2.3 A comparison of matriptase and SLIGKV-mediated canonical activation

SLIGKV (as well as the equivalent rat sequence, SLIGRL) are commonly used as agonists for canonical PAR2 activation, able to activate PAR2 independently of receptor cleavage[314]. There is however evidence that this peptide activates PAR2 via a different mechanism to the equivalent sequence as a tethered ligand[333], although whether this results in different downstream effects is unknown. Furthermore, there is some evidence that SLIGRL lacks specificity for PAR2, with an ability to activate the GPCR neurokinin-1 receptor having been suggested[343]. It was therefore of interest to examine whether global gene expression changes following canonical PAR2 activation by SLIGKV and matriptase were similar.

Changes in genes expressed greater than 2-fold ($\log_2 > 1$) compared to basal, as well as genes down-regulated by greater than 2-fold ($\log_2 < -1$) were compared for SLIGKV vs matriptase stimulation. At 90 minutes, most differentially regulated genes were up-regulated, and there was a strong correlation between SLIGKV and matriptase, with an R^2 value of 0.96 (Figure 7.4).

At 24 hours post-stimulation, there was a greater number of down regulated genes, and an even stronger correlation between matriptase and SLIGKV, with an R^2 value of 0.99 (Figure 7.5).

Taken together, it was clear that matriptase and SLIGKV exhibited similar effects on gene expression changes in SW1353 cells, and thus subsequent analyses were performed predominantly on matriptase-stimulated samples, as these hold more physiological relevance.

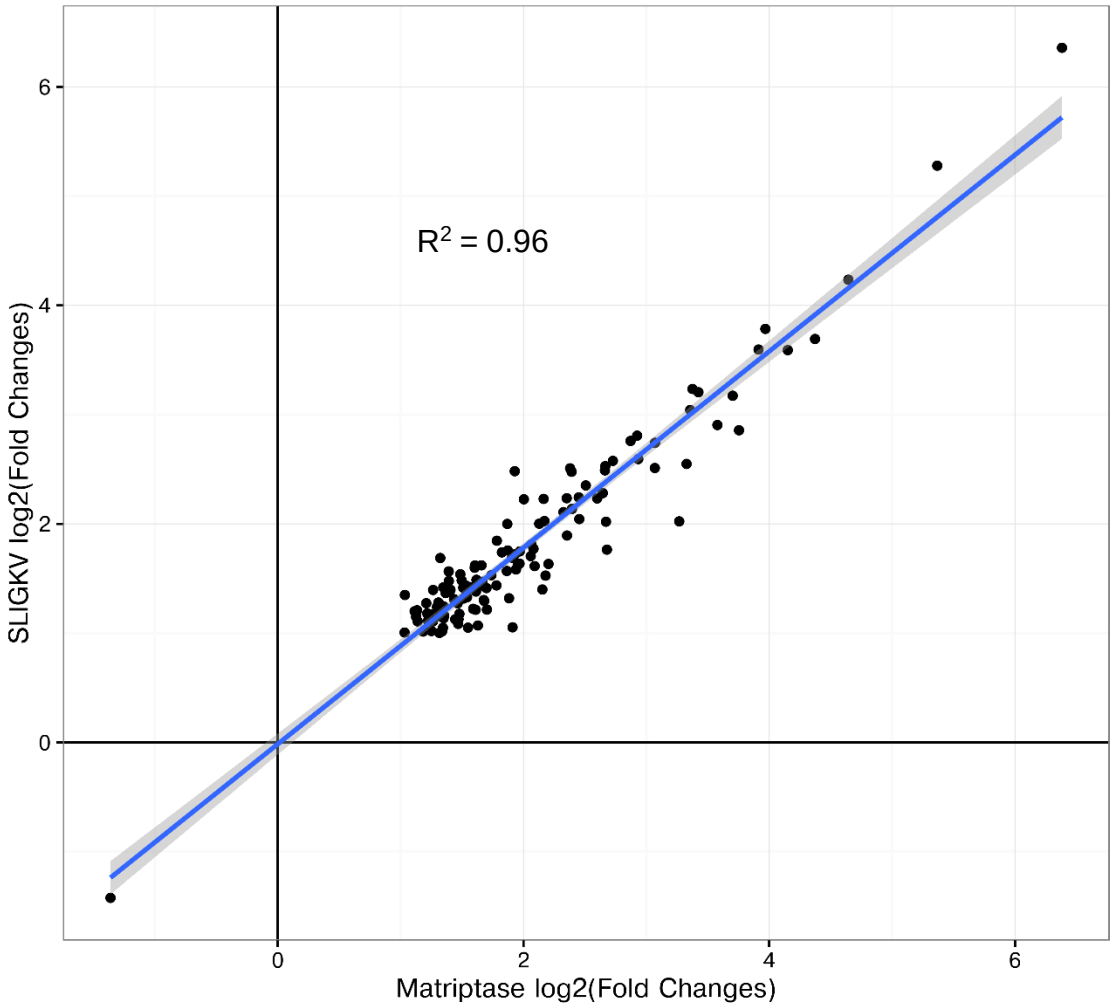

Figure 7.4: Scatter plot of matriptase vs SLIGKV induced expression changes 90 minutes post-stimulation
Scatter plot of matriptase vs SLIGKV gene expression changes (both normalised to unstimulated control) 90 minutes post-stimulation. Included are all genes with a $\log_2$ fold change of -1< and >1. The blue line represents the correlation and the grey shading represents the standard deviation. There are a total of 134 genes included in the analysis. The R^2 value refers to the correlation between the two stimulations.

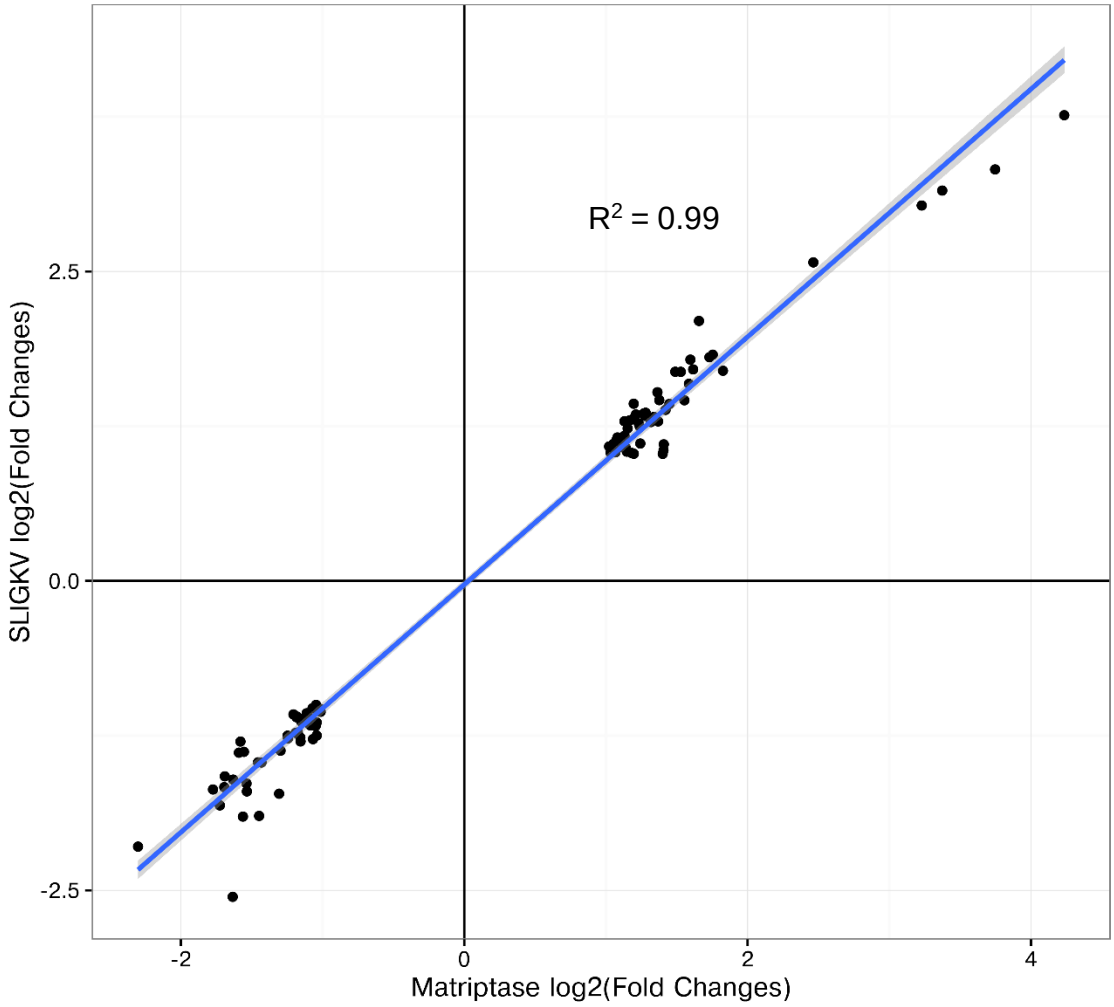

Figure 7.5: Scatter plot of matriptase vs SLIGKV induced expression changes 24 hours post-stimulation
Scatter plot of matriptase vs SLIGKV gene expression changes (both normalised to unstimulated control) 24 hours post-stimulation. Included are all genes with a $\log_2$ fold change of -1< and >1. The blue line represents the correlation and the grey shading represents the standard deviation. There are a total of 109 genes included in the analysis. The R^2 value refers to the correlation between the two stimulations.

7.2.4 An examination of genes regulated by canonical PAR2 activation in SW1353 cells

7.2.4.1 90-minute stimulation

Following 90-minute stimulation of both matriptase and SLIGKV, similar gene expression changes were observed with many genes up-regulated (Figure 7.6).

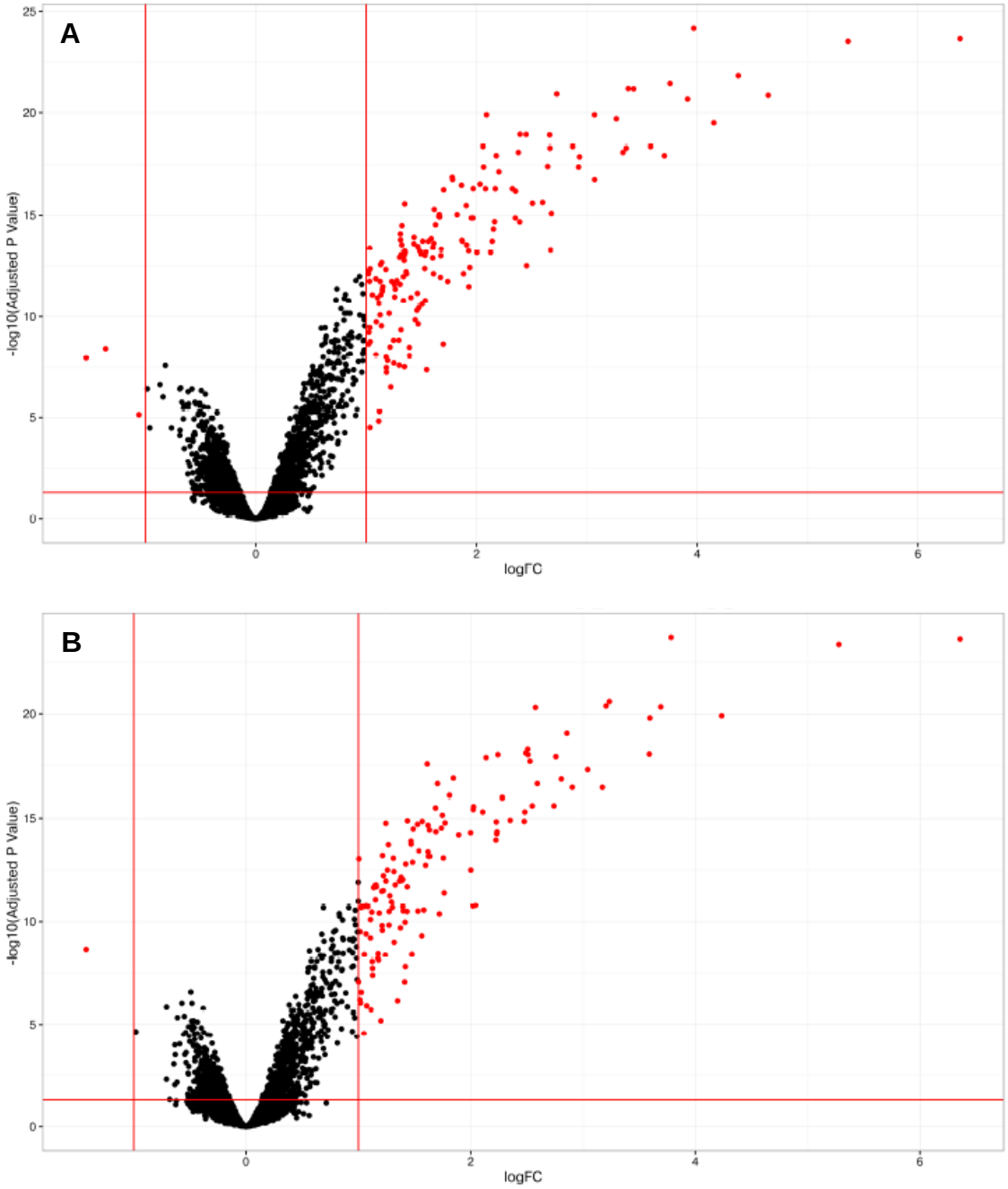

Figure 7.6: Volcano plots showing global gene expression changes following 90-minute SLIGKV or matriptase stimulation

Volcano plot of normalised microarray data, comparing either matriptase vs control (A) or SLIGKV vs control (B). The vertical red lines mark $\log_2$ fold change of -1 and 1 whereas the horizontal red line corresponds to an adjusted p-value of <0.05. The red dots therefore correspond to genes significantly expressed at either <0.5 or >2 fold change to basal.

Due to the similar gene expression changes following SLIGKV or matriptase stimulation, this chapter will focus predominantly on the expression changes following matriptase-mediated PAR2 activation as this holds more physiological relevance. Overall, 165 genes were significantly (adjusted p-value of $p < 0.05$) up-regulated by greater than 2-fold ($\log_2 > 1$) compared to basal, whereas only 3 genes were down-regulated by greater than 2-fold ($\log_2 < -1$). A list of the top 20 most up-regulated genes is presented in table 7.1.

Table 7.1: Top 20 most up-regulated genes following 90-minute matriptase stimulation

Rank	Fold Change	Adj. p-value	Gene
1	83.439	2.19441^{-24}	CXCL8
2	41.279	2.97807^{-24}	CXCL8
3	25.005	1.3742^{-21}	FOSB
4	20.718	1.4796^{-22}	FAM90A2P
5	17.764	3.16567^{-20}	NR4A2
6	15.656	6.75332^{-25}	TNFAIP3
7	15.066	2.11741^{-21}	ATF3
8	13.494	3.58251^{-22}	FOS
9	13.023	1.16156^{-18}	NR4A2
10	11.944	4.13924^{-19}	FAM90A5P
11	10.733	6.59862^{-22}	DUSP1
12	10.379	6.40802^{-22}	IER3
13	10.246	4.98809^{-19}	EGR1
14	10.038	8.02579^{-19}	FAM90A5P
15	9.631	1.99951^{-20}	KLF2
16	8.401	1.72447^{-17}	IL11
17	8.394	1.28431^{-20}	C11orf96
18	7.643	1.31625^{-18}	CSRNP1
19	7.596	4.17231^{-18}	NFKBIA
20	7.319	4.13924^{-19}	EGR2

7.2.4.2 24-hour stimulation

Following 24-hour stimulation of both matriptase and SLIGKV, similar gene expression changes were observed with many genes both up- and down-regulated (Figure 7.7).

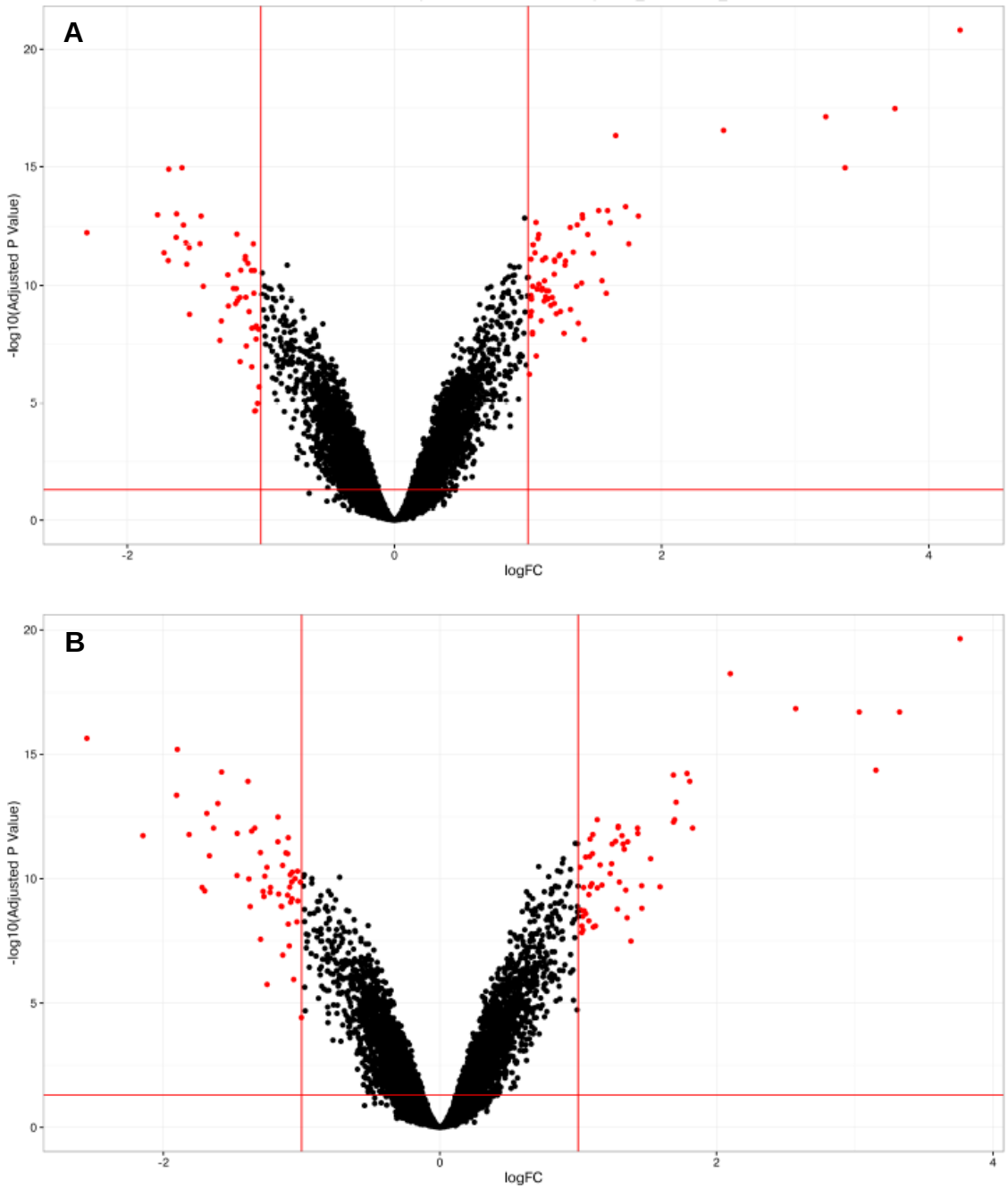

Figure 7.7: Volcano plots showing global gene expression changes following 24-hour SLIGKV or matriptase stimulation

Volcano plot of normalised microarray data, comparing either matriptase vs control (A) or SLIGKV vs control (B). The vertical red lines mark $\log_2$ fold change of -1 and 1 whereas the horizontal red line corresponds to an adjusted p-value of <0.05. The red dots therefore correspond to genes significantly expressed at either <0.5 or >2 fold change to basal.

Following 24-hour matriptase stimulation, 68 genes were significantly (adjusted p-value of p >0.05) up-regulated by greater than 2-fold (log_2 >1) compared to basal, whereas 48 genes were down-regulated by greater than 2-fold (log_2 < -1). A list of the top 20 most up-regulated genes is presented in table 7.2 and list of the 20 most down-regulated genes is presented in table 7.3. Furthermore, other genes of interest to this study outside the top 20 are included in the tables.

Table 7.2: Top 20 most up-regulated genes and other up-regulated genes of interest following 24-hour matriptase stimulation

Rank	Fold Change	Adj. p-value	Gene
1	18.82546	1.52938^{-21}	KIAA1199
2	13.42363	3.35334^{-18}	IL11
3	10.36369	1.1159^{-15}	STC1
4	9.374547	7.48334^{-18}	CXCL8
5	5.517051	2.87364^{-17}	IL24
6	3.545718	1.11196^{-13}	ITGA2
7	3.372986	1.69786^{-12}	DUSP5
8	3.31848	4.39336^{-14}	PLAUR
9	3.152777	4.75277^{-17}	MMP9
10	3.064465	2.13006^{-13}	PLAUR
11	3.023068	6.47027^{-14}	IL24
12	3.001402	2.16994^{-10}	PLAUR
13	2.93569	6.29343^{-11}	LDLR
14	2.884798	6.47027^{-14}	ARHGAP22
15	2.807649	4.29924^{-12}	IL24
16	2.727704	6.80023^{-13}	SOD2
17	2.677695	2.04302^{-08}	UPP1
18	2.654329	1.35243^{-13}	GRAMD1B
19	2.650923	9.75806^{-14}	DEFB103B
20	2.640348	7.93367^{-11}	GNG11
26	2.489293	3.39044^{-13}	SPINK1
47	2.156543	8.3662^{-12}	SERPINB8
53	2.105567	1.00703^{-12}	ADAMTS6
66	2.026306	1.9952^{-9}	CSRNP1

Table 7.3: Top 20 most down-regulated genes and other down-regulated genes of interest following 24-hour matriptase stimulation

Rank	Fold Change	Adj. p-value	Gene
1	4.931793299	5.68228^{-13}	TXNIP
2	3.418230792	9.75806^{-14}	MAFB
3	3.305468236	4.09663^{-12}	MYH8
4	3.234320017	8.74945^{-12}	BMP4
5	3.22614988	1.2789^{-15}	CNTNAP2
6	3.103671954	9.03272^{-13}	ID3
7	3.097001174	8.92322^{-14}	CADM1
8	3.011349777	1.1159^{-15}	RGCC
9	2.988116262	2.68475^{-13}	AKR1B10
10	2.952064379	1.53584^{-12}	ACKR3
11	2.93761677	1.24726^{-11}	AKR1C3
12	2.896065984	1.70762^{-9}	RHOBTB3
13	2.742393287	1.67535^{-12}	ABLIM1
14	2.727627319	1.11196^{-13}	ACKR3
15	2.473539313	2.21141^{-8}	NPPB
16	2.455910271	3.25209^{-9}	COL1A1
17	2.373306942	3.54222^{-11}	F2RL2
18	2.367435452	7.49863^{-10}	TLE4
19	2.305964608	1.33452^{-10}	COL1A2
20	2.279555578	5.91602^{-10}	ATOH8
31	2.138721772	1.152^{-11}	F2R

7.2.5 Pathway Analysis of PAR2 canonical activation

Ingenuity Pathway Analysis (IPA) was performed on matriptase-induced PAR2 canonical activation (samples normalised to controls). IPA is powerful software utilised to analyse complex "omic" data, including gene expression microarray data. IPA can perform searches for targeted information on gene and protein networks based on interactive models of experimental systems previously outlined within the literature.

7.2.5.1 Canonical Pathways

Firstly, a canonical pathway analysis was performed, which analyses associations within the experimental dataset with previously described signalling pathways. The analysis gives an indication of how strongly the pathway is in an activation or inhibitory state (Z score), as well as the significance of the association (Figure 7.8).

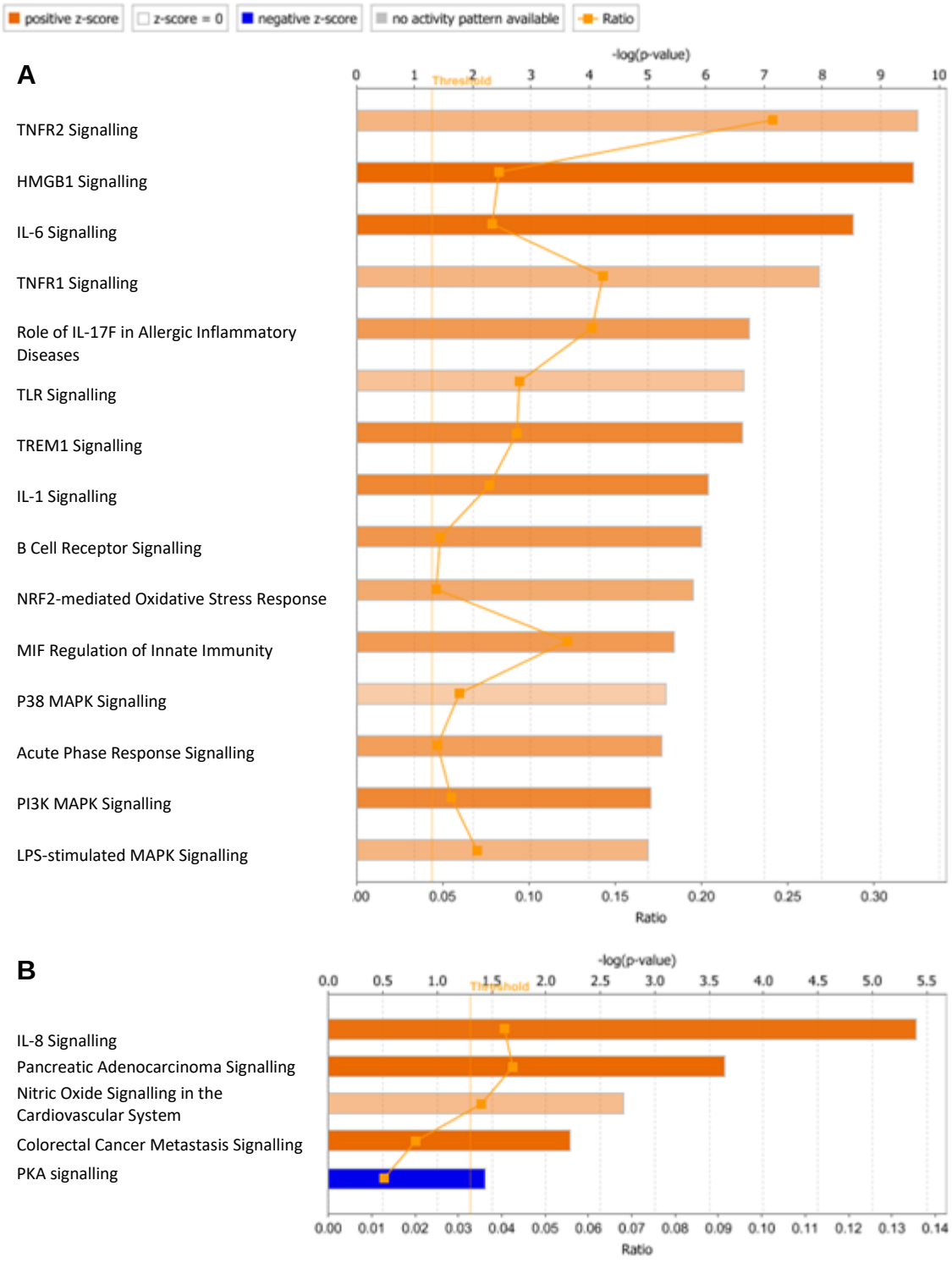

Figure 7.8: Top dysregulated canonical pathways following matriptase stimulation of PAR2
Ingenuity Pathway Analysis was performed on the microarray data: matriptase normalised to control samples, at both 90 minutes (A) and 24 hours (B) examining associated canonical pathways with the data set. The bars on the primary x axis represent the -log(p-value) for each pathway, stating the statistical significance for the association of that pathway with the microarray data set. The shade of the bar fill (orange for positive regulation, blue for negative regulation) shows the strength of the regulation: darker shade for stronger regulation. The line on the secondary x axis represent the ratio of regulated genes: the number of genes in the canonical pathway dysregulated in the examined data set.

At the 90-minute time point, all the associated pathways were in a positive activation state, with many on the list being associated with pro-inflammatory responses, such as TNF signalling, IL-6 signalling, IL-17 signalling and IL-1 signalling. The most statistically associated pathway was TNFR2 signalling, however pathways such as HMGB1 and IL-6 had higher Z-scores indicating a stronger level of activation (however at lower statistical significance due to fewer genes within the pathway being dysregulated).

An initial striking difference at the 24-hour time point was a marked reduction in the number of significantly associated pathways. Furthermore, unlike the 90-minute time point, there was an association with a negatively associated pathway in protein kinase A (PKA) signalling. The most significantly associated pathway at this time point was IL-8 signalling.

7.2.5.2 Upstream Regulators

As well as exploring canonical pathways by IPA, specific upstream regulators associated with the data set were explored. Rather than being a whole pathway, these upstream regulators represent specific gene products involved in regulation of multiple downstream targets. The analysis explores the activation state of both the upstream regulator and downstream targets within the experimental dataset, and then gives an activation Z-score, as well as significance for the association. The analysis also states a predicted activation state. Strong statistical association with a particular upstream regulator does not necessarily result from multiple activated or inhibited targets, but rather can result from a mixture. This results in a statistically associated upstream regulator without a predicted activation state, as is observed for many of the identified top associations in this study. As with the canonical pathway analysis, the upstream regulator analysis is based on previous literature for signalling networks.

At the 90-minute time point, the majority of the top 20 most significant upstream regulators are in a predicted activation state, with only CD3 being a predicted inhibited upstream regulator, and two regulators, NR3C1 and IgG having no predicted activation state (table 7.4). The most strongly associated upstream regulator is Platelet-derived growth factor (PDGF) – BB chain dimer, followed by TNF and IL-1B. Other inflammatory regulators of interest to this project within the top 20 include p38 MAPK, NF-kB, Jnk, ERK and ERK1/2.

Table 7.4: Top 20 most significantly associated upstream regulator genes with microarray data following 90-minute matriptase stimulation

Rank	Gene	Z score	p-value of overlap	Predicted Activation
1	PDGF BB	5.868	8.38^{-62}	Activated
2	TNF	5.458	7.91^{-40}	Activated
3	IL1B	5.874	6.49^{-39}	Activated
4	NR3C1	0.507	1.67^{-30}	-
5	CREB1	4.282	5.41^{-30}	Activated
6	P38 MAPK	4.016	1.55^{-28}	Activated
7	TREM1	4.452	3.69^{-26}	Activated
8	NFkB (complex)	4.339	3.22^{-25}	Activated
9	Jnk	3.196	3.74^{-23}	Activated
10	CREM	3.353	5.73^{-22}	Activated
11	EIF2AK3	2.608	7.92^{-22}	Activated
12	STAT3	3.780	1.33^{-20}	Activated
13	ERK	4.164	3.45^{-20}	Activated
14	CD3	-3.103	9.31^{-20}	Inhibited
15	ERK1/2	3.049	2.21^{-19}	Activated
16	ECSIT	3.302	8.00^{-19}	Activated
17	IgG	-1.774	2.94^{-18}	-
18	FOXL2	3.571	5.13^{-18}	Activated
19	FOXO3	2.741	2.46^{-17}	Activated
20	PRKCD	2.688	4.64^{-17}	Activated

By 24 hours, within the top 20 most strongly associated upstream regulators, only three have a predicted activation state: TNF, IL-1B and ERBB2 (table 7.5). TNF and IL1-B were both strongly associated at the 90-minute time point, however ERBB2 was the 106th most associated at this time point.

Table 7.5: Top 20 most significantly associated upstream regulator genes with microarray data following 24-hour matriptase stimulation

Rank	Gene	Z score	p-value of overlap	Predicted Activation
1	TGFB1	0.813	2.09^{-16}	-
2	TP53	-0.609	2.10^{-13}	-
3	Cg	1.599	1.05^{-12}	-
4	TNF	3.377	4.80^{-12}	Activated
5	HIF1A	0.607	1.42^{-11}	-
6	SP1		4.46^{-11}	-
7	NEDD9	1.890	1.11^{-10}	-
8	PRKCD	1.320	5.51^{-10}	-
9	SP3		5.51^{-10}	-
10	STAT5A		8.73^{-10}	-
11	IL1B	3.453	1.35^{-09}	Activated
12	TGFBR1	-1.195	1.44^{-09}	-
13	CBX5	0.333	1.49^{-09}	-
14	JUN	1.675	1.75^{-09}	-
15	AHR	1.700	2.00^{-09}	-
16	Ap1		5.01^{-09}	-
17	NR3C1	-1.497	5.28^{-09}	-
18	ERBB2	2.474	8.54^{-09}	Activated
19	KRAS	1.555	1.28^{-08}	-
20	estrogen receptor	-1.706	1.70^{-08}	-

The signalling networks of IL-1B and TNF were further explored due to their high Z-scores and significance at the 90-minute time point; the fact they were also two of the three activated regulators at the 24-hour time point; and the fact that as cytokines, TNF (specifically TNF-α) and IL-1 are both thought to be involved in OA.

As shown in table 7.4, TNF is a strongly activated upstream regulator, and by examining the downstream regulators under regulation by TNF within the microarray, it is clear that many of the genes were activated by matriptase (Figure 7.9). Further downstream of the regulators, 74 targets were also dysregulated by PAR2 activation. Two of these of particular interest, EGR2 and ATF3, were selected for inclusion in the diagram.

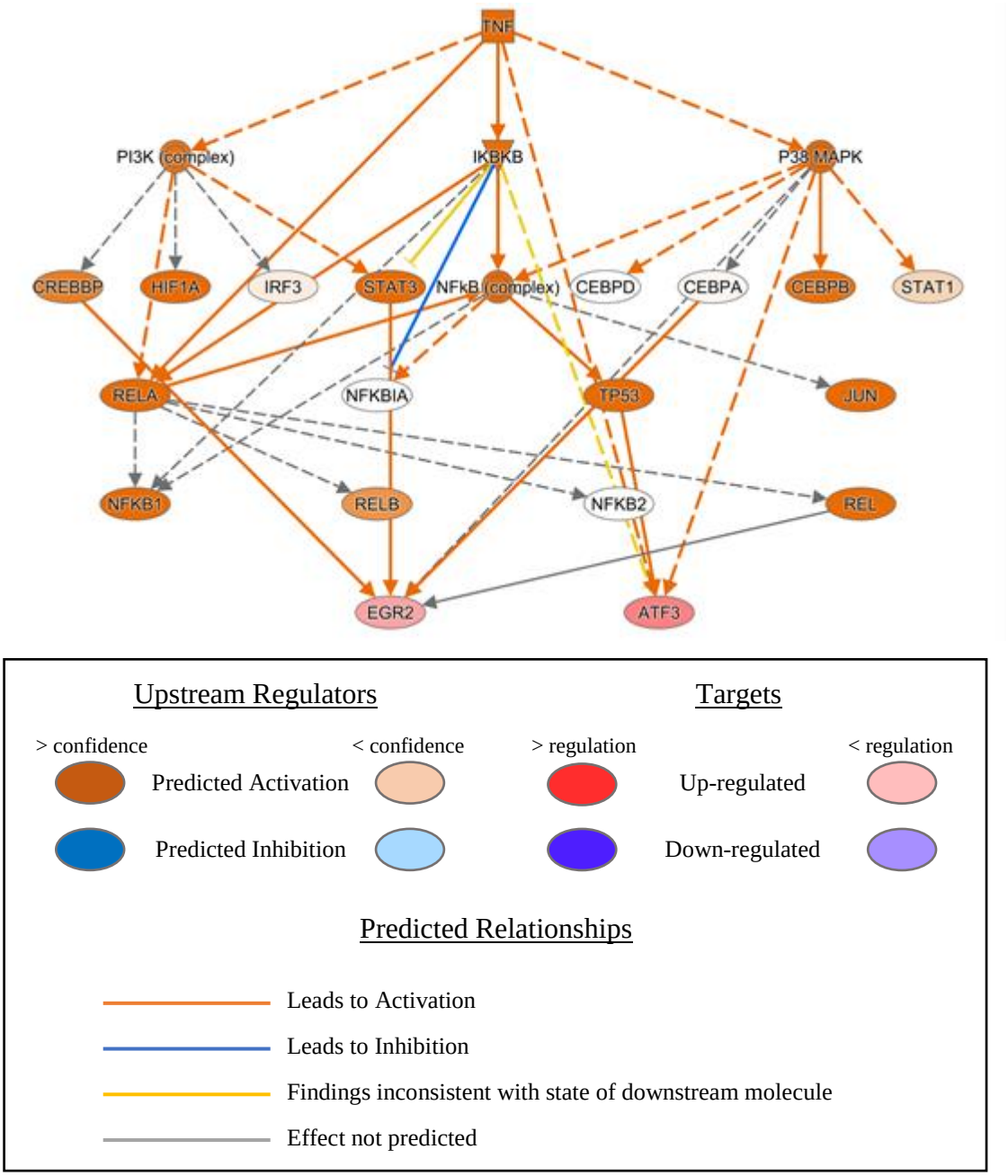

Figure 7.9: TNF pathway following 90-minute matriptase stimulation
The signalling network downstream of TNF was examined based on the activation state of the genes within the network in the microarray dataset of 90-minute PAR2 stimulation by matriptase. Included are 2 downstream targets of interest (out of 74 total targets in the network): EGR2 and ATF3.

IL-1B (IL-1β) was another strongly activated upstream regulator, and by examining the downstream regulators previously described as under its regulation, many were observed as activated within the microarray dataset following matriptase activation of PAR2 (Figure 7.10). Further downstream of the regulators, 72 targets were also dysregulated by PAR2 activation. Three of these were of particular interest: ATF3, CSRNP1 and EGR2, and were selected for inclusion in the diagram.

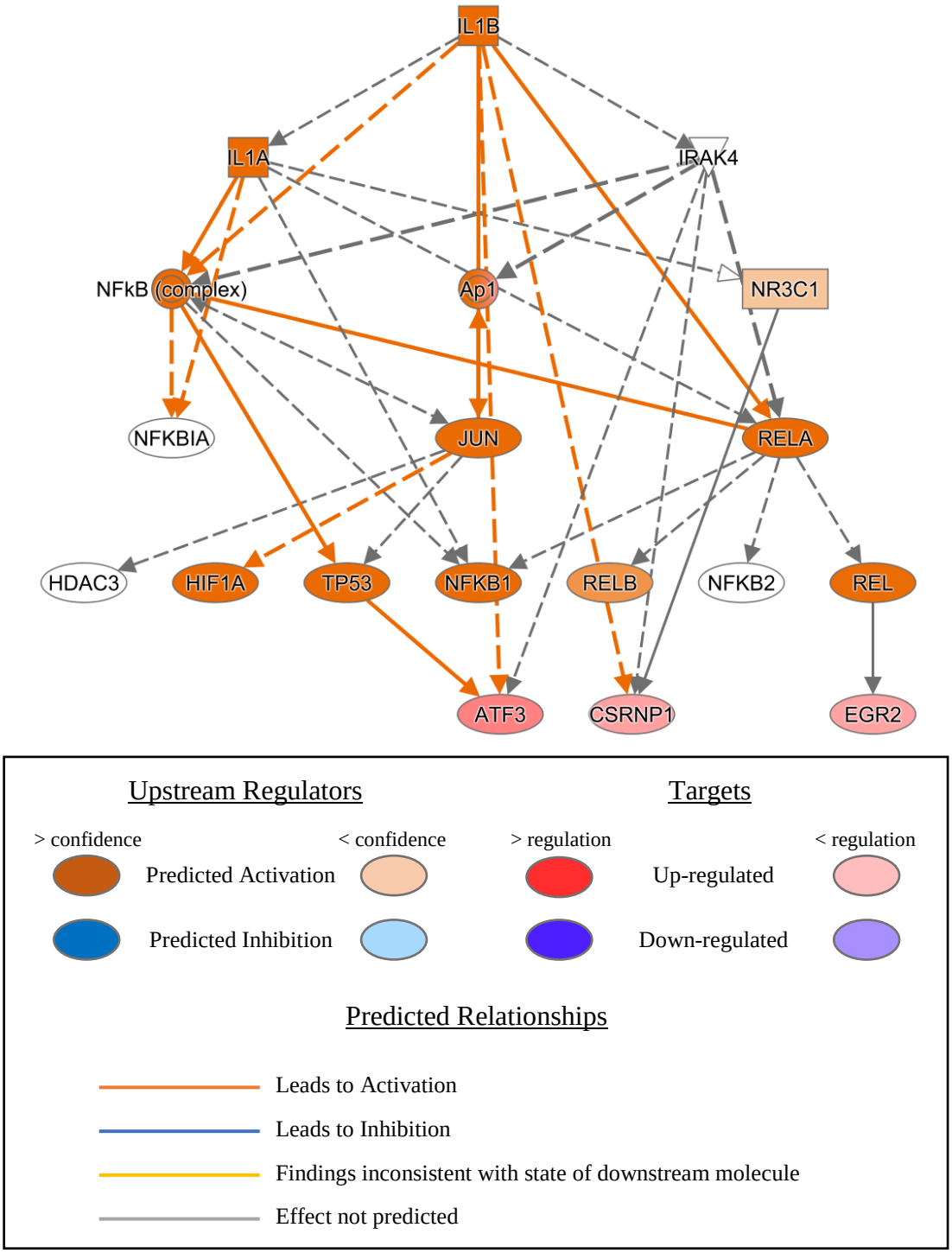

Figure 7.10: IL-1B pathway following 90 minute matriptase stimulation
The signalling network downstream of IL-1B was examined based on the activation state of the genes within the network in the microarray dataset of 90-minute PAR2 stimulation by matriptase. Included are 3 downstream targets of interest (out of 72 total targets in the network): ATF3, CSRNP1 and EGR2.

7.3 Discussion

Work presented in this chapter optimised the time points to be utilised for a gene expression microarray following canonical PAR2 activation. The selected time points were based on how SW1353 cells responded to IL-1+OSM stimulation in terms of *ATF3* and *MMP* expression. *ATF3* was subsequently identified as a PAR2 target, and 90 minutes was chosen as an early time point and 24 hours as a later time point for microarray analysis. A gene expression microarray was performed by stimulating PAR2-expressing SW1353 cells with either matriptase or SLIGKV, after which these responses were compared, and further analysis performed on matriptase-stimulated samples.

In examining the top 20 most up-regulated genes following 90-minute matriptase stimulation, a multitude of early response genes (*FOSB*, *FOS*, *ATF3*, *IER3*, *EGR1*, *EGR2* and *CSRNP1*), transcription factors (*NR4A2* and *KLF2*), cyto/chemokines (*CXCL8* and *IL-11*) and other inflammatory regulators (*NFKBIA* and *TNFAIP3*) were found to be significantly up-regulated. An initial and striking observation was that *ATF3*, *EGR2* and *CSNRP1* were all identified as being robustly up-regulated following PAR2 activation. These three genes were explored in chapter 3 as being regulated by the mechanical loading of chondrocytes. A previous study has also identified these three genes as key regulators of collagenase activation following IL-1+OSM stimulation of chondrocytes (Chris MacDonald, unpublished).

The gene with the highest fold increase of expression following 90-minute matriptase stimulation was *CXCL8* (the gene which encodes IL-8), which validates the use of this gene as a readout for canonical PAR2 activation in previous chapters, as well as in previous studies[315,316]. IL-8 has also been implicated in OA pathogenesis. IL-8[344] and its receptor[345] are up-regulated by OA chondrocytes, and whilst this expression of IL-8 has not been linked to PAR2, data presented in this study suggests that the involvement of PAR2 is a reasonable hypothesis. IL-11 which was also up-regulated at this time point has also been implicated in OA, with an elevated expression in OA chondrocytes[346]. However, this is contrary to the pro-inflammatory outcomes of PAR2 signalling, as it is suggested that IL-11 is anti-inflammatory in chondrocytes, leading to TIMP-1 upregulation[346]. IL-11 has however also been shown to promote MMP expression similarly to IL-6 when combined with IL-1 (A.D. Rowan, personal communication).

Nuclear receptor subfamily 4, group A, member 2 (NR4A2) had a robustly elevated expression level following 90-minute matriptase stimulation. NR4A2 has been identified as a transcription factor involved in multiple arthritic diseases, particularly inflammatory arthritic diseases[347]. NR4A2 has however also been shown to have elevated expression in OA synovial tissues[348]. Furthermore, the overexpression of *NR4A2* in an immortalised synovial fibroblast cell line leads to a synergistic increase in *MMP13* expression following TNFα stimulation[348].

Other genes strongly up-regulated following 90 minutes include various early response genes which have been previously implicated in OA. For example, *FOSB* had the second highest fold increase in expression following 90 minutes, and family member *FOS* was also highly up-regulated. The gene products of the *FOS* family form heterodimers with gene products of the *JUN* family to form the AP-1 transcription factor, which has key roles in the transcription of a variety of genes including the collagenolytic MMPs, in a response to a variety of stimuli, including cytokines. Indeed, the inhibition of c-Fos (the gene product of *FOS*)/AP-1 results in a reduced induction of *MMP13* following IL-1 stimulation, and was found to be protective against OA in the CIA model of mouse disease[349].

To our knowledge, this is the first study to identify *ATF3* and *CSRNP1* as downstream targets of PAR2 canonical signalling, however *EGR2* has previously been identified as being induced following trypsin activation of PAR2 in HEK293 cells, although not as robustly as in SW1353 cells[340]. Little is currently known about the signalling pathways involved in matriptase-induced up-regulated expression of collagenases. The observation that *ATF3*, *CSRNP1* and *EGR2* are all targets of PAR2 signalling is therefore a fascinating one, as it suggests the potential for similar and overlapping mechanisms of collagenase expression following distinct stimuli, be it IL-1+OSM, abnormal mechanical load, or PAR2 activation. It is noteworthy that DNA microarray analysis of SW1353 cells following IL-1+OSM identified *CXCL8* as the most up-regulated gene, in complete agreement with the data presented here[350], further suggesting overlapping common pathways.

In order to further explore this overlap and association with other defined signalling pathways, pathway analysis was undertaken. Unsurprisingly, canonical PAR2 activation was strongly associated with a whole host of defined inflammatory canonical pathways,

such as TNF signalling, IL-6 signalling, IL-17 signalling, TLR-signalling, IL-1 signalling, and p38 MAPK signalling. Furthermore, many of these canonical pathways have also been associated with OA. For example, IL-1 and TNF have long been strongly associated with OA. IL-1 (namely, IL-1β) and TNF are expressed and released by multiple cells of the joint, including chondrocytes, cells of the synovial membrane, osteoblasts and infiltrated mononuclear cells[351]. Elevated levels of IL-1β and TNF are observed in the synovial fluid and cartilage of patients with OA[352], and the receptor for IL-1 also exhibits a higher expression level in OA chondrocytes[353]. These cytokines are catabolic in nature, stimulating the expression of multiple genes detrimental to cartilage health such as the collagenolyic MMPs[351]. *IL-1B* and *TNF* were both identified in this study as very strongly associated upstream regulators within the microarray dataset, suggesting several downstream regulators and targets of IL-1β and TNF are also induced by canonical PAR2 activation. Multiple other upstream regulators identified in this study have also been previously shown to be involved in IL-1β and TNF signalling, such as p38 MAPK, JUN and STAT3. Furthermore, at 24 hours post-stimulation, *IL-1B* and *TNF* remained two of the three top upstream regulators which retained a predicted activation state, further establishing their association with PAR2 signalling.

Taking together the canonical pathway analysis and the upstream regulator analysis, it is clear that canonical PAR2 activation is highly pro-inflammatory in nature, with many overlapping pathways with those observed by pro-inflammatory cytokine stimulation. Futhermore, IL-6 and IL-17 have also been implicated in OA[351], as has TLR signalling[354].

The later time point utilised in this study was 24 hours. A striking observation was that 24 hours post-stimulation there was a more equal number of down and up-regulated genes, whereas at 90 minutes, only three genes were significantly down-regulated below the threshold of $\log_2 < -1$. This was not observed in a previous microarray analysis of canonical PAR2 activation[340] and could reflect differences in cell line or differences in sensitives of the microarray chips utilised.

After 24-hour stimulation, several cytokines remained highly up-regulated, including IL-8 and IL-11 as observed at 90 minutes, with the addition of IL-24, a cytokine which has been associated with RA, however not with OA[355]. Other genes up-regulated at 24 hours post-stimulation include cell surface receptors such as *PLAUR*, the uPA receptor and

LDLR, the Low-Density Lipoprotein receptor. Other cell surface receptors such as *F2R* (PAR1) and *F2RL2* (PAR3) were however down-regulated at this time point.

The only proteases to be significantly up-regulated at 24 hours at the set threshold were *ADAMTS6* and *MMP9*, despite RT-qPCR clearly showing the upregulation of *MMP1* at this time point in the same samples. This is likely a reflection of the relative sensitivities of DNA microarray analysis and RT-qPCR. Indeed, it is generally accepted that RT-qPCR is more sensitive than microarray analysis[356-358]. MMP-9 is a gelatinase which has an elevated expression level in OA[359,360], whereas ADAMTS-6 is an incompletely understood protease with no current link to the disease.

Interestingly, at 24 hours two protease inhibitors were up-regulated: *SPINK1* and *SERPINB8*. SPINK1 is a kazal-type serine-protease inhibitor, best known as a pancreatic-expressed trypsin inhibitor[361]. To our knowledge, this is the first time SPINK1 has been shown to be regulated by PAR2 activation, which might suggest the presence of a negative feedback system whereby canonical PAR2 activation can upregulate a trypsin inhibitor. Despite being able to inhibit trypsin, there is however evidence that SPINK1 does not inhibit matriptase[362]. SERPINB8 is an intracellular serine protease inhibitor and is best known as a furin inhibitor[363], with no current links to arthritic diseases.

The most down-regulated gene at 24 hours was Thioredoxin-interacting protein (*TXNIP*), which is an interesting observation as this gene has recently been implicated in OA[364]. The regulation of this gene by PAR2 is not a novel observation, and this was indeed also the most down-regulated gene observed in a previous microarray analysis of canonical PAR2 activation[340]. *TXNIP* was found to be expressed at relatively high levels in normal human and mouse cartilage, however expression was significantly reduced in both OA, and with aging[364].

The second most down-regulated gene at 24 hours was *MAFB*, a transcription factor, which has also been implicated in OA. *MAFB* is regulated by retinoic acid and the genetic knockdown of *MAFB* in chondrocytes however results in an increased expression of aggrecan and a decreased expression of *MMP3* and *MMP13*[365]. *MAFB* deficiency is therefore anabolic, which conflicts with the generally catabolic effects of PAR2 activation.

Another strongly down-regulated gene at 24 hours was bone morphogenic protein 4 (*BMP4*), a growth factor from the TGF-β family, which also has a decreased expression level in patients with OA[366].

Under the criteria used for the pathway analysis, only a single down-regulated canonical pathway was associated with the microarray data set, which was protein kinase A (PKA). Interestingly, decreased PKA activity has recently been associated with activation of another GPCR, GPR22, in chondrocytes[367], with GPR22 having previously been linked to OA[368].

Taking together the data presented within this chapter, it is clear that canonical PAR2 activation is pro-inflammatory in nature, and multiple genes regulated by PAR2 have links to arthritic diseases, with links to OA of particular interest to this study. In exploring canonical PAR2 activation on a global level within chondrocytes, many potentially interesting novel avenues of exploration have been identified.

7.4 Summary

- ATF3 expression reaches a peak at 1.5 hours post-stimulation when stimulated with either IL-1+OSM or via PAR2 activation.

- Matriptase and SLIGKV both induce highly similar gene expression changes in SW1353 cells.

- Multiple pathways and upstream regulators are significantly associated with the microarray data set, and the responses of PAR2 activation are generally pro-inflammatory in nature.

- Genes such as *ATF3*, *CSRNP1* and *EGR2* are highly induced by PAR2 activation, identifying overlaps with chondrocyte responses following PAR2 activation, mechanical loading of chondrocytes or IL-1+OSM stimulation.

Chapter 8 – General Discussion

8.1 General Perspectives

OA is a disease which is characterised by the enzymatic breakdown of articular cartilage, where the balance between ECM synthesis and degradation is disturbed and proteases such as the collagenases, MMP-1 and MMP-13 are up-regulated. It is becoming increasingly clear that as important as the collagenases are, many other enzymes have roles in cartilage turnover and disease, including metalloproteinases such as the aggrecanases - ADAMTS-4 and ADAMTS-5[42], as well as proteases from the serine and cysteine protease families.

Serine proteases have been implicated in OA, from simple associations (e.g. elevated expression), to others with more detailed pathogenic mechanisms. The serine protease matriptase was identified as having a role in OA. Matriptase has an elevated expression level in OA patients, as does the receptor PAR2, which can be potently activated by matriptase to induce *MMP* expression[1]. Various cysteine proteases have also had roles implicated in the disease, with the strongest links being the cathepsin proteases, cathepsin B and cathepsin K.

This project had two major aims: to explore how matriptase expression is regulated in chondrocytes, and to explore how proteases expressed by chondrocytes interact with PAR2 compared to matriptase. Understanding the regulation of previously described pathogenic mechanisms such as matriptase-mediated PAR2 activation, as well as the discovery of novel mechanisms of disease are important for understanding OA, and the development of future therapeutics.

To date, the therapeutic inhibition of active cartilage degrading proteases has been unsuccessful. The inhibition of the collagenases or MMP-3 has been shown to be protective in preventing cartilage degradation in animal models of OA[369,370], however when in clinical trials, low selectivity and severe side effects were observed[371], highlighting the importance of these enzymes in normal physiology. The targeting of MMPs in OA has, however, shown that the overall aim: the prevention of MMP-mediated cartilage degradation, is a valid target for therapy. Understanding the regulation of MMPs

in cartilage, from physiology to pathology, will potentially identify new targets elsewhere in the pathway which could prevent specific MMP activity without directly inhibiting any MMPs with a small molecule inhibitor.

8.2 Regulation of collagenase gene expression

The initial aims of chapter 3 were to explore whether matriptase was regulated by mechanical load. In performing this work, limitations in the model were identified with a major issue of long-term viability of BNCs following loading. Data generated at earlier time points were however more robust in terms of reproducibility and cell viability, therefore the focus of this chapter shifted towards an exploration of genes involved in collagenase expression. A previous study performed by our group has identified ATF3, CSRNP1 and EGR2 as all having roles in the regulation of collagenase expression following pro-inflammatory stimulation by IL-1+OSM, specifically ATF3 and EGR2 in the regulation of *MMP13* and CSRNP1 in the regulation of *MMP1* (C. MacDonald, unpublished). As these regulators are induced early following pro-inflammatory regulation, they were candidates for exploration with the mechanical loading models. This work identified all three of them to be induced by the mechanical loading of chondrocytes.

In chapter 7, a gene expression microarray was performed to explore global gene expression changes following canonical PAR2 activation. Multiple genes were regulated with strong associations to multiple defined pro-inflammatory signalling pathways and networks. One of the strongest associations with canonical PAR2 signalling in chondrocytes was with IL-1 signalling. Furthermore, *ATF3*, *CSRNP1* and *EGR2* were all found to be strongly induced by PAR2 activatio. It is well established that mechanical loading, PAR2 activation and IL-1+OSM stimulation are all able to robustly induce *MMP* expression, however work presented in this study suggests that the signalling networks involved may have overlap (Figure 8.1).

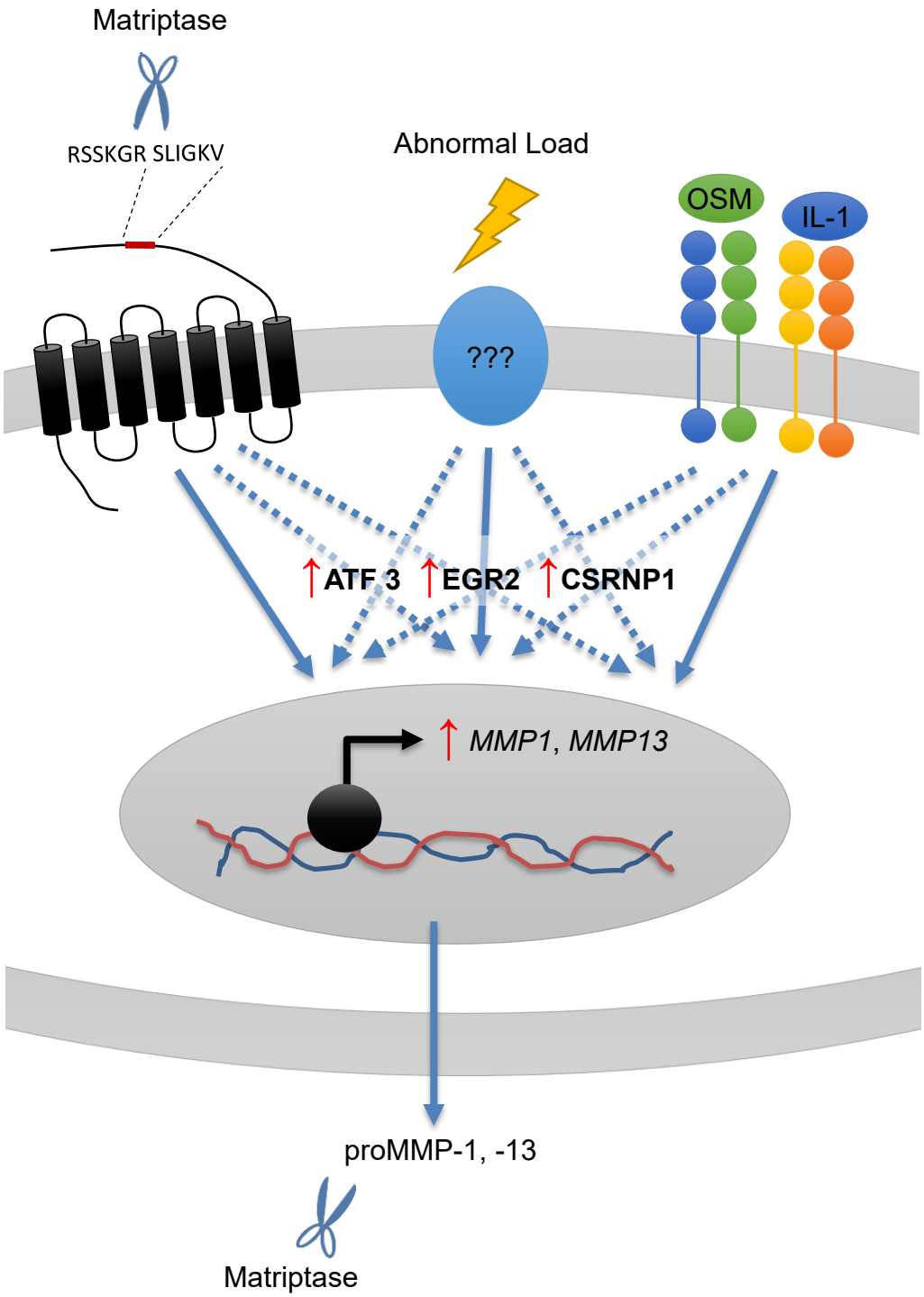

Figure 8.1: Canonical PAR2 activation, mechanical loading and IL-1+OSM stimulation result in collagenase expression
Work presented in this thesis identified ATF3, EGR2 and CSRNP1 as being regulated by mechanical loading in chondrocytes, as well as being downstream targets of PAR2 canonical activation. This follows on from previous work by this group which identified them as being collagenase regulators following IL-1+OSM stimulation.

The identification of potential overlapping signalling pathways from distinct stimuli is interesting, yet not unique in biology. For example, in the context of bone, another tissue with important mechanical roles, osteocytes respond to both mechanical loads and

hormonal stimulation. Despite being distinct stimuli, many of the downstream signalling pathways are known to overlap, such as Wnt signalling and ERK signalling[372]. Within OA, abnormal mechanical load, IL-1 and OSM, and matriptase/PAR2 signalling have all been implicated in the disease, and identifying common downstream regulators could provide interesting and novel therapeutic targets. As discussed previously, MMP inhibition has not yielded success due to the lack of specificity of inhibitors and the importance of these proteases in physiology. In understanding further how different pathological stimuli can induce *MMP* expression, it may be possible to identify specific regulators in chondrocytes where the different incoming stimuli converge, before inducing the expression of *MMPs*.

8.3 PAR2 disarming and biased agonism

The work presented in this study was performed in the context of cartilage biology and OA, however PAR2 and the examined proteases are expressed in multiple tissues. Therefore, work presented in this study could hold relevance in other physiological and pathological systems. Indeed, despite being identified in this study as having the ability to cleave PAR2, one of the identified proteases has limited relevance to cartilage biology based on our current understanding of cartilage. As discussed in chapter 6, there is little evidence of extracellular proteolysis by cathepsin V and it is not known to be present in cartilage. This protease has however been linked to multiple pathological conditions including atherosclerosis[336], as well as breast and colorectal cancers[175], diseases in which PAR2 is also implicated[200]. As there is evidence that cathepsin V can be secreted from cells such as a fibrosarcoma cell line[337], a role for cathepsin V cleavage of PAR2 under certain conditions cannot be excluded.

The other cathepsins identified as able to cleave PAR2 are however better candidates as being relevant to cartilage biology. As discussed in chapter 6, cathepsin L has been detected in synovial fluid of patients with RA[338], secretion has been observed in chondrocytes extracted from OA cartilage[191], and it has the ability to cleave aggrecan[192]. This places cathepsin L as being expressed and present in the correct compartment to cleave PAR2 in a physiological manner. Furthermore, data presented in chapter 6 showed that cathepsin L was the most potent cathepsin at PAR2 cleavage. The similar cleavage profiles of cathepsins V and L against PAR2 in the present study, as well as the high level

of homology between the two enzymes[175] mean that it would be reasonable to hypothesise that the two enzymes behave similarly. Cathepsin V was able to disarm against matriptase-induced canonical PAR2 activation, resulting in an attenuation of collagenase expression. Whilst not explored in this study, one could hypothesise that both cathepsins V and L would be biased agonists for PAR2 based on previous work with cathepsin S which showed induction via Gαs-mediated cAMP accumulation[226].

Taken together, it is possible that cathepsin L expression in osteoarthritic cartilage could be protective against the disease. Aside from the disarming of PAR2 activation, there could be further protection in terms of the biased signalling pathways induced. Should cathepsin L prove to mimic the action of cathepsin S on PAR2 activation and result in cAMP accumulation, this could further offer protection in OA. The hormone calcitonin, which signals via a GPCR (the calcitonin receptor), has been shown to be protective against cartilage degradation in a cAMP-dependent mechanism[373]. *MMP* expression following TNF+OSM cytokine stimulation in bovine articular cartilage explant culture was found to be attenuated by cAMP[373]. It has been suggested that cAMP has anti-inflammatory properties in arthritic diseases[374], and indeed PKA (a downstream target of cAMP) activity has recently been found to be reduced in OA[367]. Interestingly, pathway analysis of global gene expression changes following canonical PAR2 activation in chapter 7 of this study found PKA activity to be reduced further suggesting links between PAR2 activation and previously described outcomes of OA.

Although cathepsin S cleavage of PAR2 was not a novel observation, a role of cathepsin S cleavage of PAR2 in cartilage biology has not been explored previously. Cathepsin S cleavage of PAR2 is another strong candidate for a pathological mechanism in OA, as cathepsin S has well established extracellular roles where it is considered the most stable cathepsin at neutral pH levels[168]. Cathepsin S activity has been detected in OA cartilage[191], and secreted cathepsin S following TNFα or IL-1β stimulation of chondrocytes has been described[190]. Based on data presented in this study, it is likely cathepsin S and L would exert similar signalling and disarming outcomes.

Of the cathepsin enzymes studied, cathepsin K exhibited a markedly different cleavage profile of PAR2. Despite also being a lysosomal cathepsin protease, cathepsin K is best described as an extracellular-localised ECM degrading protease, and a potent collagenase vital in bone remodelling[160]. The observation that cathepsin K can cleave PAR2 is a

fascinating discovery as cathepsin K has been linked to OA with cathepsin K degradation of type II collagen being detected in human OA cartilage[184]. This provides evidence for the presence of active cathepsin K in the correct compartment for activity against PAR2. The outcomes of cathepsin K cleavage of PAR2 are currently unknown, however work presented in chapter 6 with the putative activator peptide suggests that canonical PAR2 signalling is not induced. Cathepsin K was found to cleave downstream of the canonical activation site, therefore it is likely that disarming would occur against canonical activation. However, it remains to be elucidated whether cathepsin K can act as a disarmer experimentally, or whether cathepsin K can act as a biased agonist for PAR2 responses. Cathepsin K has also been implicated in a wide array of cancers with a variety of suggested roles, which are generally detrimental such as the enabling of tumour metastasis[375], a role generally attributed to collagenase activity. The observation that cathepsin K can cleave PAR2 could therefore have wider implications outside of arthritic diseases.

Data presented in chapter 4 identified the classical collagenases, MMP-1, -8 and -13 as having the ability to cleave PAR2. Further work presented in chapter 5 identified an MMP-specific cleavage site on PAR2, a single amino acid downstream of the canonical site, after leucine-37. Studies performed on the putative activator peptide, LIGKVD, suggested that cleavage at this site could result in biased agonism. The only signalling pathway identified as being stimulated by this ligand was the phosphorylation of ERK1/2.

Despite ERK1/2 signalling known to be important in *MMP1* expression[320], LIGKVD was unable to stimulate *MMP1* expression in the present study. The signalling outcomes following LIGKVD-mediated ERK1/2 phosphorylation remain to be elucidated. The activation of ERK1/2 signalling is a fairly ubiquitous event following receptor activation, and in terms of PAR2 activation, multiple pathways have been identified as being able to stimulate ERK1/2 phosphorylation, with a wide range of potential outcomes for cell behaviour. ERK1/2 phosphorylation has been identified as a downstream pathway of Gα-dependent pathways (Gαq, $G\alpha_{12/13,}$ Gαs); Gβγ-dependent pathways and G protein-independent pathways[200,204,225,227].

It is difficult to speculate the potential roles of MMP-mediated PAR2 “activation”, however, it is unlikely to be positive feedback based on the lack of *MMP1* expression following LIGKVD stimulation. ERK1/2 is involved in a variety of cellular functions,

and has been associated with generally pro-inflammatory processes, however anti-inflammatory roles for ERK1/2 have also been identified[376,377]. With respect to PAR2 biology, ERK1/2 is thought to be important in the internalisation of the receptor following activation in a β-arrestin-dependent manner, however this was found to also involve Gαq activation and associated Ca^{2+} mobilisation not observed in the present study[378]. Neutrophil elastase has been identified as a biased agonist able to stimulate ERK1/2 phosphorylation, but not Ca^{2+} mobilisation[225]. However, this neutrophil elastase-mediated PAR2 biased agonism was suggested to be a result of receptor conformational change following cleavage, whereas in the present study the biased signalling observed with LIGKVD is unlikely to result from a receptor conformational change as the receptor likely remains intact. Depending on the mechanism of ERK1/2 activation by PAR2, cellular localisation can be regulated. For example, when interacting with β-arrestin, ERK1/2 activity is retained within the cytoplasm, whereas in the absence of β-arrestin, ERK1/2 is able to translocate to the nucleus[378], thus ERK1/2 has the potential to regulate different targets. It is therefore of vital importance to further elucidate the regulation of ERK1/2 by LIGKVD/active MMP in order to begin to understand an outcome for the cleavage.

In addition to the lack of evidence for a potential positive feedback situation by the putative MMP revealed ligand LIGKVD, data presented in chapter 5 highlighted the possibility that MMPs might be antagonistic to canonical PAR2 activation by blocking matriptase from cleaving PAR2. These experiments were performed with recombinant non-catalytic domains of MMP-1 and MMP-13, however there appeared to be a modest blocking effect. It would be of interest to explore whether full-length MMP can block PAR2 activation by matriptase. Matriptase is a very potent activator of PAR2 which results in expression of *MMP1* and *MMP13*, both potent collagenases. All these proteins have been implicated in OA, and if the disease pathogenesis were as simple as this mechanism, then one could hypothesise a rapid disease progression. OA is however generally described as a slowly progressing disease[24]; thus the underlying pathological mechanisms are likely much more complex. Within simplistic pathogenic pathways such as the matriptase-PAR2-MMP axis, it is likely that additional levels of regulation are present and yet to be elucidated. Work presented in this thesis such as the cleavage of PAR2 by the collagenases, and the antagonism of PAR2 activation by MMP-1 and MMP-13 CTDs, potentially provides indications of some of these unknown levels of regulation, and warrants further investigation.

8.4 Future Work

8.4.1 Mechanical Loading of Chondrocytes

- Work presented in this chapter provided no evidence that mechanical loading is a regulator of matriptase expression, however did show regulation of pro-inflammatory genes such as *CSRNP*, *ATF3* and *EGR2*. There were however severe limitations in the system, namely the cells had limited viability following loading. Furthermore, the loading regimens were not very physiological, nor was the "matrix" that the cells were cultured in. There were sufficient results from this chapter however to warrant future work in the field of mechanical loading of chondrocytes. A better system to explore the mechanical loading of chondrocytes would be one which applies mechanical load directly to cartilage in explant culture, as the cells will have a physiological matrix to transmit mechanical signals, and more physiological loads could be utilised.

8.4.2 Serine protease cleavage of PAR2

- Data presented in chapter 4 identified the serine proteases HTRA1 and uPA as having the ability to cleave PAR2. Constraints with reagents and time meant that these cleavages were not further explored. Both proteases have been implicated in OA, and are known to partake in extracellular proteolysis and indeed uPA is already known to induce cell signalling by binding its receptor uPAR. A further exploration of these proteases and their role in PAR2 cleavage would therefore be of interest.

8.4.3 The role of MMP-mediated PAR2 cleavage

- The putative MMP cleavage revealed ligand LIGKVD was identified as a biased agonist for PAR2, able to stimulate ERK1/2 phosphorylation. It is therefore vital to firstly explore whether active MMP is able to induce ERK1/2 phosphorylation when added to cell culture.

- LIGKVD was unable to induce calcium mobilisation, therefore the ERK1/2 activation is unlikely to be a result of Gαq-coupled PAR2 activation and subsequent ERK activation by PKC[379] or calcium[380]. ERK signalling however has

multiple activators which are known to be targets of PAR2, such as Gαs, Gαi, Gαs, $G\alpha_{12/13}$, βγ subunit and β-arrestin signalling[381]. It would therefore be of interest to ascertain which pathways are required for the observed LIGVKD-induced ERK1/2 activation.

- In line with deducing the pathway by which LIGKVD signals, and working under the assumption that active MMP also activates ERK signalling, it is of interest to ascertain the signalling outcomes of MMP-mediated PAR2 activation and explore whether there is a more negative feedback situation of anti-inflammatory outcomes, or whether there is a positive feedback situation of more pro-inflammatory outcomes.

- Experiments performed with the pre-incubation of MMP CTD on PAR2-expressing cells suggested the potential for a blocking effect by MMP-1 and MMP-13 CTDs on matriptase-induced PAR2 activation. This potential antagonistic action of MMP CTD warrants further investigation with full-length MMP including a catalytically inactive enzyme.

8.4.4 The role of cathepsin-mediated PAR2 cleavage

- Cathepsin V was able to disarm against matriptase-induced canonical activation of PAR2, however as discussed in chapter 6, cathepsin V is unlikely to hold a great deal of physiological relevance in cartilage biology and OA. Cathepsin V was used for these assays primarily due to availability of sufficient recombinant enzyme, however cathepsins S and L are likely more relevant. Furthermore, cathepsin B has associations with OA, and also cleaved multiple downstream sites to the canonical site thus is a candidate for being a PAR2 disarmer in cartilage. Therefore, future work testing the ability for cathepsins L, S and B to disarm against canonical PAR2 activation would be of great interest.

- Cathepsin S is described as a biased agonist in the literature (able to induce Gαs-mediated cAMP accumulation)[365]. Data presented in chapter 6 showed that cathepsin V, and to some extent cathepsin L, have similar cleavage profiles to cathepsin S. It would therefore be of interest to explore whether cathepsins V and L are able to act as biased agonists for cAMP accumulation.

- Cathepsin K primarily cleaved at a distinct site to the other cathepsin enzymes, at a location which makes it a candidate for either biased agonism or disarming. The putative activator peptide (KVDGTS) did not induce calcium mobilisation, however this is not sufficient to conclude the peptide has no effect (as shown by data in chapter 5 with the LIGKVD peptide). Future work would therefore require the exploration of other signalling pathways known to be regulated by PAR2. Furthermore, for a greater level of physiological relevance, the addition of active cathepsin K would need to be tested on cells and compared with KVDGTS.

8.4.5 Exploration of canonical PAR2 activation in chondrocytes

- It is known that matriptase-induced PAR2 activation in chondrocytes leads to an upregulation of collagenase (*MMP1* and *MMP13*) expression, however little is currently known about the signalling pathways involved. This study identified several downstream targets of PAR2 activation which are also downstream targets of IL-1+OSM stimulation of chondrocytes. It is therefore of interest to further examine these and explore whether they are required for collagenase expression. For example, experiments such as siRNA knockdown of ATF3, EGR2 and CSRNP1 prior to matriptase stimulation of cells would be interesting to perform.

- Studies in chapter 3 was performed in bovine nasal chondrocytes, whereas the microarray in chapter 7 was performed in human SW1353 cells. Previous investigation with IL-1+OSM was performed in human articular chondrocytes (HAC). Despite, ATF3, EGR2 and CSRNP1 being regulated in all three cell types, for direct comparison, all studies should be performed on a single cell type. As HAC represent the most physiologically relevant cell, the regulation of these effectors following PAR2 activation or mechanical loading should be explored in them.

8.5 Summary

Data presented in this thesis identified several novel cleavages of PAR2 by proteases from the metalloproteinase family (the collagenases: MMP-1, -8 and -13), the cysteine protease family (cathepsin V, K, L and B) and the serine protease family (HTRA1, uPA). The collagenases were found to cleave PAR2 at a specific site, a single amino acid C-terminal to the canonical activation site, to reveal a putative ligand, LIGKVD. When added to cells as a synthetic peptide, LIGKVD could induce biased signalling in PAR2-overexpressing SW1353 cells as measured by the phosphorylation of ERK1/2, but not p38 MAPK, both of which are phosphorylated by canonical PAR2 activation. The cathepsins cleaved at multiple sites, however primary sites after glutamic acid-56 for cathepsins V and L, and after glycine-40 for cathepsin K, were identified.

A gene expression microarray was performed exploring canonical PAR2 activation in SW1353 cells following matriptase stimulation. It was clear that the signalling outcomes were pro-inflammatory in nature, with significant overlap with other pathways known to be involved in OA. Some of the most up-regulated genes included *ATF3*, *EGR2* and *CSRNP1*, which had already been identified as mechanosensitive in this project, and identified as key regulators of collagenase expression following IL-1+OSM stimulation by previous study. Data presented in this thesis suggest that disparate stimuli all appear to have some common downstream elements that facilitate *MMP* expression. Further elucidation of the signalling networks involved could highlight novel therapeutic targets for the treatment of OA.

Appendix 1: Known PAR2 cleavages

Protein	Gene	Site	Cleavage sequence	Evidence	Reference
kallikrein-related peptidase 5	*KLK5*	31	G-T-N-R↓S-S-K-G	SP, RE, MS	210
kallikrein-related peptidase 6	*KLK6*	36	S-K-G-R↓S-L-I-G	SP, RE, MS	210
		41	L-I-G-K↓V-D-G-T	SP, RE, MS	210
		51	V-T-G-K↓G-V-T-V	SP, RE, MS	210
kallikrein-related peptidase 14	*KLK14*	31	G-T-N-R↓S-S-K-G	SP, RE, MS	210
		36	S-K-G-R↓S-L-I-G	SP, RE, MS	210
		41	L-I-G-K↓V-D-G-T	SP, RE, MS	210
		51	V-T-G-K↓G-V-T-V	SP, RE, MS	210
Trypsin 1	*PRSS1*	34	R-S-S-K↓G-R-S-L	rPAR2, RE, MS	301
		36	S-K-G-R↓S-L-I-G	rPAR2, RE, MS	301
		41	L-I-G-K↓V-D-G-T	SP, RE, MS	210
		51	V-T-G-K↓G-V-T-V	rPAR2, RE, MS	301
		72	L-T-G-K↓L-T-T-V	rPAR2, RE, MS	301
Plasmin	*PLG*	34	R-S-S-K↓G-R-S-L	rPAR2, RE, MS	301
		36	S-K-G-R↓S-L-I-G	rPAR2, RE, MS	301
Tryptase alpha/beta-1	*TPSAB1*	36	S-K-G-R↓S-L-I-G	SP, RE, MS	206
		41	L-I-G-K↓V-D-G-T	SP, RE, MS	206
Thrombin	*F2*	36	S-K-G-R↓S-L-I-G	rPAR2, RE, MS	301
Matriptase	*ST14*	36	S-K-G-R↓S-L-I-G		
Coagulation factor X	*F10*	36	S-K-G-R↓S-L-I-G	SDM, RE	127
Coagulation factor VII	*F7*	36	S-K-G-R↓S-L-I-G	SDM, RE	127
Trypsin IV/mesotrypsin	*PRSS3*	36	S-K-G-R↓S-L-I-G	SP, RE, MS	207
Cathepsin G	*CTSG*	38	G-R-S-L↓I-G-K-V	rPAR2, RE, MS	301
		59	E-T-V-F↓S-V-D-E	rPAR2, RE, MS	301
		64	V-D-E-F↓S-A-S-V	SP, rPAR2, RE, MS	225,301
Neutrophil Elastase	*ELANE*	42	I-G-K-V↓D-G-T-S	rPAR2, RE, MS	301
		48	T-S-H-V↓T-G-K-G	rPAR2, RE, MS	301
		53	G-K-G-V↓T-V-E-T	rPAR2, RE, MS	301
		58	V-E-T-V↓F-S-V-D	rPAR2, RE, MS	301
		67	F-S-A-S↓V-L-T-G	SP, RE, MS	225

		74	G-K-L-T↓T-V-F-L	rPAR2, RE, MS	301
		76	L-T-T-V↓F-L-P-I	rPAR2, RE, MS	301
Calpain 1	*CAPN1*	59	E-T-V-F↓S-V-D-E	rPAR2, RE, MS	301
Calpain 2	*CAPN2*	45	V-D-G-T↓S-H-V-T	rPAR2, RE, MS	301
		71	V-L-T-G↓K-L-T-T	rPAR2, RE, MS	301
Proteinase 3	*PRTN3*	48	T-S-H-V↓T-G-K-G	rPAR2, RE, MS	301
		55	G-V-T-V↓E-T-V-F	rPAR2, RE, MS	301
		57	T-V-E-T↓V-F-S-V	rPAR2, RE, MS	301
		61	V-F-S-V↓D-E-F-S	SP, rPAR2, RE, MS	225,301
		62	F-S-V-D↓E-F-S-A	rPAR2, RE, MS	301
		72	L-T-G-K↓L-T-T-V	rPAR2, RE, MS	301
		74	G-K-L-T↓T-V-F-L	rPAR2, RE, MS	301
		75	K-L-T-T↓V-F-L-P	rPAR2, RE, MS	301
		76	L-T-T-V↓F-L-P-I	rPAR2, RE, MS	301
Interstitial collagenase	*MMP1*	N/A	N/A	Indirect: MMP-1 addition to A549 cells with PAR2 antagonist	303
Chitinase-3-like protein 1	*CHI3L1*	N/A	N/A	Indirect: cell response with PAR2 blocking antibody	382
Cathepsin S		56	V-T-V-E↓T-V-F-S	SP, RE, MS	226
		38	G-R-S-L↓I-G-K-V	SP, RE, MS	300
		40	S-L-I-G↓K-V-D-G	SP, RE, MS	300

rPAR2 = recombinant PAR2, SP = synthetic peptide, RE = recombinant enzyme, MS = mass spectrometry, SDM = site-directed mutagenesis

Appendix 2: Example Mass Spectometry Traces

Electrospray MS: MMP1 - Ser-37 / Leu-38

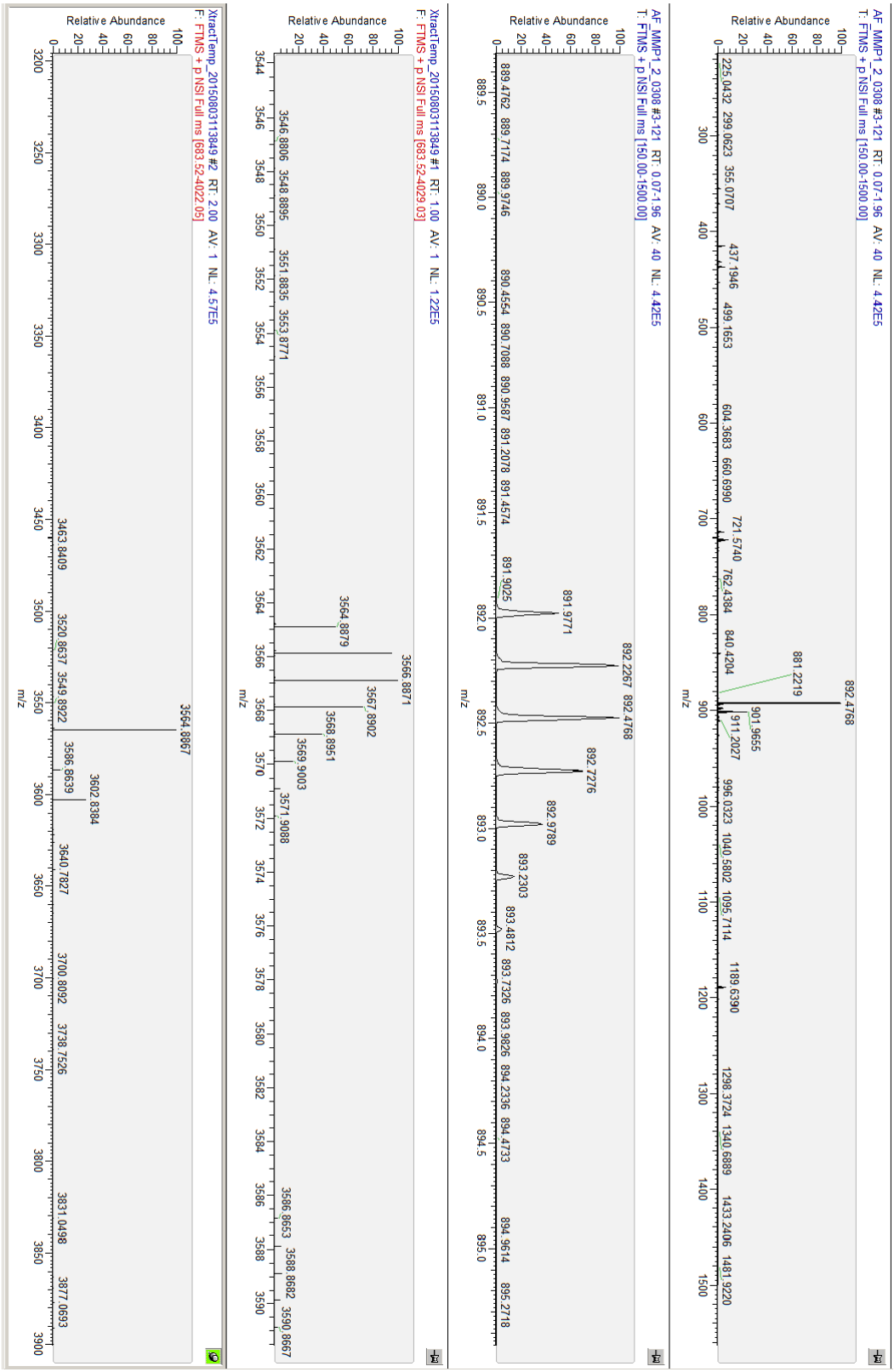

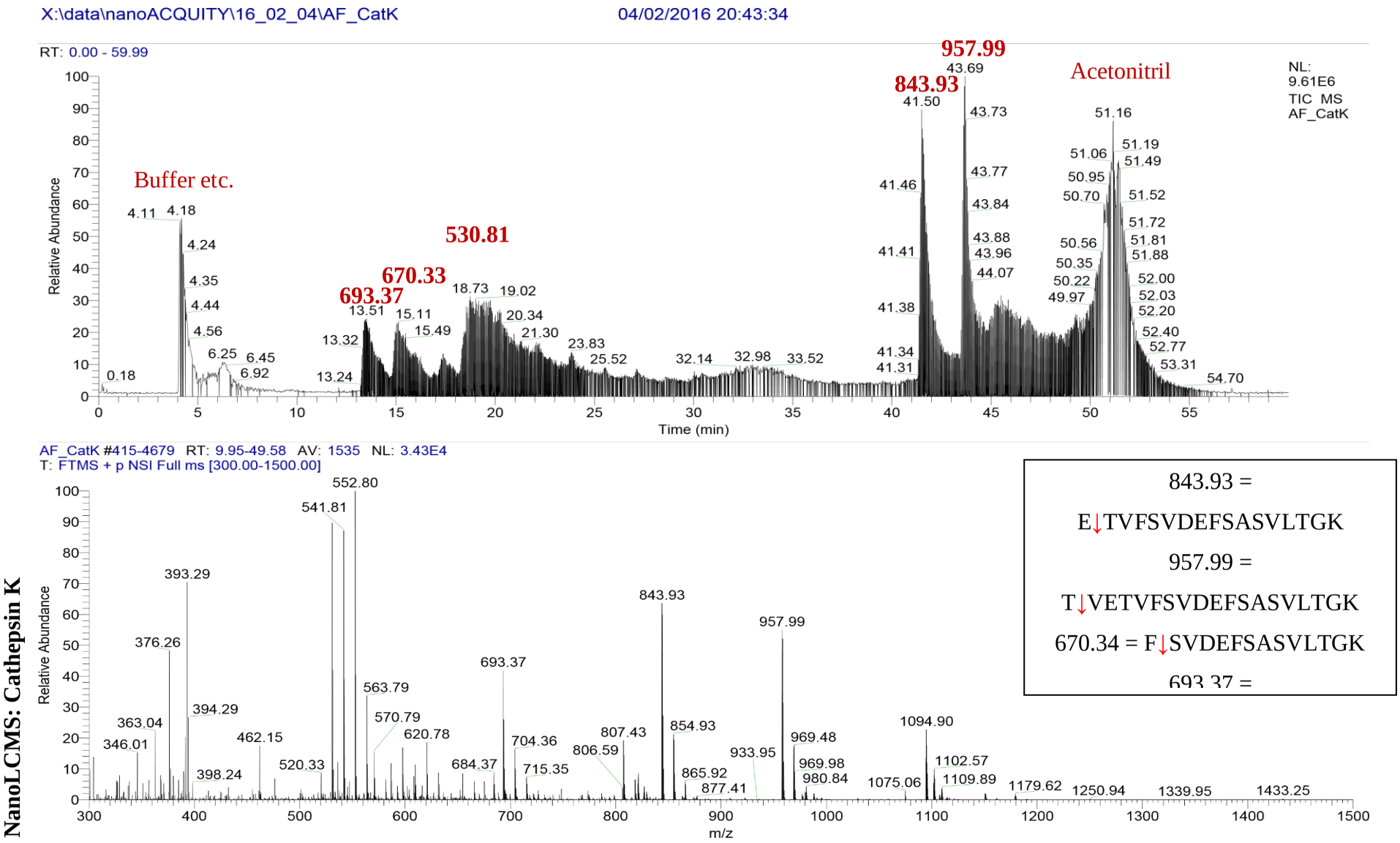

843.93 =

E↓TVFSVDEFSASVLTGK

957.99 =

T↓VETVFSVDEFSASVLTGK

670.34 = F↓SVDEFSASVLTGK

693.37 =

NanoLCMS: Cathepsin K

Appendix 3: Active-site titrations

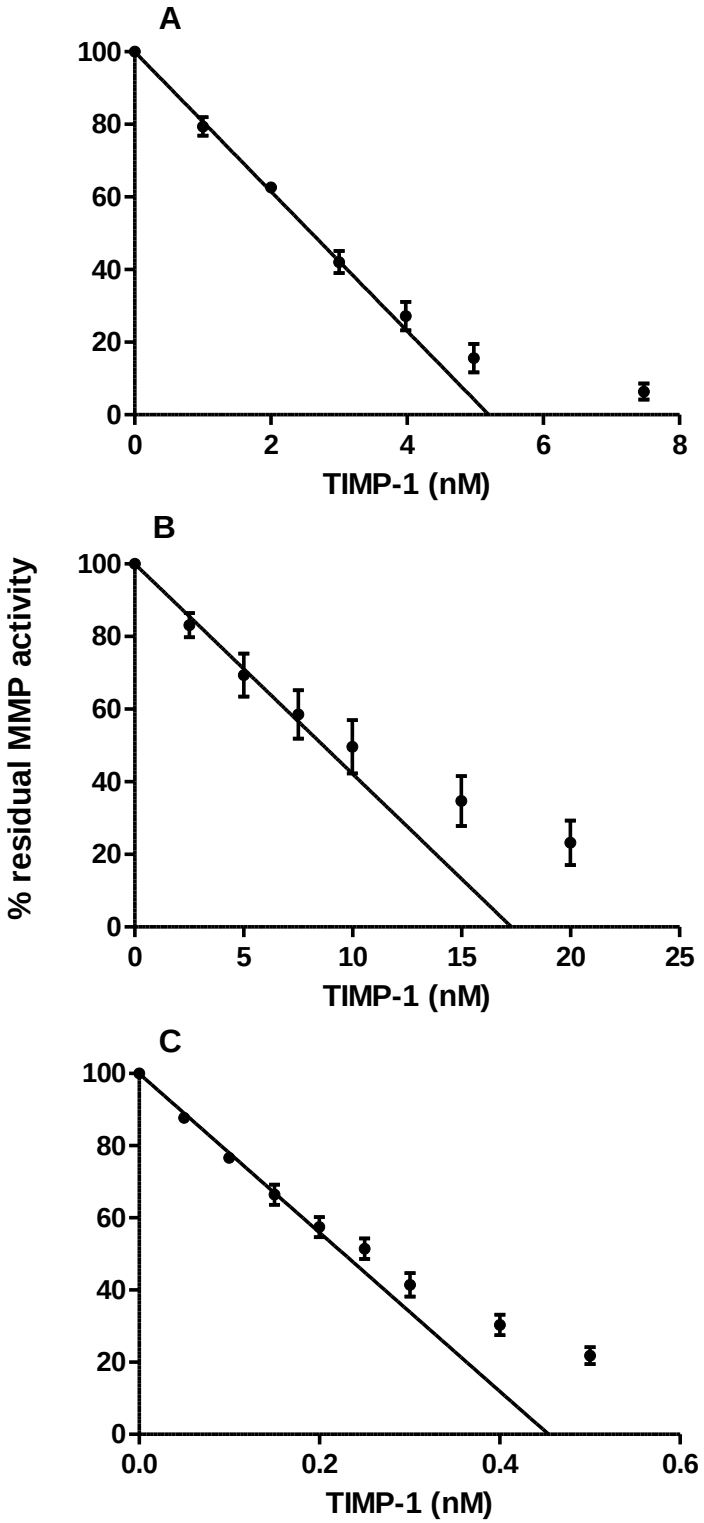

Appendix 3.1: MMP active-site titration
MMP-1 (A), MMP-8 (B) and MMP-13 (C) were active-site titrated by TIMP-1 as outlined in chapter 2.15.5.2. Curves shown are n=2 independent experiments, mean ± SD.

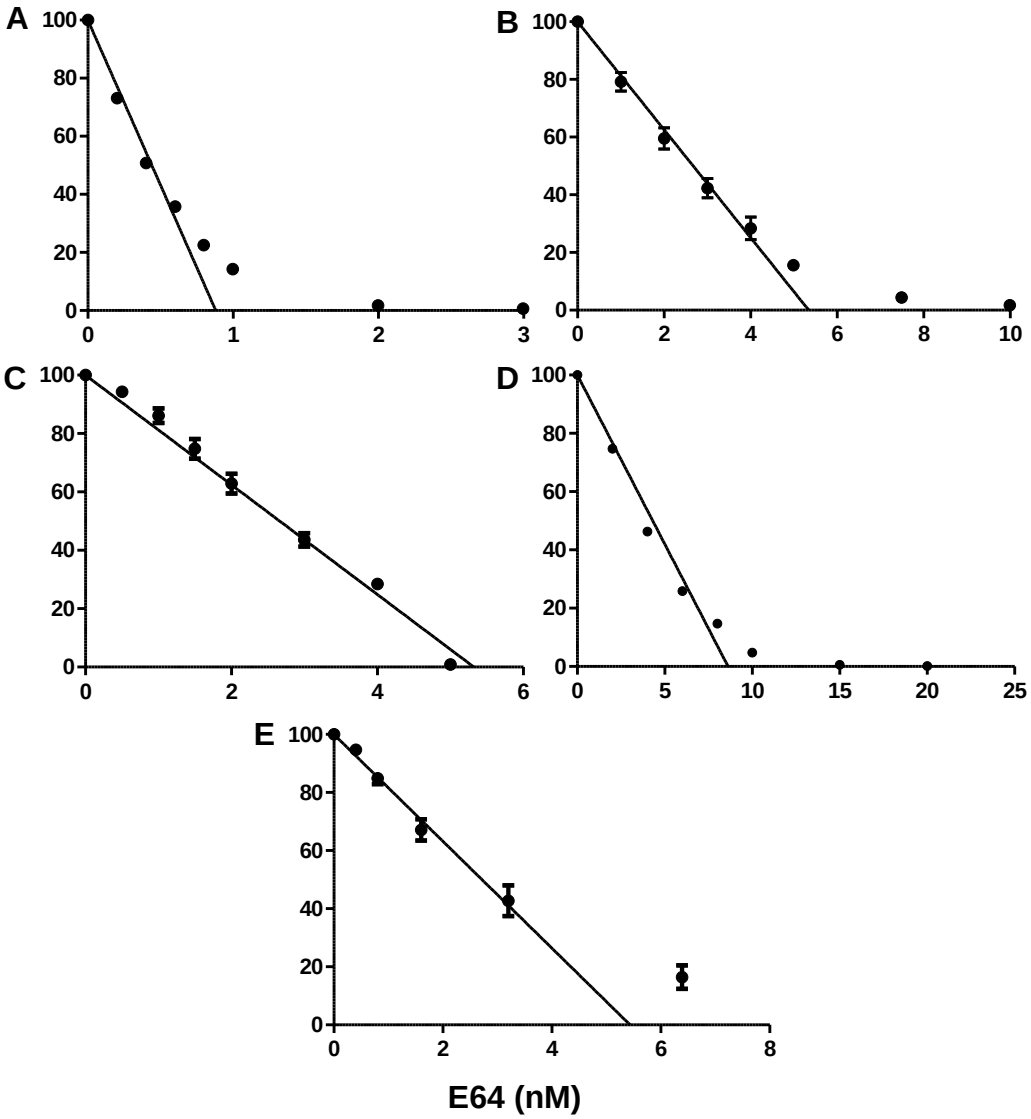

Appendix 3.2: MMP active-site titration
Cathepsins B (A), K (B), V (C), S (D) and L (E) were active-site titrated by E64 as outlined in chapter 2.15.5.1. Curves shown are n=2 independent experiments, mean ± SD.

Appendix 4: Example of raw enzyme kinetic data

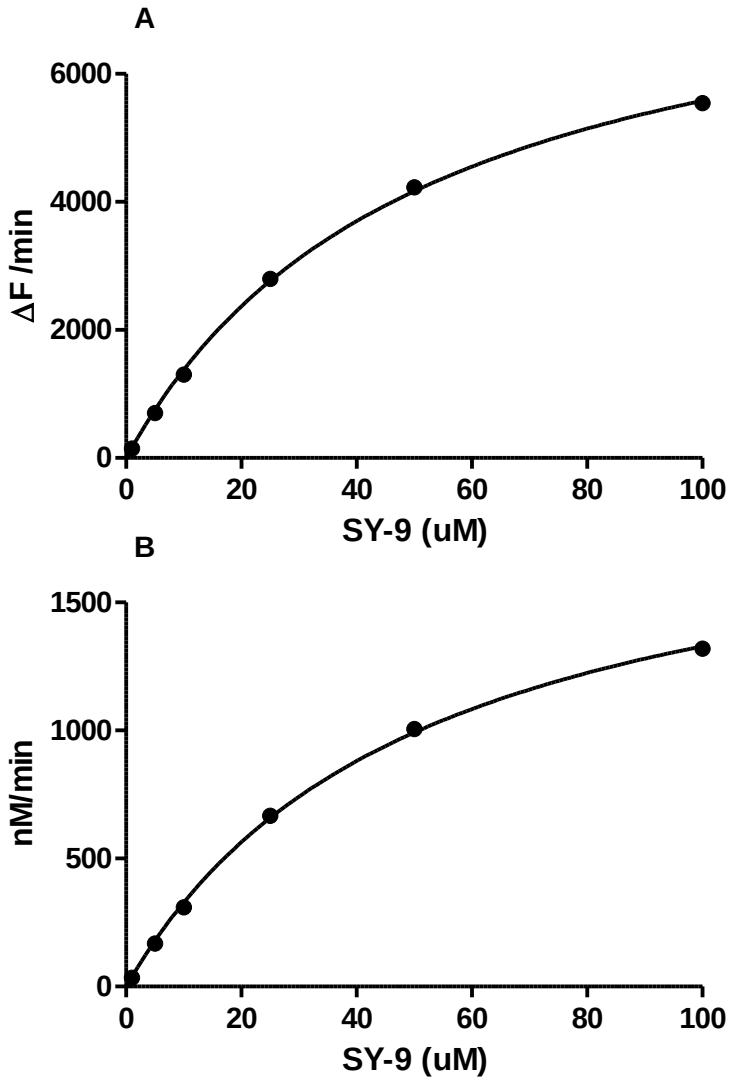

Appendix 4.1: Example of raw fluorescence data
Data showing the same enzyme assay before (A) and after (B) using a total hydrolysis standard curve to calculate substrate turnover, and thus subsequently being able to perform Michaelis-Menten kinetics.

References

1 Milner, J. M., Patel, A., Davidson, R. K., Swingler, T. E., Desilets, A., Young, D. A., Kelso, E. B., Donell, S. T., Cawston, T. E., Clark, I. M., Ferrell, W. R., Plevin, R., Lockhart, J. C., Leduc, R. & Rowan, A. D. Matriptase Is a Novel Initiator of Cartilage Matrix Degradation in Osteoarthritis. *Arthritis and Rheumatism* **62**, 1955-1966, doi:10.1002/art.27476 (2010).

2 Roughley, P. J. The structure and function of cartilage proteoglycans. *European Cells & Materials* **12**, 92-101 (2006).

3 Barbara, Y., Lowe, J. S., Stevens, A. & Heath, J. W. *Wheater's Functional Histology*. Fifth edn, (Elsevier, 2006).

4 Halloran, J. P., Sibole, S., van Donkelaar, C. C., van Turnhout, M. C., Oomens, C. W. J., Weiss, J. A., Guilak, F. & Erdemir, A. Multiscale Mechanics of Articular Cartilage: Potentials and Challenges of Coupling Musculoskeletal, Joint, and Microscale Computational Models. *Annals of Biomedical Engineering* **40**, 2456-2474, doi:10.1007/s10439-012-0598-0 (2012).

5 Heinegard, D. Proteoglycans and more - from molecules to biology. *International Journal of Experimental Pathology* **90**, 575-586, doi:10.1111/j.1365-2613.2009.00695.x (2009).

6 Buckwalter, J. A., Mow, V. C. & A, R. Restoration of Injured or Degenerated Articular Cartilage. *Journal of the American Academy of Orthopaedic Surgeons* **2**, 192-201 (1994).

7 Poole, C. A. Articular cartilage chondrons: Form, function and failure. *Journal of Anatomy* **191**, 1-13, doi:10.1046/j.1469-7580.1997.19110001.x (1997).

8 Fosang, A. J. & Beier, F. Emerging Frontiers in cartilage and chondrocyte biology. *Best Practice & Research in Clinical Rheumatology* **25**, 751-766, doi:10.1016/j.berh.2011.11.010 (2011).

9 Archer, C. W. & Francis-West, P. The chondrocyte. *International Journal of Biochemistry & Cell Biology* **35**, 401-404, doi:10.1016/s1357-2725(02)00301-1 (2003).

10 van der Kraan, P. M. & van den Berg, W. B. Chondrocyte hypertrophy and osteoarthritis: role in initiation and progression of cartilage degeneration? *Osteoarthritis and Cartilage* **20**, 223-232, doi:10.1016/j.joca.2011.12.003 (2012).

11 Murphy, G. & Nagase, H. Reappraising metalloproteinases in rheumatoid arthritis and osteoarthritis: destruction or repair? *Nature Clinical Practice Rheumatology* **4**, 128-135, doi:10.1038/ncprheum0727 (2008).

12 Verzijl, N., DeGroot, J., Thorpe, S. R., Bank, R. A., Shaw, J. N., Lyons, T. J., Bijlsma, J. W. J., Lafeber, F., Baynes, J. W. & TeKoppele, J. M. Effect of collagen turnover on the accumulation of advanced glycation end products. *Journal of Biological Chemistry* **275**, 39027-39031, doi:10.1074/jbc.M006700200 (2000).

13 Thomas, L. Reversible collapse of rabbit ears after intravenous papain, and prevention of recovery by cortisone. *The Journal of experimental medicine* **104**, 245-252, doi:10.1084/jem.104.2.245 (1956).

14 Shoulders, M. D. & Raines, R. T. in *Annual Review of Biochemistry* Vol. 78 *Annual Review of Biochemistry* 929-958 (2009).

15 Fields, G. B. Interstitial Collagen Catabolism. *Journal of Biological Chemistry* **288**, 8785-8793, doi:10.1074/jbc.R113.451211 (2013).

16 Ikenoue, T., Trindade, M. C. D., Lee, M. S., Lin, E. Y., Schurman, D. J., Goodman, S. B. & Smith, R. L. Meehanoregulation of human articular chondrocyte aggrecan and type II collagen expression by intermittent hydrostatic

pressure in vitro. *Journal of Orthopaedic Research* **21**, 110-116, doi:10.1016/s0736-0266(02)00091-8 (2003).

17 Valhmu, W. B., Stazzone, E. J., Bachrach, N. M., Saed-Nejad, F., Fischer, S. G., Mow, V. C. & Ratcliffe, A. Load-controlled compression of articular cartilage induces a transient stimulation of aggrecan gene expression. *Archives of Biochemistry and Biophysics* **353**, 29-36, doi:10.1006/abbi.1998.0633 (1998).

18 Manninen, P., Riihimaki, H., Heliovaara, M. & Suomalainen, O. Physical exercise and risk of severe knee osteoarthritis requiring arthroplasty. *Rheumatology* **40**, 432-437, doi:10.1093/rheumatology/40.4.432 (2001).

19 Roos, E. M. & Dahlberg, L. Positive effects of moderate exercise on glycosaminoglycan content in knee cartilage - A four-month, randomized controlled trial in patients at risk of osteoarthritis. *Arthritis and Rheumatism* **52**, 3507-3514, doi:10.1002/art.21415 (2005).

20 Loening, A. M., James, I. E., Levenston, M. E., Badger, A. M., Frank, E. H., Kurz, B., Nuttall, M. E., Hung, H. H., Blake, S. M., Grodzinsky, A. J. & Lark, M. W. Injurious mechanical compression of bovine articular cartilage induces chondrocyte apoptosis. *Archives of Biochemistry and Biophysics* **381**, 205-212, doi:10.1006/abbi.2000.1988 (2000).

21 Sun, H. B. in *Molecular and Integrative Physiology of the Musculoskeletal System* Vol. 1211 *Annals of the New York Academy of Sciences* (eds J. I. Mechanick, L. Sun, & M. Zaidi) 37-50 (2010).

22 Blain, E. J. Mechanical regulation of matrix metalloproteinases. *Frontiers in Bioscience* **12**, 507-527, doi:10.2741/2078 (2007).

23 McInnes, I. B. & Schett, G. The Pathogenesis of Rheumatoid Arthritis. *New England Journal of Medicine* **365**, 2205-2219 (2011).

24 Goldring, M. B. & Goldring, S. R. Osteoarthritis. *Journal of Cellular Physiology* **213**, 626-634, doi:10.1002/jcp.21258 (2007).

25 Felson, D. T., Lawrence, R. C., Dieppe, P. A., Hirsch, R., Helmick, C. G., Jordan, J. M., Kington, R. S., Lane, N. E., Nevitt, M. C., Zhang, Y., Sowers, M., McAlindon, T., Spector, T. D., Poole, A. R., Yanovski, S. Z., Ateshian, G., Sharma, L., Buckwalter, J. A., Brandt, K. D. & Fries, J. F. Osteoarthritis: new insights. Part 1: the disease and its risk factors. *Annals of internal medicine* **133**, 635-646 (2000).

26 Pratta, M. A., Yao, W. Q., Decicco, C., Tortorella, M. D., Liu, R. Q., Copeland, R. A., Magolda, R., Newton, R. C., Trzaskos, J. M. & Arner, E. C. Aggrecan protects cartilage collagen from proteolytic cleavage. *Journal of Biological Chemistry* **278**, 45539-45545, doi:10.1074/jbc.M303737200 (2003).

27 Hedlund, H., Hedbom, E., Heinegard, D., Mengarelli-Widholm, S., Reinholt, F. P. & Svensson, O. Association of the aggrecan keratan sulfate-rich region with collagen in bovine articular cartilage. *Journal of Biological Chemistry* **274**, 5777-5781, doi:10.1074/jbc.274.9.5777 (1999).

28 Maroudas, A. Balance between swelling pressure and collagen tension in normal and degenerate cartilage. *Nature* **260**, 808-809, doi:10.1038/260808a0 (1976).

29 Aigner, T. & McKenna, L. Molecular pathology and pathobiology of osteoarthritic cartilage. *Cellular and Molecular Life Sciences* **59**, 5-18, doi:10.1007/s00018-002-8400-3 (2002).

30 Hollander, A. P., Heathfield, T. F., Webber, C., Iwata, Y., Bourne, R., Rorabeck, C. & Poole, A. R. Increased damage to type II collagen in osteoarthritic articular cartilage detected by a new immunoassay. *Journal of Clinical Investigation* **93**, 1722-1732, doi:10.1172/jci117156 (1994).

31 Hollander, A. P., Pidoux, I., Reiner, A., Rorabeck, C., Bourne, R. & Poole, A. R. Damage to type II collagen in aging and osteoarthritis starts at the articular

surface, originates around chondrocytes, and extends into the cartilage with progressive degeneration. *Journal of Clinical Investigation* **96**, 2859-2869, doi:10.1172/jci118357 (1995).

32 Kiani, C., Chen, L., Wu, Y. J., Yee, A. J. & Yang, B. B. Structure and function of aggrecan. *Cell Research* **12**, 19-32, doi:10.1038/sj.cr.7290106 (2002).

33 Fosang, A. J., Neame, P. J., Hardingham, T. E., Murphy, G. & Hamilton, J. A. Cleavage of cartilage proteoglycan between G1 and G2 domains by stromelysins. *Journal of Biological Chemistry* **266**, 15579-15582 (1991).

34 Fosang, A. J., Neame, P. J., Last, K., Hardingham, T. E., Murphy, G. & Hamilton, J. A. The interglobular domain of cartilage aggrecan is cleaved by PUMP, gelatinases, and cathepsin B. *Journal of Biological Chemistry* **267**, 19470-19474 (1992).

35 Fosang, A. J., Last, K., Knauper, V., Neame, P. J., Murphy, G., Hardingham, T. E., Tschesche, H. & Hamilton, J. A. Fibroblast and neutrophil collagenases cleave at two sites in the cartilage aggrecan interglobular domain. *Biochemical Journal* **295**, 273-276 (1993).

36 Fosang, A. J., Last, K., Knauper, V., Murphy, G. & Neame, P. J. Degradation of cartilage aggrecan by collagenase-3 (MMP-13). *Febs Letters* **380**, 17-20, doi:10.1016/0014-5793(95)01539-6 (1996).

37 Sandy, J. D., Flannery, C. R., Neame, P. J. & Lohmander, L. S. The structure of aggrecan fragments in human synovial fluid. Evidence for the involvement in osteoarthritis of a novel proteinase which cleaves the Glu 373-Ala 374 bond of the interglobular domain. *Journal of Clinical Investigation* **89**, 1512-1516, doi:10.1172/jci115742 (1992).

38 Hughes, C. E., Little, C. B., Buttner, F. H., Bartnik, E. & Caterson, B. Differential expression of aggrecanase and matrix metalloproteinase activity in chondrocytes isolated from bovine and porcine articular cartilage. *Journal of Biological Chemistry* **273**, 30576-30582, doi:10.1074/jbc.273.46.30576 (1998).

39 Tortorella, M. D., Burn, T. C., Pratta, M. A., Abbaszade, I., Hollis, J. M., Liu, R., Rosenfeld, S. A., Copeland, R. A., Decicco, C. P., Wynn, R., Rockwell, A., Yang, F., Duke, J. L., Solomon, K., George, H., Bruckner, R., Nagase, H., Itoh, Y., Ellis, D. M., Ross, H., Wiswall, B. H., Murphy, K., Hillman, M. C., Hollis, G. F., Newton, R. C., Magolda, R. L., Trzaskos, J. M. & Arner, E. C. Purification and cloning of aggrecanase-1: A member of the ADAMTS family of proteins. *Science* **284**, 1664-1666, doi:10.1126/science.284.5420.1664 (1999).

40 Hurskainen, T. L., Hirohata, S., Seldin, M. F. & Apte, S. S. ADAM-TS5, ADAM-TS6, and ADAM-TS7, novel members of a new family of zinc metalloproteases - General features and genomic distribution of the ADAM-TS family. *Journal of Biological Chemistry* **274**, 25555-25563, doi:10.1074/jbc.274.36.25555 (1999).

41 Stanton, H., Rogerson, F. M., East, C. J., Golub, S. B., Lawlor, K. E., Meeker, C. T., Little, C. B., Last, K., Farmer, P. J., Campbell, I. K., Fourie, A. M. & Fosang, A. J. ADAMTS5 is the major aggrecanase in mouse cartilage in vivo and in vitro. *Nature* **434**, 648-652, doi:10.1038/nature03417 (2005).

42 Glasson, S. S., Askew, R., Sheppard, B., Carito, B., Blanchet, T., Ma, H. L., Flannery, C. R., Peluso, D., Kanki, K., Yang, Z. Y., Majumdar, M. K. & Morris, E. A. Deletion of active ADAMTS5 prevents cartilage degradation in a murine model of osteoarthritis. *Nature* **434**, 644-648, doi:10.1038/nature03369 (2005).

43 Song, R.-H., Tortorella, M. D., Malfait, A.-M., Alston, J. T., Yang, Z., Arner, E. C. & Griggs, D. W. Aggrecan degradation in human articular cartilage explants is mediated by both ADAMTS-4 and ADAMTS-5. *Arthritis and Rheumatism* **56**, 575-585, doi:10.1002/art.22334 (2007).

44 Naito, S., Shiomi, T., Okada, A., Kimura, T., Chijiiwa, M., Fujita, Y., Yatabe, T., Komiya, K., Enomoto, H., Fujikawa, K. & Okada, Y. Expression of ADAMTS4 (aggrecanase-1) in human osteoarthritic cartilage. *Pathology International* **57**, 703-711, doi:10.1111/j.1440-1827.2007.02167.x (2007).

45 Perez-Silva, J. G., Espanol, Y., Velasco, G. & Quesada, V. The Degradome database: expanding roles of mammalian proteases in life and disease. *Nucleic Acids Research* **44**, D351-D355, doi:10.1093/nar/gkv1201 (2016).

46 Schechter, I. & Berger, A. On the size of the active site in proteases. I. Papain. *Biochemical and biophysical research communications* **27**, 157-162, doi:10.1016/s0006-291x(67)80055-x (1967).

47 Pelmenschikov, V., Blomberg, M. R. A. & Siegbahn, P. E. A theoretical study of the mechanism for peptide hydrolysis by thermolysin. *Journal of Biological Inorganic Chemistry* **7**, 284-298, doi:10.1007/s007750100295 (2002).

48 Erez, E., Fass, D. & Bibi, E. How intramembrane proteases bury hydrolytic reactions in the membrane. *Nature* **459**, 371-378, doi:10.1038/nature08146 (2009).

49 Bode, W., Gomisruth, F. X. & Stockler, W. Astacins, serralysins, snake venom and matrix metalloproteinases exhibit identical zinc-binding environments (HEXXHXXGXXH and Met-turn) and topologies and should be grouped into a common family, the metzincins. *Febs Letters* **331**, 134-140, doi:10.1016/0014-5793(93)80312-i (1993).

50 Tallant, C., Garcia-Castellanos, R., Baumann, U. & Xavier Gomis-Rueth, F. On the Relevance of the Met-turn Methionine in Metzincins. *Journal of Biological Chemistry* **285**, 13951-13957, doi:10.1074/jbc.M109.083378 (2010).

51 Huxley-Jones, J., Clarke, T.-K., Beck, C., Toubaris, G., Robertson, D. L. & Boot-Handford, R. P. The evolution of the vertebrate metzincins; insights from Ciona intestinalis and Danio rerio. *Bmc Evolutionary Biology* **7**, doi:10.1186/1471-2148-7-63 (2007).

52 Gross, J. & Lapiere, C. M. Collagenolytic activity in amphibian tissues : a tissue culture assay. *Proceedings of the National Academy of Sciences of the United States of America* **48**, 1014-1022, doi:10.1073/pnas.48.6.1014 (1962).

53 Nagase, H., Visse, R. & Murphy, G. Structure and function of matrix metalloproteinases and TIMPs. *Cardiovascular Research* **69**, 562-573, doi:10.1016/j.cardiores.2005.12.002 (2006).

54 Boire, A., Covic, L., Agarwal, A., Jacques, S., Sherifl, S. & Kuliopulos, A. PAR1 is a matrix metalloprotease-1 receptor that promotes invasion and tumorigenesis of breast cancer cells. *Cell* **120**, 303-313, doi:10.1016/j.cell.2004.12.018 (2005).

55 Aimes, R. T. & Quigley, J. P. Matrix metalloproteinase-2 is an interstitial collagenase. *Journal of Biological Chemistry* **270**, 5872-5876 (1995).

56 Bigg, H. F., Rowan, A. D., Barker, M. D. & Cawston, T. E. Activity of matrix metalloproteinase-9 against native collagen types I and III. *Febs Journal* **274**, 1246-1255, doi:10.1111/j.1742-4658.2007.05669.x (2007).

57 Van Wart, H. E. & Birkedal-Hansen, H. The cysteine switch: a principle of regulation of metalloproteinase activity with potential applicability to the entire matrix metalloproteinase gene family. *Proceedings of the National Academy of Sciences of the United States of America* **87**, 5578-5582 (1990).

58 Nagase, H., Enghild, J. J., Suzuki, K. & Salvesen, G. Stepwise activation mechanisms of the precursor of matrix metalloproteinase 3 (stromelysin) by proteinases and (4-aminophenyl)mercuric acetate. *Biochemistry* **29**, 5783-5789, doi:10.1021/bi00476a020 (1990).

59 Pei, D. Q. & Weiss, S. J. Furin-dependent intracellular activation of the human stromelysin-3 zymogen. *Nature* **375**, 244-247, doi:10.1038/375244a0 (1995).

60 Yana, I. & Weiss, S. J. Regulation of membrane type-1 matrix metalloproteinase activation by proprotein convertases. *Molecular Biology of the Cell* **11**, 2387-2401 (2000).
61 Rowan, A. D., Litherland, G. J., Hui, W. & Milner, J. M. Metalloproteases as potential therapeutic targets in arthritis treatment. *Expert Opinion on Therapeutic Targets* **12**, 1-18, doi:10.1517/14728222.12.1.1 (2008).
62 Milner, J. M., Rowan, A. D., Elliott, S. F. & Cawston, T. E. Inhibition of furin-like enzymes blocks interleukin-1 alpha/oncostatin M-stimulated cartilage degradation. *Arthritis and Rheumatism* **48**, 1057-1066, doi:10.1002/art.10873 (2003).
63 Fingleton, B. Matrix metalloproteinases as valid clinical targets. *Current Pharmaceutical Design* **13**, 333-346, doi:10.2174/138161207779313551 (2007).
64 Piccard, H., Van den Steen, P. E. & Opdenakker, G. Hemopexin domains as multifunctional liganding modules in matrix metal loproteinases and other proteins. *Journal of Leukocyte Biology* **81**, 870-892, doi:10.1189/jlb.1006629 (2007).
65 Troeberg, L. & Nagase, H. Proteases involved in cartilage matrix degradation in osteoarthritis. *Biochimica Et Biophysica Acta-Proteins and Proteomics* **1824**, 133-145, doi:10.1016/j.bbapap.2011.06.020 (2012).
66 Clark, I. M. & Cawston, T. E. Fragments of human fibroblast collagenase - Purification and characterization. *Biochemical Journal* **263**, 201-206 (1989).
67 Knauper, V., Osthues, A., Declerck, Y. A., Langley, K. E., Blaser, J. & Tschesche, H. Fragmentation of human polymorphonuclear-leucocyte collagenase. *Biochemical Journal* **291**, 847-854 (1993).
68 Knauper, V., Cowell, S., Smith, B., LopezOtin, C., Oshea, M., Morris, H., Zardi, L. & Murphy, G. The role of the c-terminal domain of human collagenase-3 (MMP-13) in the activation of procollagenase-3, substrate specificity, and tissue inhibitor of metalloproteinase interaction. *Journal of Biological Chemistry* **272**, 7608-7616 (1997).
69 Murphy, G., Allan, J. A., Willenbrock, F., Cockett, M. I., Oconnell, J. P. & Docherty, A. J. P. The role of the C-terminal domain in collagenase and stromelysin specificity. *Journal of Biological Chemistry* **267**, 9612-9618 (1992).
70 Hirose, T., Patterson, C., Pourmotabbed, T., Mainardi, C. L. & Hasty, K. A. Structure-function relationship of human neutrophil collagenase: identification of regions responsible for substrate specificity and general proteinase activity. *Proceedings of the National Academy of Sciences of the United States of America* **90**, 2569-2573, doi:10.1073/pnas.90.7.2569 (1993).
71 Harris, E. D., Jr., Cohen, G. L. & Krane, S. M. Synovial collagenase: its presence in culture from joint disease of diverse etiology. *Arthritis and rheumatism* **12**, 92-102, doi:10.1002/art.1780120206 (1969).
72 Welgus, H. G., Jeffrey, J. J. & Eisen, A. Z. The collagen substrate specificity of human skin fibroblast collagenase. *Journal of Biological Chemistry* **256**, 9511-9515 (1981).
73 Hasty, K. A., Jeffrey, J. J., Hibbs, M. S. & Welgus, H. G. The collagen substrate specificity of human neutrophil collagenase. *Journal of Biological Chemistry* **262**, 10048-10052 (1987).
74 Stremme, S., Duerr, S., Bau, B., Schmid, E. & Aigner, T. MMP-8 is only a minor gene product of human adult articular chondrocytes of the knee. *Clinical and Experimental Rheumatology* **21**, 205-209 (2003).
75 Shlopov, B. V., Lie, W. R., Mainardi, C. L., Cole, A. A., Chubinskaya, S. & Hasty, K. A. Osteoarthritic lesions - Involvement of three different collagenases. *Arthritis and Rheumatism* **40**, 2065-2074, doi:10.1002/art.1780401120 (1997).

76 Tetlow, L. C. & Woolley, D. E. Comparative immunolocalization studies of collagenase 1 and collagenase 3 production in the rheumatoid lesion, and by human chondrocytes and synoviocytes in vitro. *British Journal of Rheumatology* **37**, 64-70 (1998).

77 Lindy, O., Konttinen, Y. T., Sorsa, T., Ding, Y. L., Santavirta, S., Ceponis, A. & LopezOtin, C. Matrix metalloproteinase 13 (collagenase 3) in human rheumatoid synovium. *Arthritis and Rheumatism* **40**, 1391-1399, doi:10.1002/art.1780400806 (1997).

78 Knauper, V., LopezOtin, C., Smith, B., Knight, G. & Murphy, G. Biochemical characterization of human collagenase-3. *Journal of Biological Chemistry* **271**, 1544-1550 (1996).

79 Zhang, L., Yang, M., Yang, D., Cavey, G., Davidson, P. & Gibson, G. Molecular Interactions of MMP-13 C-Terminal Domain with Chondrocyte Proteins. *Connective Tissue Research* **51**, 230-239, doi:10.3109/03008200903288902 (2010).

80 Galasso, O., Familiari, F., De Gori, M. & Gasparini, G. Recent findings on the role of gelatinases (matrix metalloproteinase-2 and -9) in osteoarthritis. *Advances in orthopedics* **2012**, 834208-834208, doi:10.1155/2012/834208 (2012).

81 Mohtai, M., Smith, R. L., Schurman, D. J., Tsuji, Y., Torti, F. M., Hutchinson, N. I., Stetlerstevenson, W. G. & Goldberg, G. I. Expression of 92-kD type IV collagenase/gelatinase (gelatinase B) in osteoarthritic cartilage and its induction in normal human articular cartilage by interleukin *Journal of Clinical Investigation* **92**, 179-185, doi:10.1172/jci116547 (1993).

82 Soder, S., Roach, H. I., Oehler, S., Bau, B., Haag, J. & Aigner, T. MMP-9/gelatinase B is a gene product of human adult articular chondrocytes and increased in osteoarthritic cartilage. *Clinical and experimental rheumatology* **24**, 302-304 (2006).

83 Duerr, S., Stremme, S., Soeder, S., Bau, B. & Aigner, T. MMP-2/gelatinase A is a gene product of human adult articular chondrocytes and is increased in osteoarthritic cartilage. *Clinical and Experimental Rheumatology* **22**, 603-608 (2004).

84 Hulejova, H., Baresova, V., Klezl, Z., Polanska, M., Adam, M. & Senolt, L. Increased level of cytokines and matrix metalloproteinases in osteoarthritic subchondral bone. *Cytokine* **38**, 151-156, doi:10.1016/j.cyto.2007.06.001 (2007).

85 Poe, M., Stein, R. L. & Wu, J. K. High pressure gel-permeation assay for the proteolysis of human aggrecan by human stromelysin-1: kinetic constants for aggrecan hydrolysis. *Archives of Biochemistry and Biophysics* **298**, 757-759, doi:10.1016/0003-9861(92)90477-e (1992).

86 Bord, S., Horner, A., Hembry, R. M. & Compston, J. E. Stromelysin-1 (MMP-3) and stromelysin-2 (MMP-10) expression in developing human bone: Potential roles in skeletal development. *Bone* **23**, 7-12, doi:10.1016/s8756-3282(98)00064-7 (1998).

87 Kevorkian, L., Young, D. A., Darrah, C., Donell, S. T., Shepstone, L., Porter, S., Brockbank, S. M. V., Edwards, D. R., Parker, A. E. & Clark, I. M. Expression profiling of metalloproteinases and their inhibitors in cartilage. *Arthritis and Rheumatism* **50**, 131-141, doi:10.1002/art.11433 (2004).

88 Barksby, H. E., Milner, J. M., Patterson, A. M., Peake, N. J., Hui, W., Robson, T., Lakey, R., Middleton, J., Cawston, T. E., Richards, C. D. & Rowan, A. D. Matrix metalloproteinase 10 promotion of collagenolysis via procollagenase activation - Implications for cartilage degradation in arthritis. *Arthritis and Rheumatism* **54**, 3244-3253, doi:10.1002/art.22167 (2006).

89 Knauper, V., Murphy, G. & Tschesche, H. Activation of human neutrophil procollagenase by stromelysin 2. *European Journal of Biochemistry* **235**, 187-191, doi:10.1111/j.1432-1033.1996.00187.x (1996).
90 Chen, J.-J., Huang, J.-F., Du, W.-X. & Tong, P.-J. Expression and significance of MMP3 in synovium of knee joint at different stage in osteoarthritis patients. *Asian Pacific Journal of Tropical Medicine* **7**, 297-300, doi:10.1016/s1995-7645(14)60042-0 (2014).
91 Murphy, G. & Nagase, H. Localizing matrix metalloproteinase activities in the pericellular environment. *Febs Journal* **278**, 2-15, doi:10.1111/j.1742-4658.2010.07918.x (2011).
92 Lee, M. H., Rapti, M. & Murphy, G. Unveiling the surface Epitopes that render tissue inhibitor of metalloproteinase-1 inactive against membrane type 1-matrix metalloproteinase. *Journal of Biological Chemistry* **278**, 40224-40230, doi:10.1074/jbc.M305678200 (2003).
93 Edwards, D. R., Handsley, M. M. & Pennington, C. J. The ADAM metalloproteinases. *Molecular Aspects of Medicine* **29**, 258-289, doi:10.1016/j.mam.2008.08.001 (2008).
94 Zack, M. D., Malfait, A.-M., Skepner, A. P., Yates, M. P., Griggs, D. W., Hall, T., Hills, R. L., Alston, J. T., Nemirovskiy, O. V., Radabaugh, M. R., Leone, J. W., Arner, E. C. & Tortorella, M. D. ADAM-8 Isolated From Human Osteoarthritic Chondrocytes Cleaves Fibronectin at Ala(271). *Arthritis and Rheumatism* **60**, 2704-2713, doi:10.1002/art.24753 (2009).
95 Kerna, I., Kisand, K., Laitinen, P., Tamm, A. E., Kumm, J., Lintrop, M. & Tamm, A. O. Association of ADAM12-S protein with radiographic features of knee osteoarthritis and bone and cartilage markers. *Rheumatology International* **32**, 519-523, doi:10.1007/s00296-010-1717-6 (2012).
96 Bohm, B. B., Burkhardt, H., Aigner, T., Blobel, C. P. & Kalden, J. R. Upregulation of MDC15 (metargidin) mRNA in human osteoarthritic cartilage. *Arthritis and Rheumatism* **42**, S252-S252 (1999).
97 Bohm, B. B., Aigner, T., Roy, B., Brodie, T. A., Blobel, C. P. & Burkhardt, H. Homeostatic effects of the metalloproteinase disintegrin ADAM15 in degenerative cartilage remodeling. *Arthritis and Rheumatism* **52**, 1100-1109, doi:10.1002/art.20974 (2005).
98 Reiss, K. & Saftig, P. The "A Disintegrin And Metalloprotease" (ADAM) family of sheddases: Physiological and cellular functions. *Seminars in Cell & Developmental Biology* **20**, 126-137, doi:10.1016/j.semcdb.2008.11.002 (2009).
99 Roghani, M., Becherer, J. D., Moss, M. L., Atherton, R. E., Erdjument-Bromage, H., Arribas, J., Blackburn, R. K., Weskamp, G., Tempst, P. & Blobel, C. P. Metalloprotease-disintegrin MDC9: Intracellular maturation and catalytic activity. *Journal of Biological Chemistry* **274**, 3531-3540, doi:10.1074/jbc.274.6.3531 (1999).
100 Seals, D. F. & Courtneidge, S. A. The ADAMs family of metalloproteases: multidomain proteins with multiple functions. *Genes & Development* **17**, 7-30, doi:10.1101/gad.1039703 (2003).
101 Porter, S., Clark, I. M., Kevorkian, L. & Edwards, D. R. The ADAMTS metalloproteinases. *Biochemical Journal* **386**, 15-27, doi:10.1042/bj20040424 (2005).
102 Longpre, J.-M., McCulloch, D. R., Koo, B.-H., Alexander, J. P., Apte, S. S. & Leduc, R. Characterization of proADAMTS5 processing by proprotein convertases. *International Journal of Biochemistry & Cell Biology* **41**, 1116-1126, doi:10.1016/j.biocel.2008.10.008 (2009).

103 Gao, G., Plaas, A., Thompson, V. P., Jin, S., Zuo, F. R. & Sandy, J. D. ADAMTS4 (aggrecanase-1) activation on the cell surface involves C-terminal cleavage by glycosylphosphatidyl inositol-anchored membrane type 4-matrix metalloproteinase and binding of the activated proteinase to chondroitin sulfate and heparan sulfate on syndecan-1. *Journal of Biological Chemistry* **279**, 10042-10051, doi:10.1074/jbc.M312100200 (2004).

104 Flannery, C. R., Zeng, W. L., Corcoran, C., Collins-Racie, L. A., Chockalingam, P. S., Hebert, T., Mackie, S. A., McDonagh, T., Crawford, T. K., Tomkinson, K. N., LaVallie, E. R. & Morris, E. A. Autocatalytic cleavage of ADAMTS-4 (Aggrecanase-1) reveals multiple glycosaminoglycan-binding sites. *Journal of Biological Chemistry* **277**, 42775-42780, doi:10.1074/jbc.M205309200 (2002).

105 Gendron, C., Kashiwagi, M., Lim, N. H., Enghild, J. J., Thogersen, I. B., Hughes, C., Caterson, B. & Nagase, H. Proteolytic activities of human ADAMTS-5 - Comparative studies with ADAMTS-4. *Journal of Biological Chemistry* **282**, 18294-18306, doi:10.1074/jbc.M701523200 (2007).

106 Plaas, A., Osborn, B., Yoshihara, Y., Bai, Y., Bloom, T., Nelson, F., Mikecz, K. & Sandy, J. D. Aggrecanolysis in human osteoarthritis: confocal localization and biochemical characterization of ADAMTS5 - hyaluronan complexes in articular cartilages. *Osteoarthritis and Cartilage* **15**, 719-734, doi:10.1016/j.joca.2006.12.008 (2007).

107 Szabo, R. & Bugge, T. H. Type II transmembrane serine proteases in development and disease. *International Journal of Biochemistry & Cell Biology* **40**, 1297-1316, doi:10.1016/j.biocel.2007.11.013 (2008).

108 Miller, G. S. & List, K. The matriptase-prostasin proteolytic cascade in epithelial development and pathology. *Cell and Tissue Research* **351**, 245-253, doi:10.1007/s00441-012-1348-1 (2013).

109 Blow, D. M., Birktoft, J. J. & Hartley, B. S. Role of a buried acid group in the mechanism of action of chymotrypsin. *Nature* **221**, 337-340, doi:10.1038/221337a0 (1969).

110 Kraut, J. Serine Proteases: Structure and Mechanism of Catalysis. *Annual Review of Biochemistry* **46**, 331-358, doi:10.1146/annurev.bi.46.070177.001555 (1977).

111 List, K., Haudenschild, C. C., Szabo, R., Chen, W. J., Wahl, S. M., Swaim, W., Engelholm, L. H., Behrendt, N. & Bugge, T. H. Matriptase/MT-SP1 is required for postnatal survival, epidermal barrier function, hair follicle development, and thymic homeostasis. *Oncogene* **21**, 3765-3779, doi:10.1038/sj/onc/1205502 (2002).

112 List, K., Szabo, R., Wertz, P. W., Segre, J., Haudenschild, C. C., Kim, S. Y. & Bugge, T. H. Loss of proteolytically processed filaggrin caused by epidermal deletion of matriptase/MT-SP1. *Journal of Cell Biology* **163**, 901-910, doi:10.1083/jcb.200304161 (2003).

113 Basel-Vanagaite, L., Attia, R., Ishida-Yamamoto, A., Rainshtein, L., Ben Amitai, D., Lurie, R., Pasmanik-Chor, M., Indelman, M., Zvulunov, A., Saban, S., Magal, N., Sprecher, E. & Shohat, M. Autosomal recessive ichthyosis with hypotrichosis caused by a mutation in ST14, encoding type II transmembrane serine protease matriptase. *American Journal of Human Genetics* **80**, 467-477, doi:10.1086/512487 (2007).

114 Uhland, K. Matriptase and its putative role in cancer. *Cellular and Molecular Life Sciences* **63**, 2968-2978, doi:10.1007/s0018-006-6298-x (2006).

115 Takeuchi, T., Harris, J. L., Huang, W., Yan, K. W., Coughlin, S. R. & Craik, C. S. Cellular localization of membrane-type serine protease 1 and identification of protease-activated receptor-2 and single-chain urokinase-type plasminogen

activator as substrates. *Journal of Biological Chemistry* **275**, 26333-26342, doi:10.1074/jbc.M002941200 (2000).
116 Cho, E. G., Kim, M. G., Kim, C., Kim, S. R., Seong, I. S., Chung, C. H., Schwartz, R. H. & Park, D. N-terminal processing is essential for release of epithin, a mouse type II membrane serine protease. *Journal of Biological Chemistry* **276**, 44581-44589, doi:10.1074/jbc.M107059200 (2001).
117 Kim, C., Cho, Y. C., Kang, C. H., Kim, M. G., Lee, H. S., Cho, E. G. & Park, D. Filamin is essential for shedding of the transmembrane serine protease, epithin. *Embo Reports* **6**, 1045-1051, doi:10.1038/sj.embor.7400534 (2005).
118 Oberst, M. D., Williams, C. A., Dickson, R. B., Johnson, M. D. & Lin, C. Y. The activation of matriptase requires its noncatalytic domains, serine protease domain, and its cognate inhibitor. *Journal of Biological Chemistry* **278**, 26773-26779, doi:10.1074/jbc.M304282200 (2003).
119 Inouye, K., Yasumoto, M., Tsuzuki, S., Mochida, S. & Fushiki, T. The optimal activity of a pseudozymogen form of recombinant matriptase under the mildly acidic pH and low ionic strength conditions. *Journal of Biochemistry* **147**, 485-492, doi:10.1093/jb/mvp190 (2010).
120 Satomi, S., Yamasaki, Y., Tsuzuki, S., Hitomi, Y., Iwanaga, T. & Fushiki, T. A role for membrane-type serine protease (MT-SP1) in intestinal epithelial turnover. *Biochemical and Biophysical Research Communications* **287**, 995-1002, doi:10.1006/bbrc.2001.5686 (2001).
121 Milner, J. M., Patel, A. & Rowan, A. D. Emerging Roles of Serine Proteinases in Tissue Turnover in Arthritis. *Arthritis and Rheumatism* **58**, 3644-3656, doi:10.1002/art.24046 (2008).
122 Okroj, M., Heinegard, D., Holmdahl, R. & Blom, A. M. Rheumatoid arthritis and the complement system. *Annals of Medicine* **39**, 517-530, doi:10.1080/07853890701477546 (2007).
123 Wang, Q., Rozelle, A. L., Lepus, C. M., Scanzello, C. R., Song, J. J., Larsen, D. M., Crish, J. F., Bebek, G., Ritter, S. Y., Lindstrom, T. M., Hwang, I. Y., Wong, H. D. H., Punzi, L., Encarnacion, A., Shamloo, M., Goodman, S. B., Wyss-Coray, T., Goldring, S. R., Banda, N. K., Thurman, J. M., Gobezie, R., Crow, M. K., Holers, V. M., Lee, D. M. & Robinson, W. H. Identification of a central role for complement in osteoarthritis. *Nature Medicine* **17**, 1674-U1196, doi:10.1038/nm.2543 (2011).
124 Busso, N. & Hamilton, J. A. Extravascular coagulation and the plasminogen activator/plasmin system in rheumatoid arthritis. *Arthritis and Rheumatism* **46**, 2268-2279, doi:10.1002/art.10498 (2002).
125 Yang, Y. H., Hall, P., Little, C. B., Fosang, A. J., Milenkovski, G., Santos, L., Xue, J., Tipping, P. & Morand, E. F. Reduction of arthritis severity in protease-activated receptor-deficient mice. *Arthritis and Rheumatism* **52**, 1325-1332, doi:10.1002/art.21001 (2005).
126 Marty, I., Peclat, V., Kirdaite, G., Salvi, R., So, A. & Busso, N. Amelioration of collagen-induced arthritis by thrombin inhibition. *Journal of Clinical Investigation* **107**, 631-640, doi:10.1172/jci11064 (2001).
127 Camerer, E., Huang, W. & Coughlin, S. R. Tissue factor- and factor X-dependent activation of protease-activated receptor 2 by factor VIIa. *Proceedings of the National Academy of Sciences of the United States of America* **97**, 5255-5260, doi:10.1073/pnas.97.10.5255 (2000).
128 Boileau, C., Amiable, N., Martel-Pelletier, J., Fahmi, H., Duval, N. & Pelletier, J.-P. Activation of proteinase-activated receptor 2 in human osteoarthritic cartilage upregulates catabolic and proinflammatory pathways capable of

inducing cartilage degradation: a basic science study. *Arthritis Research & Therapy* **9**, doi:10.1186/ar2329 (2007).

129 Hu, S. I., Carozza, M., Klein, M., Nantermet, P., Luk, D. & Crowl, R. M. Human HtrA, an evolutionarily conserved serine protease identified as a differentially expressed gene product in osteoarthritic cartilage. *Journal of Biological Chemistry* **273**, 34406-34412, doi:10.1074/jbc.273.51.34406 (1998).

130 Vande Walle, L., Lamkanfi, M. & Vandenabeele, P. The mitochondrial serine protease HtrA2/Omi: an overview. *Cell Death and Differentiation* **15**, 453-460, doi:10.1038/sj.cdd.4402291 (2008).

131 Tsuchiya, A., Yano, M., Tocharus, J., Kojima, H., Fukumoto, M., Kawaichi, M. & Oka, C. Expression of mouse HtrA1 serine protease in normal bone and cartilage and its upregulation in joint cartilage damaged by experimental arthritis. *Bone* **37**, 323-336, doi:10.1016/j.bone.2005.03.015 (2005).

132 Tocharus, J., Tsuchiya, A., Kajikawa, M., Ueta, Y., Oka, C. & Kawaichi, M. Developmentally regulated expression of mouse HtrA3 and its role as an inhibitor of TGF-beta signaling. *Development Growth & Differentiation* **46**, 257-274 (2004).

133 Chamberland, A., Wang, E., Jones, A. R., Collins-Racie, L. A., LaVallie, E. R., Huang, Y., Liu, L., Morris, E. A., Flannery, C. R. & Yang, Z. Identification of a novel HtrA1-susceptible cleavage site in human aggrecan: evidence for the involvement of HtrA1 in aggrecan proteolysis in vivo. *Journal of Biological Chemistry* **284**, 27352-27359, doi:10.1074/jbc.M109.037051 (2009).

134 Lopez-Otin, C. & Matrisian, L. M. Tumour micro environment - Opinion - Emerging roles of proteases in tumour suppression. *Nature Reviews Cancer* **7**, 800-808, doi:10.1038/nrc2228 (2007).

135 Berti, P. & Storer, A. Alignment/phylogeny of the papain superfamily of cysteine proteases. *Journal of Molecular Biology* **246**, 273-283 (1995).

136 Thornberry, N. A., Bull, H. G., Calaycay, J. R., Chapman, K. T., Howard, A. D., Kostura, M. J., Miller, D. K., Molineaux, S. M., Weidner, J. R., Aunins, J., Elliston, K. O., Ayala, J. M., Casano, F. J., Chin, J., Ding, G. J. F., Egger, L. A., Gaffney, E. P., Limjuco, G., Palyha, O. C., Raju, S. M., Rolando, A. M., Salley, J. P., Yamin, T. T., Lee, T. D., Shively, J. E., Maccross, M., Mumford, R. A., Schmidt, J. A. & Tocci, M. J. A novel heterodimeric cysteine protease is required for inteleukin-1 beta processing in monocytes. *Nature* **356**, 768-774, doi:10.1038/356768a0 (1992).

137 Saido, T. C., Sorimachi, H. & Suzuki, K. Calpain: new perspectives in molecular diversity and physiological-pathological involvement. *Faseb Journal* **8**, 814-822 (1994).

138 Turk, V., Turk, B. & Turk, D. Lysosomal cysteine proteases: facts and opportunities. *Embo Journal* **20**, 4629-4633, doi:10.1093/emboj/20.17.4629 (2001).

139 Korkmaz, B., Moreau, T. & Gauthier, F. Neutrophil elastase, proteinase 3 and cathepsin G: Physicochemical properties, activity and physiopathological functions. *Biochimie* **90**, 227-242, doi:10.1016/j.biochi.2007.10.009 (2008).

140 McDonald, J. & Barrett, A. in *Mammalian Proteases* Vol. 2 357 (New York: Academic, 1986).

141 Takahashi, T. & Tang, J. Cathepsin D from porcine and bovine spleen. *Methods in Enzymology* **80**, 565-581 (1981).

142 Rossi, A., Deveraux, Q., Turk, B. & Sali, A. Comprehensive search for cysteine cathepsins in the human genome. *Biological Chemistry* **385**, 363-372, doi:10.1515/bc.2004.040 (2004).

143 McGrath, M. E. The lysosomal cysteine proteases. *Annual Review of Biophysics and Biomolecular Structure* **28**, 181-204, doi:10.1146/annurev.biophys.28.1.181 (1999).
144 Wang, J., Xiang, Y. F. & Lim, C. THE DOUBLE CATALYTIC TRIAD, CYS25-HIS159-ASP158 AND CYS25-HIS159-ASN175, IN PAPAIN CATALYSIS - ROLE OF ASP158 AND ASN175. *Protein Engineering* **7**, 75-82, doi:10.1093/protein/7.1.75 (1994).
145 Vernet, T., Tessier, D. C., Chatellier, J., Plouffe, C., Lee, T. S., Thomas, D. Y., Storer, A. C. & Menard, R. Structural and Functional Roles of Asparagine 175 in the Cysteine Protease Papain. *Journal of Biological Chemistry* **270**, 16645-16652 (1995).
146 Shokhen, M., Khazanov, N. & Albeck, A. Challenging a paradigm: Theoretical calculations of the protonation state of the Cys25-His159 catalytic diad in free papain. *Proteins-Structure Function and Bioinformatics* **77**, 916-926, doi:10.1002/prot.22516 (2009).
147 Ishidoh, K. & Kominami, E. Processing and activation of lysosomal proteinases. *Biological Chemistry* **383**, 1827-1831, doi:10.1515/bc.2002.206 (2002).
148 Turk, D., Podobnik, M., Kuhelj, R., Dolinar, M. & Turk, V. Crystal structures of human procathepsin B at 3.2 and 3.3 angstrom resolution reveal an interaction motif between a papain-like cysteine protease and its propeptide. *Febs Letters* **384**, 211-214, doi:10.1016/0014-5793(96)00309-2 (1996).
149 Coulombe, R., Grochulski, P., Sivaraman, J., Menard, R., Mort, J. S. & Cygler, M. Structure of human procathepsin L reveals the molecular basis of inhibition by the prosegment. *Embo Journal* **15**, 5492-5503 (1996).
150 Sivaraman, J., Lalumiere, M., Menard, R. & Cygler, M. Crystal structure of wild-type human procathepsin K. *Protein Science* **8**, 283-290 (1999).
151 LaLonde, J. M., Zhao, B. G., Janson, C. A., D'Alessio, K. J., McQueney, M. S., Orsini, M. J., Debouck, C. M. & Smith, W. W. The crystal structure of human procathepsin K. *Biochemistry* **38**, 862-869, doi:10.1021/bi9822271 (1999).
152 Pungercar, J. R., Caglic, D., Sajid, M., Dolinar, M., Vasiljeva, O., Pozgan, U., Turk, D., Bogyo, M., Turk, V. & Turk, B. Autocatalytic processing of procathepsin B is triggered by proenzyme activity. *Febs Journal* **276**, 660-668, doi:10.1111/j.1742-4658.2008.06815.x (2009).
153 Dahl, S. W., Halkier, T., Lauritzen, C., Dolenc, I., Pedersen, J., Turk, V. & Turk, B. Human recombinant pro-dipeptidyl peptidase I (cathepsin C) can be activated by cathepsins L and S but not by autocatalytic processing. *Biochemistry* **40**, 1671-1678, doi:10.1021/bi001693z (2001).
154 Nagler, D. K., Zhang, R. L., Tam, W., Sulea, T., Purisima, E. O. & Menard, R. Human cathepsin X: A cysteine protease with unique carboxypeptidase activity. *Biochemistry* **38**, 12648-12654, doi:10.1021/bi991371z (1999).
155 Schick, C., Pemberton, P. A., Shi, G. P., Kamachi, Y., Cataltepe, S., Bartuski, A. J., Gornstein, E. R., Bromme, D., Chapman, H. A. & Silverman, G. A. Cross-class inhibition of the cysteine proteinases cathepsins K, L, and S by the serpin squamous cell carcinoma antigen 1: A kinetic analysis. *Biochemistry* **37**, 5258-5266, doi:10.1021/bi972521d (1998).
156 Gondi, C. S. & Rao, J. S. Cathepsin B as a cancer target. *Expert Opinion on Therapeutic Targets* **17**, 281-291, doi:10.1517/14728222.2013.740461 (2013).
157 Fais, S. Cannibalism: A way to feed on metastatic tumors. *Cancer Letters* **258**, 155-164, doi:10.1016/j.canlet.2007.09.014 (2007).
158 Kobayashi, H., Schmitt, M., Goretzki, L., Chucholowski, N., Calvete, J., Kramer, M., Gunzler, W. A., Janicke, F. & Graeff, H. Cathepsin B Efficiently Activates the Soluble and the Tumor Cell Receptor-bound Form of the Proenzyme

Urokinase-type Plasminogen Activator (Pro-uPA). *Journal of Biological Chemistry* **266**, 5147-5152 (1991).

159 Kostoulas, G., Lang, A., Nagase, H. & Baici, A. Stimulation of angiogenesis through cathepsin B inactivation of the tissue inhibitors of matrix metalloproteinases. *Febs Letters* **455**, 286-290, doi:10.1016/s0014-5793(99)00897-2 (1999).

160 Bromme, D. & Lecaille, F. Cathepsin K inhibitors for osteoporosis and potential off-target effects. *Expert Opinion on Investigational Drugs* **18**, 585-600, doi:10.1517/13543780902832661 (2009).

161 Drake, F. H., Dodds, R. A., James, I. E., Connor, J. R., Debouck, C., Richardson, S., LeeRykaczewski, E., Coleman, L., Rieman, D., Barthlow, R., Hastings, G. & Gowen, M. Cathepsin K, but not cathepsins B, L, or S, is abundantly expressed in human osteoclasts. *Journal of Biological Chemistry* **271**, 12511-12516 (1996).

162 Garnero, P., Borel, O., Byrjalsen, I., Ferreras, M., Drake, F. H., McQueney, M. S., Foged, N. T., Delmas, P. D. & Delaisse, J. M. The collagenolytic activity of cathepsin K is unique among mammalian proteinases. *Journal of Biological Chemistry* **273**, 32347-32352, doi:10.1074/jbc.273.48.32347 (1998).

163 Kafienah, W., Bromme, D., Buttle, D. J., Croucher, L. J. & Hollander, A. P. Human cathepsin K cleaves native type I and II collagens at the N-terminal end of the triple helix. *Biochemical Journal* **331**, 727-732 (1998).

164 Lecaille, F., Broemme, D. & Lalmanach, G. Biochemical properties and regulation of cathepsin K activity. *Biochimie* **90**, 208-226, doi:10.1016/j.biochi.2007.08.011 (2008).

165 Aguda, A. H., Panwar, P., Du, X., Nguyen, N. T., Brayer, G. D. & Broemme, D. Structural basis of collagen fiber degradation by cathepsin K. *Proceedings of the National Academy of Sciences of the United States of America* **111**, 17474-17479, doi:10.1073/pnas.1414126111 (2014).

166 Panwar, P., Soe, K., Guido, R. V. C., Bueno, R. V. C., Delaisse, J.-M. & Broemme, D. A novel approach to inhibit bone resorption: exosite inhibitors against cathepsin K. *British Journal of Pharmacology* **173**, 396-410, doi:10.1111/bph.13383 (2016).

167 Gupta, S., Singh, R. K., Dastidar, S. & Ray, A. Cysteine cathepsin S as an immunomodulatory target: present and future trends. *Expert Opinion on Therapeutic Targets* **12**, 291-299, doi:10.1517/14728222.12.3.291 (2008).

168 Liuzzo, J. P., Petanceska, S. S., Moscatelli, D. & Devi, L. A. Inflammatory mediators regulate cathepsin S in macrophages and microglia: A role in attenuating heparan sulfate interactions. *Molecular Medicine* **5**, 320-333 (1999).

169 Vasiljeva, O., Dolinar, M., Pungercar, J. R., Turk, V. & Turk, B. Recombinant human procathepsin S is capable of autocatalytic processing at neutral pH in the presence of glycosaminoglycans. *Febs Letters* **579**, 1285-1290, doi:10.1016/j.febslet.2004.12.093 (2005).

170 Xin, X. Q., Gunesekera, B. & Mason, R. W. The specificity and elastinolytic activities of bovine cathepsins S and H. *Archives of Biochemistry and Biophysics* **299**, 334-339, doi:10.1016/0003-9861(92)90283-3 (1992).

171 Nakagawa, T. Y., Brissette, W. H., Lira, P. D., Griffiths, R. J., Petrushova, N., Stock, J., McNeish, J. D., Eastman, S. E., Howard, E. D., Clarke, S. R. M., Rosloniec, E. F., Elliott, E. A. & Rudensky, A. Y. Impaired invariant chain degradation and antigen presentation and diminished collagen-induced arthritis in cathepsin S null mice. *Immunity* **10**, 207-217, doi:10.1016/s1074-7613(00)80021-7 (1999).

172 Beck, H., Schwarz, G., Schroter, C. J., Deeg, M., Baier, D., Stevanovic, S., Weber, E., Driessen, C. & Kalbacher, H. Cathepsin S and an asparagine-specific

endoprotease dominate the proteolytic processing of human myelin basic protein in vitro. *European Journal of Immunology* **31**, 3726-3736, doi:10.1002/1521-4141(200112)31:12<3726::aid-immu3726>3.0.co;2-o (2001).

173 Fajardo, I., Svensson, L., Bucht, A. & Pejler, G. Increased levels of hypoxia-sensitive proteins in allergic airway inflammation. *American Journal of Respiratory and Critical Care Medicine* **170**, 477-484, doi:10.1164/rccm.200402-1780C (2004).

174 Lankelma, J. M., Voorend, D. M., Barwari, T., Koetsveld, J., Van der Spek, A. H., De Porto, A. P. N. A., Van Rooijen, G. & Van Noorden, C. J. F. Cathepsin L, target in cancer treatment? *Life Sciences* **86**, 225-233, doi:10.1016/j.lfs.2009.11.016 (2010).

175 Santamaria, I., Velasco, G., Cazorla, M., Fueyo, A., Campo, E. & Lopez-Otin, C. Cathepsin L2, a novel human cysteine proteinase produced by breast and colorectal carcinomas. *Cancer Research* **58**, 1624-1630 (1998).

176 Bromme, D., Li, Z. Q., Barnes, M. & Mehler, E. Human cathepsin V functional expression, tissue distribution, electrostatic surface potential, enzymatic characterization, and chromosomal localization. *Biochemistry* **38**, 2377-2385, doi:10.1021/bi982175f (1999).

177 Puzer, L., Cotrin, S. S., Alves, M. F. M., Egborge, T., Araujo, M. S., Juliano, M. A., Juliano, L., Bromme, D. & Carmona, A. K. Comparative substrate specificity analysis of recombinant human cathepsin V and cathepsin L. *Archives of Biochemistry and Biophysics* **430**, 274-283, doi:10.1016/j.abb.2004.07.006 (2004).

178 Werle, B., Julke, B., Lah, T., Spiess, E. & Ebert, W. Cathepsin B fraction active at physiological pH of 7.5 is of prognostic significance in squamous cell carcinoma of human lung. *British Journal of Cancer* **75**, 1137-1143, doi:10.1038/bjc.1997.196 (1997).

179 Buck, M. R., Karustis, D. G., Day, N. A., Honn, K. V. & Sloane, B. F. Degradation of extracellular-matrix proteins by human cathepsin B from normal and tumour tissues. *Biochemical Journal* **282**, 273-278 (1992).

180 Bromme, D., Okamoto, K., Wang, B. B. & Biroc, S. Human cathepsin O-2, a matrix protein-degrading cysteine protease expressed in osteoclasts - Functional expression of human cathepsin O-2 in Spodoptera frugiperda and characterization of the enzyme. *Journal of Biological Chemistry* **271**, 2126-2132 (1996).

181 Turk, B., Dolenc, I., Turk, V. & Bieth, J. G. Kinetics of the pH-induced inactivation of human cathepsin L. *Biochemistry* **32**, 375-380, doi:10.1021/bi00052a046 (1993).

182 Dehrmann, F. M., Coetzer, T. H. T., Pike, R. N. & Dennison, C. Mature cathepsin L is substantially active in the ionic milieu of the extracellular medium. *Archives of Biochemistry and Biophysics* **324**, 93-98, doi:10.1006/abbi.1995.9924 (1995).

183 Konttinen, Y. T., Mandelin, J., Li, T. F., Salo, J., Lassus, J., Liljestrom, M., Hukkanen, M., Takagi, M., Virtanen, I. & Santavirta, S. Acidic cysteine endoproteinase cathepsin K in the degeneration of the superficial articular hyaline cartilage in osteoarthritis. *Arthritis and Rheumatism* **46**, 953-960, doi:10.1002/art.10185 (2002).

184 Dejica, V. M., Mort, J. S., Laverty, S., Percival, M. D., Antoniou, J., Zukor, D. J. & Poole, A. R. Cleavage of type II collagen by cathepsin K in human osteoarthritic cartilage. *American Journal of Pathology* **173**, 161-169, doi:10.2353/ajpath.2008.070494 (2008).

185 Bayliss, M. T. & Yousufali, S. Studies on cathepsin B in human articular cartilage. *Biochemical Journal* **171**, 149-154 (1978).

186 Baici, A., Horler, D., Lang, A., Merlin, C. & Kissling, R. Cathepsin B in osteoarthritis: zonal variation of enzyme activity in human femoral head cartilage. *Annals of the Rheumatic Diseases* **54**, 281-288, doi:10.1136/ard.54.4.281 (1995).
187 Mehraban, F., Tindal, M. H., Proffitt, M. M. & Moskowitz, R. W. Temporal pattern of cysteine endopeptidase (cathepsin B) expression in cartilage and synovium from rabbit knees with experimental osteoarthritis: Gene expression in chondrocytes in response to interleukin-1 and matrix depletion. *Annals of the Rheumatic Diseases* **56**, 108-115, doi:10.1136/ard.56.2.108 (1997).
188 Mort, J. S., Magny, M. C. & Lee, E. R. Cathepsin B: an alternative protease for the generation of an aggrecan 'metalloproteinase' cleavage neoepitope. *Biochemical Journal* **335**, 491-494 (1998).
189 Dvir-Ginzberg, M., Gagarina, V., Lee, E. J., Booth, R., Gabay, O. & Hall, D. J. Tumor Necrosis Factor alpha-Mediated Cleavage and Inactivation of SirT1 in Human Osteoarthritic Chondrocytes. *Arthritis and Rheumatism* **63**, 2363-2373, doi:10.1002/art.30279 (2011).
190 Caglic, D., Repnik, U., Jedeszko, C., Kosec, G., Miniejew, C., Kindermann, M., Vasiljeva, O., Turk, V., Wendt, K. U., Sloane, B. F., Goldring, M. B. & Turk, B. The proinflammatory cytokines interleukin-1 alpha and tumor necrosis factor alpha promote the expression and secretion of proteolytically active cathepsin S from human chondrocytes. *Biological Chemistry* **394**, 307-316, doi:10.1515/hsz-2012-0283 (2013).
191 Ben-Aderet, L., Merquiol, E., Fahham, D., Kumar, A., Reich, E., Ben-Nun, Y., Kandel, L., Haze, A., Liebergall, M., Kosinska, M. K., Steinmeyer, J., Turk, B., Blum, G. & Dvir-Ginzberg, M. Detecting cathepsin activity in human osteoarthritis via activity-based probes. *Arthritis Research & Therapy* **17**, doi:10.1186/s13075-015-0586-5 (2015).
192 Hou, W. S., Li, Z. Q., Buttner, F. H., Bartnik, E. & Bromme, D. Cleavage site specificity of cathepsin K toward cartilage proteoglycans and protease complex formation. *Biological Chemistry* **384**, 891-897, doi:10.1515/bc.2003.100 (2003).
193 Fonovic, M. & Turk, B. Cysteine cathepsins and extracellular matrix degradation. *Biochimica Et Biophysica Acta-General Subjects* **1840**, 2560-2570, doi:10.1016/j.bbagen.2014.03.017 (2014).
194 Morko, J., Kiviranta, R., Joronen, K., Saamanen, A. M., Vuorio, E. & Salminen-Mankonen, H. Spontaneous development of synovitis and cartilage degeneration in transgenic mice overexpressing cathepsin K. *Arthritis and Rheumatism* **52**, 3713-3717, doi:10.1002/art.21423 (2005).
195 Vinardell, T., Dejica, V., Poole, A. R., Mort, J. S., Richard, H. & Laverty, S. Evidence to suggest that cathepsin K degrades articular cartilage in naturally occurring equine osteoarthritis. *Osteoarthritis and Cartilage* **17**, 375-383, doi:10.1016/j.joca.2008.07.017 (2009).
196 Connor, J. R., LePage, C., Swift, B. A., Yamashita, D., Bendele, A. M., Maul, D. & Kumar, S. Protective effects of a cathepsin K inhibitor, SB-553484, in the canine partial medial meniscectomy model of osteoarthritis. *Osteoarthritis and Cartilage* **17**, 1236-1243, doi:10.1016/j.joca.2009.03.015 (2009).
197 Takahashi, D., Iwasaki, N., Kon, S., Matsui, Y., Majima, T., Minami, A. & Uede, T. Down-Regulation of Cathepsin K in Synovium Leads to Progression of Osteoarthritis in Rabbits. *Arthritis and Rheumatism* **60**, 2372-2380, doi:10.1002/art.24718 (2009).
198 Hayami, T., Zhuo, Y., Wesolowski, G. A., Pickarski, M. & Duong, L. T. Inhibition of cathepsin K reduces cartilage degeneration in the anterior cruciate ligament transection rabbit and murine models of osteoarthritis. *Bone* **50**, 1250-1259, doi:10.1016/j.bone.2012.03.025 (2012).

199 Robbins, M., Judge, A. & MacLachlan, I. siRNA and Innate Immunity. *Oligonucleotides* **19**, 89-101, doi:10.1089/oli.2009.0180 (2009).
200 Adams, M. N., Ramachandran, R., Yau, M.-K., Suen, J. Y., Fairlie, D. P., Hollenberg, M. D. & Hooper, J. D. Structure, function and pathophysiology of protease activated receptors. *Pharmacology & Therapeutics* **130**, 248-282, doi:10.1016/j.pharmthera.2011.01.003 (2011).
201 Kahn, M. L., Hammes, S. R., Botka, C. & Coughlin, S. R. Gene and locus structure and chromosomal localization of the protease-activated receptor gene family. *Journal of Biological Chemistry* **273**, 23290-23296, doi:10.1074/jbc.273.36.23290 (1998).
202 Nieman, M. T. & Schmaier, A. H. Interaction of thrombin with PAR1 and PAR4 at the thrombin cleavage site. *Biochemistry* **46**, 8603-8610, doi:10.1021/bi700597p (2007).
203 Sprang, S. R. & DeCamp, D. L. in *Encyclopedia of the Neurological Sciences (Second Edition)* 560–563 (2014).
204 Soh, U. J. K., Dores, M. R., Chen, B. & Trejo, J. Signal transduction by protease-activated receptors. *British Journal of Pharmacology* **160**, 191-203, doi:10.1111/j.1476-5381.2010.00705.x (2010).
205 Nystedt, S., Emilsson, K., Larsson, A. K., Strombeck, B. & Sundelin, J. Molecular cloning and functional expression of the gene encoding the human proteinase-activated receptor 2. *European Journal of Biochemistry* **232**, 84-89, doi:10.1111/j.1432-1033.1995.tb20784.x (1995).
206 Molino, M., Barnathan, E. S., Numerof, R., Clark, J., Dreyer, M., Cumashi, A., Hoxie, J. A., Schechter, N., Woolkalis, M. & Brass, L. F. Interactions of mast cell tryptase with thrombin receptors and PAR-2. *Journal of Biological Chemistry* **272**, 4043-4049 (1997).
207 Knecht, W., Cottrell, G. S., Amadesi, S., Mohlin, J., Skaregarde, A., Gedda, K., Peterson, A., Chapman, K., Hollenberg, M. D., Vergnolle, N. & Bunnett, N. W. Trypsin IV or mesotrypsin and p23 cleave protease-activated receptors 1 and 2 to induce inflammation and hyperalgesia. *Journal of Biological Chemistry* **282**, 26089-26100, doi:10.1074/jbc.M703840200 (2007).
208 Hansen, K. K., Sherman, P. M., Cellars, L., Andrade-Gordon, P., Pan, Z. Y., Baruch, A., Wallace, J. L., Hollenberg, M. D. & Vergnolle, N. A major role for proteolytic activity and proteinase-activated receptor-2 in the pathogenesis of infectious colitis. *Proceedings of the National Academy of Sciences of the United States of America* **102**, 8363-8368, doi:10.1073/pnas.0409535102 (2005).
209 Mize, G. J., Wang, W. & Takayama, T. K. Prostate-specific kallikreins-2 and-4 enhance the proliferation of DU-145 prostate cancer cells through protease-activated receptors-1 and-2. *Molecular Cancer Research* **6**, 1043-1051, doi:10.1158/1541-7786.mcr-08-0096 (2008).
210 Oikonomopoulou, K., Hansen, K. K., Saifeddine, M., Tea, I., Blaber, M., Blaber, S. I., Scarisbrick, I., Andrade-Gordon, P., Cottrell, G. S., Bunnett, N. W., Diamandis, E. P. & Hollenberg, M. D. Proteinase-activated receptors, targets for kallikrein signaling. *Journal of Biological Chemistry* **281**, 32095-32112, doi:10.1074/jbc.M513138200 (2006).
211 Wilson, S., Greer, B., Hooper, J., Zijlstra, A., Walker, B., Quigley, J. & Hawthorne, S. The membrane-anchored serine protease, TMPRSS2, activates PAR-2 in prostate cancer cells. *Biochemical Journal* **388**, 967-972, doi:10.1042/bj20041066 (2005).
212 Smith, R., Jenkins, A., Lourbakos, A., Thompson, P., Ramakrishnan, V., Tomlinson, J., Deshpande, U., Johnson, D. A., Jones, R., Mackie, E. J. & Pike, R. N. Evidence for the activation of PAR-2 by the sperm protease, acrosin:

expression of the receptor on oocytes. *Febs Letters* **484**, 285-290, doi:10.1016/s0014-5793(00)02146-3 (2000).

213 Miki, M., Nakamura, Y., Takahashi, A., Nakaya, Y., Eguchi, H., Masegi, T., Yoneda, K., Yasuoka, S. & Sone, S. Effect of human airway trypsin-like protease on intracellular free Ca2+ concentration in human bronchial epithelial cells. *The journal of medical investigation : JMI* **50**, 95-107 (2003).

214 Mihara, K., Ramachandran, R., Saifeddine, M., Hansen, K. K., Renaux, B., Polley, D., Gibson, S., Vanderboor, C. & Hollenberg, M. D. Thrombin-Mediated Direct Activation of Proteinase-Activated Receptor-2: Another Target for Thrombin Signaling. *Molecular Pharmacology* **89**, 606-614, doi:10.1124/mol.115.102723 (2016).

215 Chiu, L.-L., Perng, D.-W., Yu, C.-H., Su, S.-N. & Chow, L.-P. Mold allergen, Pen c 13, induces IL-8 expression in human airway epithelial cells by activating protease-activated receptor 1 and 2. *Journal of Immunology* **178**, 5237-5244 (2007).

216 Sun, G., Stacey, M. A., Schmidt, M., Mori, L. & Mattoli, S. Interaction of mite allergens Der P3 and Der P9 with protease-activated receptor-2 expressed by lung epithelial cells. *Journal of Immunology* **167**, 1014-1021 (2001).

217 Asokananthan, N., Graham, P. T., Stewart, D. J., Bakker, A. J., Eidne, K. A., Thompson, P. J. & Stewart, G. A. House dust mite allergens induce proinflammatory cytokines from respiratory epithelial cells: The cysteine protease allergen, Der p 1, activates protease-activated receptor (PAR)-2 and inactivates PAR-1. *Journal of Immunology* **169**, 4572-4578 (2002).

218 Kauffman, H. F., Tamm, M., Timmerman, J. A. B. & Borger, P. House dust mite major allergens Der p 1 and Der p 5 activate human airway-derived epithelial cells by protease-dependent and protease-independent mechanisms. *Clinical and molecular allergy : CMA* **4**, 5-5, doi:10.1186/1476-7961-4-5 (2006).

219 Lourbakos, A., Potempa, J., Travis, J., D'Andrea, M. R., Andrade-Gordon, P., Santulli, R., Mackie, E. J. & Pike, R. N. Arginine-specific protease from Porphyromonas gingivalis activates protease-activated receptors on human oral epithelial cells and induces interleukin-6 secretion. *Infection and Immunity* **69**, 5121-5130, doi:10.1128/iai.69.8.5121-5130.2001 (2001).

220 Uehara, A., Muramoto, K., Imamura, T., Nakayama, K., Potempa, J., Travis, J., Sugawara, S. & Takada, H. Arginine-specific gingipains from Porphyromonas gingivalis stimulate production of hepatocyte growth factor (scatter factor) through protease-activated receptors in human gingival fibroblasts in culture. *Journal of Immunology* **175**, 6076-6084 (2005).

221 Hong, J. H., Hong, J. Y., Park, B., Lee, S.-I., Seo, J. T., Kim, K.-E., Sohn, M. H. & Shin, D. M. Chitinase Activates Protease-Activated Receptor-2 in Human Airway Epithelial Cells. *American Journal of Respiratory Cell and Molecular Biology* **39**, 530-535, doi:10.1165/rcmb.2007-0410OC (2008).

222 Hollenberg, M. D., Renaux, B., Hyun, E., Houle, S., Vergnolle, N., Saifeddine, M. & Ramachandran, R. Derivatized 2-furoyl-LIGRLO-amide, a versatile and selective probe for proteinase-activated receptor 2: Binding and visualization. *Journal of Pharmacology and Experimental Therapeutics* **326**, 453-462, doi:10.1124/jpet.108.136432 (2008).

223 McGuire, J. J., Saifeddine, M., Triggle, C. R., Sun, K. & Hollenberg, M. D. 2-Furoyl-LIGRLO-amide: A potent and selective proteinase-activated receptor 2 agonist. *Journal of Pharmacology and Experimental Therapeutics* **309**, 1124-1131, doi:10.1124/jpet.103.064584 (2004).

224 Dulon, S., Cande, C., Bunnett, N. W., Hollenberg, M. D., Chignard, M. & Pidard, D. Proteinase-activated receptor-2 and human lung epithelial cells - Disarming by

neutrophil serine proteinases. *American Journal of Respiratory Cell and Molecular Biology* **28**, 339-346, doi:10.1165/rcmb.4908 (2003).

225 Ramachandran, R., Mihara, K., Chung, H., Renaux, B., Lau, C. S., Muruve, D. A., DeFea, K. A., Bouvier, M. & Hollenberg, M. D. Neutrophil Elastase Acts as a Biased Agonist for Proteinase-activated Receptor-2 (PAR(2)). *Journal of Biological Chemistry* **286**, 24638-24648, doi:10.1074/jbc.M110.201988 (2011).

226 Zhao, P., Lieu, T., Barlow, N., Metcalf, M., Veldhuis, N. A., Jensen, D. D., Kocan, M., Sostegni, S., Haerteis, S., Baraznenok, V., Henderson, I., Lindstrom, E., Guerrero-Alba, R., Valdez-Morales, E. E., Liedtke, W., McIntyre, P., Vanner, S. J., Korbmacher, C. & Bunnett, N. W. Cathepsin S Causes Inflammatory Pain via Biased Agonism of PAR(2) and TRPV4. *Journal of Biological Chemistry* **289**, 27215-27234, doi:10.1074/jbc.M114.599712 (2014).

227 Stalheim, L., Ding, Y., Gullapalli, A., Paing, M. M., Wolfe, B. L., Morris, D. R. & Trejo, J. Multiple independent functions of arrestins in the regulation of protease-activated receptor-2 signaling and trafficking. *Molecular Pharmacology* **67**, 78-87, doi:10.1124/mol.104.006072 (2005).

228 Luo, W. B., Wang, Y. F., Hanck, T., Stricker, R. & Reiser, G. Jab1, a novel protease-activated receptor-2 (PAR-2)-interacting protein, is involved in PAR-2-induced activation of activator protein-1. *Journal of Biological Chemistry* **281**, 7927-7936, doi:10.1074/jbc.M510784200 (2006).

229 Ricks, T. K. & Trejo, J. Phosphorylation of Protease-activated Receptor-2 Differentially Regulates Desensitization and Internalization. *Journal of Biological Chemistry* **284**, 34444-34457, doi:10.1074/jbc.M109.048942 (2009).

230 Kang, D. S., Tian, X. & Benovic, J. L. Role of beta-arrestins and arrestin domain-containing proteins in G protein-coupled receptor trafficking. *Current Opinion in Cell Biology* **27**, 63-71, doi:10.1016/j.ceb.2013.11.005 (2014).

231 Bohm, S. K., Khitin, L. M., Grady, E. F., Aponte, G., Payan, D. G. & Bunnett, N. W. Mechanisms of desensitization and resensitization of proteinase-activated receptor-2. *Journal of Biological Chemistry* **271**, 22003-22016 (1996).

232 Jensen, D. D., Zhao, P., Jimenez-Vargas, N. N., Lieu, T., Gerges, M., Yeatman, H. R., Canals, M., Vanner, S. J., Poole, D. P. & Bunnett, N. W. Protein Kinase D and G Subunits Mediate Agonist-evoked Translocation of Protease-activated Receptor-2 from the Golgi Apparatus to the Plasma Membrane. *Journal of Biological Chemistry* **291**, 11285-11299, doi:10.1074/jbc.M115.710681 (2016).

233 Perry, S. R., Xu, W. J., Wirija, A., Lim, J. X., Yau, M. K., Stoermer, M. J., Lucke, A. J. & Fairlie, D. P. Three Homology Models of PAR2 Derived from Different Templates: Application to Antagonist Discovery. *Journal of Chemical Information and Modeling* **55**, 1181-1191, doi:10.1021/acs.jcim.5b00087 (2015).

234 Xiang, Y., Masuko-Hongo, K., Sekine, T., Nakamura, H., Yudoh, K., Nishioka, K. & Kato, T. Expression of proteinase-activated receptors (PAR)-2 in articular chondrocytes is modulated by IL-1 beta, TNF-alpha and TGF-beta. *Osteoarthritis and Cartilage* **14**, 1163-1173, doi:10.1016/j.joca.2006.04.015 (2006).

235 Ferrell, W. R., Kelso, E. B., Lockhart, J. C., Plevin, R. & McInnes, I. B. Protease-activated receptor 2: a novel pathogenic pathway in a murine model of osteoarthritis. *Annals of the Rheumatic Diseases* **69**, 2051-2054, doi:10.1136/ard.2010.130336 (2010).

236 Amiable, N., Martel-Pelletier, J., Lussier, B., Tat, S. K., Pelletier, J.-P. & Boileau, C. Proteinase-activated Receptor-2 Gene Disruption Limits the Effect of Osteoarthritis on Cartilage in Mice: A Novel Target in Joint Degradation. *Journal of Rheumatology* **38**, 911-920, doi:10.3899/jrheum.100710 (2011).

237 Huesa, C., Ortiz, A., Dunning, L., McGavin, L., Bennett, L., McIntosh, K., Crilly, A., Kurowska-Stolarska, M., Plevin, R., van 't Hof, R., Rowan, A. D., McInnes,

I. B., Goodyear, C., lockhart, J. C. & Ferrell, P. W. Proteinase-activated receptor 2 modulates OA-related pain, cartilage and bone pathology. *Ann Rheum Dis* **In Press** (2015).

238 Staunton, D., Hudson, K. R. & Heath, J. K. The interactions of the cytokine-binding homology region and immunoglobulin-like domains of gp130 with oncostatin M: implications for receptor complex formation. *Protein Engineering* **11**, 1093-1102, doi:10.1093/protein/11.11.1093 (1998).

239 Bougault, C., Paumier, A., Aubert-Foucher, E. & Mallein-Gerin, F. Investigating conversion of mechanical force into biochemical signaling in three-dimensional chondrocyte cultures. *Nature Protocols* **4**, 928-938, doi:10.1038/nprot.2009.63 (2009).

240 Laemmli, U. K. Cleavage of structural proteins during the assembly of the head of bacteriophage T4. *Nature* **227**, 680-&, doi:10.1038/227680a0 (1970).

241 Schagger, H. & Vonjagow, G. Tricine–sodium dodecyl sulfate polyacrylamide gel electrophoresis for the separation of proteins in the range from 1–100 kDa. *Analytical Biochemistry* **166**, 368-379, doi:10.1016/0003-2697(87)90587-2 (1987).

242 Matthews, J. in *Fundamentals of Receptor, Enzyme, and Transport Kinetics* (CRC Press, 1993).

243 Barrett, A. J., Kembhavi, A. A., Brown, M. A., Kirschke, H., Knight, C. G., Tamai, M. & Hanada, K. L-trans-Epoxysuccinyl-leucylamido(4-guanidino)butane (E-64) and its analogues as inhibitors of cysteine proteinases including cathepsins B, H and L. *Biochemical Journal* **201**, 189-198 (1982).

244 Bougault, C., Paumier, A., Aubert-Foucher, E. & Mallein-Gerin, F. Molecular analysis of chondrocytes cultured in agarose in response to dynamic compression. *Bmc Biotechnology* **8**, doi:10.1186/1472-6750-8-71 (2008).

245 Bougault, C., Aubert-Foucher, E., Paumier, A., Perrier-Groult, E., Huot, L., Hot, D., Duterque-Coquillaud, M. & Mallein-Gerin, F. Dynamic Compression of Chondrocyte-Agarose Constructs Reveals New Candidate Mechanosensitive Genes. *Plos One* **7**, doi:10.1371/journal.pone.0036964 (2012).

246 Fanning, P. J., Emkey, G., Smith, R. J., Grodzinsky, A. J., Szasz, N. & Trippel, S. B. Mechanical regulation of mitogen-activated protein kinase signaling in articular cartilage. *Journal of Biological Chemistry* **278**, 50940-50948, doi:10.1074/jbc.M305107200 (2003).

247 Li, K. W., Wang, A. S. & Sah, R. L. Microenvironment regulation of extracellular signal-regulated kinase activity in chondrocytes - Effects of culture configuration, interleukin-1, and compressive stress. *Arthritis and Rheumatism* **48**, 689-699, doi:10.1002/art.10849 (2003).

248 Wang, L. & Stegemann, J. P. Extraction of high quality RNA from polysaccharide matrices using cetlytrimethylammonium bromide. *Biomaterials* **31**, 1612-1618, doi:10.1016/j.biomaterials.2009.11.024 (2010).

249 Mio, K., Kirkham, J. & Bonass, W. A. Tips for extracting total RNA from chondrocytes cultured in agarose gel using a silica-based membrane kit. *Analytical Biochemistry* **351**, 314-316, doi:10.1016/j.ab.2005.12.031 (2006).

250 Melzak, K. A., Sherwood, C. S., Turner, R. F. B. & Haynes, C. A. Driving forces for DNA adsorption to silica in perchlorate solutions. *Journal of Colloid and Interface Science* **181**, 635-644, doi:10.1006/jcis.1996.0421 (1996).

251 Knight, M. M., Lee, D. A. & Bader, D. L. The influence of elaborated pericellular matrix on the deformation of isolated articular chondrocytes cultured in agarose. *Biochimica Et Biophysica Acta-Molecular Cell Research* **1405**, 67-77, doi:10.1016/s0167-4889(98)00102-5 (1998).

252 Gebauer, M., Saas, J., Sohler, F., Haag, J., Soder, S., Pieper, M., Bartnik, E., Beninga, J., Zimmer, R. & Aigner, T. Comparison of the chondrosarcoma cell line SW1353 with primary human adult articular chondrocytes with regard to their gene expression profile and reactivity to IL-1 beta. *Osteoarthritis and Cartilage* **13**, 697-708, doi:10.1016/j.joca.2005.04.004 (2005).

253 Akiyama, H., Chaboissier, M. C., Martin, J. F., Schedl, A. & de Crombrugghe, B. The transcrintion factor Sox9 has essential roles in successive steps of the chondrocyte differentiation pathway and is required for expression of Sox5 and Sox6. *Genes & Development* **16**, 2813-2828, doi:10.1101/gad.1017802 (2002).

254 Bi, W. M., Deng, J. M., Zhang, Z. P., Behringer, R. R. & de Crombrugghe, B. Sox9 is required for cartilage formation. *Nature Genetics* **22**, 85-89 (1999).

255 Zhao, Q., Eberspaecher, H., Lefebvre, V. & deCrombrugghe, B. Parallel expression of Sox9 and Col2a1 in cells undergoing chondrogenesis. *Developmental Dynamics* **209**, 377-386, doi:10.1002/(sici)1097-0177(199708)209:4<377::aid-aja5>3.0.co;2-f (1997).

256 Ng, L. J., Wheatley, S., Muscat, G. E. O., ConwayCampbell, J., Bowles, J., Wright, E., Bell, D. M., Tam, P. P. L., Cheah, K. S. E. & Koopman, P. SOX9 binds DNA, activates transcription, and coexpresses with type II collagen during chondrogenesis in the mouse. *Developmental Biology* **183**, 108-121, doi:10.1006/dbio.1996.8487 (1997).

257 Sekiya, I., Tsuji, K., Koopman, P., Watanabe, H., Yamada, Y., Shinomiya, K., Nifuji, A. & Noda, M. SOX9 enhances aggrecan gene promoter/enhancer activity and is up-regulated by retinoic acid in a cartilage-derived cell line, TC6. *Journal of Biological Chemistry* **275**, 10738-10744, doi:10.1074/jbc.275.15.10738 (2000).

258 Han, Y. & Lefebvre, V. L-Sox5 and Sox6 drive expression of the aggrecan gene in cartilage by securing binding of Sox9 to a far-upstream enhancer. *Molecular and Cellular Biology* **28**, 4999-5013, doi:10.1128/mcb.00695-08 (2008).

259 Mwale, F., Stachura, D., Roughley, P. & Antoniou, J. Limitations of using aggrecan and type X collagen as markers of chondrogenesis in mesenchymal stem cell differentiation. *Journal of Orthopaedic Research* **24**, 1791-1798, doi:10.1002/jor.20200 (2006).

260 Xu, J., Wang, W., Ludeman, M., Cheng, K., Hayami, T., Lotz, J. C. & Kapila, S. Chondrogenic differentiation of human mesenchymal stem cells in three-dimensional alginate gels. *Tissue Engineering Part A* **14**, 667-680, doi:10.1089/tea.2007.0272 (2008).

261 Poole, C. A., Flint, M. H. & Beaumont, B. W. Chondrons in cartilage: ultrastructural analysis of the pericellular microenvironment in adult human articular cartilages. *Journal of Orthopaedic Research* **5**, 509-522, doi:10.1002/jor.1100050406 (1987).

262 Marcelino, J. & McDevitt, C. A. Attachment of articular cartilage chondrocytes to the tissue form of type VI collagen. *Biochimica Et Biophysica Acta-Protein Structure and Molecular Enzymology* **1249**, 180-188, doi:10.1016/0167-4838(95)00026-q (1995).

263 Guilak, F., Alexopoulos, L. G., Upton, M. L., Youn, I., Choi, J. B., Cao, L., Setton, L. A. & Haider, M. A. in *Skeletal Development and Remodeling in Health, Disease, and Aging* Vol. 1068 *Annals of the New York Academy of Sciences* (ed M. Zaidi) 498-512 (2006).

264 Vincent, T. L., McLean, C. J., Full, L. E., Peston, D. & Saklatvala, J. FGF-2 is bound to perlecan in the pericellular matrix of articular cartilage, where it acts as a chondrocyte mechanotransducer. *Osteoarthritis and Cartilage* **15**, 752-763, doi:10.1016/j.joca.2007.01.021 (2007).

265 Honda, K., Ohno, S., Tanimoto, K., Ijuin, C., Tanaka, N., Doi, T., Kato, Y. & Tanne, K. The effects of high magnitude cyclic tensile load on cartilage matrix metabolism in cultured chondrocytes. *European Journal of Cell Biology* **79**, 601-609, doi:10.1078/0171-9335-00089 (2000).

266 Pufe, T., Lemke, A., Kurz, B., Petersen, W., Tillmann, B., Grodzinsky, A. J. & Mentlein, R. Mechanical overload induces VEGF in cartilage discs via hypoxia-inducible factor. *American Journal of Pathology* **164**, 185-192, doi:10.1016/s0002-9440(10)63109-4 (2004).

267 Nicodemus, G. D. & Bryant, S. J. Mechanical loading regimes affect the anabolic and catabolic activities by chondrocytes encapsulated in PEG hydrogels. *Osteoarthritis and Cartilage* **18**, 126-137, doi:10.1016/j.joca.2009.08.005 (2010).

268 Xu, Z. F., Buckley, M. J., Evans, C. H. & Agarwal, S. Cyclic tensile strain acts as an antagonist of IL-1 beta actions in chondrocytes. *Journal of Immunology* **165**, 453-460 (2000).

269 Sharp, W. W., Terracio, L., Borg, T. K. & Samarel, A. M. Contractile activity modulates actin synthesis and turnover in cultured neonatal rat heart cells. *Circulation Research* **73**, 172-183 (1993).

270 Byron, K. L., Puglisi, J. L., Holda, J. R., Eble, D. & Samarel, A. M. Myosin heavy chain turnover in cultured neonatal rat heart cells: Effects of Ca2+ (i) and contractile activity. *American Journal of Physiology-Cell Physiology* **271**, C1447-C1456 (1996).

271 Flynn, B. P., Bhole, A. P., Saeidi, N., Liles, M., DiMarzio, C. A. & Ruberti, J. W. Mechanical Strain Stabilizes Reconstituted Collagen Fibrils against Enzymatic Degradation by Mammalian Collagenase Matrix Metalloproteinase 8 (MMP-8). *Plos One* **5**, doi:10.1371/journal.pone.0012337 (2010).

272 Blott, S. C., Williams, J. L. & Haley, C. S. Genetic variation within the Hereford breed of cattle. *Animal Genetics* **29**, 202-211 (1998).

273 Gibbs, R. A., Taylor, J. F., Van Tassell, C. P., Barendse, W., Eversoie, K. A., Gill, C. A., Green, R. D., Hamernik, D. L., Kappes, S. M., Lien, S., Matukumalli, L. K., McEwan, J. C., Nazareth, L. V., Schnabel, R. D., Taylor, J. F., Weinstock, G. M., Wheeler, D. A., Ajmone-Marsan, P., Barendse, W., Boettcher, P. J., Caetano, A. R., Garcia, J. F., Hanotte, O., Mariani, P., Skow, L. C., Williams, J. L., Caetano, A. R., Diallo, B., Green, R. D., Hailemariam, L., Hanotte, O., Martinez, M. L., Morris, C. A., Silva, L. O. C., Spelman, R. J., Taylor, J. F., Mulatu, W., Zhao, K., Abbey, C. A., Agaba, M., Araujo, F. R., Bunch, R. J., Burton, J., Gill, C. A., Gorni, C., Olivier, H., Harrison, B. E., Luff, B., Machado, M. A., Mariani, P., Morris, C. A., Mwakaya, J., Plastow, G., Sim, W., Skow, L. C., Smith, T., Sonstegard, T. S., Spelman, R. J., Taylor, J. F., Thomas, M. B., Valentini, A., Williams, P., Womack, J., Wooliams, J. A., Liu, Y., Qin, X., Worley, K. C., Gao, C., Gill, C. A., Jiang, H., Liu, Y., Moore, S. S., Nazareth, L. V., Ren, Y., Song, X.-Z., Bustamante, C. D., Hernandez, R. D., Muzny, D. M., Nazareth, L. V., Patil, S., Lucas, A. S., Fu, Q., Kent, M. P., Moore, S. S., Vega, R., Abbey, C. A., Gao, C., Gill, C. A., Green, R. D., Matukumalli, L. K., Matukumalli, A., McWilliam, S., Schnabel, R. D., Sclep, G., Ajmone-Marsan, P., Bryc, K., Bustamante, C. D., Choi, J., Gao, H., Grefenstette, J. J., Murdoch, B., Stella, A., Villa-Angulo, R., Wright, M., Aerts, J., Jann, O., Negrini, R., Sonstegard, T. S., Williams, J. L., Taylor, J. F., Villa-Angulo, R., Goddard, M. E., Hayes, B. J., Barendse, W., Bradley, D. G., Boettcher, P. J., Bustamante, C. D., da Silva, M. B., Lau, L. P. L., Liu, G. E., Lynn, D. J., Panzitta, F., Sclep, G., Wright, M. & Dodds, K. G. Genome-Wide Survey of SNP Variation Uncovers the Genetic Structure of Cattle Breeds. *Science* **324**, 528-532, doi:10.1126/science.1167936 (2009).

274 Smeyne, R. J., Vendrell, M., Hayward, M., Baker, S. J., Miao, G. G., Schilling, K., Robertson, L. M., Curran, T. & Morgan, J. I. Continuous c-fos expression precedes programmed cell death in vivo. *Nature* **363**, 166-169, doi:10.1038/363166a0 (1993).
275 Marti, A., Jehn, B., Costello, E., Keon, N., Ke, G., Martin, F. & Jaggi, R. Protein kinase A and AP-1 (c-Fos/JunD) are induced during apoptosis of mouse mammary epithelial cells. *Oncogene* **9**, 1213-1223 (1994).
276 Preston, G. A., Lyon, T. T., Yin, Y. X., Lang, J. E., Solomon, G., Annab, L., Srinivasan, D. G., Alcorta, D. A. & Barrett, J. C. Induction of apoptosis by c-Fos protein. *Molecular and Cellular Biology* **16**, 211-218 (1996).
277 Zhang, X., Zhang, L., Yang, H., Huang, X., Otu, H., Libermann, T. A., DeWolf, W. C., Khosravi-Far, R. & Olumi, A. F. c-Fos as a proapoptotic agent in TRAIL-induced apoptosis in prostate cancer cells. *Cancer Research* **67**, 9425-9434, doi:10.1158/0008-5472.can-07-1310 (2007).
278 Liang, Y., Jorgensen, A., Kaestel, C. G., Wiencke, A. K., Lui, G. M., la Cour, M., Ropke, C. & Nissen, M. H. Bcl-2, Bax, and c-Fos expression correlates to RPE cell apoptosis induced by UV-light and daunorubicin. *Current Eye Research* **20**, 25-34 (2000).
279 Yu, R.-A., He, L.-F. & Chen, X.-M. Effects of cadmium on hepatocellular DNA damage, proto-oncogene expression and apoptosis in rats. *Biomedical and environmental sciences : BES* **20**, 146-153 (2007).
280 Chung, C., Erickson, I. E., Mauck, R. L. & Burdick, J. A. Differential behavior of auricular and articular chondrocytes in hyaluronic acid hydrogels. *Tissue Engineering Part A* **14**, 1121-1131, doi:10.1089/ten.tea.2007.0291 (2008).
281 Boutell, J., Maciewicz, R. A. & Parker, A. E. Cartilage ECM molecules are differentially expressed between nasal and articular bovine chondrocytes. *Int J Exp Pathol* **81**, A7-A8 (2000).
282 Arai, M., Anderson, D., Kurdi, Y., Annis-Freeman, B., Shields, K., Collins-Racie, L. A., Corcoran, C., DiBlasio-Smith, E., Pittman, D. D., Dorner, A. J., Morris, E. & LaVallie, E. R. Effect of adenovirus-mediated overexpression of bovine ADAMTS-4 and human ADAMTS-5 in primary bovine articular chondrocyte pellet culture system. *Osteoarthritis and Cartilage* **12**, 599-613, doi:10.1016/j.joca.2004.05.001 (2004).
283 Candrian, C., Vonwil, D., Barbero, A., Bonacina, E., Miot, S., Farhadi, J., Wirz, D., Dickinson, S., Hollander, A., Jakob, M., Li, Z., Alini, M., Heberer, M. & Martin, I. Engineered cartilage generated by nasal chondrocytes is responsive to physical forces resembling joint loading. *Arthritis and Rheumatism* **58**, 197-208, doi:10.1002/art.23155 (2008).
284 Dos Santos, C., Akram, A., Masoom, H., Han, B., Haitsma, J. J., Peng, C., Shan, Y., Zhang, H., Liu, M., Hai, T. & Slutsky, A. S. ATF3 is activated in ventilator induced lung injury. *Faseb Journal* **24** (2010).
285 Koivisto, E., Acosta, A. J., Moilanen, A.-M., Tokola, H., Aro, J., Pennanen, H., Sakkinen, H., Kaikkonen, L., Ruskoaho, H. & Rysa, J. Characterization of the Regulatory Mechanisms of Activating Transcription Factor 3 by Hypertrophic Stimuli in Rat Cardiomyocytes. *Plos One* **9**, doi:10.1371/journal.pone.0105168 (2014).
286 Wang, X., Fan, J., Zhang, M., Sun, Z. & Xu, G. Gene Expression Changes under Cyclic Mechanical Stretching in Rat Retinal Glial (Muller) Cells. *Plos One* **8**, doi:10.1371/journal.pone.0063467 (2013).
287 Ott, C.-E., Bauer, S., Manke, T., Ahrens, S., Roedelsperger, C., Gruenhagen, J., Kornak, U., Duda, G., Mundlos, S. & Robinson, P. N. Promiscuous and Depolarization-Induced Immediate-Early Response Genes Are Induced by

Mechanical Strain of Osteoblasts. *Journal of Bone and Mineral Research* **24**, 1247-1262, doi:10.1359/jbmr.090206 (2009).

288 Zaman, G., Sunters, A., Galea, G. L., Javaheri, B., Saxon, L. K., Moustafa, A., Armstrong, V. J., Price, J. S. & Lanyon, L. E. Loading-related Regulation of Transcription Factor EGR2/Krox-20 in Bone Cells Is ERK1/2 Protein-mediated and Prostaglandin, Wnt Signaling Pathway-, and Insulin-like Growth Factor-I Axis-dependent. *Journal of Biological Chemistry* **287**, 3946-3962, doi:10.1074/jbc.M111.252742 (2012).

289 Diercke, K., Kohl, A., Lux, C. J. & Erber, R. Compression of human primary cementoblasts leads to apoptosis A possible cause of dental root resorption? *Journal of Orofacial Orthopedics-Fortschritte Der Kieferorthopadie* **75**, 430-445, doi:10.1007/s00056-014-0237-5 (2014).

290 Verma, P. & Dalal, K. ADAMTS-4 and ADAMTS-5: Key Enzymes in Osteoarthritis. *Journal of Cellular Biochemistry* **112**, 3507-3514, doi:10.1002/jcb.23298 (2011).

291 Werb, Z., Mainardi, C. L., Vater, C. A. & Harris, E. D. Endogenous activiation of latent collagenase by rheumatoid synovial cells. Evidence for a role of plasminogen activator. *New England Journal of Medicine* **296**, 1017-1023, doi:10.1056/nejm197705052961801 (1977).

292 Schaegger, H. Tricine-SDS-PAGE. *Nature Protocols* **1**, 16-22, doi:10.1038/nprot.2006.4 (2006).

293 Camerer, E., Barker, A., Duong, D. N., Ganesan, R., Kataoka, H., Cornelissen, I., Darragh, M. R., Hussain, A., Zheng, Y.-W., Srinivasan, Y., Brown, C., Xu, S.-M., Regard, J. B., Lin, C.-Y., Craik, C. S., Kirchhofer, D. & Coughlin, S. R. Local Protease Signaling Contributes to Neural Tube Closure in the Mouse Embryo. *Developmental Cell* **18**, 25-38, doi:10.1016/j.devcel.2009.11.014 (2010).

294 Hollenberg, M. D., Mihara, K., Polley, D., Suen, J. Y., Han, A., Fairlie, D. P. & Ramachandran, R. Biased signalling and proteinase-activated receptors (PARs): targeting inflammatory disease. *British Journal of Pharmacology* **171**, 1180-1194, doi:10.1111/bph.12544 (2014).

295 Tanaka, M., Arai, H., Liu, N., Nogaki, F., Nomura, K., Kasuno, K., Oida, E., Kita, T. & Ono, T. Role of coagulation factor Xa and protease-activated receptor 2 in human mesangial cell proliferation. *Kidney International* **67**, 2123-2133, doi:10.1111/j.1523-1755.2005.00317.x (2005).

296 Jin, T., Tarkowski, A., Carmeliet, P. & Bokarewa, M. Urokinase, a constitutive component of the inflamed synovial fluid, induces arthritis. *Arthritis Research & Therapy* **5**, R9-R17, doi:10.1186/ar606 (2003).

297 Trivedi, V., Boire, A., Tchemychev, B., Kaneider, N. C., Leger, A. J., O'Callaghan, K., Covic, L. & Kuliopulos, A. Platelet Matrix Metalloprotease-1 Mediates Thrombogenesis by Activating PAR1 at a Cryptic Ligand Site. *Cell* **137**, 332-343, doi:10.1016/j.cell.2009.02.018 (2009).

298 Jaffre, F., Friedman, A. E., Hu, Z., Mackman, N. & Blaxall, B. C. beta-Adrenergic Receptor Stimulation Transactivates Protease-Activated Receptor 1 via Matrix Metalloproteinase 13 in Cardiac Cells. *Circulation* **125**, 2993-+, doi:10.1161/circulationaha.111.066787 (2012).

299 Albericio, F. Developments in peptide and amide synthesis. *Current Opinion in Chemical Biology* **8**, 211-221, doi:10.1016/j.cbpa.2004.03.002 (2004).

300 Elmariah, S. B., Reddy, V. B. & Lerner, E. A. Cathepsin S Signals via PAR2 and Generates a Novel Tethered Ligand Receptor Agonist. *Plos One* **9**, doi:10.1371/journal.pone.0099702 (2014).

301 Loew, D., Perrault, C., Morales, M., Moog, S., Ravanat, C., Schuhler, S., Arcone, R., Pietropaolo, C., Cazenave, J. P., van Dorsselaer, A. & Lanza, L. O. Proteolysis

of the exodomain of recombinant protease-activated receptors: Prediction of receptor activation or inactivation by MALDI mass spectrometry. *Biochemistry* **39**, 10812-10822, doi:10.1021/bi0003341 (2000).

302 KB, U. *UniProtKB - P55085 (PAR2_HUMAN)*, <http://www.uniprot.org/uniprot/P55085> (2016).

303 Li, X. & Tai, H.-H. Thromboxane A(2) Receptor-Mediated Release of Matrix Metalloproteinase-1 (MMP-1) Induces Expression of Monocyte Chemoattractant Protein-1 (MCP-1) by Activation of Protease-Activated Receptor 2 (PAR2) in A549 Human Lung Adenocarcinoma Cells. *Molecular Carcinogenesis* **53**, 659-666, doi:10.1002/mc.22020 (2014).

304 Tiaden, A. N. & Richards, P. J. The Emerging Roles of HTRA1 in Musculoskeletal Disease. *American Journal of Pathology* **182**, 1482-1488, doi:10.1016/j.ajpath.2013.02.003 (2013).

305 Grau, S., Richards, P. J., Kerr, B., Hughes, C., Caterson, B., Williams, A. S., Junker, U., Jones, S. A., Clausen, T. & Ehrmann, M. The role of human HtrA1 in arthritic disease. *Journal of Biological Chemistry* **281**, 6124-6129, doi:10.1074/jbc.M500361200 (2006).

306 Wu, J., Liu, W., Bemis, A., Wang, E., Qiu, Y., Morris, E. A., Flannery, C. R. & Yang, Z. Comparative proteomic characterization of articular cartilage tissue from normal donors and patients with osteoarthritis. *Arthritis and Rheumatism* **56**, 3675-3684, doi:10.1002/art.22876 (2007).

307 Eigenbrot, C., Ultsch, M., Lipari, M. T., Moran, P., Lin, S. J., Ganesan, R., Quan, C., Tom, J., Sandoval, W., Campagne, M. v. L. & Kirchhofer, D. Structural and Functional Analysis of HtrA1 and Its Subdomains. *Structure* **20**, 1040-1050, doi:10.1016/j.str.2012.03.021 (2012).

308 Carmeliet, P., Moons, L., Lijnen, H. R., Baes, M., Lemaitre, V., Tipping, P., Drew, A., Eeckhout, Y., Shapiro, S., Lupu, F. & Collen, D. Urokinase-generated plasmin activates matrix metalloproteinases during aneurysm formation. *Nature Genetics* **17**, 439-444, doi:10.1038/ng1297-439 (1997).

309 Smith, H. W. & Marshall, C. J. Regulation of cell signalling by uPAR. *Nature Reviews Molecular Cell Biology* **11**, 23-36, doi:10.1038/nrm2821 (2010).

310 Rawlings, N. D., Barrett, A. J. & Finn, R. Twenty years of the MEROPS database of proteolytic enzymes, their substrates and inhibitors. *Nucleic Acids Research* **44**, D343-D350, doi:10.1093/nar/gkv1118 (2016).

311 Park, J. E., Lenter, M. C., Zimmermann, R. N., Garin-Chesa, P., Old, L. J. & Rettig, W. J. Fibroblast activation protein, a dual specificity serine protease expressed in reactive human tumor stromal fibroblasts. *Journal of Biological Chemistry* **274**, 36505-36512, doi:10.1074/jbc.274.51.36505 (1999).

312 Aggarwal, S., Brennen, W. N., Kole, T. P., Schneider, E., Topaloglu, O., Yates, M., Cotter, R. J. & Denmeade, S. R. Fibroblast activation protein peptide substrates identified from human collagen I derived gelatin cleavage sites. *Biochemistry* **47**, 1076-1086, doi:10.1021/bi701921b (2008).

313 Huang, C.-H., Suen, C.-S., Lin, C.-T., Chien, C.-H., Lee, H.-Y., Chung, K.-M., Tsai, T.-Y., Jiaang, W.-T., Hwang, M.-J. & Chen, X. Cleavage-site specificity of prolyl endopeptidase FAP investigated with a full-length protein substrate. *Journal of Biochemistry* **149**, 685-692, doi:10.1093/jb/mvr017 (2011).

314 Kanke, T., Ishiwata, H., Kabeya, M., Saka, M., Doi, T., Hattori, Y., Kawabata, A. & Plevin, R. Binding of a highly potent protease-activated receptor-2 (PAR2) activating peptide, H-3 2-furoyl-LIGRL-NH2, to human PAR2. *British Journal of Pharmacology* **145**, 255-263, doi:10.1038/sj.bjp.0706189 (2005).

315 Yoshida, N., Katada, K., Handa, O., Takagi, T., Kokura, S., Naito, Y., Mukaida, N., Soma, T., Shimada, Y., Yoshikawa, T. & Okanoue, T. Interleukin-8

production via protease-activated receptor 2 in human esophageal epithelial cells. *International Journal of Molecular Medicine* **19**, 335-340 (2007).

316 Tanaka, Y., Sekiguchi, F., Hong, H. & Kawabata, A. PAR2 triggers IL-8 release via MEK/ERK and PI3-kinase/Akt pathways in GI epithelial cells. *Biochemical and Biophysical Research Communications* **377**, 622-626, doi:10.1016/j.bbrc.2008.10.018 (2008).

317 Seitz, I., Hess, S., Schulz, H., Eckl, R., Busch, G., Montens, H. P., Brandl, R., Seidl, S., Schomig, A. & Ott, I. Membrane-type serine protease-1/matriptase induces interleukin-6 and-8 in endothelial cells by activation of protease-activated receptor-2 - Potential implications in atherosclerosis. *Arteriosclerosis Thrombosis and Vascular Biology* **27**, 769-775, doi:10.1161/01.atv.0000258862.61067.14 (2007).

318 Deroanne, C. F., Hamelryckx, D., Ho, T. T. G., Lambert, C. A., Catroux, P., Lapiere, C. M. & Nusgens, B. V. Cdc42 downregulates MMP-1 expression by inhibiting the ERK1/2 pathway. *Journal of Cell Science* **118**, 1173-1183, doi:10.1242/jcs.01707 (2005).

319 Weiss, M. B., Abel, E. V., Mayberry, M. M., Basile, K. J., Berger, A. C. & Aplin, A. E. TWIST1 Is an ERK1/2 Effector That Promotes Invasion and Regulates MMP-1 Expression in Human Melanoma Cells. *Cancer Research* **72**, 6382-6392, doi:10.1158/0008-5472.can-12-1033 (2012).

320 Raymond, L., Eck, S., Mollmark, J., Hays, E., Tomek, I., Kantor, S., Elliott, S. & Vincenti, M. Interleukin-1 beta induction of matrix metal loproteinase-1 transcription in chondrocytes requires ERK-dependent activation of CCAAT enhancer-binding protein-beta. *Journal of Cellular Physiology* **207**, 683-688, doi:10.1002/jcp.20608 (2006).

321 Cawston, T. E., Ellis, A. J., Humm, G., Lean, E., Ward, D. & Curry, V. Interleukin-1 and oncostatin-M in combination promotes the release of collagen fragments from bovine nasal cartilage in culutre. *Biochemical and Biophysical Research Communications* **215**, 377-385, doi:10.1006/bbrc.1995.2476 (1995).

322 Cleaver, C. S., Rowan, A. D. & Cawston, T. E. Interleukin 13 blocks the release of collagen from bovine nasal cartilage treated with proinflammatory cytokines. *Annals of the Rheumatic Diseases* **60**, 150-157, doi:10.1136/ard.60.2.150 (2001).

323 Shingleton, W. D., Ellis, A. J., Rowan, A. D. & Cawston, T. E. Retinoic acid combines with interleukin-1 to promote the degradation of collagen from bovine nasal cartilage: Matrix metalloproteinases-1 and-13 are involved in cartilage collagen breakdown. *Journal of Cellular Biochemistry* **79**, 519-531, doi:10.1002/1097-4644(20001215)79:4<519::aid-jcb10>3.0.co;2-u (2000).

324 Wu, J. J., Rush, T. S., Hotchandani, R., Du, X. M., Geck, M., Collins, E., Xu, Z. B., Skotnicki, J., Levin, J. I. & Lovering, F. E. Identification of potent and selective MMP-13 inhibitors. *Bioorganic & Medicinal Chemistry Letters* **15**, 4105-4109, doi:10.1016/j.bmcl.2005.06.019 (2005).

325 Matter, H., Schwab, W., Barbier, D., Billen, G., Haase, B., Neises, B., Schudok, M., Thorwart, W., Schreuder, H., Brachvogel, V., Lonze, P. & Weithmann, K. U. Quantitative structure-activity relationship of human neutrophil collagenase (MMP-8) inhibitors using comparative molecular field analysis and X-ray structure analysis. *Journal of Medicinal Chemistry* **42**, 1908-1920, doi:10.1021/jm980631s (1999).

326 Turk, B. E., Huang, L. L., Piro, E. T. & Cantley, L. C. Determination of protease cleavage site motifs using mixture-based oriented peptide libraries. *Nature Biotechnology* **19**, 661-667, doi:10.1038/90273 (2001).

327 Netzelarnett, S., Fields, G., Birkedalhansen, H. & Vanwart, H. E. Sequence Specificities of Human Fibroblast and Neutrophil Collagenases. *Journal of Biological Chemistry* **266**, 6747-6755 (1991).

328 Beliveau, F., Desilets, A. & Leduc, R. Probing the substrate specificities of matriptase, matriptase-2, hepsin and DESC1 with internally quenched fluorescent peptides. *Febs Journal* **276**, 2213-2226, doi:10.1111/j.1742-4658.2009.06950.x (2009).

329 Nagase, H. & Visse, R. in *Extracellular Matrix Degradation* Vol. 2 Ch. 5, 95-122 (2011).

330 Al-Ani, B., Hansen, K. K. & Hollenberg, M. D. Proteinase-activated receptor-2: Key role of amino-terminal dipeptide residues of the tethered ligand for receptor activation. *Molecular Pharmacology* **65**, 149-156, doi:10.1124/mol.65.1.149 (2004).

331 Ferrell, W. R., Lockhart, J. C., Kelso, E. B., Dunning, L., Plevin, R., Meek, S. E., Smith, A. J. H., Hunter, G. D., McLean, J. S., McGarry, F., Ramage, R., Jiang, L., Kanke, T. & Kawagoe, J. Essential role for proteinase-activated receptor-2 in arthritis. *Journal of Clinical Investigation* **111**, 35-41, doi:10.1172/jci200316913 (2003).

332 Ramachandran, R., Mihara, K., Mathur, M., Rochdi, M. D., Bouvier, M., Defea, K. & Hollenberg, M. D. Agonist-Biased Signaling via Proteinase Activated Receptor-2: Differential Activation of Calcium and Mitogen-Activated Protein Kinase Pathways. *Molecular Pharmacology* **76**, 791-801, doi:10.1124/mol.109.055509 (2009).

333 Al-Ani, B., Wijesuriya, S. J. & Hollenberg, M. D. Proteinase-activated receptor 2: Differential activation of the receptor by tethered ligand and soluble peptide analogs. *Journal of Pharmacology and Experimental Therapeutics* **302**, 1046-1054, doi:10.1124/jpet.302.3.1046 (2002).

334 Lin, C. B., Chen, N., Scarpa, R., Guan, F., Babiarz-Magee, L., Liebel, F., Li, W. H., Kizoulis, M., Shapiro, S. & Seiberg, M. LIGR, a protease-activated receptor-2-derived peptide, enhances skin pigmentation without inducing inflammatory processes. *Pigment Cell & Melanoma Research* **21**, 172-183, doi:10.1111/j.1755-148X.2008.00441.x (2008).

335 Foskett, J. K., White, C., Cheung, K.-H. & Mak, D.-O. D. Inositol trisphosphate receptor Ca2+ release channels. *Physiological Reviews* **87**, 593-658, doi:10.1152/physrev.00035.2006 (2007).

336 Yasuda, Y., Li, Z. Q., Greenbaum, D., Bogyo, M., Weber, E. & Bromme, D. Cathepsin V, a novel and potent elastolytic activity expressed in activated macrophages. *Journal of Biological Chemistry* **279**, 36761-36770, doi:10.1074/jbc.M403986200 (2004).

337 Niwa, Y., Suzuki, T., Dohmae, N., Umezawa, K. & Simizu, S. Determination of cathepsin V activity and intracellular trafficking by N-glycosylation. *Febs Letters* **586**, 3601-3607, doi:10.1016/j.febslet.2012.08.001 (2012).

338 Ikeda, Y., Ikata, T., Mishiro, T., Nakano, S., Ikebe, M. & Yasuoka, S. Cathepsins B and L in synovial fluids from patients with rheumatoid arthritis and the effect of cathepsin B on the activation of pro-urokinase. *The journal of medical investigation : JMI* **47**, 61-75 (2000).

339 Keyszer, G. M., Heer, A. H., Kriegsmann, J., Geiler, T., Trabandt, A., Keysser, M., Gay, R. E. & Gay, S. Comparative analysis of cathepsin L, cathepsin D, and collagenase messenger RNA expression in synovial tissues of patients with rheumatoid arthritis and osteoarthritis, by in situ hybridization. *Arthritis and Rheumatism* **38**, 976-984, doi:10.1002/art.1780380714 (1995).

340 Suen, J. Y., Gardiner, B., Grimmond, S. & Fairlie, D. P. Profiling Gene Expression Induced by Protease-Activated Receptor 2 (PAR2) Activation in Human Kidney Cells. *Plos One* **5**, doi:10.1371/journal.pone.0013809 (2010).
341 Stenton, G. R., Nohara, O., Dery, R. E., Vliagoftis, H., Gilchrist, M., Johri, A., Wallace, J. L., Hollenberg, M. D., Moqbel, R. & Befus, A. D. Proteinase-activated receptor (PAR)-1 and-2 agonists induce mediator release from mast cells by pathways distinct from PAR-1 and PAR-2. *Journal of Pharmacology and Experimental Therapeutics* **302**, 466-474, doi:10.1124/jpet.302.2.466 (2002).
342 Huang, H. L., Hsing, H. W., Lai, T. C., Chen, Y. W., Lee, T. R., Chan, H. T., Lyu, P. C., Wu, C. L., Lu, Y. C., Lin, S. T., Lin, C. W., Lai, C. H., Chang, H. T., Chou, H. C. & Chan, H. L. Trypsin-induced proteome alteration during cell subculture in mammalian cells. *Journal of Biomedical Science* **17**, doi:10.1186/1423-0127-17-36 (2010).
343 Abey, H. T., Fairlie, D. P., Moffatt, J. D., Balzary, R. W. & Cocks, T. M. Protease-activated receptor-2 peptides activate neurokinin-1 receptors in the mouse isolated trachea. *Journal of Pharmacology and Experimental Therapeutics* **317**, 598-605, doi:10.1124/jpet.105.097121 (2006).
344 Borzi, R. M., Mazzetti, I., Macor, S., Silvestri, T., Bassi, A., Cattini, L. & Facchini, A. Flow cytometric analysis of intracellular chemokines in chondrocytes in vivo: constitutive expression and enhancement in osteoarthritis and rheumatoid arthritis. *Febs Letters* **455**, 238-242, doi:10.1016/s0014-5793(99)00886-8 (1999).
345 Borzi, R. M., Mazzetti, I., Cattini, L., Uguccioni, M., Baggiolini, M. & Facchini, A. Human chondrocytes express functional chemokine receptors and release matrix-degrading enzymes in response to C-X-C and C-C chemokines. *Arthritis and Rheumatism* **43**, 1734-1741, doi:10.1002/1529-0131(200008)43:8<1734::aid-anr9>3.0.co;2-b (2000).
346 Yan, D. Y., Kc, R., Chen, D., Xiao, G. Z. & Im, H. J. Bovine Lactoferricin-induced Anti-inflammation Is, in Part, via Up-regulation of Interleukin-11 by Secondary Activation of STAT3 in Human Articular Cartilage. *Journal of Biological Chemistry* **288**, 31655-31669, doi:10.1074/jbc.M112.440420 (2013).
347 Ralph, J. A., McEvoy, A. N., Kane, D., Bresnihan, B., FitzGerald, O. & Murphy, E. P. Modulation of orphan nuclear receptor NURR1 expression by methotrexate in human inflammatory joint disease involves adenosine A2A receptor-mediated responses. *Journal of Immunology* **175**, 555-565 (2005).
348 Mix, K. S., McMahon, K., McMorrow, J. P., Walkenhorst, D. E., Smyth, A. M., Petrella, B. L., Gogarty, M., Fearon, U., Veale, D., Attur, M. G., Abramson, S. B. & Murphy, E. P. Orphan nuclear receptor NR4A2 induces synoviocyte proliferation, invasion, and matrix metalloproteinase 13 transcription. *Arthritis and Rheumatism* **64**, 2126-2136, doi:10.1002/art.34399 (2012).
349 Aikawa, Y., Morimoto, K., Yamamoto, T., Chaki, H., Hashiramoto, A., Narita, H., Hirono, S. & Shiozawa, S. Treatment of arthritis with a selective inhibitor of c-Fos/activator protein-1. *Nature Biotechnology* **26**, 817-823, doi:10.1038/nbt1412 (2008).
350 Barksby, H. E., Hui, W., Wappler, I., Peters, H. H., Milner, J. M., Richards, C. D., Cawston, T. E. & Rowan, A. D. Interleukin-1 in combination with oncostatin M up-regulates multiple genes in chondrocytes - Implications for cartilage destruction and repair. *Arthritis and Rheumatism* **54**, 540-550, doi:10.1002/art.21574 (2006).
351 Wojdasiewicz, P., Poniatowski, L. A. & Szukiewicz, D. The Role of Inflammatory and Anti-Inflammatory Cytokines in the Pathogenesis of Osteoarthritis. *Mediators of Inflammation*, doi:10.1155/2014/561459 (2014).

352 Melchiorri, C., Meliconi, R., Frizziero, L., Silvestri, T., Pulsatelli, L., Mazzetti, I., Borzi, R. M., Uguccioni, M. & Facchini, A. Enhanced and coordinated in vivo expression of inflammatory cytokines and nitric oxide synthase by chondrocytes from patients with osteoarthritis. *Arthritis and Rheumatism* **41**, 2165-2174, doi:10.1002/1529-0131(199812)41:12<2165::aid-art11>3.0.co;2-o (1998).

353 Martelpelletier, J., McCollum, R., Dibattista, J., Faure, M. P., Chin, J. A., Fournier, S., Sarfati, M. & Pelletier, J. P. The interleukin-1 receptor in normal and osteoarthritic human articular chondrocytes: identification as the type I receptor and analysis of binding kinetics and biologic function. *Arthritis and Rheumatism* **35**, 530-540, doi:10.1002/art.1780350507 (1992).

354 Sillat, T., Barreto, G., Clarijs, P., Soininen, A., Ainola, M., Pajarinen, J., Korhonen, M., Konttinen, Y. T., Sakalyte, R., Hukkanen, M., Ylinen, P. & Nordstrom, D. C. E. Toll-like receptors in human chondrocytes and osteoarthritic cartilage. *Acta Orthopaedica* **84**, 585-592, doi:10.3109/17453674.2013.854666 (2013).

355 Kragstrup, T. W., Otkjaer, K., Hohn, C., Jorgensen, A., Hokland, M., Iversen, L. & Deleuran, B. The expression of IL-20 and IL-24 and their shared receptors are increased in rheumatoid arthritis and spondyloarthropathy. *Cytokine* **41**, 16-23, doi:10.1016/j.cyto.2007.10.004 (2008).

356 Raymond, F., Carbonneau, J., Boucher, N., Robitaille, L., Boisvert, S., Wu, W. K., De Serres, G., Boivin, G. & Corbeil, J. Comparison of Automated Microarray Detection with Real-Time PCR Assays for Detection of Respiratory Viruses in Specimens Obtained from Children. *Journal of Clinical Microbiology* **47**, 743-750, doi:10.1128/jcm.01297-08 (2009).

357 Allanach, K., Mengel, M., Einecke, G., Sis, B., Hidalgo, L. G., Mueller, T. & Halloran, P. F. Comparing microarray versus RT-PCR assessment of renal allograft biopsies: Similar performance despite different dynamic ranges. *American Journal of Transplantation* **8**, 1006-1015, doi:10.1111/j.1600-6143.2008.02199.x (2008).

358 Wang, Y. L., Barbacioru, C., Hyland, F., Xiao, W. M., Hunkapiller, K. L., Blake, J., Chan, F., Gonzalez, C., Zhang, L. & Samaha, R. R. Large scale real-time PCR validation on gene expression measurements from two commercial long-oligonucleotide microarrays. *Bmc Genomics* **7**, doi:10.1186/1471-2164-7-59 (2006).

359 Zeng, G. Q., Chen, A. B., Li, W., Song, J. H. & Gao, C. Y. High MMP-1, MMP-2, and MMP-9 protein levels in osteoarthritis. *Genetics and Molecular Research* **14**, 14811-14822, doi:10.4238/2015.November.18.46 (2015).

360 Lipari, L. & Gerbino, A. Expression of gelatinases (MMP-2, MMP-9) in human articular cartilage. *International Journal of Immunopathology and Pharmacology* **26**, 817-823 (2013).

361 Ohmuraya, M., Sugano, A., Hirota, M., Takaoka, Y. & Yamamura, K. Role of intrapancreatic SPINK1/Spink3 expression in the development of pancreatitis. *Frontiers in Physiology* **3**, doi:10.3389/fphys.2012.00126 (2012).

362 Yamasaki, Y., Satomi, S., Murai, N., Tsuzuki, S. & Fushiki, T. Inhibition of membrane-type serine protease 1/matriptase by natural and synthetic protease inhibitors. *Journal of Nutritional Science and Vitaminology* **49**, 27-32 (2003).

363 Izaguirre, G., Qi, L. X., Lima, M. & Olson, S. T. Identification of Serpin Determinants of Specificity and Selectivity for Furin Inhibition through Studies of alpha(1) PDX (alpha(1)-Protease Inhibitor Portland)-Serpin B8 and Furin Active-site Loop Chimeras. *Journal of Biological Chemistry* **288**, doi:10.1074/jbc.M113.462804 (2013).

364 Alvarez-Garcia, O., Olmer, M., Akagi, R., Akasaki, Y., Fisch, K. M., Shen, T., Su, A. I. & Lotz, M. K. Suppression of REDD1 in osteoarthritis cartilage, a novel mechanism for dysregulated mTOR signaling and defective autophagy. *Osteoarthritis and Cartilage* **24**, 1639-1647, doi:10.1016/j.joca.2016.04.015 (2016).

365 Zhang, Y. & Ross, A. C. Retinoic acid and the transcription factor MafB act together and differentially to regulate aggrecan and matrix metalloproteinase gene expression in neonatal chondrocytes. *Journal of Cellular Biochemistry* **114**, 471-479, doi:10.1002/jcb.24387 (2013).

366 Bramlage, C. P., Haupl, T., Kaps, C., Ungethum, U., Krenn, V., Pruss, A., Muller, G. A., Strutz, F. & Burmester, G. R. Decrease in expression of bone morphogenetic proteins 4 and 5 in synovial tissue of patients with osteoarthritis and rheumatoid arthritis. *Arthritis Research & Therapy* **8**, doi:10.1186/ar1923 (2006).

367 Guns, L., Calebiro, D., Lohse, M., Loires, R. & Cailotto, F. The GPR22 receptor, genetically linked to osteoarthritis stimulates chondrocyte hypertrophy and decreases protein kinase a activity. *Ann Rheum Dis* **75** (2016).

368 Kerkhof, H. J. M., Lories, R. J., Meulenbelt, I., Jonsdottir, I., Valdes, A. M., Arp, P., Ingvarsson, T., Jhamai, M., Jonsson, H., Stolk, L., Thorleifsson, G., Zhai, G. J., Zhang, F., Zhu, Y. Y., van der Breggen, R., Carr, A., Doherty, M., Doherty, S., Felson, D. T., Gonzalez, A., Halldorsson, B. V., Hart, D. J., Hauksson, V. B., Hofman, A., Ioannidis, J. P. A., Kloppenburg, M., Lane, N. E., Loughlin, J., Luyten, F. P., Nevitt, M. C., Parimi, N., Pols, H. A. P., Rivadeneira, F., Slagboom, E. P., Styrkarsdottir, U., Tsezou, A., van de Putte, T., Zmuda, J., Spector, T. D., Stefansson, K., Uitterlinden, A. G. & van Meurs, J. B. J. A Genome-Wide Association Study Identifies an Osteoarthritis Susceptibility Locus on Chromosome 7q22. *Arthritis and Rheumatism* **62**, 499-510, doi:10.1002/art.27184 (2010).

369 Lewis, E. J., Bishop, J., Bottomley, K. M. K., Bradshaw, D., Brewster, M., Broadhurst, M. J., Brown, P. A., Budd, J. M., Elliott, L., Greenham, A. K., Johnson, W. H., Nixon, J. S., Rose, F., Sutton, B. & Wilson, K. Ro 32-3555, an orally active collagenase inhibitor, prevents cartilage breakdown in vitro and in vivo. *British Journal of Pharmacology* **121**, 540-546, doi:10.1038/sj.bjp.0701150 (1997).

370 MacPherson, L. J., Bayburt, E. K., Capparelli, M. P., Carroll, B. J., Goldstein, R., Justice, M. R., Zhu, L. J., Hu, S. I., Melton, R. A., Fryer, L., Goldberg, R. L., Doughty, J. R., Spirito, S., Blancuzzi, V., Wilson, D., Obyrne, E. M., Ganu, V. & Parker, D. T. Discovery of CGS 27023A, a non-peptidic, potent, and orally active stromelysin inhibitor that blocks cartilage degradation in rabbits. *Journal of Medicinal Chemistry* **40**, 2525-2532, doi:10.1021/jm960871c (1997).

371 Vandenbroucke, R. E. & Libert, C. Is there new hope for therapeutic matrix metalloproteinase inhibition? *Nature Reviews Drug Discovery* **13**, 904-927, doi:10.1038/nrd4390 (2014).

372 Plotkin, L. & Bellido, T. Osteocytic signalling pathways as therapeutic targets for bone fragility. *Nature Reviews Endocrinology* **12**, 593–605 (2016).

373 Karsdal, M. A., Sumer, E. U., Wulf, H., Madsen, S. H., Christiansen, C., Fosang, A. J. & Sondergaard, B.-C. Induction of increased cAMP levels in articular chondrocytes blocks matrix metalloproteinase-mediated cartilage degradation, but not aggrecanase-mediated cartilage degradation. *Arthritis and Rheumatism* **56**, 1549-1558, doi:10.1002/art.22599 (2007).

374 Morovic-Vergles, J., Culo, M. I., Gamulin, S. & Culo, F. Cyclic adenosine 5 '-monophosphate in synovial fluid of rheumatoid arthritis and osteoarthritis

patients. *Rheumatology International* **29**, 167-171, doi:10.1007/s00296-008-0663-z (2008).

375 Verbovsek, U., Van Noorden, C. J. F. & Lah, T. T. Complexity of cancer protease biology: Cathepsin K expression and function in cancer progression. *Seminars in Cancer Biology* **35**, 71-84, doi:10.1016/j.semcancer.2015.08.010 (2015).

376 Roux, P. P. & Blenis, J. ERK and p38 MAPK-activated protein kinases: a family of protein kinases with diverse biological functions. *Microbiology and Molecular Biology Reviews* **68**, 320-+, doi:10.1128/mmbr.68.2.320-344.2004 (2004).

377 Maeng, Y. S., Min, J. K., Kim, J. H., Yamagishi, A., Mochizuki, N., Kwon, J. Y., Park, Y. W., Kim, Y. M. & Kwon, Y. G. ERK is an anti-inflammatory signal that suppresses expression of NF-kappa B-dependent inflammatory genes by inhibiting IKK activity in endothelial cells. *Cellular Signalling* **18**, 994-1005, doi:10.1016/j.cellsig.2005.08.007 (2006).

378 DeFea, K. A., Zalevsky, J., Thoma, M. S., Dery, O., Mullins, R. D. & Bunnett, N. W. beta-Arrestin-dependent endocytosis of proteinase-activated receptor 2 is required for intracellular targeting of activated ERK1/2. *Journal of Cell Biology* **148**, 1267-1281, doi:10.1083/jcb.148.6.1267 (2000).

379 Ueda, Y., Hirai, S., Osada, S., Suzuki, A., Mizuno, K. & Ohno, S. Protein kinase C delta activates the MEK-ERK pathway in a manner independent of Ras and dependent on Raf. *Journal of Biological Chemistry* **271**, 23512-23519 (1996).

380 Schmitt, J. M., Wayman, G. A., Nozaki, N. & Soderling, T. R. Calcium activation of ERK mediated by calmodulin kinase I. *Journal of Biological Chemistry* **279**, 24064-24072, doi:10.1074/jbc.M401501200 (2004).

381 Eishingdrelo, H. & Kongsamut, S. Minireview: Targeting GPCR Activated ERK Pathways for Drug Discovery. *Current chemical genomics and translational medicine* **7**, 9-15, doi:10.2174/2213988501307010009 (2013).

382 Goergens, S. W., Eckardt, K., Elsen, M., Tennagels, N. & Eckel, J. Chitinase-3-like protein 1 protects skeletal muscle from TNF alpha-induced inflammation and insulin resistance. *Biochemical Journal* **459**, 479-488, doi:10.1042/bj20131151 (2014).